University of
Strathclyde
Glasgow

Strathclyde Institute of Pharmacy
and Biomedical Sciences

Impact of end groups of PLGA on polymer properties and ocular implant performance

Mariam Badawi

Thesis presented in fulfilment of the requirement for the degree of
Doctor of Philosophy (PhD)

2017

Declaration of Authenticity and Author's Rights

This thesis is the result of the author's original research. It has been composed by the author and has not been previously submitted for examination which has led to the award of a degree.

Signed: Mariam Badawi

Date: 22nd of January 2018

"This thesis is dedicated to mom and dad.

For without you I wouldn't be"

ACKNOWLEDGMENTS

When ***thank you*** is not enough! I would like to thank my principal supervisor Professor Clive G. Wilson, for giving me three years of experience that have shaped my career forever. Thank you for helping me develop and allowing me to grow into the independent researcher and confident thinker I have become. Thank you for giving me the freedom to fail and encouraging me to tap on new approaches throughout my lab work. Thank you for being my role model not only as a researcher but also on the human aspect of matters. To Mrs. Stephanie Wilson Thank you for hosting all the amazing barbeques I will miss those! Thanks for our last night boot camp that was much needed! I would also like to thank my second supervisor Professor Peter Cormack for his guidance and support as well as giving me the opportunity to work in his lab where I have found my new love “polymer chemistry”.

I am utterly grateful to my industrial supervisor Dr. Ruiwen Shi. Not only for his guidance and support during my stay at Allergan, but also his patience and kindness as a teacher. Thank you for taking the time to explain the basics, I’m taking a lot of what you have taught me with me forever. I would also like to thank Dr. Patrick Hughes for facilitating my research and enabling my industrial experience at Allergan laboratories. I also would like to thank Dr. James Cunningham and Dr. Sesha Neervannan for facilitating my visits and interaction at the last stages of this Allergan funded studentship.

That being said there are so many people I am grateful for without whom this thesis would have never come to life. I would like to say thank you to Professor Sandy Grey who taught me how to analyse my first NMR chart! Ibrahim thank you for the support and troubleshooting every time I was in panic mode, Claire thank you for being my soundboard when I was losing it. Jen thank you for every time you saved me. Ivan and Jeremy thank you for all the fun days in the lab. Tim and Amaia thank you for bridging all my chemistry gaps. Thank you Anna and Gaetan for making Glasgow my second home.

Thanks to Professor Tim Long at Virginia Tech for enabling my research in his lab and the invaluable knowledge gained from his group. In particular thank you Justin and Evan for helping me out even when you had more important things to do – like writing up your thesis! Thank you Katie your support and kindness. Special thanks to Raouf for all the tips and tricks in the lab.

Last but not least I'm forever indebted to my parents who have been cheering me all the way. Without you I would not be where I am today. Mom I don't know how you kept your enthusiasm and encouragement for so long. Not doubting my ability even when I doubted myself. Dad thank you for your love and generous care. For all the times you helped me see the lesson presenting itself. For all the suggestions you made to help with my lab work, they actually worked! To my siblings who had to cope with a lot of drama during the past 3 years thank you. To Sara thanks for flying over every time I had a mental breakdown, and posting chocolate to fix all PhD problems. Mohamed thank you for being my internal barometer for all the late night phone calls in the lab we did it! It is official we are Nerds! Ahmad thank you for being the source of joy in my life for all the times I wanted to cry but you made me laugh. A group hug is well deserved right now!

In the end thank you God, for giving me an experience that has shaped my personality forever, for the strength and patience to learn even when the lesson was not clear. Thank you for sending my way all the people who have showered me with generosity, love and kindness. ***Gratitude*** in my case would be an understatement…

Sincerely,

Mariam

CONTENTS

CHAPTER 5: FUNDAMENTAL UNDERSTANDING OF ENDCAPPING STRUCTURE-PROPERTY RELATIONSHIP OF PLGA POLYMERS

ABSTRACT

The unique anatomy of the eye and its efficient barrier mechanisms challenge the development of ophthalmic dosage forms. Conventionally, most ophthalmic drugs are delivered topically in the form of eye drops. However, the short pre-corneal residence time requires frequent instillation which results in fluctuations in therapeutic concentration, and low patient compliance coupled with high health care cost. Glaucoma is the second leading cause of vision loss after cataract in the world. Approximately 10% of people with glaucoma who receive proper treatment still experience loss of vision. This makes the long-term effectiveness and efficacy of current therapies questionable. Biodegradable polymeric implants offer potential for exact drug delivery at the intraocular target site. The FDA-approved PLGA has been investigated for implantable ocular dosage forms. From a manufacturing stand point, the copolymer provides several merits. However, the risk of distortion on hydration causing endothelial contact, the biological fate of the polymeric system and the physico-chemical properties of the active compound are all issues that need to be integrated into the design. The effect of the copolymer composition and molecular weight has been addressed. However the effect of endcapping of PLGA polymers on hydrophilicity and drug-polymer interaction in attempts to tune drug delivery is scarce in the literature. The current study investigates the utilization of end capping in achieving desired drug release kinetics and implant mechanical profiles upon intraocular exposure.

List of Abbreviations

Abbreviation	
C_{ss}	Saturated solution
CMV	cytomegalovirus
DDS	Drug Delivery System
DSC	Differential Scanning Calorimetry
DVS	Dynamic Vapour Sorption
EVA	Ethylene vinyl acetate
FDA	Food and Drug Administration
FT-IR	Fourier Transform Infrared
GA	Glycolic acid
GPC	Gel Permeation Chromatography
LA	Lactic acid
MC	Moisture content
MW	Molecular Weight
NMR	Nuclear Magnetic Resonance
PCF	Polysulfone capillary fiber
PDI	Poly Dispersity Index
PGA	Poly glycolic acid
PLGA	Poly lactide-co-glycolide
PLA	Poly Lactic acid
PVA	Polyvinyl alcohol
RH	Relative Humidity
ROP	Ring Open Polymerization
SEC	Size Exclusion Chromatography
$Sn(Oct)_2$	Stannous octoate
TGA	Thermogravimetric Analysis
XRPD	X- Ray Powder Diffraction
$Zn(Lact)_2$	Zinc Lactate
EDC	N-ethyl-N'-(3-(dimethylamino)propyl)carbodiimide
NHS	N-hydroxysuccinimide

CHAPTER 1: INTRODUCTION

The eye is a sensory organ prone to a wide variety of diseases which result principally from infection, inflammation and inappropriate angiogenesis. The vulnerability of the tissue due to injury is in part ameliorated by barriers preventing the ingress of foreign compounds and pathogens. Isolation from the circulation by aqueous and blood barriers limit successful drug delivery excluding local delivery of active products. As a consequence, the efficacy of topical drug delivery via eye-drops *per se* is limited to the treatment of anterior segment eye diseases. The slowly progressive ocular diseases affect approximately 67 million people. This alarming high number of anticipated patients prompts urgent intervention to the current therapeutic care model.

1.1. Glaucoma: the silent thief

According to the World Health Organization, glaucoma a long-term ocular neuropathy has been ranked as the second leading cause of blindness worldwide (Quigley, 2011). Quigley & Broman, writing in the British Journal of Ophthalmology in 2006, estimated that the number of people with glaucoma will be nearly 79.6 million worldwide by 2020 (Quigley and Broman, 2006). 10% of whom will become bilaterally blind (Mantravadi and Vadhar, 2015). Partial vision loss or blindness increases the health care costs of treating the disease by at least 46% (Fedorchak *et alet al*., 2014).

Glaucoma is a collection of ocular pathological conditions typically characterized by an increase in intraocular pressure (IOP) (Costa *et alet al*., 2003). Uncontrolled IOP greater than 21 mmHg ultimately compromises blood flow to the retina. This results in acquired loss of retinal ganglion cells and permanent damage to the optic nerve with subsequent loss of vision and/or irreversible blindness (Mealy *et al*., 2014). Early diagnosis is thus critical to prevent irreversible vision loss and ensure better prognosis (Cantor, 2006). A less common form of glaucoma where a normal intraocular pressure is maintained has also been identified. It is more prevalent in the Japanese population; however, treatment follows the same therapeutic objective of lowering intraocular pressure (Mallick *et al*., 2016).

Based on the configuration of the angle between the cornea and the iris diaphragm where reabsorption of the aqueous humour occurs, two major types of high pressure glaucoma have been identified; open and closed-angle glaucoma. Closed-angle glaucoma, which is a medical emergency, is ultimately treated surgically. Open-angle glaucoma has a more gradual and insidious onset and thus requires drug therapy on a permanent basis, often with changes of treatment over a year (Coleman *et al*., 2016).

1.1.1. Current Non-Surgical Therapies

Current non-surgical treatment options for glaucoma are limited to medicated eye drops taken multiple times per day for maintaining IOP at normal levels, through either decreased production or increased outflow of aqueous

humour. Decreased production of aqueous humour is achieved by the use of beta-blockers, carbonic anhydrase inhibitors. Sympathomimetics often with prostaglandin analogues are used to increase the aqueous humour outflow (Bucolo *et al*., 2013, Mealy *et al*., 2014,). Nevertheless, optimal control of intraocular pressure in glaucomatous patients does not seem to stop retinal ganglion cell death and subsequent vision loss. This suggests that a neuroprotective agent should be used in conjunction with current therapeutic treatment.

1.1.2. New pharmacological treatment of Open-Angle Glaucoma

Novel agents to treat primary open-angle glaucoma have recently been reviewed by Lu and colleagues. Since the introduction of the original latanoprost analogues, researchers have described the rho kinase inhibitors such as ripasudil and netarsudil which decrease trabecular- meshwork resistance; the adenosine receptor agonist traodenoson which akin to the prostanoids, diverts more aqueous humour outflow through the scleral route and the newly modified prostanoid analogues latanosprostene and ONO-9054, which are more potent than the first and second line prostanoids (Lu *et al*., 2017).

1.1.3. Brimonidine

Brimonidine [5-bromo-6-(2-imidazolidinylideneamino)quinoxaline] is a highly selective α_2-adrenergic agonist approved for topical ocular administration in the treatment of open-angle glaucoma. It is also administered prior to

phacoemulsification cataract surgery and after argon laser trabeculoplasty to prevent the post-operative increase of intraocular pressure. In addition, it has been used to induce miosis in patients suffering from poor night vision after Lasik surgery (Naik *et al*., 2010).

Clinical studies suggest that Brimonidine has a dual mechanism of action. First, it reduces intra-ocular pressure (IOP) by reducing aqueous humour production through the activation of the Gi alpha subunit. This reduces cAMP and hence aqueous humour production by the ciliary body. Second, it increases the aqueous humour outflow via the uveoscleral pathway (Cantor, 2006, Naik *et al*., 2010).

There has been evidence to suggest that Brimonidine also exhibits important neuroprotective actions by interacting with its target receptors in the retina, which can release various neurotrophins including brain-derived neurotrophic factor (BDNF) and ciliary neurotrophic factor (CNTF). These neurotrophins have a potential to prevent apoptosis of photoreceptors, thus limiting the progression to visual loss in glaucoma (Lonngren *et al*., 2006). This proposition has however been challenged by Weinreb (Weinreb, 2016).

Due to its selectivity Brimonidine, eye drops reduce elevated IOP with minimal effect on cardiovascular and pulmonary parameters when compared with other drugs, namely clonidine and apraclonidine adopted for glaucoma treatment (Insel, 1996, Munk *et al*., 1995).

Commercially, Brimonidine is available in its tartrate salt form as 0.1% and 0.15% w/v sterile ophthalmic solution (Alphagan® P) and as a 0.2% w/v sterile ophthalmic solution (Alphagan®). Brimonidine tartrate is also available in combination with timolol in the commercial product Combigan™ (Brimonidine Tartrate, Timolol Maleate Ophthalmic Solution 0.2%/0.5%).

In salt form, it has a molecular weight of 442.24 Da with pka 7.78±0.05. It is a white, odourless, crystalline powder with hydrophilic nature having a melting point at 207 ± 0.5°C. The empirical chemical formula is $C_{15}H_{16}N_5O_6Br$ and the chemical structure is as shown in Figure 1.1. Brimonidine tartrate is highly soluble in water at low pH and solvents such as Dimethylsulfoxide (DMSO). Brimonidine has a rapid onset of action, with the peak ocular hypotensive effect occurring at two hours post-dosing. The duration of effect is 12 hours or greater.

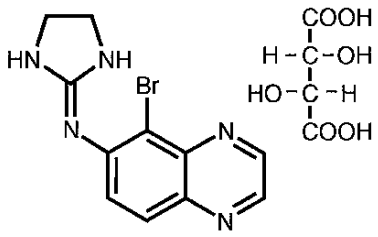

Figure 1.1: Chemical structure of Brimonidine tartrate

1.2. Physiological-ocular barriers: an impediment to intraocular drug delivery

The eye is a relatively isolated organ divided into an anterior and posterior segment with numerous avascular structures. This unique anatomy and efficient protective mechanisms of the eye challenge the development of

effective ophthalmic dosage forms. In this regard, the efficacy of topical drug delivery via eye-drops is only limited to the treatment of anterior segment eye diseases. The anterior segment includes the cornea, iris, crystalline lens, ciliary body and aqueous humour while the posterior segment comprises the vitreous body, retina, and choroid. Due to the number of protective anterior segment barriers, typically less than 5% of an applied dose via an eye-drop will be delivered to the ocular tissues of the anterior segment and almost negligible quantities to none may enter the posterior segment if required (Lee and Robinson, 1986, Mikkelson *et al*., 1973).

The orbit receives a small fraction of the total systemic blood flow and therefore the amount of drug delivered to the eye following oral administration does not support a potential avenue for therapy. High doses would be necessary to achieve effective drug concentrations at the target tissue with systemic adverse effects as a consequence. Such approach is thus not feasible for potent drugs with narrow therapeutic indices (del Amo and Urtti, 2008).

Eye drops are the most commonly applied pharmaceutical dosage forms used in the treatment of glaucoma and other ocular diseases affecting the anterior segment of the eye. These dosage forms are easy to instil. However, the ocular bioavailability of the drugs is extremely poor, with only 1-7% of the dose reaching the aqueous humour as illustrated in Figure 1.2 (Mikkelson *et al*., 1973).

The inherent drawback of this route is related to the precorneal factors such as tear turnover and dilution by tear flow, lacrimo-nasal drainage, reflex blinking and highly selective corneal epithelial barrier (Figure 1.2). These factors lower the concentration gradient that drives the absorption of the drug across the cornea and conjunctiva. As a result, the amount given in each eye drop is significantly higher than the amount actually required for IOP reduction (Fedorchak *et al*., 2014).

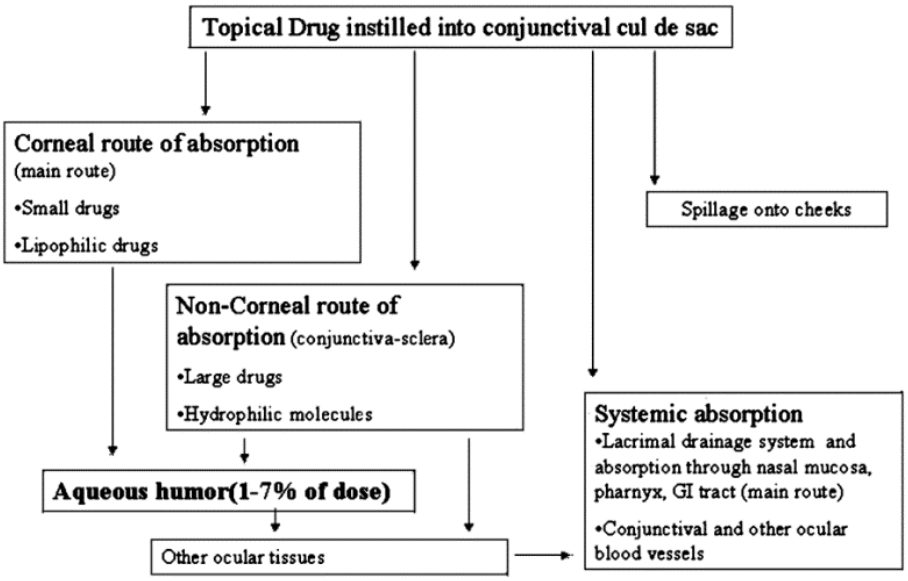

Figure 1.2: Typical profile of a topically applied drug: in the best case only 1% to 7% of the topically applied drug reaches the anterior segment (i.e. by ointment).

In fact, up to 50% of the given dose is absorbed systemically by the lacrimal drainage system, nasal mucosa, and pharynx, causing systemic side effects and significantly affecting overall tolerability of the drug. These anatomical and physiological elements lead to the ineffective lowering of the IOP and progression of glaucoma (Fedorchak *et al*., 2014, Ghate and Edelhauser, 2008).

For these reasons reducing intraocular pressure is accomplished by rigorous dosing schedules where administration of the drug as drops multiple times daily is required to achieve an adequate level of therapeutic effect. Consequently, decreasing the expectations of the patients to the daily therapy (Vaishya *et al*., 2014, De Souza *et al*., 2016, Servat and Bernardino, 2011). Patient non-adherence to therapy greatly reduces the efficacy of topical treatments. Studies have demonstrated that patient adherence rates with eye drop medication range from 5 to 80% for ocular hypotensive treatments, with one study showing that 37% of patients incorrectly followed the treatment schedule when multiple drops daily were required (Patel and Spaeth, 1995, Olthoff *et al*., 2005). Brimonidine tartrate, which requires dosing as drops as often as every 8 h has been associated with a reported average 64% adherence rate (Hermann *et al*., 2011).

Poor response to medical glaucoma treatment, whether as a result of non-adherence or lack of efficacy, typically leads to more invasive surgical interventions such as laser surgery, filtering, trabeculectomy and tube-shunt surgeries (Mermoud *et al*., 1993, Quigley, 2011).

In order to overcome the drawbacks of the conventional eye drops, many researchers have attempted to increase the pre-corneal residence time to improve the bioavailability of eye-drop formulations. These include increasing the viscosity of ophthalmic delivery systems through inclusion of drugs in hydrogel-based polymers or mucoadhesives thermoresponsive gels, and ointments (Wilson *et al*., 1998).

As well as the use of penetration enhancers, such as chelating agents, surfactants, bile salts, the use of prodrugs and liposomal carriers, and colloidal particulate formulations. These approaches have the ability to prolong the precorneal residence time and improve the bioavailability of drugs within the anterior segment when compared with their eye drops counterparts. However, they suffer from disadvantages that include a sticky sensation, blurred vision and induced reflex blinking which also increases patient non-compliance.

1.3. Approaches employed to overcome the ocular barriers

The main prerequisites for an ideal ophthalmic drug delivery system would, therefore, be first the ability to be administrated accurately with little loss, thereby reducing the concentration of drug needed and accompanied local and systemic side effects. Second the ability to improve drug retention in the pre-corneal area leading to increased drug bioavailability without causing irritation. This reduces the need for frequent dosing thus leading to improved patient compliance.

Selected drugs for the treatment of glaucoma have been incorporated into sustained release formulations to decrease the need for frequent dosing. Attempts to design controlled release dosage forms of Brimonidine have been previously discussed in the literature. To date, the proposed long-term sustained release formulations include direct injection of drug solutions,

intraocular injectables (including carriers such as microspheres, nanospheres, and liposomes) or implants (Deokule *et al*., 2012, De Souza *et al*., 2016, Mealy *et al*., 2014).

1.3.1. Ocular Inserts

To overcome the drawbacks of conventional eye drops, ocular drug delivery systems, such as inserts, have the potential for use as a patient-administered (non-injectable) device. Ocular inserts are defined as sterile, multi-layered, drug-impregnated polymeric devices which are placed into the cul-de-sac or conjunctival sac to deliver drugs in the anterior segment of the eye. Their size and shape are specially designed for ophthalmic application. After insertion they exhibit a gelling behaviour, releasing drugs at a slow and constant rate resulting in an extended residence and bioavailability at the site of drug action (Saettone and Salminen, 1995).

In spite of the numerous advantages demonstrated by ocular inserts, its capital disadvantage is the foreign body sensation accompanied by its initial administration. However, this disadvantage did not prevent the adoption of this technology in several successfully marketed ocular inserts (Ocusert®, Ocufit® SR, and Minidisc®) as their numerous advantages extremely supersede their sole disadvantage. As a consequence, ocular inserts could be applied to improve the glaucomatous patient compliance due to the efficacy of the therapy and the reduced frequency of administration. Several

recent studies have attempted to take steps toward long-term delivery of new medications to the eye through the development of ocular inserts for the glaucoma medication.

Ocusert® (Alza; Vacaville, CA) an ocular device based on pilocarpine alginate enclosed in ethylene-vinyl acetate delivers therapeutic concentrations of the pilocarpine for 7 days, reducing significantly the IOP in patients. The primary advantage of this device was the decreased dosing frequency relative to topical treatment (a four times daily drop) and ease of removal by patients any time. Despite its eventual discontinuation due to the side effects caused by pilocarpine, the inserts provided a marked improvement over topical medications and were preferred by a significant number of patients. Therefore, a key area for improvement is the choice of drug (Macoul and Pavan-Langston, 1975).

Other studies have been performed to demonstrate the development of ocular inserts containing different types of drugs to treat glaucoma, including bimatoprost,(J.R. Franca *et al*., 2014) timolol maleate (Fulgêncio *et al*., 2012) and betaxolol hydrochloride (Hitesh and Jayvadan, 2013). Wheeler's work suggests that Brimonidine tartrate can be released over a period of several days through the use of both diffusion and degradation mediated release mechanisms (Wheeler *et al*., 2003). However, the development of a device that can provide weeks of release for Brimonidine has yet to be achieved (De Souza *et al*., 2016).

1.3.2. Implantable Device Technology

Surgically inserted ocular implantable polymeric devices offer long-term pharmacotherapeutic exposure at the desired location giving the advantage of local drug delivery. This method bypasses ocular barriers, provides prolonged release times and improved therapeutic efficacy. Moreover, it diminishes the side effects and avoids systemic complications, ultimately improving compliance. Ocular implants have been developed using both biodegradable and nonbiodegradable polymeric matrices with various geometries (Bourges *et al*., 2006, Choonara *et al*., 2009, Eljarrat-Binstock *et al*., 2010). Figure 1.3 illustrates the potential sites for ocular implant administration.

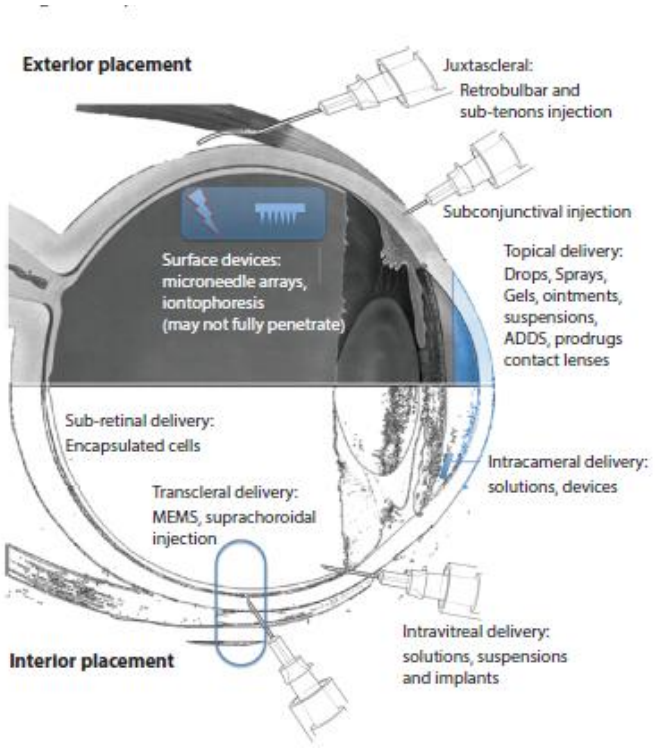

Figure 1.3: Potential sites for ocular drug delivery device administration (Wilson *et al*., 2016).

Although insertion of the implants is an invasive procedure as it requires minor surgery, the implants have the benefit of by-passing the blood–ocular barriers to deliver constant therapeutic levels of drug directly at the site of action. In addition, although the surface of tissues to be targeted is large, the volume of the ocular fluids circulating is small therefore smaller quantity of drug needed during the treatment decreasing the risk of the side effects associated with high dosing (del Amo and Urtti, 2008). Many reports have recorded the successful applications of intraocular implants containing a wide range of drugs such as antimicrobial, antiviral and anti‑inflammatory agents (Bourges *et al*., 2006, Choonara *et al*., 2009, Eljarrat-Binstock *et al*., 2010, Thrimawithana *et al*., 2011).

Intravitreal intraocular implants have been developed to achieve controlled and sustained drug delivery for cases of proliferative vitreoretinopathy, cytomegalovirus (CMV), retinitis, endophthalmitis, and posterior capsule opacification (Bourges *et al*., 2006), thus improving their delivery to the posterior retina where the majority of sight-threatening diseases occur (Choonara *et al*., 2009). Deokule and colleagues developed an intravitreal implant loaded with Brimonidine tartrate that was used to achieve statistically significant IOP reduction for one month in normotensive rabbits (Deokule *et al*., 2012). In fact, Brimonidine has successfully been tested for its safety and efficacy upon sustained delivery from a Poly lactide-co-glycolide (PLGA) intravitreal implant with two doses (200 µg, µ400 g) of Brimonidine tartrate (Manickavasagam and Oyewumi, 2013).

On the other hand, intracameral injection in the anterior chamber offers potential benefits from an “immune privilege” particularly observed in the limiting the risk of exaggerated inflammatory reaction to foreign antigens (Bourges *et al*., 2006). Another advantage to this route is the avoidance of adverse effects associated with intravitreal implants, including cataract formation, retinal detachment, vitreous haemorrhage, and endophthalmitis (Fedorchak *et al*., 2014).

1.4. Polymers used for intraocular implants

The diverse applications and functionalities of polymers make them among the most widely used excipients in pharmaceutical development (Jain, 2000). Continued research has focused on the invention of polymeric matrices for the improvement of the release profiles of long-term drug release systems (Silva *et al*., 2015). Polymeric viscous or semi-solid materials can be localized in the eye as intraocular “implants” after simple injection (Bourges *et al*., 2006). Ocular implants which provide a platform for the sustained release of molecules are constructed from either biodegradable or non-biodegradable polymers, with various geometries releasing actives from several weeks to years (Thrimawithana *et al*., 2011).

There are several major factors to consider with regard to these implantable polymeric devices. Biocompatibility is essential and all components are required to be chemically inert, non-carcinogenic, hypoallergenic, and

mechanically stable at the implantation site. Furthermore, the material should not be physically or chemically modified by local tissue nor cause any unexpected immune or inflammatory response at the site of implantation (Choonara *et al*., 2009).

1.4.1. Non-biodegradable Polymers

In the early 70s, non-bioerodible implants were introduced offering controlled release over prolonged periods. The delivery of the drug from these systems is based on diffusion of a dissolution medium into the device dissolving the drug, creating a saturated solution (C_{ss}) which is subsequently released to the medium by diffusion. For as long as the internal solution is at C_{ss}, the release rate is constant (Velez and Whitcup, 1999). Probably the first commercial intraocular implant used clinically was Vitasert©. Retisert© and Medidur© were later approved (Figure 1.4). Details of these marketed reservoir non-biodegradable implants are discussed below.

Figure 1.4: Comparison of the sizes of Medidur®, Retisert® and Vitrasert® implants(Choonara *et al*., 2009).

- **Vitrasert®:** a reservoir-type device was developed by Ashton and colleagues in 1992 for the release of ganciclovir in patients requiring treatment for cytomegalovirus retinitis. It provided long-term (more than 80 days) drug delivery and was approved for clinical use by the Food and Drug Administration in 1996 (Chiron Vision Inc., Irvine, CA). The implant is composed of ganciclovir and polymeric coats of polyvinyl alcohol (PVA) and ethylene vinyl acetate (EVA) as shown in Figure 1.5.

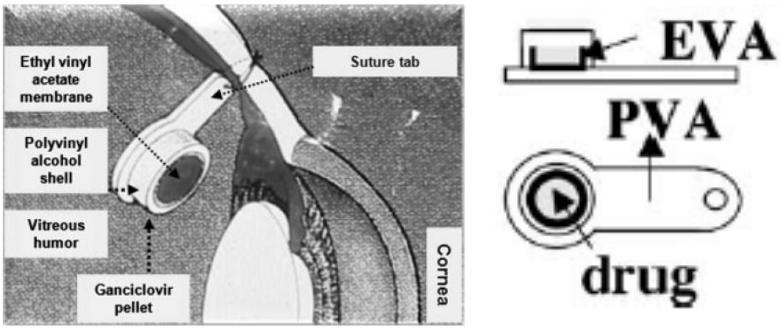

Figure 1.5: Non-biodegradable Vitrasert® implanted in the eye (Choonara *et al*., 2009, Yasukawa *et al*., 2004).

PVA, a permeable polymer, acts as the framework of the device and regulates the rate of ganciclovir release. EVA an impermeable polymer controls the surface area that is permeable to the drug. This polymeric arrangement enables zero order sustained release of the drug without an initial or a final burst release (Choonara *et al*., 2009, Yasukawa *et al*., 2004).

- **Retisert®**: the first marketed fluocinolone acetonide implant for the treatment of chronic non-infectious uveitis (Bausch & Lomb Inc., Rochester, NY) is a reservoir-based implant designed to provide drug release over a

period of approximately 1000 days (Figure 1.4). (del Amo and Urtti, 2008) The device has shown significant reduced recurrence of uveitis to 5.4% compared with 46% in the control eye 1 year post-implantation (Choonara *et al*., 2009).

- **Medidur®:** a non-biodegradable reservoir-type implant also contains fluocinolone, for the treatment of the retinal and choroidal diseases. It is much smaller than Retisert® (Figure 1.4). This makes it easier to surgically insert the implant during an outpatient visit through a 3.5 mm incision with a 25G needle into the back of the eye enabling self-sealing of the wound (Alimera Sciences Inc., Atlanta, GA and Sivida Inc., Watertown, MA). The implant is not sutured to the eye wall and floats freely in the vitreous space releasing the drug constantly for at least 3 months (Choonara *et al*., 2009).

Inspite, the advantages of the aforementioned implants such as convenience, long-term controlled release, reduced cost and lack of systemic toxicity. Relatively large incisions (4–5-mm sclerotomy at the pars plana) for implantation may be required. Temporary decrease in visual acuity was attributed to the surgical procedure and the surgical removal of the exhausted implant is usually associated with serious side effects or retention until death (Lee *et al*., 2010, Bourges *et al*., 2006). Other complications in the posterior segment including vitreous haemorrhage, risks of infection, retinal detachment, endophthalmitis, and cystoid macular oedema with epiretinal membrane post-implantation have also been reported (Choonara *et al*.,

2009). These problems cannot be ignored because postoperative complications are associated with decreased visual acuity despite treatment (Yasukawa *et al*., 2004).

1.4.2. Biodegradable Polymers

Biodegradable polymers allow for sustained release without post-treatment removal. They are converted through enzymatic or non-enzymatic pathways in the body into soluble fragments and are excreted by the body.(Lee *et al*., 2010) Unfortunately, they show more erratic drug-release profiles which makes their development and optimization a more complex task.(Thrimawithana *et al*., 2011) Numerous variables influence the spontaneous degradation and erosion kinetics of these polymers (Bourges *et al*., 2006). These factors include alterations in body pH or temperature that may cause a transient increase or decrease in the erosion rate. The surface area of the drug delivery device also plays a significant role in its erosion. A more pressing challenge is that the diffusion of the drug usually occurs at a slower rate than the degradation of the device. This poses a significant challenge when the drug has a narrow therapeutic index (Choonara *et al*., 2009).

Among renowned biodegradable materials widely used in medicine and pharmacy are poly (D,L-lactide)s (PLAs) and the copolymers with glycolide; poly(d,l-lactic-co-glycolic acid)s (PLGAs)

These copolymers belong to the FDA-approved aliphatic polyesters class of polymers. Their biodegradation occurs through bulk erosion upon cleavage of the polymer chains by hydrolysis into natural metabolites (lactic acid and/or glycolic acid). The acids are eliminated by the Kreb's cycle in the form of carbon dioxide and water (Félix Lanao *et al*., 2011), as shown in Figure 1.6 reducing any concern about their long-term toxicity as well as any need for debris removal post-therapeutic duration.(Allison, 2008, Fredenberg *et al*., 2011)

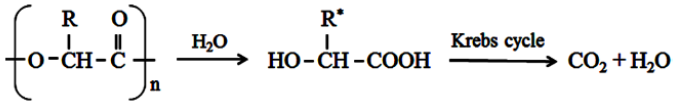

Figure 1.6: R = H (glycolic acid) or R = CH_3 (lactic acid). Degradation products: 1) lactic acid (if the polymer is PLA), 2) glycolic acid (if the polymer is PGA), 3) both (polymer source is PLGA).

1.5. Poly Lactide-co-glycolide (PLGA)

The versatility of PLGA to form various shapes has made it attractive in the production of biomedical devices. The first product based on PLGA copolymer (Vicryl®), was commercialized in the 1970s.(Silva *et al*., 2015) Although the first applications of these polymers have been as materials for surgical sutures and implants to repair fractures, the proven safety, mechanical strength and tuneable degradation rate of the copolymer make it a preferred polymeric candidate for fabricating solid implants.(Jain, 2000, Koopaei *et al*., 2012) Their use in drug release devices has been extensively investigated for formulation of ocular dosage forms. In fact, PLGA has been

reported to be one of the best-defined biomaterials available for intraocular drug delivery with respect to design and performance.(Lee *et al*., 2010, Choonara *et al*., 2009)

1.5.1. PLGA based Ocular Implants

Surodex™ (Oculex Pharmaceuticals, Inc., Sunnyvale, CA) is a rod-shaped biodegradable implant (1.0×0.5 mm) consisting of 60 mg dexamethasone and PLGA with hydroxypropyl methylcellulose (HPMC) which provides sustained drug release at a constant rate (7–10 days). The implant is inserted in the anterior chamber following cataract surgery at the conclusion of surgery to control postoperative inflammation without suture fixation. In cataract patients, Surodex was shown to reduce flare in the postoperative period and to have anti-inflammatory effects as good as topical steroids.(Lee *et al*., 2010)

In comparison with conventional postoperative eye drops, the intraocular implants require significantly lower drug concentrations and hence reduced systemic side effects and systemic drug toxicity, provide a controlled drug concentrations at the target site with near-zero order pharmacokinetics and reduced complications related to patient noncompliance. However the difficulty of removal of the device if required, potential corneal endothelium damage from the physical migration of the device, and localized damage at the site of the implantation all present challenges to the development of the DDS. (Bourges *et al*., 2006)

Ozurdex® formerly known as Posurdex®, (Allergan Inc., Irvine,CA) is a sterile, single-use system that has been successfully used to deliver one solid, rod-shaped PLGA copolymer implant 6.0X0.46mm (Novadur™ matrix, Allergan, Inc.) containing of 0.7 mg dexamethasone into the vitreous for the treatment of macular oedema (Figures 1.7). (Whitcup and Robinson, 2015)

Figure 1.7: Ozurdex® sustained-release drug delivery system. The dexamethasone drug pellet at a dose of 350 or 700 µg is inserted using a 22-gauge microinjector. (Adapted from Ozurdex®, Allergan, Inc., Irvine, CA).

The rationale of the design is to overcome ocular drug delivery barriers and extend the duration of dexamethasone effect in the eye. The implant releases dexamethasone biphasically, with peak doses for the initial 2 months, followed by lower therapeutic doses for up to 6 months in the target area. (Lee *et al*., 2011) Moreover, the plasma concentrations of the drug have been found to be below quantification levels overcoming systemic side effects. (Roy and Hegde, 2013) A novel single-use applicator is used to insert the implant into the vitreous through a 22-gauge pars plana injection. The procedure is performed in-office rather than in a surgical setting and does not require sutures for wound closure. (Agrawal *et al*., 2014)

Brimonidine has successfully been tested for its safety and efficacy upon sustained delivery from a PLGA intravitreal implant similar to Ozurdex® (known as Brimo DDS PS). This demonstrates the PLGA platform technology's applicability in the intravitreal delivery of neuroprotective agents for the treatment of both the intraocular pressure and neurodegenerative aspects of glaucoma. (Manickavasagam and Oyewumi, 2013) In spite of their success in controlled drug release profiles, the extruded intraocular implants displayed physical defects upon injection. Incidents of fractured and segmented implants have been reported in several studies as seen in Figure 1.8.(Agrawal *et al*., 2014, Rishi *et al*., 2012, Roy and Hegde, 2013, Cabrerizo and Garay-Aramburu, 2013)

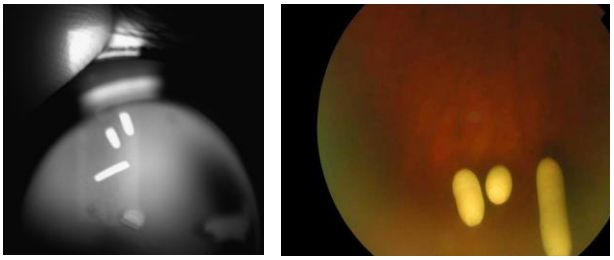

Figure 1.8: Fundus examination revealed a broken Ozurdex™ implant in the vitreous cavity (Rishi *et al*., 2012, Agrawal *et al*., 2014)

One hypothesis for the fragmentation was attributed to implant cracking during manufacturing or packing, friction or misalignment with the injector. However, injector inspection for any residual drug pellets was the negative confirming delivery of an intact implant. (Rishi *et al*., 2012, Roy and Hegde, 2013)

Another possible explanation to explain the curvature taken by the implant prior to fragmentation as seen in Figure 1.9 is induced stress fracture and ageing. Changes in these particular mechanical properties are attributed to the sensitivity of the PLGA's physical structure to its surrounding hydrating phase.(Tsai *et al*., 2016) Therefore the moisture barrier properties of the polymer are of particular interest; however, there are only a few published reports on the transport of water in PLGA. This will be the focus of Chapter 3 in this thesis.

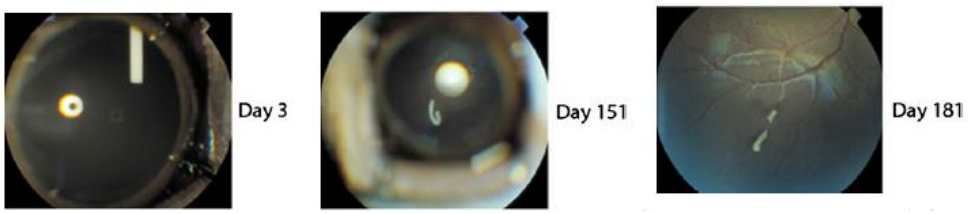

Figure 1.9: Photographic images showing biodegradation of PLGA dexamethasone 700-µg implant (Ozurdex®) in a monkey eye over a 6-month period.(Susan S. Lee *et al*., 2011)

1.5.2. Mechanisms of drug release in PLGA based delivery systems

Although a zero-order release profile is the most commonly preferred profile, mono-phasic release from PLGA-based DDSs is rare. Drug release is sometimes bi-phasic or tri-phasic due to the heterogeneity of the drug/polymer matrix and polymer degradation. In a classic tri-phasic release profile, Phase I is usually attributed to the initial burst release. This is followed by an often slower release Phase II, which is a diffusion driven phase governed by the polymer matrix density and porosity.

Phase III is usually a period of faster release, often attributed to the onset of erosion as polymer degradation and hydration ensue also known as the second burst. (Fredenberg *et al*., 2011)

The initial burst in the PLGA release profile is generally characterized as a spike in drug release rate profiles. This is attributed to uncontrolled drug release from the implant surface prior to the onset of polymer degradation. This is usually undesirable, especially in drugs with low therapeutic indices.(Yasukawa *et al*., 2004)

Control over burst release, continues to be an impediment to product development of controlled release systems. Even in the absence of toxicity, a variable initial release will adversely affect subsequent drug release rate and duration. The rate and extent of burst release must then be accounted for during manufacturing since higher quantities of the drug might be required to ensure adequate delivery over the intended duration.(Allison, 2008)

The rate and degree of this initial phase are affected by intrinsic factors such as drug molecular weight, implant dimension, the partition coefficient of the drug between the polymer and release medium and drug-polymer interaction. Moreover processing parameters during manufacturing as well as storage conditions of the final product that may affect the physical properties of the amorphous polymers, in turn, affect burst release. (Yeo and Park, 2004, Siepmann *et al*., 2004)

The second diffusive phase of stable drug release occurs due to the outward diffusion of drugs and surface erosion of the matrix.(Yasukawa *et al*., 2004, Lee *et al*., 2010) This phase is governed by the rate of polymer degradation, total surface area of the implant, percentage and hydrophilicity of the loaded drug. When a drug is homogenously distributed in an amorphous matrix its diffusion is governed by chemical factors of the polymers such as hydrophilicity/hydrophobicity and stiffness of polymer chains, and the physical factors such as polymer matrix density and porosity.(Klose *et al*., 2006, Narasimhan and Langer, 1997)

Polymer matrix density and porosity are a function of a number of formulation and processing variables. Polymer matrix density is based on the distance between polymer chains within the solid matrix and is a dynamic property of amorphous materials that is affected by structural relaxation. This is caused by the thermodynamic departure of the system from an equilibrium state, which can further affect implant structure and drug release performance.(Allison, 2008) The mobility of polymer chains depends on the glass transition temperature (Tg). The transport resistance is higher for PLGAs in the vitreous state, and water absorption and hydrolysis proceed more slowly. The glass transition temperature decreases with decreasing molecular weight and increase in water content. (Zolnik *et al*., 2006)

Porosity, on the other hand, accounts for the voids and channels throughout the matrix and influences the surface available for diffusion.(Yeo and Park, 2004, Sasaki *et al*., 2005) Upon immersion in dissolution media or

administration in the eye, water is initially absorbed by the polymer. The rate of water absorption, or hydration, is rapid compared to drug release.(Batycky *et al*., 1997, Blasi *et al*., 2005) Water absorption may lower glass transition temperature and lead to higher mobility of polymer chains, which may result in the formation of pores in the matrix. Small pores grow and coalesce with neighbouring ones to form larger channels. Pores may also be closed. This phenomenon is related to the mobility of the polymer chains, and their ability to subsequently rearrange.(Yamaguchi *et al*., 2002) Consequently, pore formation and pore closure influence the resistance to drug transport.(Fredenberg *et al*., 2011)

Finally, biodegradation and mass loss due to the bulk erosion of the polymer throughout the matrix result in the final burst. This is generally uncontrollable, poorly predictable and therefore, largely undesirable. (Yasukawa *et al*., 2004, Bourges *et al*., 2006) Consequently, as illustrated in Figure 1.10, there are three possible routes for drug molecules to be released from a PLGA-based DDS.

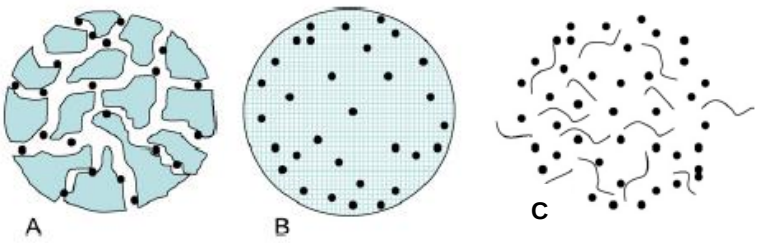

Figure 1.10: Mechanisms of drug release from PLGA based drug delivery systems (A) Diffusion through water filled pores (B) diffusion through the polymer (C) diffusion through pores formed upon polymer erosion. (Fredenberg *et al*., 2011)

Transport through water-filled pores; this is the case when the encapsulated drug is too hydrophilic to diffuse through the polymer phase (Figure 1.10.A). When the drug is small and hydrophobic, transport occurs primarily through the polymer phase (Figure 1.10.B). Finally, the encapsulated drug may be released through erosion of the polymer (Figure 1.10.C). (Fredenberg *et al*., 2011, Wang *et al*., 2002, Raman *et al*., 2005)

Describing the processes controlling the release rate such as water absorption, pore closure, swelling, drug dissolution, the rate of drug diffusion, polymer–drug interaction and degradation kinetics to name a few, is more informative than describing the route of drug release when it comes to considering how drug release can be modified.(Kang and Schwendeman, 2007)

1.5.3. Controlling drug release from PLGA DDS

An important point to bear in mind is the dynamic nature of PLGA, as its properties and behaviour change with degradation. Of particular interest in their use in drug delivery is that the degradation rate of PLGAs and subsequent drug release rate can be modulated. Three main factors determine the degradation rate of PLGA copolymers, the lactide: glycolide ratio, lactide stereoisomeric composition and molecular weight. The lactide: glycolide ratio and stereoisomeric composition are most important as they determine polymer hydrophilicity and crystallinity.(Lee *et al*., 2010) The

higher ratios of the more hydrophobic PLA decrease the penetration of water and overall degradation rate of the polymer while higher ratios of the more hydrophilic PGA have the opposite effect as seen in Figure 1.11.(Park *et al*., 2011, Park and Kang, 2013)

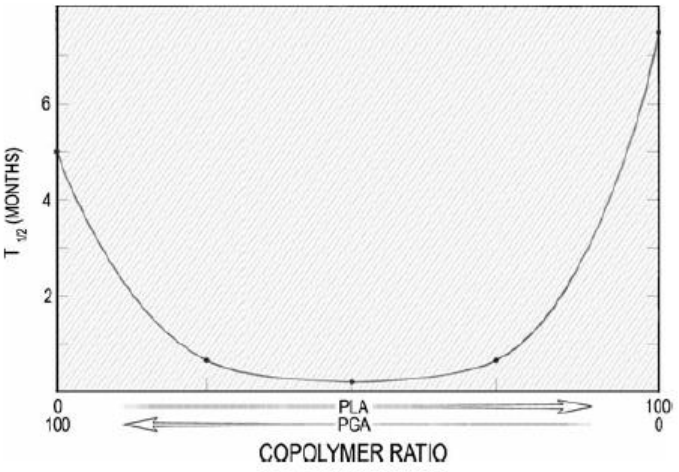

Figure 1.11: Relationship between lactide/glycolide polymer ratio and degradation rate of PLGA (Lee *et al*., 2010)

This broad range of properties has made these polymers ideal candidates as controlled drug release vehicles due to the ability to tailor the polymer degradation time. (Sharp *et al*., 2001) Other attempts to improve the release pattern of these polymeric implants have been by using blends of polymers of different molecular weight at different ratios.(Bourges *et al*., 2006) The higher molecular weight polymers act as a framework while hydrolysis of polymers with a lower molecular weight regulates the drug release.(Yasukawa *et al*., 2004) However, this approach does not allow for a wide range of controlled release rates (Tsuji and Muramatsu, 2001).

Surface modification of polymers is also routinely induced by chemically grafting small molecules on the surface (Tobiesen and Michielsen, 2002, Tsuji and Muramatsu, 2001). However, PLGA lacks functional chemical groups on its aliphatic polyester backbone, which limits surface modification via the aforementioned routes (Keegan *et al*., 2006). Moreover, the covalent conjugation of motifs in an attempt to modify the polymer's surface properties after fabrication into a delivery system may potentially expose the polymer to hydrolysis and denaturation. Thereby usually inducing undesirable radical changes in the bulk properties, such as melting temperature and crystallinity. (Park *et al*., 2011)

Another method that has yet to be exploited for tunable drug delivery involves subtly controlling the chemistry of the PLGA polymer-end groups. Endcapping with functional groups for polymers is a good technique to modify the surface properties while limiting the changes to the bulk properties of polymeric materials.(Kobori *et al*., 2004) By controlling the acid-terminating groups on PLGA polymers, a range of new release profiles can be established, perhaps in a predictable manner.(Huang *et al*., 2013)

1.6. PLGA end capping

End-capping of PLGA with functional groups has been reported to substantially change several properties such as water absorption, mass loss, polymer degradation, kinetic rate constant, and drug release profiles, with little to no effect on other bulk properties as mechanical and thermal

properties which are more likely influenced by the polymer's molecular weight.(Huang *et al*., 2013)

Compared to other surface functionalization techniques, endcapping through synthetic pathways spares the polyesters liable backbone from harsh post manufacturing processes while, achieving high coverage of chemically bonded motifs with significant homogeneity. Thus with very small variations in the structure of a given polymer formulation, its characteristics can significantly change, resulting in new functions and applications.

The end structure of PLGA polymer is a factor that affects primarily its hydrophilicity and hence related properties.(Walter *et al*., 2001) The presence of free carboxyl-end groups renders the copolymer more hydrophilic. Thus, delivery systems made of the copolymer with free carboxyl groups have a more hydrophilic surface than those where the carboxyl-end groups are esterified.(Gasper *et al*., 1998)

PLGA of the same molecular weight and copolymer composition but different end caps have elicited different degradation profiles. It has been reported that PLGA acid terminated films had half-lives half that of their ester terminated counterparts of the same molecular weight. The nature and length of the alkyl ester/amide end cap can further modulate the degradation rate, initial burst release profiles, encapsulation efficiency, swelling properties, drug interactions. (de Jong *et al*., 2001, Wu and Wang, 2001)

This is in part because of the higher water penetration into non-endcapped matrices due to their greater hydrophilicity resulting in faster ester bond hydrolysis and thus faster molecular weight decrease.

Degradation in the non-endcapped polymer n is initially faster because the acidic end groups catalyse hydrolysis of the ester bonds resulting in the production of more acidic groups in an autocatalytic cycle. The nature and length of the alkyl ester end cap can further modulate the degradation rate.(Tracy *et al*., 1999) Consequently, drug release rates are also affected.

Contradictory results have been published regarding end capping effect on polymer's thermal properties. Huang and colleagues reported that acid-terminated PLGA films displayed a lower Tg when compared to the ester-terminated films over time, due to the faster ester cleavage kinetics of the acid-terminated PLGA films.(Huang *et al*., 2013) Conversely, other research indicated that in polymers with equal copolymer compositions and molecular weights, a slightly lower glass trasition temperature (Tg) for PLGA-capped was observed. This suggests that the end group may act as a plasticizer.(Samadi *et al*., 2013)

In addition, endcapping may affect surface and cross-sectional morphology; the acid-terminated polymers have a high affinity for water absorption leading to pore formation and consequent mass loss. Whereas endcapped polymers show a lag phase before morphological changes or degradation occurs.

(Huang *et al*., 2013) Endcapping has also been shown to influence encapsulation efficiency. Where free carboxylic PLGAs interacted with cationic charged drugs and increased their encapsulation as illustrated by Yeo and colleagues.(Yeo and Park, 2004)

On the other hand, end capped polymers would prove more efficient in encapsulating hydrophobic drugs. (Walter *et al*., 2001) In other words, drug polymer interaction will be influenced by the overall hydrophilicity of the polymer which can be modulated through endcapping. (Bendix, 1998)

1.6.1. Synthesis and Modification of PLGA

The two most commonly used methods to synthesize PLGAs are first the direct polycondensation reactions of lactic and glycolic acids resulting in low molecular weight copolymers. The second is ring open polymerization (ROP) of the cyclic dimers, lactide and glycolide (Figure 1.12) which allows for higher control of the resultant product, hence its wide application.(Gao *et al*., 2002, Zhou *et al*., 2004)

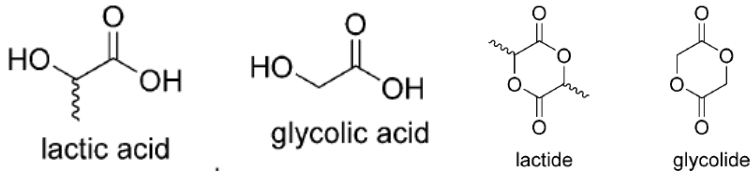

Figure 1.12: Structure of Lactic and glycolic acids and their cyclic dimers

Compared to the poly-condensation route, ROP is much more suited for control of the polymer chain ends (Dechy-Cabaret *et al*., 2004) and will be studied further in this work.

1.6.2. Ester Endcapped PLGA

Polymers with higher molecular weights are exclusively produced by the ring-opening polymerization of the cyclic monomers. Where a catalyst is always necessary to start the polymerization, a metal catalyst is predominantly used. (Erbetta *et al*., 2012, Bendix, 1998) For the production of polymers for medical applications, stannous (II) 2-ethylhexanoate, abbreviated as tin octoate (Figure 1.13), is the most widely used complex for the industrial preparation of PLGA. The scope of the current work will focus on the use of stannous (II) 2-ethylhexanoate in coordination-*insertion polymerization of PLGA.

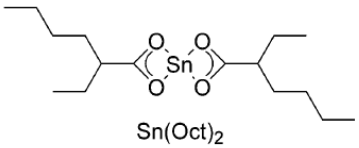

$Sn(Oct)_2$

Figure 1.13: Structure of tin (II) Octanoate [Sn(Oct)2].(Dechy-Cabaret *et al*., 2004)

$Sn(Oct)_2$, is commercially available, easy to handle, and soluble in common organic solvents and in melt monomers. It is highly active (typical reaction times in bulk at 140-180°C range from minutes to a few hours) and allows for

the preparation of high-molecular-weight polymers, it has proven to be very efficient and prevents racemization. (Dechy-Cabaret *et al*., 2004)

$Sn(Oct)_2$ provides a kinetically persistent living polymerization system. The polymerization is even faster and better controlled when $Sn(Oct)_2$ is combined with a proton-donating reagent such as an alcohol. In general trace impurities containing hydroxyl groups as the initiator (such as alcohol or water) coordinate with Sn to form the tin alkoxide. The tin alkoxide then coordinates with lactide/glycolide to push the polarization of the carbonyl group and reacts further with alcohol. In fact, it is the Sn–OH bond that initiates the ring-opening of the monomer to form the Sn–alkoxide group. The proposed reaction mechanisms and possible side reactions are shown in Figure 1.14-1.15 (Ouyang *et al*., 2011)

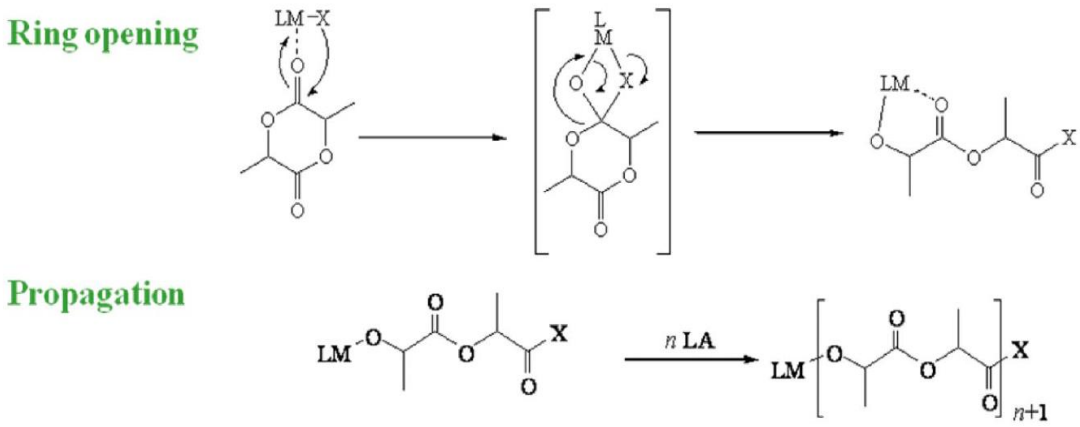

Figure 1.14: Reaction mechanism of PLGA prepared by coordination insertion ring-opening polymerization.(Chisholm, 2010)

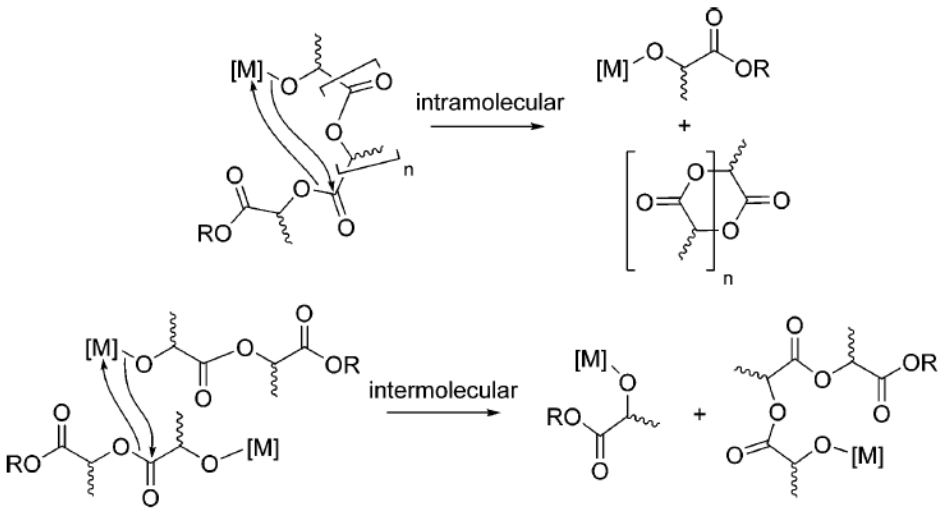

Figure 1.15: Schematic Representations for the Intramolecular and Intermolecular Transesterification Side Reactions.(Dechy-Cabaret *et al*., 2004)

As described above, the hydroxyl-contained compounds play a predominant role in ring-opening polymerization of PLGA. Any impurities present in the monomer (alcohols, lactic acid, water, etc.) may act as co-initiators, especially when $Sn(Oct)_2$ is used without proton-donating additives. The amount of the hydroxyl-contained compounds within a certain range affects the molecular weight of PLGA.(Korhonen *et al*., 2001, Bendix, 1998)

The proton-donating agents are involved in the reversible chain transfer within the growing chain, making it essential that the ROH to $Sn(Oct)_2$ ratio be carefully optimized. (Dechy-Cabaret *et al*., 2004) These compounds affect not only the molecular weight of the resulting polymers but can be used to manipulate the polymer's physical properties since they cap the polymers with ester end groups.(Ouyang *et al*., 2011)

1.6.3. Amide Endcapped PLGA

A rather interesting and promising synthetic pathway is the carbodiimide coupling chemistry. This very mild, fast, reaction done at room temperature at neutral pH has been routinely used as a starting point for surface modification of several polymers through immobilization of NH_2-containing biomolecules onto carboxyl-containing substrates via a covalent amide bond. This method has been previously used to increase (or decrease) the hydrophilicity of nylon surfaces (Tobiesen and Michielsen, 2002)

The method uses N-ethyl-N'-(3-(dimethyl amino propyl) carbodiimide (EDC) and N-hydroxysuccinimide (NHS) as the amidization accelerators (molecular structures of EDC and NHS are shown in Figure 1.16). The EDC/NHS activation approach possesses many merits such as: high conversion efficiency, mild reaction conditions, excellent biocompatibility and much cleaner products.(Wang *et al*., 2011) Using EDC/NHS activation, a series of alkyl amines will be coupled to the carboxylic end of PLGA through the reaction scheme depicted in Figure 1.17-1.19.

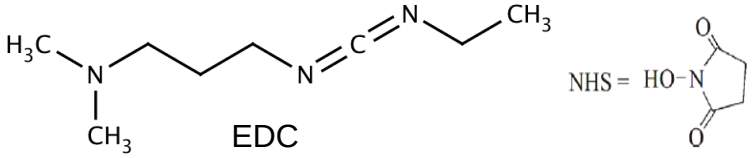

Figure 1.16: Molecular structure of EDC and NHS

The molecular activation mechanism of EDC/NHS is generally believed to be a two-step activation protocol. The first step is the addition of the OH group of the carboxylic acid across one of the double bonds of the carbodiimide reactant, forming an O-acyl urea adduct (Figure 1.17).

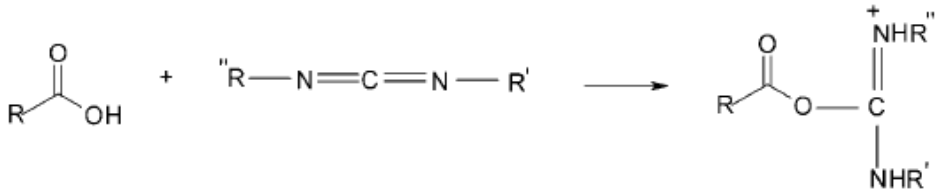

Figure 1.17: Activation of carboxylic acid end by EDC forming O-acyl adduct (Tobiesen and Michielsen, 2002)

The terminal O-acylurea can then be transformed according to three competitive paths:

(i) a nucleophilic attack by NHS which yields the succinimidyl ester product with the release of the urea corresponding to the initial carbodiimide reactant with a high yield under optimized reaction conditions (Figure 1.18).

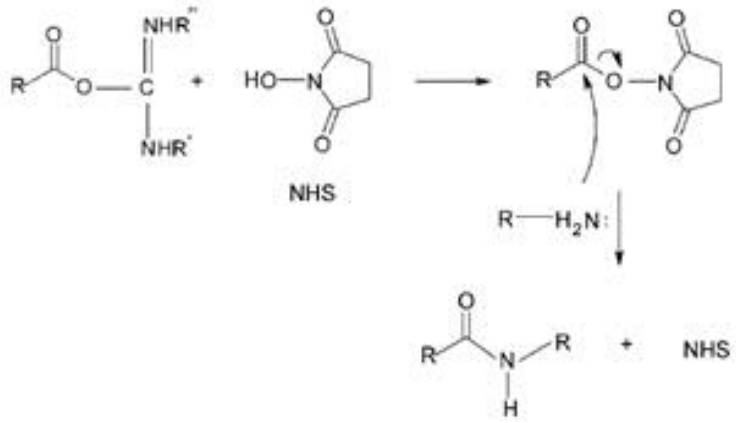

Figure 1.18: Amidization of a carboxylic acid with a primary amine via NHS activation of the acid (Tobiesen and Michielsen, 2002)

NHS is precisely used to improve the EDC-mediated coupling reaction by efficiently providing a more stable NHS-ester intermediate acting as a “rescuer” of the *O*-acyl isourea intermediate that is amine-reactive to form an amide bond, competing with the latter reactions.(Navarro *et al*., 2008)

(ii) a dehydration reaction with a neighbouring carboxyl group to yield an anhydride product, with a similar urea release (Figure 1.19). However, the anhydride formed by the competitive path is also a linking moiety and can react directly with the primary amines, resulting in equal quantities of two products, amide and carboxylic acid. It may further evolve to NHS-ester depending on its structural stability. Therefore, anhydride formation appears as a secondary pathway for succinimidyl ester formation, available at high acid concentration. (Wang *et al*., 2011)

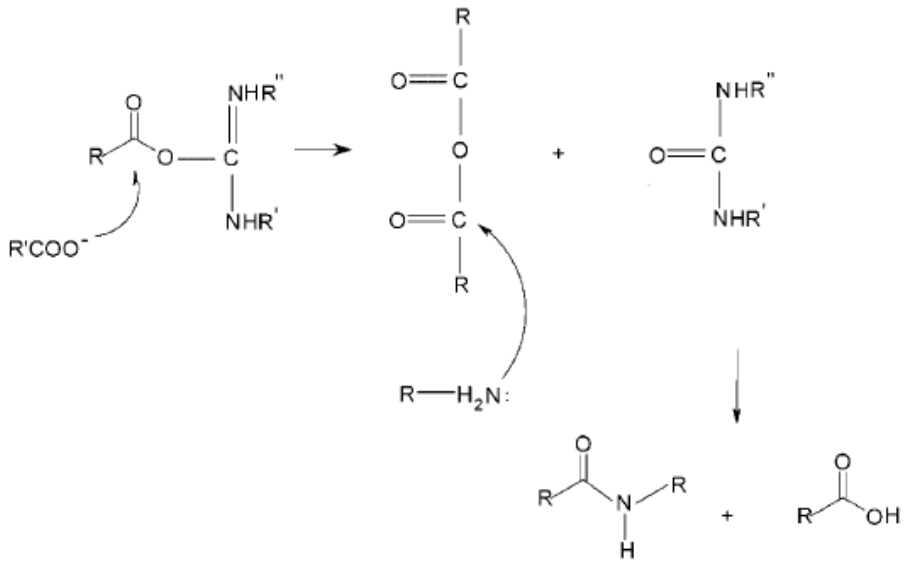

Figure 1.19: Amidization of carboxylic acid with an amine via the acid anhydride formed through the attack of the activated ester by another acid (Tobiesen and Michielsen, 2002).

NHS-ester, however, reacts with the primary amine to produce only a single product of amide. From the product viewpoints, obviously, the cross-linking efficiency of anhydride is only half that of NHS-ester. Therefore, NHS-ester is preferred in amidation even though anhydride can be easily obtained by using only EDC for dehydration of carboxylic acids (Wang *et al*., 2011). Kinetic studies have shown that the importance of this rearrangement can be reduced if the concentration of the nucleophile is sufficiently high (Tobiesen and Michielsen, 2002).

(iii) Finally a rearrangement via an intramolecular acyl transfer to yield an N-acyl urea may occur which is negligible at the well-accepted reaction conditions and only becomes serious under extreme conditions such as high temperatures and high concentrations. (Sam *et al*., 2010)

1.7. PLGA Characterization

Polymer synthesis and tailoring for particular applications require selection of appropriate characterization techniques to ensure reproducibility and effectiveness of the designed product. Biodegradable polymers have numerous physical and chemical characteristics which rely on defined properties such as molecular weight averages and distribution, glass transition and/or melting temperatures, monomer ratios, sequencing for copolymers and so forth (Figure 1.20) all of which could be used to manipulate the physical behaviour of pristine polymers. (Hausberger and DeLuca, 1995)

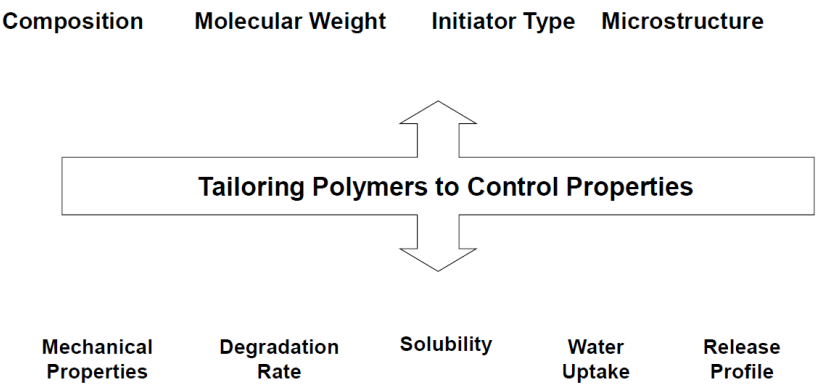

Figure 1.20: Tailoring of polymers mechanical properties to control polymer behaviour *in vitro/in vivo*

Moreover, when polymers are fabricated into controlled drug delivery systems, additional characterization is required such as surface area, bulk density, surface morphology, etc. since these properties may affect both degradation and drug release. Thus thorough analysis is necessary for a complete understanding and probable prediction of the system's behaviour.

Analytical techniques to characterize these different aspects of the polymers/polymer systems ranges from end-group analysis, gel permeation chromatography for molecular weight determination, thermogravimetric analysis and differential scanning calorimetry for thermal analysis, and scanning electron microscopy for morphological examination. Thus, working with polymer systems requires careful selection and validation of a collection of techniques that fully characterize and significantly discriminate polymer attributes. A spectrum of characterization techniques to comprehensively analyse and discriminate between different endcapped PLGA polymers will be conducted in this work.

1.7.1. Effect of endcapping on moisture uptake properties

Characterizing the physical stability of the polymeric delivery systems at increasing relative humidity is important in the assessment of their storage as well as *in vivo* lifetime and performance.(Sharp *et al*., 2001) Few data on the solubility of water and its diffusion coefficient in PLGA is available. Diffusion generally governs water movement through a polymeric matrix. Traditionally diffusion coefficient measurements could be obtained using saturated salt solutions to equilibrate samples to specified relative humidity values which require long data collection times and is cumbersome. New automated water sorption instruments, which can conveniently and precisely control both relative humidity and temperature, provide a faster, and more robust method.

A typical commercially available one is the automatic dynamic vapour sorption (DVS) instrument available from Surface Measurement Systems Ltd. offer many advantages compared to saturated salt solutions listed in Table 1.1.(Yu *et al*., 2008) Although DVS facilitates continuous data acquisition for diffusion coefficient calculations, there are relatively few reports utilizing these automated water sorption instruments for obtaining polymeric sorption.(Roman-Gutierrez *et al*., 2003) This could be due to the difficulty in the selection of the appropriate mathematical model which relies on the type and geometry of the sample, the DVS pan selected, and the diffusion mechanism (case I or case II diffusion) encountered.(Yu *et al*., 2008)

Table 1.1: Comparison between the saturated salt solution method and DVS

Feature	Saturated Salt Solution Method	DVS Instrument
Sample size	1 – 2 g	5 – 100 mg
Experimental time	Weeks to months	Days
Experimental design	Less flexible, discrete relative humidity values dependant on salt selection and experimental temperature	More flexible relative humidity control, can obtain absorption and desorption data on the same sample in a short time
Air flow	Static to slow movement with use of a fan or stir bar inside the chamber	Dynamic, air continuously flows past the sample
Data collection	Weight measurements disturb the environmental relative humidity; fewer discrete data points	Weight measurements do not disturb environmental relative humidity, nearly contious data points
Labour	More labour intensive (manual periodic weighing)	Less labour intensive (instrument weighs sample)
Cost	low	High

1.7.2. Effect of endcapping on thermal properties

Differential Scanning Calorimetry (DSC)

Differential scanning calorimetry (DSC) is used to investigate the thermal characteristics of polymers. It provides data on thermal critical points like melting point, enthalpy specific heat or glass transition temperature. A sample and an empty reference crucible are heated at same constant heat flow rate, the energy which is absorbed or evolved by the sample during endothermic or exothermic events, respectively, is electrically compensated for by an equivalent amount of energy to the sample, maintaining isothermal conditions between the sample and reference holders. (Hausberger and

DeLuca, 1995) Hence, critical points of the sample and can be detected. A schematic principle of the DSC is described in Figure 1.21

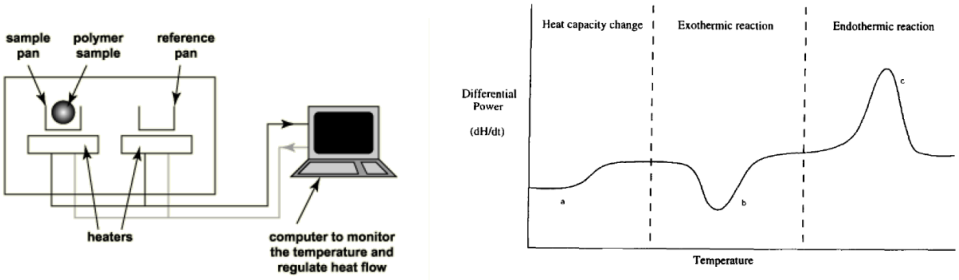

(i) (ii)

Figure 1.21: (i) Schematic principle of DSC measurements setup (ii) DSC Thermal Events: (a) a normal glass transition; (b) crystallization exotherm and (c) a melting endotherm

Figure 1.21(ii) shows a DSC thermogram in which the heat flow rate, dH/dt, is plotted vs temperature or time. An endothermic transition is represented by a positive peak and an exothermic transition by a negative peak. Thermochemical parameters such as heat capacity and heat of fusion can be determined, making this an excellent technique for thermal characterization of polymers. (Hausberger and DeLuca, 1995)

Thermogravimetric analysis (TGA)

Another essential technique adopted is thermogravimetric analysis (TGA), to measure the change in mass with the increase in temperature, thermal stability, and maximum degradation temperature for the polymers indicated by their mass loss curves. The schematic principle of the TGA measurement is shown in Figure 1.22. The sample is heated under nitrogen or synthetic air

with constant heat rate while the difference of the mass during this process is measured. A mass loss indicates that degradation of the substance takes place. The reaction with oxygen from the synthetic air, for example, could lead to an increase in mass.

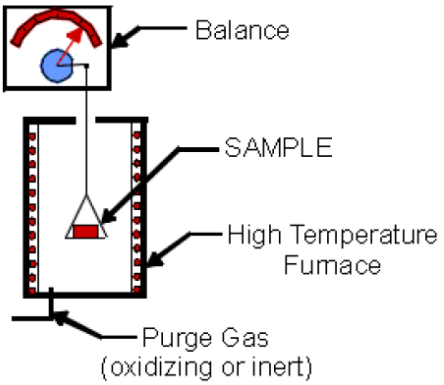

Figure 1.22: Schematic principle of TGA measurement

1.8. Procedures for making implants

Implants may be moulded, extruded, or prepared as films (Figure 1.23). When moulded, the polymers are heated and compressed into a closed container into the desired shape. Polymer films can be prepared by melt pressing or solution-casting. In solution-casting, the polymers with or without drugs are dissolved in a common solvent in desirable proportion to form a viscous solution that then is spread on a flat, non-adhesive surface, followed by evaporation of the solvent. Finally, the resulting film is peeled from the surface.(Yasukawa *et al*., 2004) However, solvent-casting methods are not ideal for industrial scale-up for many reasons. First, the process requires large amounts of organic. Such systems are also open to the risk of denaturation of drugs during encapsulation. Second, this process requires a

very long time to completely remove solvents from the film. Third, solvent-casting is not a continuous process, which may increase batch-to-batch variation in the composition of implants as well as cost of manufacturing.(Widmer *et al*., 1998)

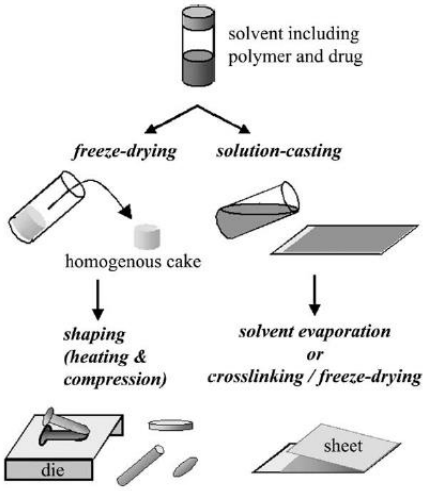

Figure 1.24: Procedures to prepare biodegradable implants with various shapes. (Yasukawa *et al*., 2004)

Unlike solvent-casting, extrusion is a continuous process of drawing polymer-drug mixture through a die to create implants of fixed cross-sectional profile without any use of solvent. The process requires an extruder and polymer-drug mixture with required micron size feed material. During the process, the polymer-drug mixture is heated to a semi-liquid state by a combination of heating elements and shear stress from the extrusion screw. The screw pushes the mixture through the die. The resulting extrudate is then cooled and solidified before cutting into desired lengths for implants or other applications.(Wang *et al*., 2010) Thus, both procedures include heating, drying, or both. Exposure of drug to high temperature can be disadvantageous as denaturation can take place. Therefore, method limitation will be based on drug and PLGA melting point, polymorph stability and chemical interactions.

1.9. Research objective

The aim and objectives of this thesis was to investigate the effects of endcapping on the physicochemical properties of PLGA and subsequent effect on the performance of PLGA based intraocular implants. In order to achieve this goal, a basic understanding of structure activity relationship of polymer endcaps was necessary and PLGA drug loaded implants had to be fabricated. With this in mind, the following studies have been performed to achieve the above objectives.

1. Synthesis of endcapped linear PLGA copolymers in Chapter 2 and examining a spectrum of characterization techniques to validate their capability in comprehensively analysing and discriminating between different endcapped PLGAs.
2. Definition of the the effect of endcapping on the polymer's moisture uptake properties and investigate the mechanism of water uptake in bulk polymer and polymer films in Chapter 3
3. Fabrication, tuning and characterization of PLGA based Brimonidine loaded intraocular implants intended for intracameral implantation as alternative delivery systems to treat ocular diseases in Chapter 4.
4. Investigation of the mechanism of drug release from PLGA implants and understanding of the capability of endcapping in fine tuning the drug release profile in Chapter 4

5. Finally, identification of the structure/property relationships of the endcapped polymers. This requires correlating the different physical and chemical properties of the polymers to their *in vitro* behaviour and to set a platform for synthesis of end function oriented, i.e. working with the end in mind. This was done using surface response methodology to implement a D-optimal design to understand the design space and key determinants in polymer performance in Chapter 5

CHAPTER 2: SYNTHESIS AND CHARACTERIZATION OF ENDCAPPED PLGA COPOLYMERS

2.1. Introduction and Objectives

Copolymers of PLGA have attracted considerable attention in the drug delivery area due to flexibility in establishing different periods of release through molecular architecture, generating an array of biodegradation patterns (Koopaei *et al*., 2012). In addition, there is a requirement to accommodate both hydrophilic and hydrophobic drugs to service the requirements of the potential applications (Karikari, 2006). Both physical and chemical modification techniques have been routinely utilised to generate polymer compositions with the appropriate properties (Park and Kang, 2013). Examples of approaches include varying the molecular weight of the polymer or the monomer ratio, blending with other polymers, and grafting.

Although attractive, these methods not only modify surface properties of PLGA but also promote radical changes in the bulk properties, such as crystallinity (Kobori *et al*., 2004). During the last decade academic chemists have placed particular emphasis on the control of polymer microstructure. (Chisholm, 2010) A rather less investigated route commonly referred to as “endcapping” has been reported to substantially impart several changes in polymer properties according to the selected functional group while limiting the changes to the bulk properties (Huang *et al*., 2013).

For instance, the presence of free carboxyl-end groups affects the polymer's hydrophilicity, the consequences of which include sorption dependent properties such as drug release, burst effect, and polymer degradation (Walter *et al*., 2001). Therefore delivery systems made of PLGA of the same molecular weight and monomer ratio but different end caps will elicit different drug release and degradation profiles. The nature and length of the end cap can be explored to fine tune these properties (de Jong *et al*., 2001, Wu and Wang, 2001) .

There is much data in the literature on the optimization of PLGA properties via monomer ratio and molecular weight. However basic information on the effect of end-capping on the compositional and morphological structure of this family of polymers is still lacking in the open literature. The main objective of this chapter was to explore and optimize conditions suitable for end-capping of one of the most widely used biomaterials, PLGA. The properties of the generated polymers were analysed by a variety of characterization tools, to lay the foundation for structure–property relationships.

2.2. Materials and Methods

2.2.1. Materials

For preliminary screening a range of amorphous, commercially available PLGA copolymers with monomer ratio of 50:50 were procured, purified and characterized. Polymers were purchased from three providers. Resomer RG502H, RG502, RG503H and RG503 (Sigma Aldrich, Dorset, UK), PDLGA 5002 and PDLGA 5002A (Purac, Gorinchem Netherlands), AP40, AP41, AP55, AP63 and AP98 (PolySciTech, West Lafayette, USA). For endcapping; all chemicals were bought from Sigma-Aldrich (Dorset, UK). Ethylamine, Butylamine, Dodecylamine, Benzylamine, Aniline, N-Ethyl-N'-(3-(dimethylamino)-propyl) carbodiimide hydrochloride (EDC), and N-hydroxysuccinimide (NHS), were used in NHS/EDC coupling. For ring open polymerization; glycolide, and D,L-lactide were used as monomers. Tin(II)-ethylhexanoate $Sn(Oct)_2$ as initiator, lauryl alcohol, and ethyl alcohol as co-initiators, and anhydrous toluene (99.8%) was used as a solvent. D,L-lactide was recrystallized and Tin(II)-ethylhexanoate was distilled prior to use. All the monomers, initiators, and catalysts were stored under dry nitrogen in a glove box. Toluene was stirred over calcium hydride and distilled. Anhydrous methylene chloride, anhydrous methanol, anhydrous chloroform, diethyl ether, and heptane were used without further purification. For gel permeation chromatography, polystyrene standards from 500 to 2000,000 Da were used for calibration, THF was used as a solvent.

2.2.1.1. PLGA Purification

Chloroform and methanol were used as solvent and non-solvent, respectively in purification and precipitation. The commercial PLGA samples (5 g) were dissolved in 5 ml anhydrous chloroform and precipitated in excess anhydrous methanol (100 ml) with continuous stirring. The product was re-dissolved and re-precipitated three times. The isolated PLGA was freeze dried at -70°C to remove solvent traces for 48h then stored in a freezer (-25^{o}C) until further characterization.

2.2.2. PLGA Functionalisation

A range of amide and ester end–capped PLGAs were synthesized by either EDC/NHS coupling or ring-opening living polymerization respectively. The target Molecular weight (Mn) of 10,000-20,000 g/mol and 50:50 monomer ratio was chosen due to the amorphous structure of PLGA produced and favourable degradation time in drug release systems. (Du, 2012, Silva *et al*., 2015, Erbetta *et al*., 2012)

2.2.2.1. EDC/NHS Coupling

In this study, a series of alkyl amines shown in Figure 2.1 were coupled to the carboxylic end of PLGA using 1-ethyl-3-(3-dimethylaminopropyl)

carbodiimide hydrochloride (EDC) and *N*-hydroxysuccinimide (NHS) as the amidization accelerators.

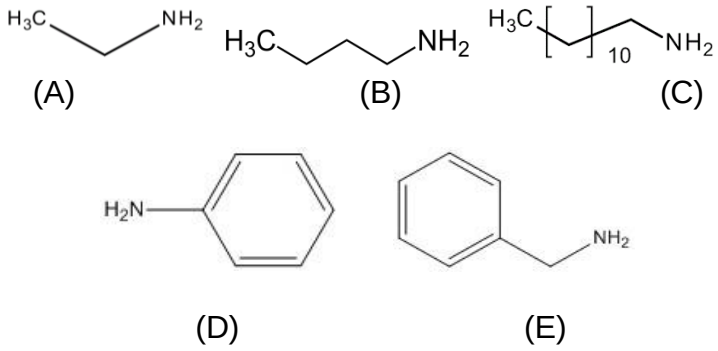

Figure 2.1: Molecular structure of primary amines used in the EDC/NHS coupling of PLGA: (A) Ethylamine, (B) Butylamine, (C) Dodecylamine, (D) Aniline, (E) Benzylamine.

Synthetic procedure

Synthesis of endcapped PLGA with a series of amines was commenced by the conjugation of a Ligand-NH_2 to the carboxylic group of PLGA. Figure 2.2 presents a schematic of the complete reaction thought to come into play for the activation of an acid-terminated polymer. Excess NHS (135 mg, 1.1 mmol) in the presence of EDC (230 mg, 1.2 mmol) was added to a stirred solution of PLGA-COOH (5 g, 0.14 mmol) in anhydrous methylene chloride (10 mL). The mixture was stirred for 2 hours at 22°C. PLGA-NHS was precipitated in excess ice-cold mixture of diethyl ether and methanol (50:50) to remove the residual NHS. After drying under vacuum, PLGA-NHS (1 g, 0.059 mmol) was dissolved in anhydrous chloroform (4 mL) followed by addition of NH_2-Ligand (1:1 ratio) and gently stirred overnight. The

endcapped copolymer was precipitated in excess ice-cold mixture of diethyl ether and methanol (50:50) and washed with the same solvent to remove excess reactants or hydrolysed esters. The resulting endcapped PLGA was dried in a vacuum oven at 40^{o}C after which it was stored at -25^{o}C till it was fully characterized as further described in Section 2.2.3.

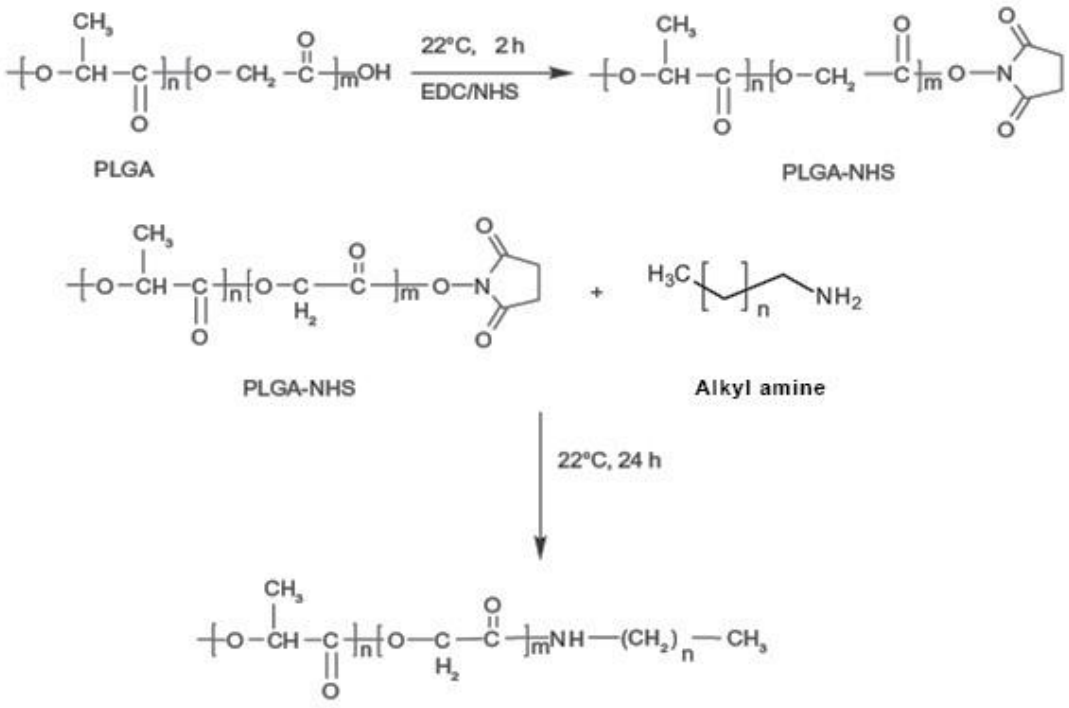

Figure 2.2: The proposed mechanism for EDC/NHS amidization

2.2.2.2. Ring Open Polymerization (ROP)

Ester endcapped PLGAs were synthesized by opening the cyclic dimer rings of the monomers D,L-lactide and glycolide. A monomer ratio of 50:50 (D,L-lactide : glycolide) was selected. The ratio of the stannous octoate initiator $Sn(Oct)_2$ and co-initiators was used to control molecular weight. Figure 2.3 shows a schematic of the synthesis.

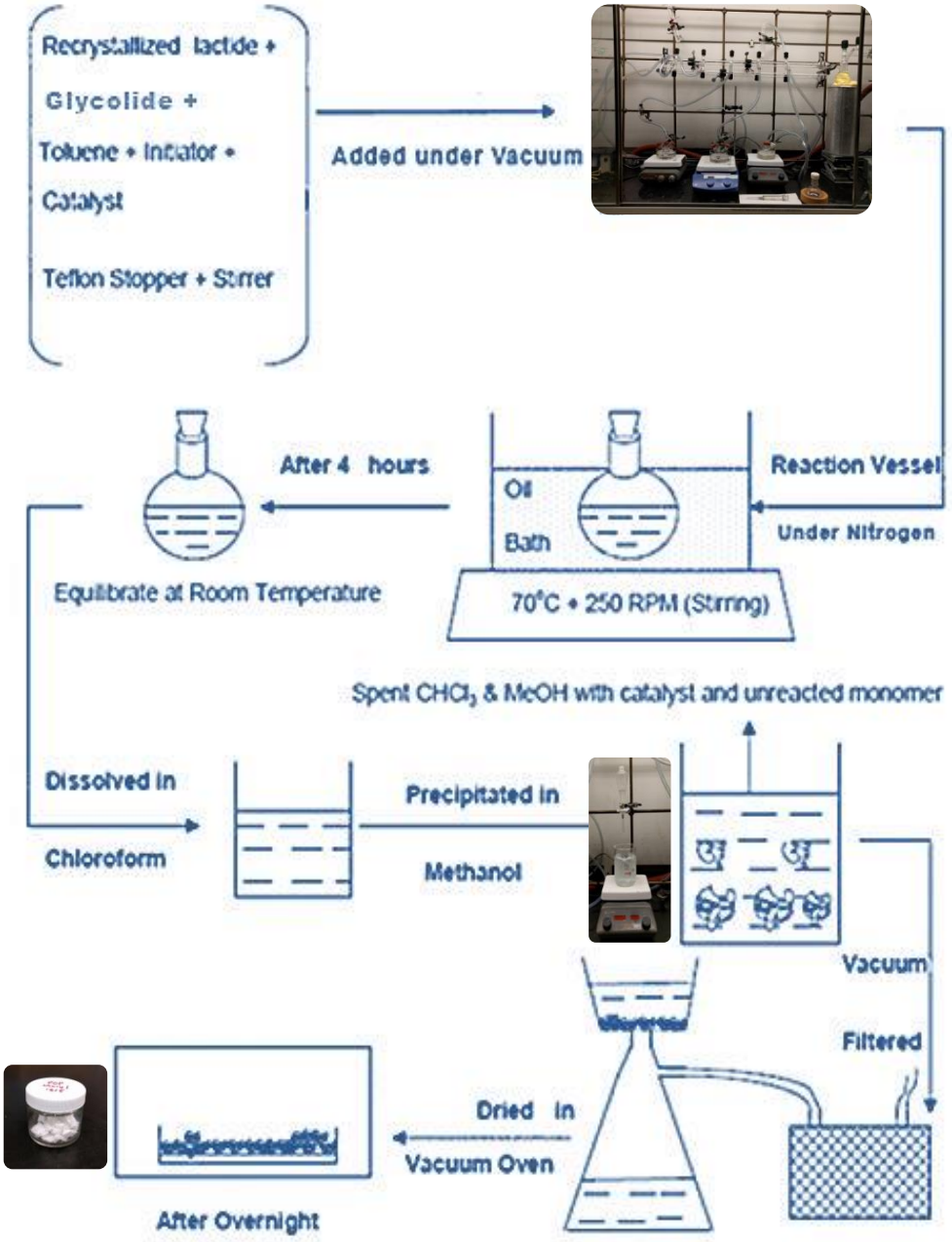

Figure 2.3: Schematic of synthesis of end-capped PLGA (Adapted from Singh *et al*., 2011b)

Purification of D,L-lactide

D,L-lactide (3,6-Dimethyl-1,4-dioxane-2,5-dione) was recrystallized twice from anhydrous ethyl acetate and dried under reduced pressure at 40^{o}C prior to use. Ethyl acetate (450-500 ml) was taken in a round bottom flask and heated to boiling by raising the temperature of the oil bath to 77^{o}C (boiling point of ethyl acetate). D,L-lactide (100 g) was taken in a 500ml beaker with a magnetic stirrer. When ethyl acetate began to reflux, it was pipetted slowly to the monomer beaker with a stirrer on a hot plate (for 5 min at70^{o}C). D,L-lactide was dissolved in the minimal amount of solvent and allowed to cool at ambient temperature. The equilibrated monomer solution was placed in the refrigerator for an hour. Subsequently, it was taken out and the resulting crystals in the beaker were scrapped with a spatula into a filter funnel, vacuum filtered and recrystallization repeated. The monomer crystals were dried overnight under the vacuum and stored in a glove box.

Synthetic procedure

Equimolar amounts of monomers were added to a flame-dried 50-mL round-bottomed flask containing a magnetic stir bar (250 rpm) and sealed under vacuum with a rubber septum to prevent moisture. The system was purged with nitrogen and reaction flask was immersed in an oil bath at 70^{o}C controlled using a temperature-regulator (IKA Labortechnik, Germany). PLGAs were initiated with either ethyl or dodecyl alcohol to induce different

end-capped polymers (Figure 2.4). The co-initiator was added via syringe under nitrogen, followed by a catalytic amount of $Sn(Oct)_2$ in toluene, and the reaction mixture was allowed to stir. The mole ratio of catalyst and initiator used was 1:1 for this polymerization as they form a living macro-initiator.(Singh *et al*., 2011b)

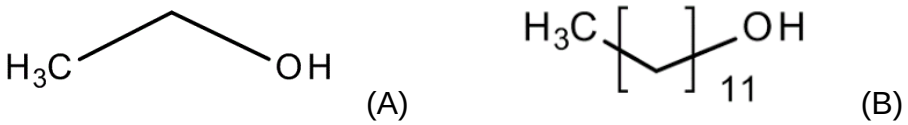

Figure 2.4: Molecular structure of alcohols used as co-initiators (A) ethyl alcohol and (B) dodecyl alcohol

Glycolide melted during the first minutes of the reaction and occupied the lower part of the flask, while D,L-lactide, was suspended in the molten glycolide until it completely melted. According to Gilding and Reed the copolymerization rates of both monomers are quite different, glycolide is more reactive than D,L-lactide. This leads to copolymers with block sequences along the polymer chain which necessitated efficient stirring to avoid preferential glycolide polymerization.(Gilding and Reed, 1979)

During the initial synthesis trials vapour formed and partially crystallised on the wall of the reaction flask. Erbetta and colleagues reported similar observation and their analyses of the crystals concluded that these were D,L-lactide produced by the evaporation and crystallization of the monomer (Erbetta *et al*., 2012). Application of a vacuum was necessary to avoid the

presence of moisture and oxygen which are detrimental to the reaction.(Bendix, 1998)

The formation of vapour became more pronounced upon suction with a vacuum pump. In order to optimize the copolymerization conditions vacuum was initially applied, without injection of nitrogen. Once D,L-lactide melted, the vacuum was terminated and replaced with a Nitrogen flow. Efficient vacuum control, absence of humidity in the reactants, and adequate stirring, were key to successful synthesis.

After four hours, the viscous solution was dissolved in anhydrous chloroform then precipitated in cold anhydrous methanol. Cold methanol was used to terminate the polymerization, with a hydroxyl group (-OH). Ideally, the hydroxyl-contained compounds should be removed under mild conditions after the polymerization reaction without affecting the molecular weight of the PLGA. The purification of the copolymers was carried out by dissolution/precipitation processes. The resultant white spongy precipitate was vacuum-filtered and dried in vacuum oven at 40˚C, for 48h to remove residual solvents then placed in sealed flasks in a freezer at -25˚C.

2.2.2.3. Sample Labelling

Both commercially bought and synthesized polymers were labelled according to their endcap: Ethyl [E], Butyl [Bu], Dodecyl [Dd], Cholesterol [C], Benzyl

[Bn], and Phenyl [Φ], while hydroxyl [OH] was designated for the free non-endcapped polymers. The amide series was shorthanded as the A series whilst the ester series as E. The approximate molecular weight was given in thousands. For example, a 10,000 g/mol molecular weight PLGA sample endcapped with a Dodecyl amide endcap would be denoted as PLGA-10K-[Dd]-A whereas a polymer with approximately the similar molecular weight but a dodecyl ester endcap would be PLGA-10K-[Dd]-E.

Figure 2.5(a) illustrates the chemical structure of a standard PLGA terminated with one hydroxyl and one carboxylic end-group referred to as non-endcapped. Figure 2.5 (b) and (c) show one ester or amide end-capped PLGA with a hydrophilic hydroxyl group on the other end respectively

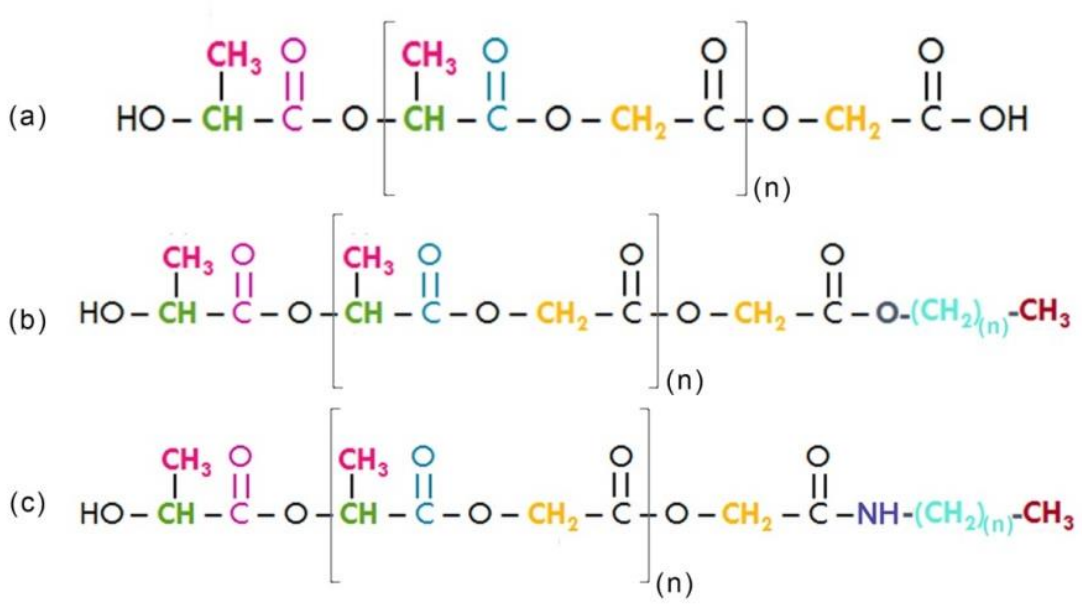

Figure 2.5: Molecular structures of PLGA copolymers; (a) non-endcapped free carboxylic acid, (b) ester endcapped, (c) amide endcapped.

2.2.3. PLGA Characterization

Analytical Balance (Mettler Toledo, Leiceser, UK), Modulated Differential Scanning Calorimetry (DSC 822^e, Mettler Toledo, Leicester, UK), Thermal Gravimetric Analyzer (TGA 822^e, Mettler Toledo, Leicester, UK), Fourier Transform Infrared (ThermoScientific Nicolet iS10 spectrophotometer Starna, UK), Nuclear Magnetic Resonance Spectrometer (JEOL JNM-LA 400 spectrophotometer (400MHz), and Bruker AVANCE-III (600MHz), Gel Permeation Chromatography (Waters® 515 GPC), X-Ray Powder Diffractometer, (Bruker D8 Advance II diffractometer, GmbH, Germany)

2.2.3.1. Gel Permeation Chromatography (GPC)

GPC was utilized to find out the average molecular weight (M_n, M_w) and Polydispersity index PDI (M_w/M_n). A Waters® GPC was used with 30 cm-long, 7.5 mm-diameter, 5 µm styrene-divinyl benzene columns. The columns were conditioned and run at 25 ºC using THF as the elution solvent at a flow rate of 0.4 ml/minute. A two-channel UV detector and a refractive index 2410 detector were used to analyse data based on polystyrene standards. GPC was carried out at a flow rate of 0.4 ml/min at 25ºC and eluted with THF. Sample concentration was 2 mg/ml. A calibration line was developed using a series of polystyrene standard having molecular weight range from 890 to 769000. The molecular weight and molecular weight distributions were obtained using Empower 2 software.

2.2.3.2. X-Ray Powder Diffractometer (XRPD)

X-ray diffraction was used to investigate the influence of end-capping on the crystallinity of the copolymers. The PLGA samples were compressed into the sample holder to provide a smooth surface. Scans were run at room temperature in symmetrical reflection mode with Cu radiation source (λ=1.54 Å) operated at 40 kV and 50 mA. Each experiment was conducted in triplicate. All diffraction patterns were normalized to the peak of highest intensity. Calibration scans were performed during a sample scan.

2.2.3.3. Fourier Transform Infrared (FT-IR)

Transmittance spectra were recorded from 400 to 4000 cm^{-1} for both monomers and copolymers samples using a ThermoScientific Nicolet iS10 spectrophotometer. Spectra were collected at a resolution of 4 cm^{-1} over 64 scans. The samples were mounted onto a de-mountable (open-end) optical glass cell with a path-length of 1 mm.

2.2.3.4. Nuclear Magnetic Resonance (NMR)

The polymer/end group composition, number average molecular weight (M_n), and percent functionalization were determined using NMR spectroscopy. NMR experiments such as ^{1}H, ^{13}C-DEPT-q-135, ^{1}H-^{1}H correlation spectroscopy (COSY), ^{1}H-^{13}C heteronuclear single quantum coherence (HSQC), and ^{1}H-^{13}C heteronuclear multiple-bond correlation (HMBC) spectra were acquired at ambient temperature. NMR samples were prepared by

dissolving the 10 w/v% co-polymers in $CDCl_3$ containing (0.03% v/v) tetramethyl silane (TMS) as an internal standard at 0.05% or DMSO in using glass NMR tubes with 5 mm outer diameter. Pulse sequence was as follows: relaxation delay (3 seconds), pulse (54.6 degree), acquisition time (1.8 second), spectral width (4,000 Hz), and total acquisition time (3.74 seconds). All NMR data were plotted with tetramethylsilane standard as 0.0 ppm. Chemical shifts in ppm were referenced relatively to chloroform at 7.26 ppm in ^{1}H-NMR and 77.23 ppm in ^{13}C-NMR spectra. Chemical shifts and coupling constants are reported in parts per million (ppm) and hertz (Hz) respectively.

2.2.3.5. Modulated Differential scanning calorimetry (MDSC)

Glass-transition temperatures were determined by modulated differential scanning calorimetry (DSC 822^{e}, Mettler Toledo, Leicester, UK). Approximately 5 mg of sample were crimped in aluminium pans (40 µl). The lid was pierced before the measurement. An empty pin-holed aluminium pan was used as a reference under a nitrogen purge. Both the reference pan and the sample pan were allowed to equilibrate isothermally for 10 min at -20^{o}C. The pans were a ramped between -20 ºC and 120 ºC at 5 ºC/min, with modulation amplitude of +/- 0.16 ºC and a period of 60 s, quench cooled to -20^{o}C (to eliminate any sample thermal history), finally heated again to 200^{o}C at 1^{o}C /min with modulation amplitude of +/- 0.16 ºC/min and a period of 60 s. The second run DSC curve was used for determining the glass transition temperature (T_g), and TA universal analysis software was used for data analysis.

2.2.3.6. Thermogravimetric Analysis (TGA)

Samples were heated from room temperature (±20^{o}C) to 500^{o}C for the copolymers and 400^{o}C for the monomers in an unsealed aluminium sample vessel, at a rate of 10^{o}C/min under a nitrogen purge (TGA 822^{e}, Mettler Toledo, Leicester, UK). The mass of the analysed samples varied between 10 and 20 mg. All TGA results were the average of a minimum of three measurements. The technique allowed us to determine the temperature at which thermal degradation commenced (T_{onset}) and the change in mass as a function of temperature increase. Derived thermogravimetric curves (DrTG) were used to identify the maximum degradation temperature (T_{degmax}).

2.3. Results and Discussion

Each of the discussed synthesis routes offered potential for PLGA endcapping but perhaps the more challenging aspect of the polymer modification was the characterization to ensure successful endcapping.

2.3.1. Molecular Weight Analysis (GPC)

The selection of PLGA with desired composition and molecular weight is critical in formulation of drug delivery systems. Composition is controlled by monitoring the feed ratio of the monomers. However, the control of molecular weight requires extra effort. Several means have been discussed in the literature which include but are not limited to the control of polymerization temperature/time, catalyst concentration, degree of vacuum, as well as addition of molecular weight controller. (Nuo *et al*., 2000)

Molecular weights and molecular weight distribution were determined by GPC. Figure 2.6 depicts a representative GPC curve showing a mono-modal peak with a polydispersity of 2.23 for the 15,000 $g.mol^{-1}$ PLGA-15k-[OH]. Table 2.1 lists the number and weight average molecular weights recorded for the commercial and synthesized polymers. The molecular weights of the synthesized PLGAs agreed with the targeted molecular weight predicted from the monomer-to-alkoxide ratio. However, the molecular-weight distributions were relatively broad (PDI from 1.36 to 2.27). This might be indicative of the occurrence of transesterification reactions whose precise nature

(intramolecular backbiting and/or intermolecular chain transfer) remains to be determined (Dechy-Cabaret *et al*., 2004).

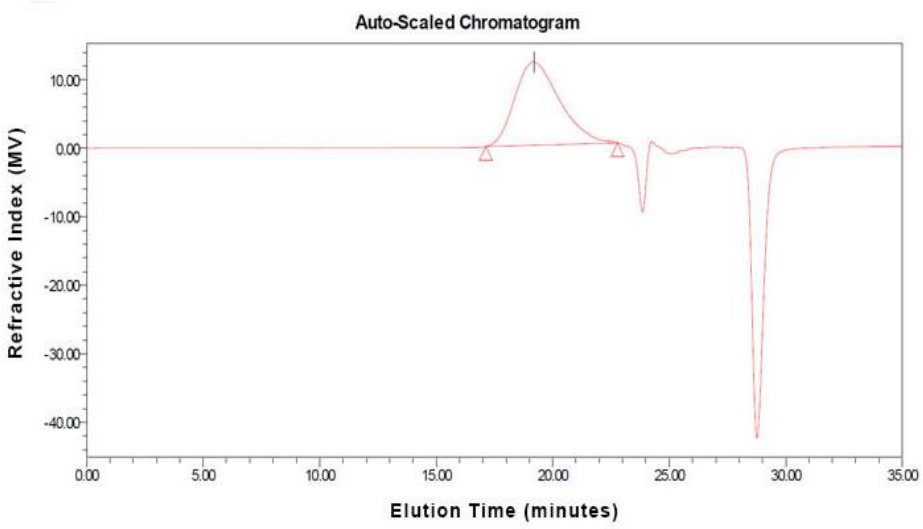

Figure 2.6: Size Exclusion Chromatogram of PLGA-15K-[OH].

Table 2.1: Molecular weights of Standard and Endcapped PLGA samples

Sample Label	M_n[a] ($g.mol^{-1}$)	M_w[a] ($g.mol^{-1}$)	PDI (M_w/M_n)
PLGA-5K-[OH]©	4335	8910	2.05
PLGA-7K-[OH]©	7201	11923	1.65
PLGA-10K-[OH]©	9980	16018	1.60
PLGA-15K-[OH]©	13790	31393	2.27
PLGA-20K-[OH]©	19771	33926	1.71
PLGA-25K-[OH]©	24507	41866	1.70
PLGA-30K-[OH]©	N/A	N/A	N/A
PLGA-35K-[OH]©	35821	60196	1.68
PLGA-15K-[E]-E	12127	21510	1.77
PLGA-15K-[Dd]-E	12127	21510	1.73
PLGA-15K-[C]-E©	11217	19430	1.36
PLGA-15K-[E]-A	17849	24288	1.99
PLGA-15K-[Bu]-A	11376	19558	1.74
PLGA-15K-[Dd]-A	12667	22056	1.70
PLGA-15K-[Bn]-A	11168	19886	1.781
PLGA-15K-[Φ]-A	12703	25297	1.67

[a]Determined via GPC
©Commercial Samples obtained from Sigma Aldrich, Purac and Corbion

2.3.2. Morphology of copolymers by XRPD

The degree of crystallinity of the commercially procured non-endcapped PLGAs was conducted using a high resolution X-ray diffractometer as shown in Figure 2.7. The main peak of XRD spectra observed from 7 (2-theta) to 25 (2-theta) was assigned to the amorphous hydrocarbon backbone as previously reported for non-endcapped PLGA. (Erbetta *et al*., 2012, Park and Kang, 2013)

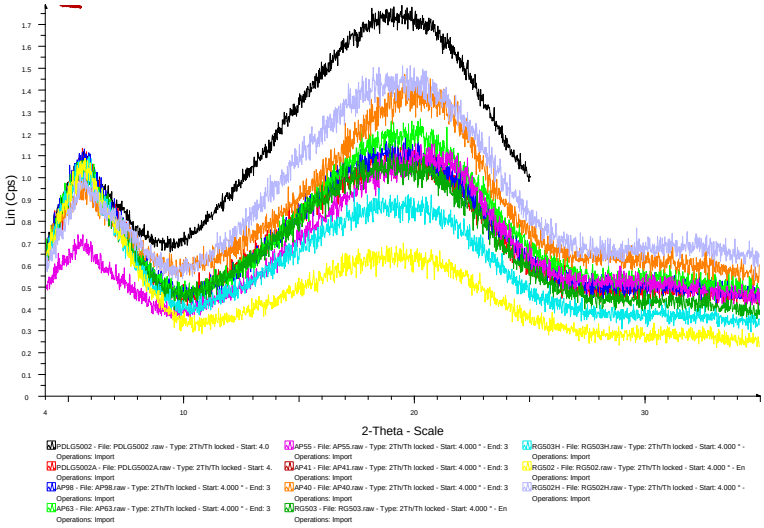

Figure 2.7: XRPD curves of non-endcapped commercially procured PLGAs

According to Gliding and Reed's phase diagram, Figure 2.8, while PGA is highly crystalline, the crystallinity rapidly disappears in copolymers of lactide and glycolide. The selected monomer ratio (50:50) lies in the amorphous range for PLGA. (Gilding and Reed, 1979) This is ideal for applications where it is necessary to have a monophasic matrix with a homogeneous dispersion of the active species such as in drug delivery (Athanasiou *et al*., 1996). The use of the racemic D,L- Lactide contributed to the amorphous nature of the polymers due to the irregularities in the polymer chain (Merkli *et al*., 1998).

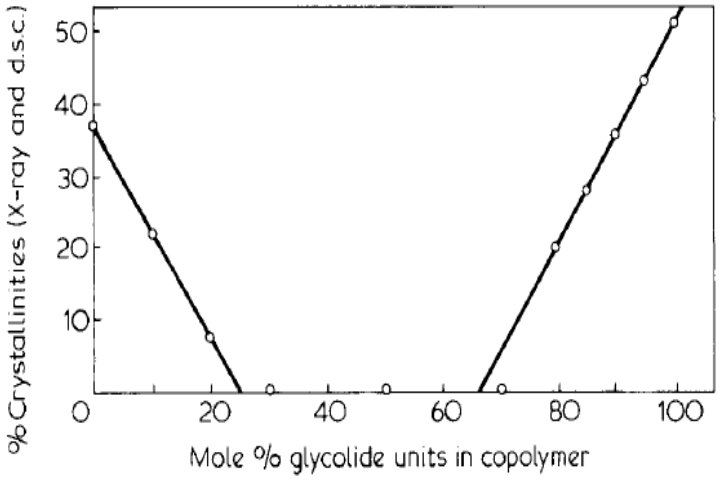

Figure 2.8: % Crystallinity for PLGA copolymers as a function of composition determined by XRPD (Gilding and Reed, 1979)

Endcapping with either ester or amide endcaps did not affect the crystallinity of the polymer. Figure 2.9 shows a representative sample of the synthesized endcapped polymers where overlapping XRD scans indicate the PLGAs were amorphous regardless of the endcap.

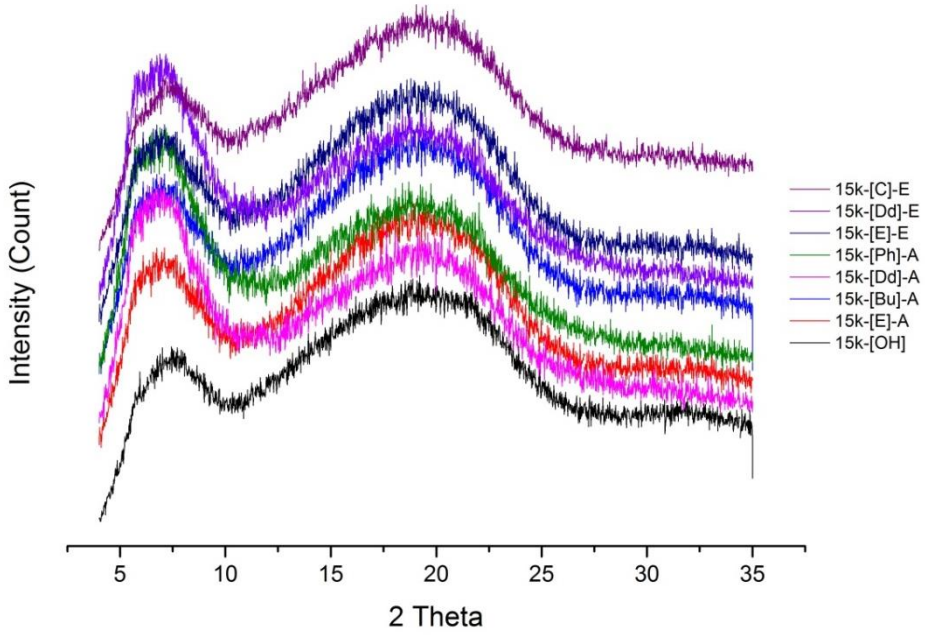

Figure 2.9: X-ray diffraction patterns of endcapped PLGAs showing superimposable hallos suggesting amorphous structure.

2.3.3. Structural Characterization

2.3.3.1. Fourier Transform Infrared (FT-IR)

(i) Characterisation of Monomers

Table 2.2 summarizes the absorption bands observed in the FTIR spectra for D,L-lactide and glycolide monomer's spectra with their respective functional groups.(Erbetta *et al*., 2012) In both spectra generated by Omnic Software, strong bands appear in the region between 1760 and 1750 cm^{-1}, due to stretch of the carbonyl groups present in the two monomers as seen in Figure 2.10 and 2.11. There are also stretching bands due to asymmetric and symmetric C-C(=O)-O vibrations between 1300 and 1150 cm^{-1}. The bands in these regions are useful in the characterization of esters.(Feng *et al*., 2015)

Table 2.2: Assignment of absorption peaks observed in the FTIR spectra of D,L-Lactide and Glycolide

Absorption Bands (cm^{-1})	Functional Group
3000 - 2700	CH, CH_2, CH_3 (stretching)
1900 – 1550	C=O (stretching)
1500 – 1250	CH_3 and CH_2 (deformation)
1350 – 1150	CH_2 and CH (wagging)
1300 - 1150	C =O (ester Stretching)

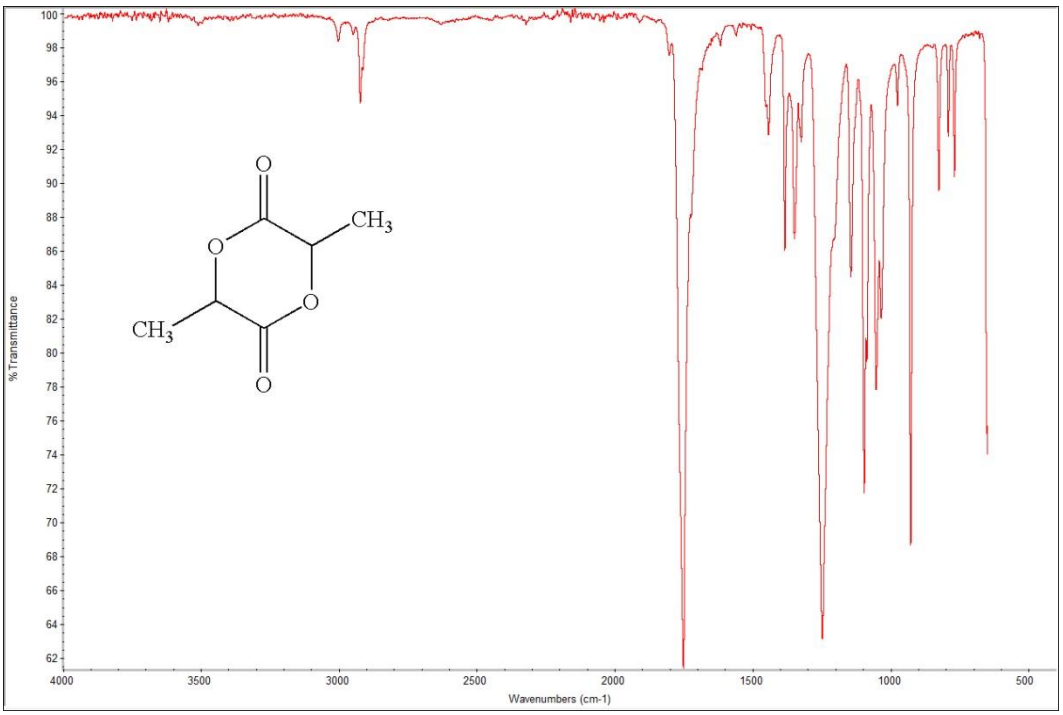

Figure 2.10: FT-IR spectrum of D/L-Lactide monomer

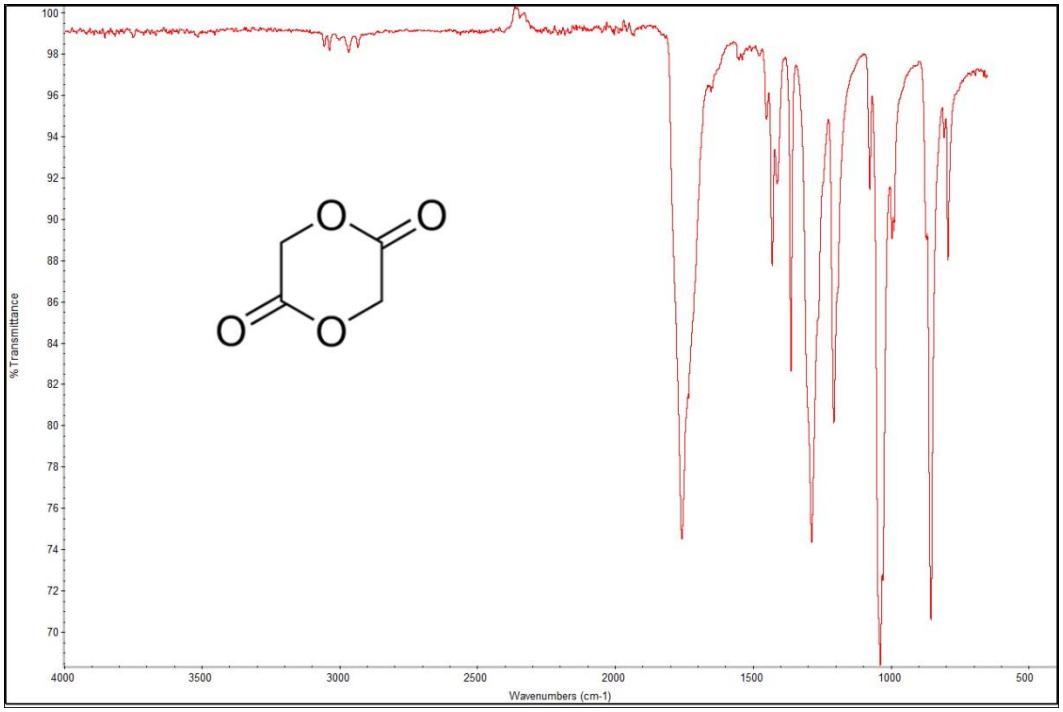

Figure 2.11: FT-IR spectrum of Glycolide monomer

(ii) Characterisation of PLGA Samples

The FTIR spectra of non-endcapped PLGA PLGA-15K-[OH] in comparison to its dodecyl ester end-capped counterpart PLGA-15K-[Dd]-E are presented in Figure 2.12. Both spectra exhibit prominent carbonyl C=O, C-C-O and C-O-C stretching bonding at 1747 cm^{-1} peak 1300, 1090 cm^{-1}, and 1130, 1083 cm^{-1} peak respectively demonstrating the presence of the ester group. (Hanafy *et al*., 2009)

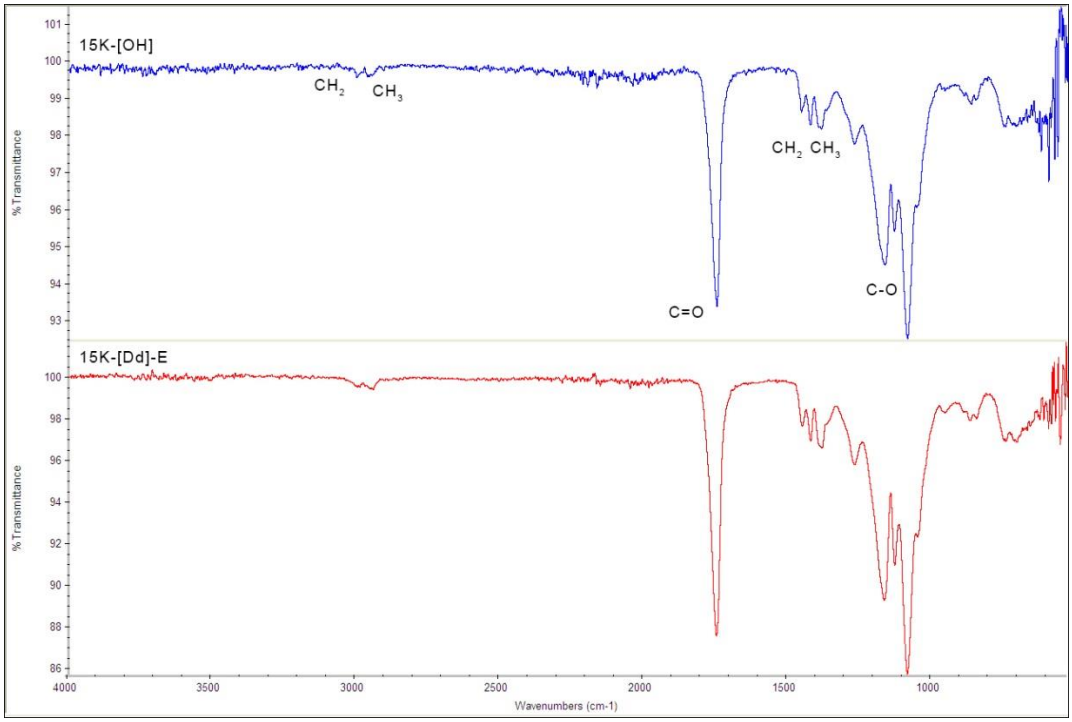

Figure 2.12: FTIR spectra of PLGA-15K-[OH] versus PLGA-15K-[Dd]-E

Peaks at 1452, 1360 and 750 cm^{-1} were due to C-H bending in methyl groups, 1047 cm^{-1} peaks were assigned to the C-CH_3 stretching vibrations. Bands around 3,000 cm^{-1} present due to the alkyl groups were consistent with the expected structure of the copolymer along with very weak bands in the region of 2860-2960 cm^{-1} assigned to C-H stretch of CH_2 and CH_3.

The assigned peaks were in agreement with previous PLGA characterization studies.(Park and Kang, 2013, Somayeh Ali mohammadi *et al*., 2012) However it was concluded that FT-IR could not be used effectively to identify the ester endcapping possibly due to the dilution in the ester backbone

On the other hand, the FTIR spectra in Figure 2.13 illustrate the transformation of carboxyl-terminated PLGA into the amide coupled endcap upon reaction with EDC/NHS. Taking dodecylamide endcap as a model ligand and comparing it with the spectra of the non-endcapped PLGA starting material two observations can be drawn.

The carbonyl stretching band (***v***C=O) broadened after activation, with a shift to 1747 cm^{-1} possibly due to the appearance of side products of anhydride and N-acylurea (Wang *et al*., 2011). This was concomitant with the appearance of two small and broad additional bands, which cannot be ascribed to the succinimidyl ester termination or to acid groups, located at 1645 and 1550 cm^{-1}. They are indicative of completion of the amidation reaction amide bond formation (C=O stretch at 1645 cm^{-1} (amide I) and CNH mode at 1550 cm^{-1}(amide II)) (Moraillon *et al*., 2008). Table 2.3 summarizes the absorption bands with their respective functional groups.

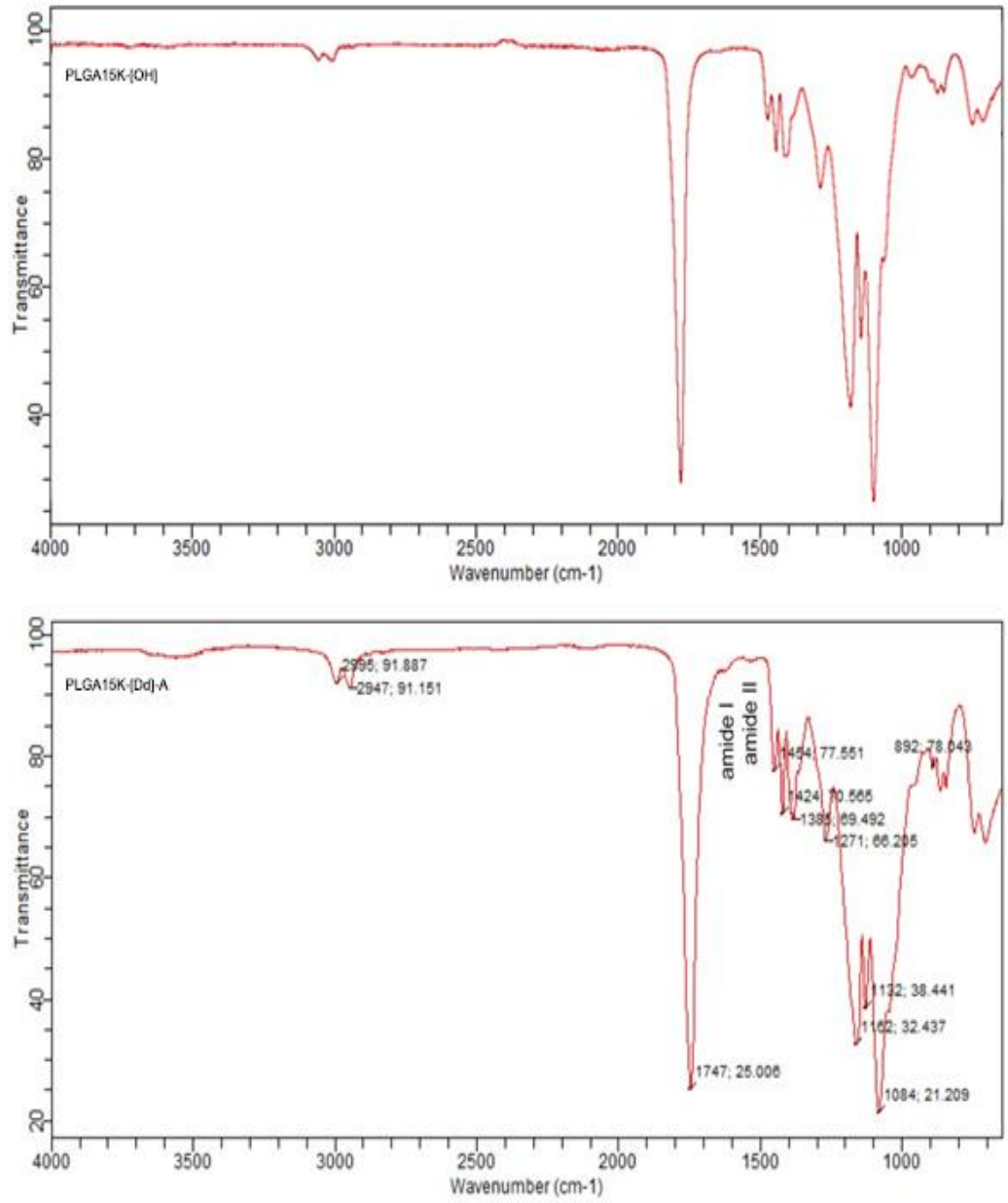

Figure 2.13: FTIR spectra of non-endcapped PLGA-15K-[OH] and its dodecyl amide capped counterpart PLGA-15K-[Dd]-A

Table 2.3: Absorption peaks assignment in the region from 1000 to 3000 cm^{-1}

Absorption Bands (cm^{-1})	Saturated Chain Related Bands	
2925	ν_{as} (CH_2)	Methylene anti-asymmetric stretch
2855	ν_s (CH_2)	Methylene symmetric stretch
1465	δ (CH_2)	Methylene scissor deformation
	Functional Group Related Bands	
1750	ν_s (C=O)	Ester, C=O stretch
1715	ν_s (C=O)	Carboxylic acid, C=O stretch
1650	ν (C=O)	Amide I, C=O stretch
1550	ν (N-H)	Amide II, N-H bend
1415	δ (C-O-H)	Acid, C-O-H in-plane deformation
1300,1090	ν (C-C-O)	Ester, C-C-O stretch
1285	ν (C-OH)	Acid, C-OH stretch
1130,1085	ν (C-O-C)	Ester, C-O-C stretch

2.3.3.2. Nuclear Magnetic Resonance (NMR)

Although chain end units have an important influence on the properties of polymers, their characterization remains challenging due to the low occurrence of these units. The chemical structures of both commercial and synthesized PLGAs were investigated by 1D and 2D-NMR which are non-destructive technique used for structure elucidation (Park and Kang, 2013) .

(i) Monomers

Figure 2.14 shows the ^1H NMR spectra of the monomers. The methylene group (CH_2) at 5.02 was taken as the reference for the glycolide monomer. While lactide methyl and methine groups (CH_3 and CH) appeared at 1.61 and 5.04 respectively.

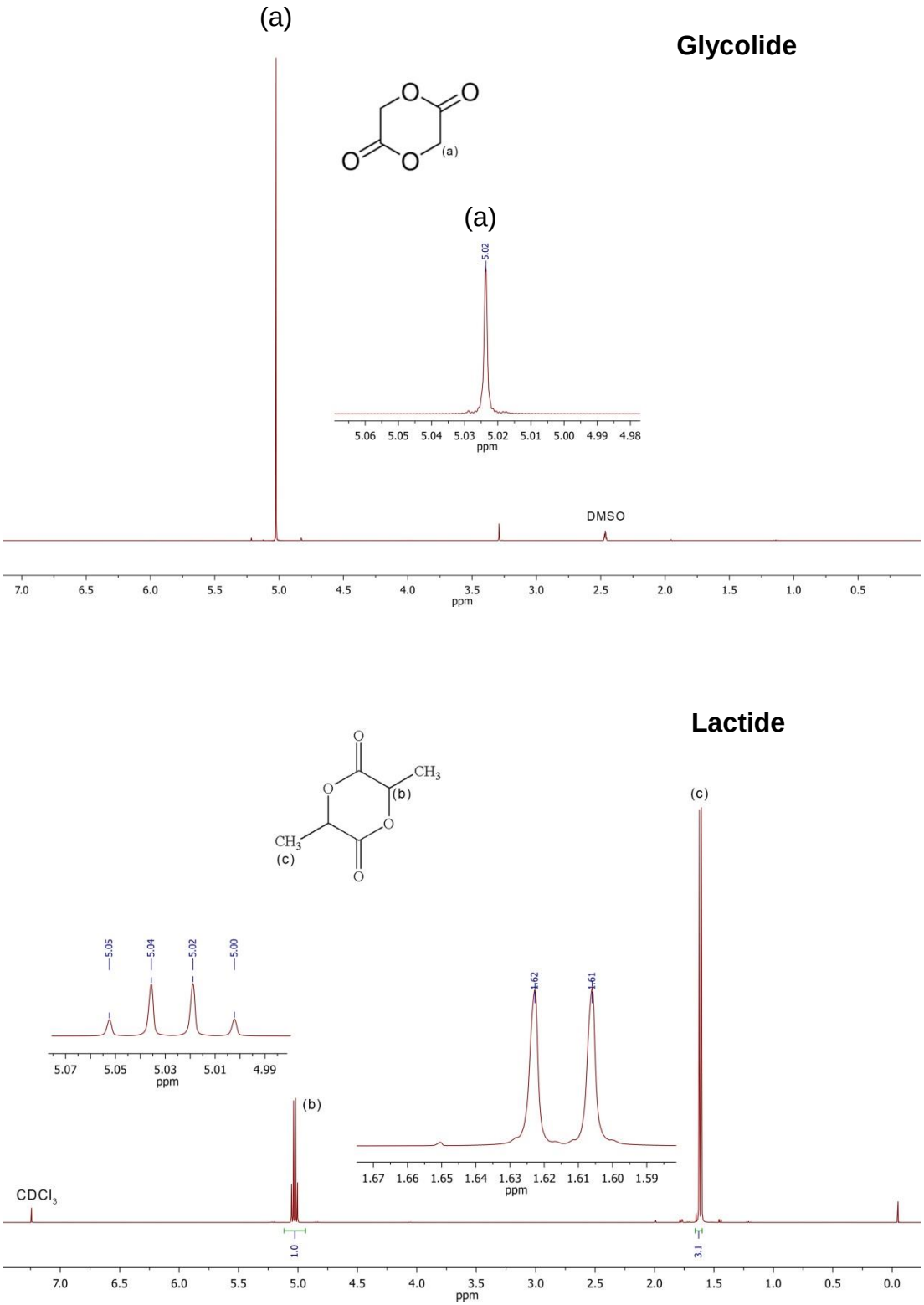

Figure 2.14: ^{1}H-NMR spectrum of monomers glycolide and D,L-lactide in DMSO and $CHCl_3$ respectively

(ii) Non- Endcapped PLGA

Figure 2.15 shows the ^{1}H NMR spectrum of the non-endcapped PLGA, PLGA-15K-[OH]. Absence or low peak intensity of residual monomers signals suggests negligible or no monomers were present in the final product. Analysis revealed the presence of three sets of peaks, characterizing the main functional groups. The first one centred at 5.25 ppm corresponds to methine protons (CH) in lactic acid and peaks centred at 4.35 ppm are due to the same protons at the end of the polymer. The second one corresponds to the methyl (CH_2) in glycolic acid at 4.77 ppm. And the third one corresponds to methyl groups (CH_3) of the D,L-Lactic acid repeated units at 1.52. Peaks at 1.5 ppm are due to the same protons at the end groups of the polymer, which often interfere with residual lactic acid monomer peaks. Results concur with previously published data. (Ping Lan and Wang, 2009, Erbetta *et al*., 2012, Takeuchi *et al*., 2017)

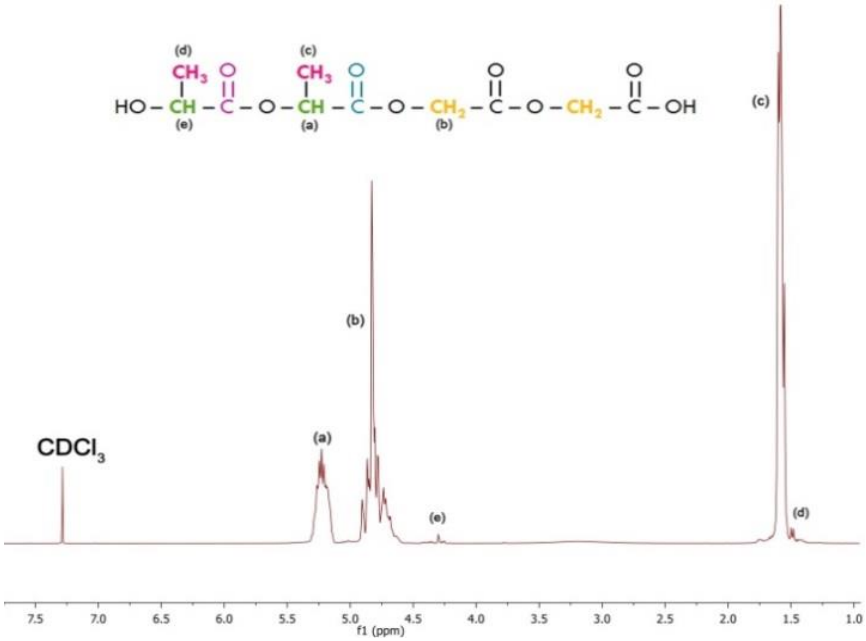

Figure 2.15: ^{1}H-NMR spectrum of non-endcapped PLGA-15K-[OH] in $CDCl_3$

Figure 2.16 shows the ^{13}C-DEPT-q-135 NMR spectra of PLGA-15K-[OH] as an example of the non-endcapped polymers. In DEPT (135°), the carbons attached to an odd number of hydrogens (methine (-CH-) and methyl carbons (-CH_3-)) produce signals with positive amplitudes while carbons coupled to an even number (-CH_2-) give signals with negative amplitudes.

Analysis revealed the presence of three sets of peaks. The first corresponds to carboxylic and carbonyl bonds (169.8 ppm). The second one (71.1-63.5 ppm) corresponds to CH bonds (69.1 ppm) in lactic acid and CH_2 (60.6 ppm) in glycolic acid due to the negative amplitude of this peak. And the third one corresponds to methyl groups of the D,L-lactic acid repeating units (18.8 ppm). (Hanafy *et al*., 2009, Deniz and Turk, 1999)

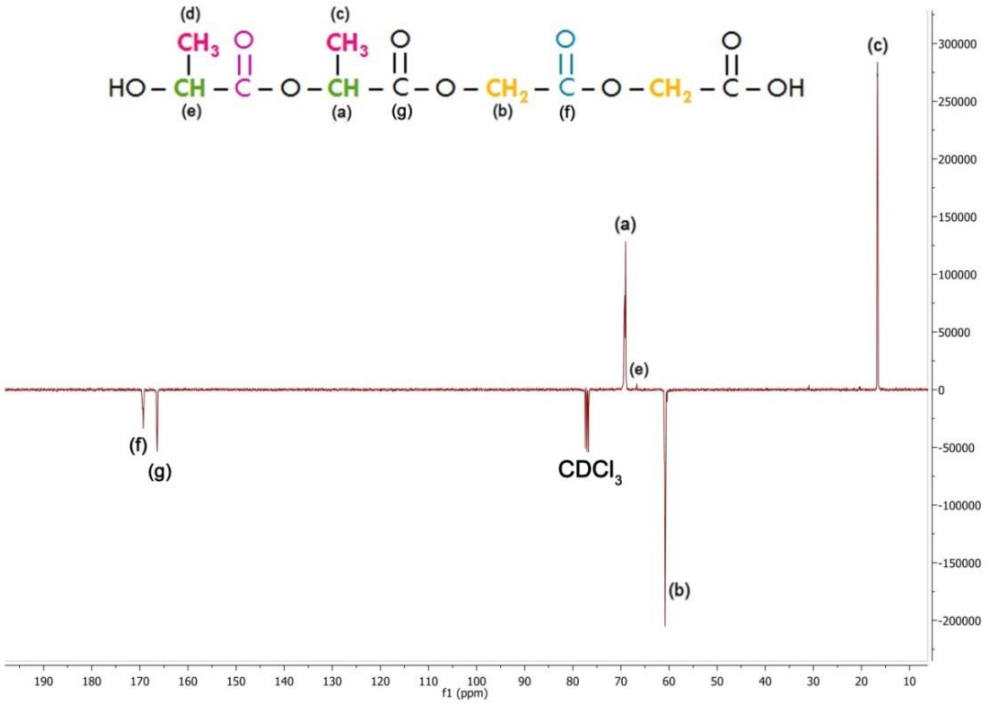

Figure 2.16: ^{13}C-DEPT-q-135 NMR spectra of non-endcapped PLGA-15k-[OH] in $CDCl_3$

To date, extensive research has been done to determine monomer sequence of polymers using 1D- and 2D- H-C correlated spectroscopy. 2D-NMR methods were combined to characterize the detailed structure of PLGA copolymers. The second dimension (^{13}C chemical shift in this case) helps to resolve the peaks that are not resolved in 1D-NMR spectra, especially ^{1}H. 2D-NMR not only confirms the resonance assignments in 1D-NMR spectra, but also provides information on atomic connectivity and confirmation of structure.

The homonuclear COSY 2D-NMR spectrum provided information on ^{1}H-^{1}H correlations, and therefore can be used to confirm whether proton signals are contributed by the same unit. 2D (^{1}H-^{1}H) COSY NMR spectrum of the copolymer PLGA-15K-[OH] shown in Figure 2.17, highlights the intra-three bond coupling of protons, and thereby represents the configurational structure of polymer chain.

In Figure 2.17, the off-diagonal peaks or cross related peaks show coupling between the oxymethine proton (–OCH–) and the methyl protons ($–CH_3$) next to the oxymethine proton in the lactide block can be seen as a cross peak at 5.18 ppm/1.59 ppm. Similar results have been published for polylactide polymers (Jung *et al*., 2010).

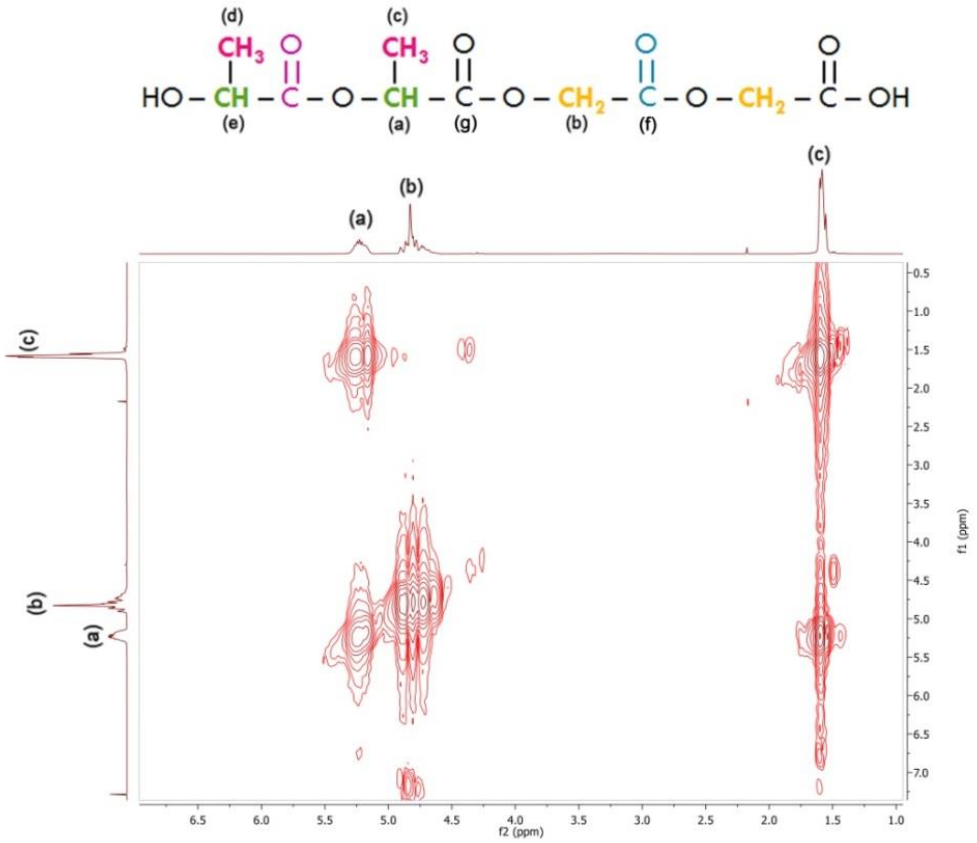

Figure 2.17: 2D COSY ^{1}H-^{1}H correlation NMR spectrum for PLGA15k-[OH] in $CDCl_3$

HSQC (which identifies one-bond correlations) and HMBC (which identifies 2- and 3-bond correlations) were combined to assign polymer resonances. From the HSQC one bond ^{1}H-^{13}C correlations of the methyl group from lactide units can be observed (Figure 2.18). In the HMBC spectrum (Figure 2.19), it can be seen that the lactide methyl proton (c) resonance is correlated with methine (a) and carbonyl (g) carbon resonance. Likewise the glycolide methylene proton (b) correlated with the carbonyl (f) carbon resonance (Linlin Li *et al*., 2011).

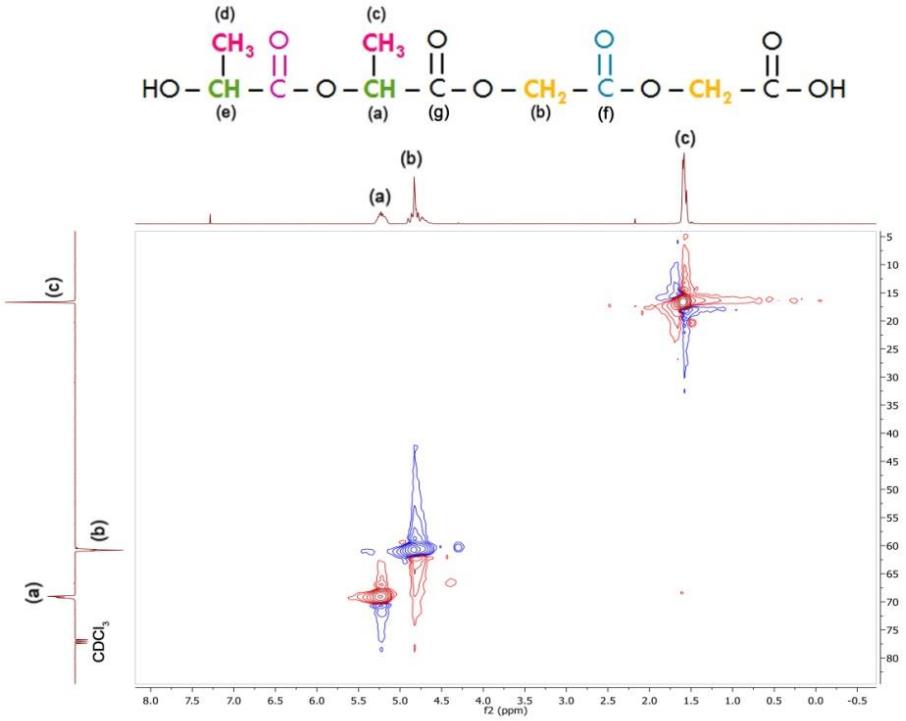

Figure 2.18: 2D HSQC ^{1}H-^{13}C correlation NMR spectrum for PLGA15k-[OH] in $CDCl_3$.

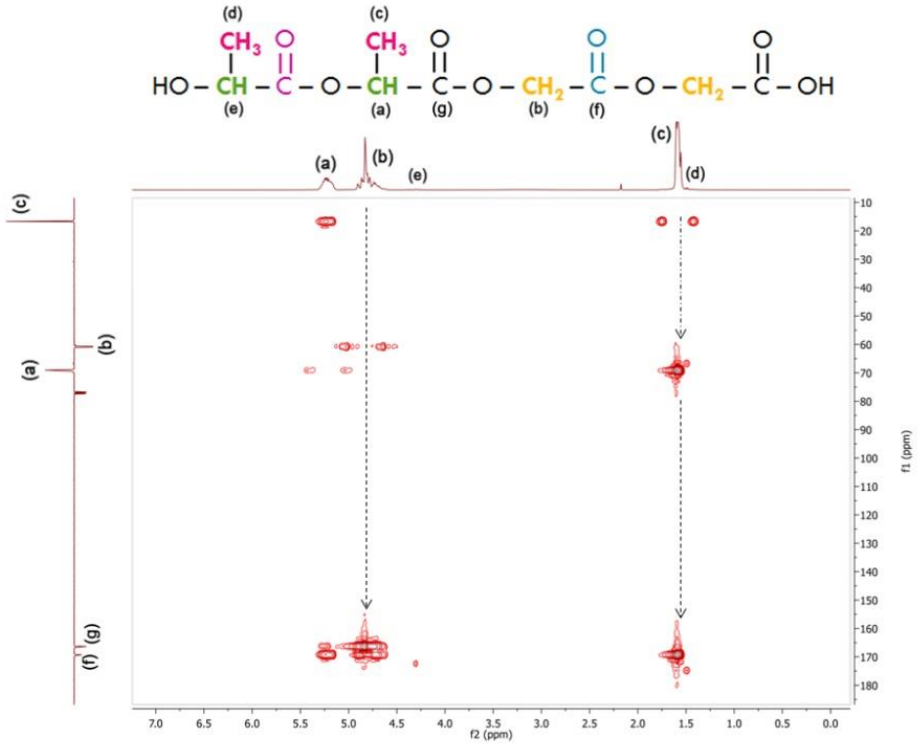

Figure 2.19: 2D HMBC ^{1}H-^{13}C correlation NMR spectrum for PLGA15k-[OH] in $CDCl_3$.

(iii) Ester Endcapped PLGA

Ester endcapped PLGA-15K-[E]-E, and PLGA-15K-[Dd]-E samples show the typical ^{1}H NMR spectra of non-endcapped PLGA polymers in Figure 2.20 Where peaks (a) (5.25 ppm) and (c) (1.59 ppm) were assignable to methine and methyl proton resonances of lactic acid in the main chain along with peaks (e) (4.35 ppm) and (d) (1.5ppm) due to the methinine and methyl protons in the hydroxyl terminal lactic acid unit in addition to the chemical shift assignment for each proton resonance of the ester endcap.

In Figure 2.20 (A), additional peaks (h) (4.18 ppm) and (i) (1.25 ppm) were assigned to the methylene and methyl proton in the ethyl ester group, respectively. Likewise the dodecyl ester cap in Figure 2.19(B) showed three new peaks (f) (4.19 ppm) for the methylene proton, (h) (0.92 ppm) for the methyl proton and a higher intensity signal assigned for the repeating methylene proton (g) at 1.3 ppm. Assigned peaks are in agreement with previously reported data (Kobori *et al*., 2004).

The ^{13}C-DEPT-q-135 NMR spectra of the ethyl ester endcapped PLGA-15K-[E]-E copolymer revealed an additional peak (16.3 ppm) attributed to the terminal methyl group of the ester. However, the methylene groups of both the ester and repeating glycolide unit seem to overlap coming off as a single peak at 60.6 ppm (Figure 2.21).

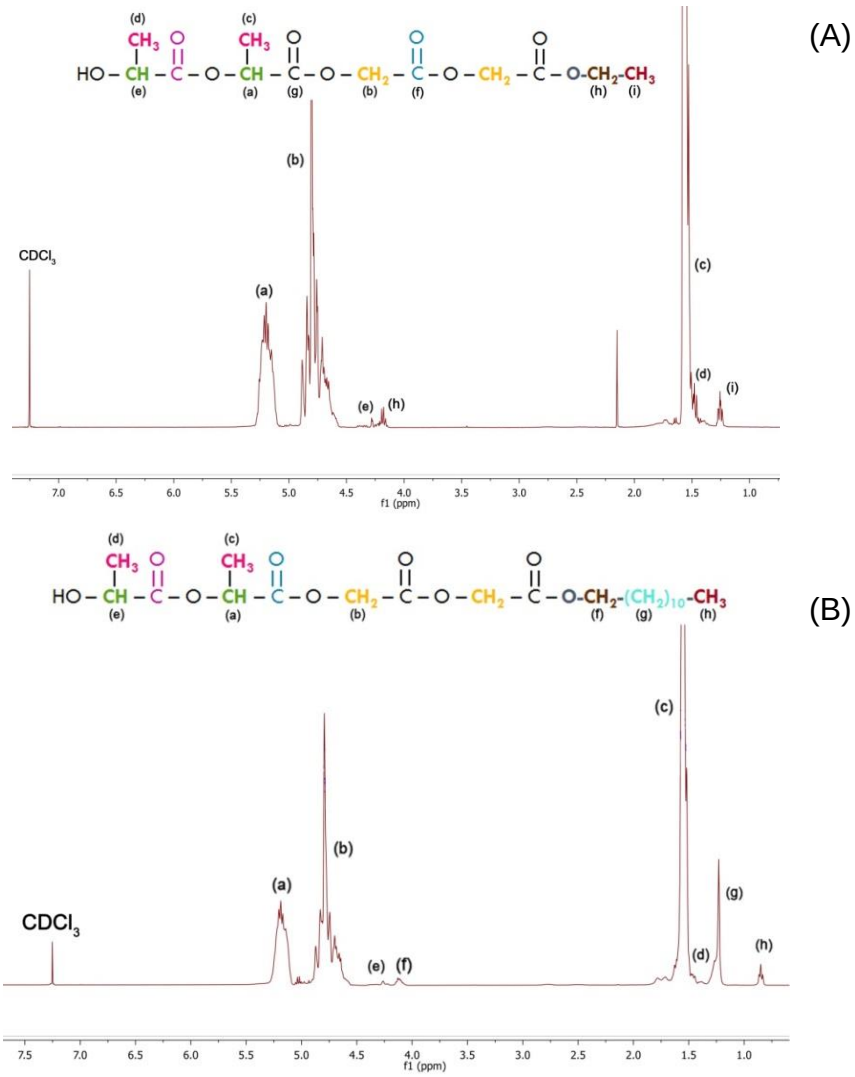

Figure 2.20: ^{1}H-NMR spectra of PLGA samples endcapped with ethyl (A), and dodecyl (B) ester

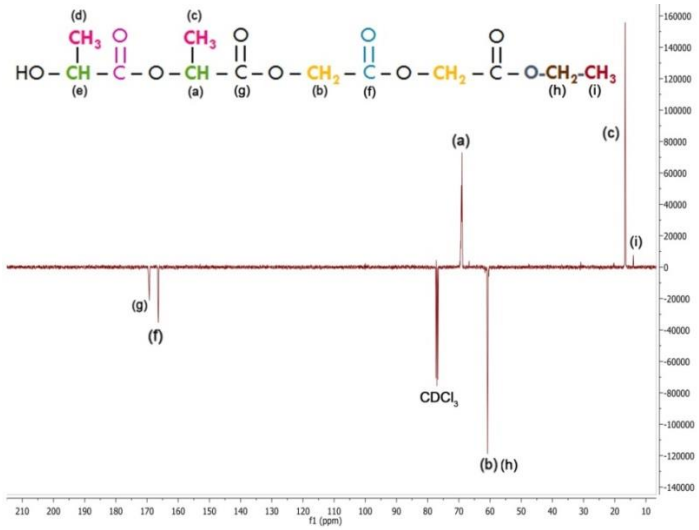

Figure 2.21: ^{13}C-DEPT-q-135 NMR spectra of endcapped PLGA-15K-[E]-E

Homo and Hetero 2D NMR spectra of the ethyl endcapped copolymer PLGA15K-[E]-E were analysed to confirm successful endcapping. In Figure 2.22 and 2.23; COSY, HSQC and HMBC spectra of PLGA-15K-[E]-E show the same basic correlations seen in PLGA-15K-[OH] scans. An additional coupling interaction between the methyl protons of the ester endcap with the methylene proton of the same unit appears in the spectra of PLGA-15K-[E]-E. The COSY ^{1}H-NMR demonstrated a construction of the endcap which was further confirmed by the HSQC and HMBC.

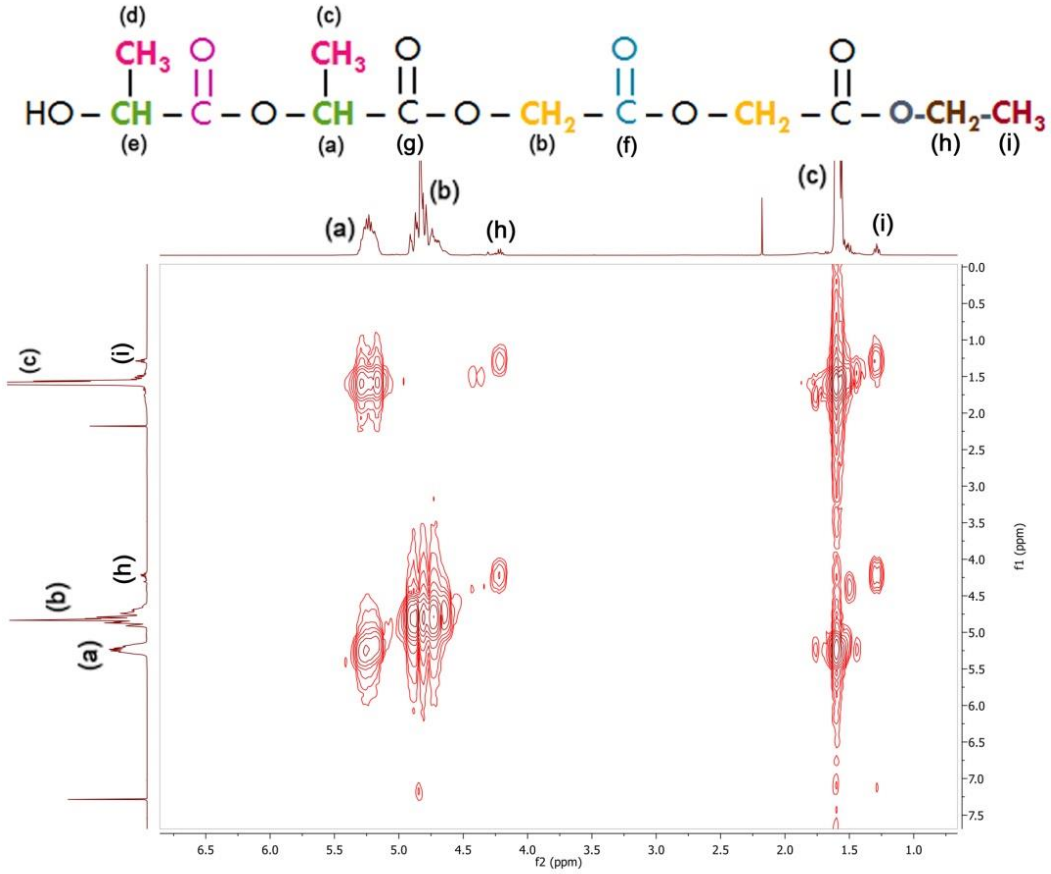

Figure 2.22**:** 2D COSY ^{1}H-^{1}H correlation NMR spectrum for PLGA15k-[E]-E in $CDCl_3$

The HSQC one bond ^{1}H-^{13}C correlations of the methyl and methylene groups of the endcap can be observed (Figure 2.23.A). In addition, the HMBC spectrum (Figure 2.23.B), confirms that the ethyl ester methyl proton (i) resonance is correlated with methylene (h) carbon resonance.

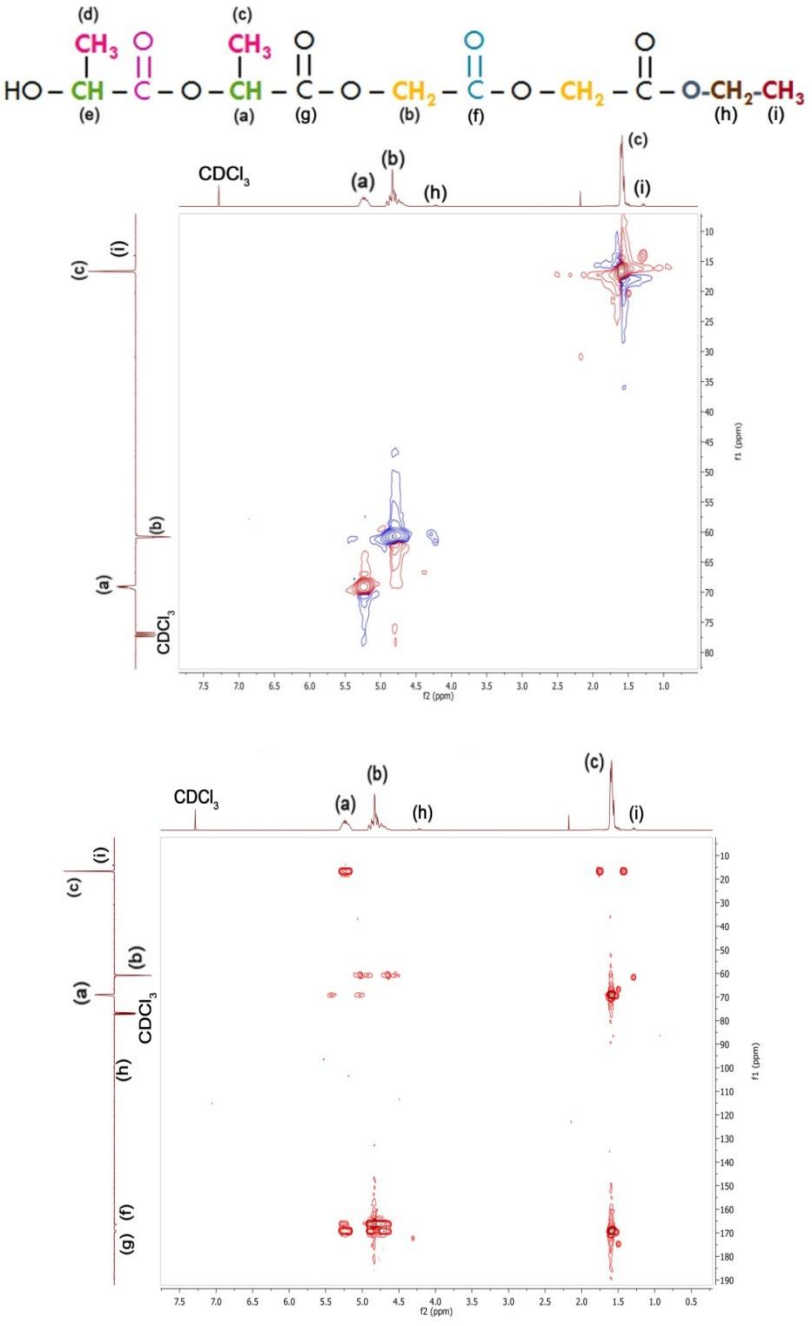

Figure 2.23: 2D HSQC (A) and HMBC (B), ^{1}H-^{13}C correlation NMR spectrum for PLGA15K-[E]-E in $CDCl_3$

(iv) Amide Endcapped PLGA

The ^{1}HNMR analysis of the PLGA amide series revealed the presence of three main sets of peaks: at 5.25 ppm corresponding to methine protons (CH) in lactic acid, the methylene (CH_2) in glycolic acid at 4.77 ppm, and the methyl groups (CH_3) of the D,L-Lactic acid repeated units at 1.52, as expected. However solvent contamination was predominant in the first synthesis trials masking the endcap peaks in preliminary data, as seen in Figure 2.24. Drying the samples under vacuum was not sufficient to rid it of the residual methanol and diethyl ether used for polymer precipitation. Methanol singlet peaks at 1.4 and 3.49 ppm assigned to the hydroxyl and methyl protons respectively are evident in Figure 2.24.A. Likewise, diethyl ether contamination is clear in Figure 2.24.B with methyl triplet and methylene quartet peak spanning the 1.21 and 3.48 space respectively.(Takeuchi *et al*., 2017)

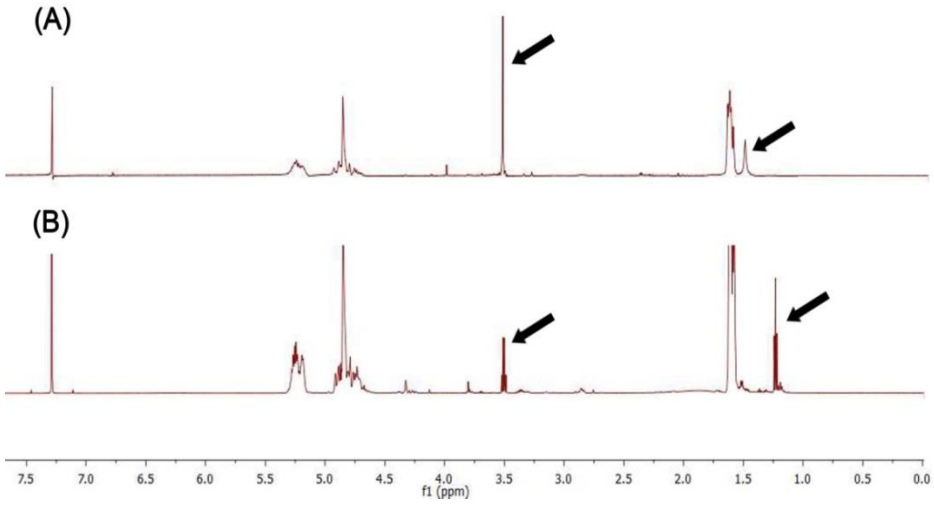

Figure 2.24: ^{1}H-NMR spectra of PLGA15k-[E]-A in $CDCl_3$ initial synthesis trials showing solvent contamination (A) methanol (B) diethyl ether in $CDCl_3$

PLGA-15K-[E]-A samples dried using a rotary evaporator showed clearer peaks (Figure 2.25) with ethyl amide peaks appearing at 1.25 and 3.75 ppm corresponding to the terminal methyl groups (CH_3) and methylene (CH_2) respectively. There was a small peak at 6.25 ppm, indicating the presence of an amide bond between PLGA and ethylamine (Figure 2.25 inset) as previously reported.(Liu and Lin, 2012, Kamaly *et al*., 2013)

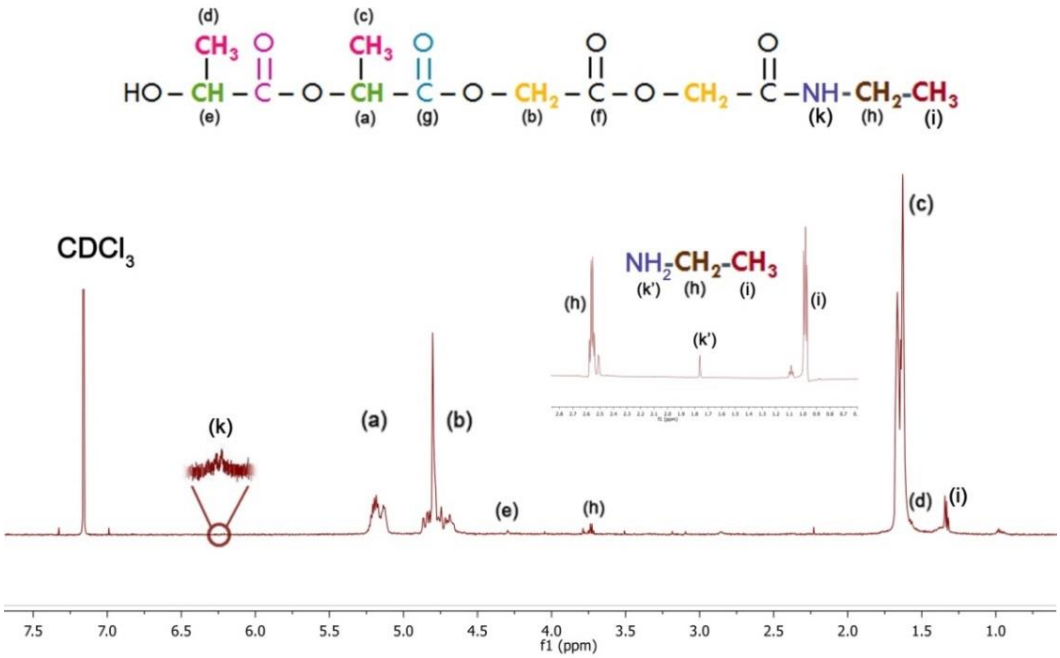

Figure 2.25: ^{1}H-NMR spectra of PLGA samples endcapped with ethyl amide $CDCl_3$

Studying the ^{1}H-NMR spectra of the synthesized PLGA-15K-[Dd]-A in Figure 2.26.A, the three backbone peaks appear at 5.30–5.17 ppm for the CH of lactide, at 4.90–4.56 ppm for the CH_2 of glycolide, at 3.61–3.55 ppm for and at 1.62–1.45 ppm for the CH_3 of lactide.

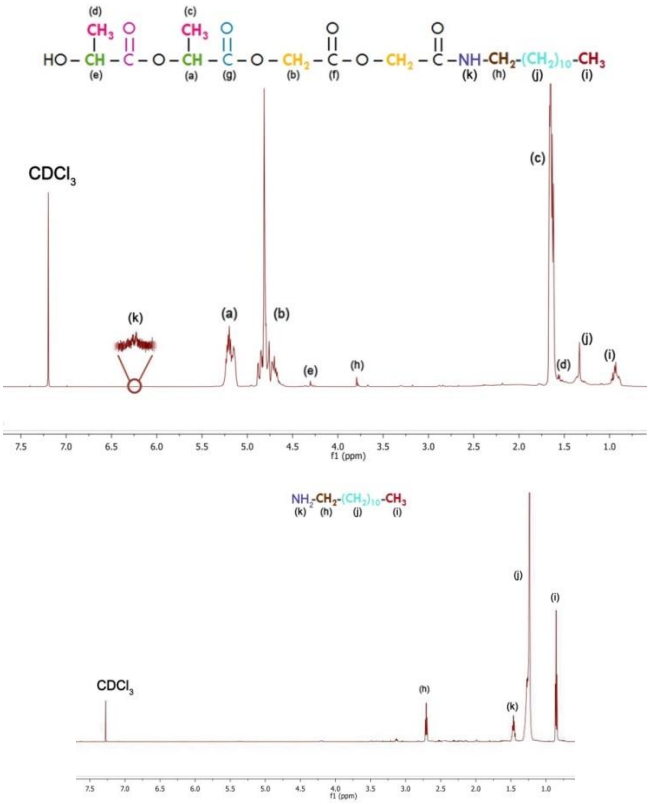

Figure 2.26: ^{1}H-NMR spectra of (A) PLGA-15K-[Dd]-A and (B) dodecyl amine in $CDCl_3$

The ^{1}H-NMR of the dodecyl amine used in the synthesis is shown in Figure 2.26(B). The shift of the alkyl chain peaks down field in Figure 2.26(A) is indicative of attachment to a more electronegative functional group. In addition to the downfield shift, the disappearance of the primary amine protons (k') at 1.5 ppm in Figure 2.26(B) in favour of the appearance of the secondary amine's proton (k) in Figure 2.26(A) and its significant shift down field is indicative of amide bond formation.

Taking the step wise synthesis of PLGA-benzyl amide as an example; Figure 2.27 illustrates the appearance of the succinimide ester characteristic peak (L) of its methylene protons at 2.6 ppm as the coupling intermediate forms.

This later disappears in the second step of the reaction as the amide endcap coupled with the appearance of the amide proton (k) and characteristic benzyl protons (h) and (m) at 3.8 and 7.2 respectively. (Singh *et al*., 2011b)

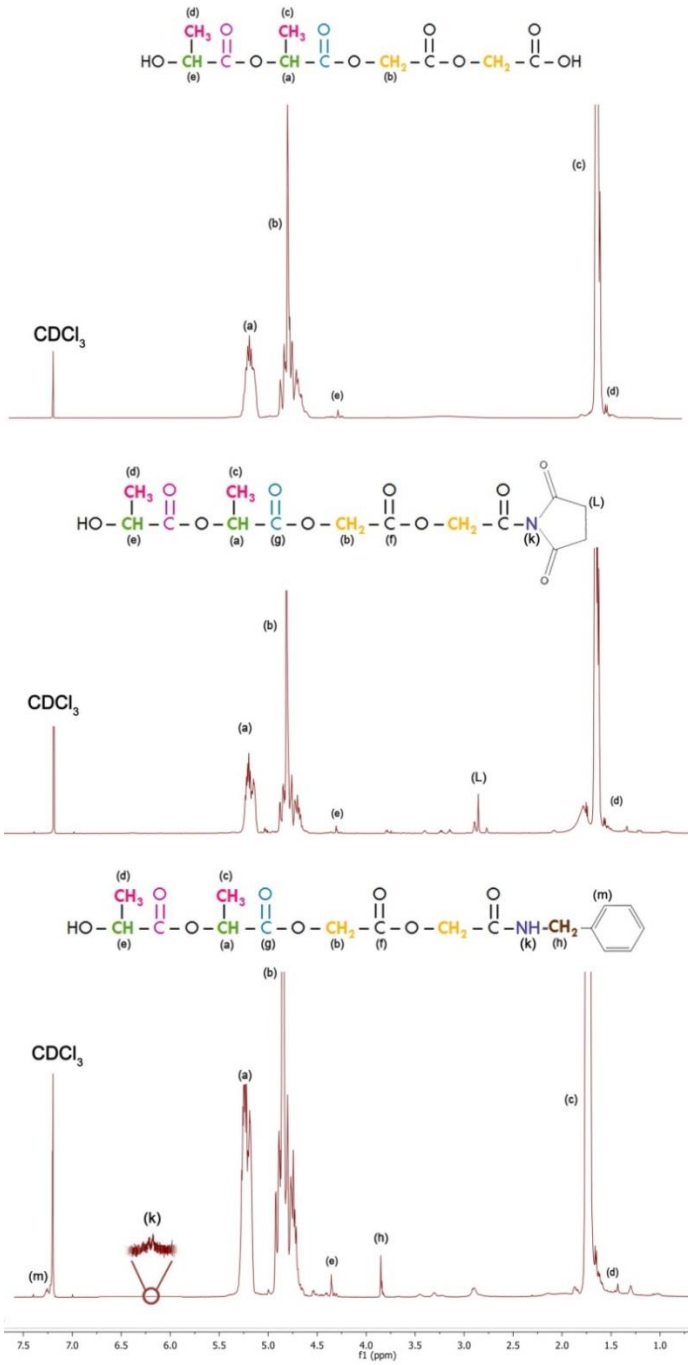

Figure 2.27: ^{1}H-NMR spectra showing the different peak shifts as the non-endcapped PLGA is activated by the EDC/NHS forming the NHS ester followed by amidation with benzyl amide in $CDCl_3$.

Figure 2.28 shows the ^{13}C-DEPT-q-135 NMR spectra of PLGA-15K-[Bn]-A. As previously discussed analysis revealed the presence of three sets of peaks. The first corresponds to carboxylic and carbonyl bonds (169.8 ppm), the second one (71.1-63.5 ppm) corresponds to CH bonds (69.1 ppm) in lactic acid and CH_2 (60.6 ppm) in glycolic acid and the third one corresponds to methyl groups of the D,L-lactic acid repeating units (18.8 ppm). In addition to three main sets of peaks the characteristic aromatic carbons appeared at 129 ppm

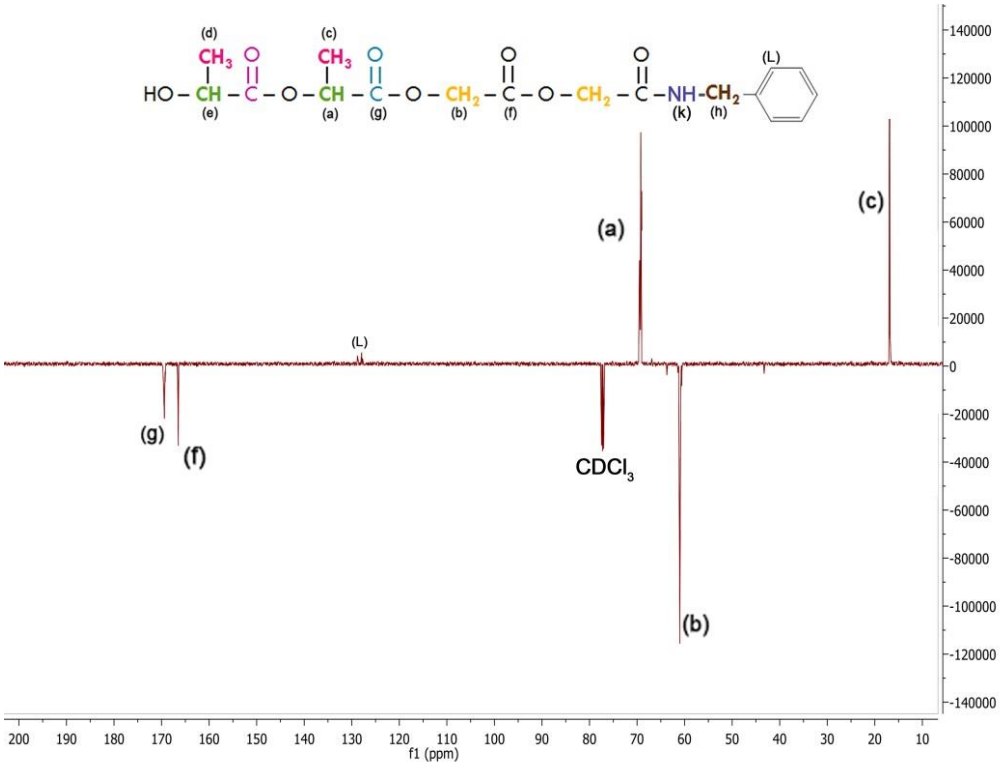

Figure 2.28:^{13}C-DEPT-q-135 NMR spectra of PLGA-15k-[Bn]-A in $CDCl_3$

The 2D (^{1}H-^{1}H) COSY NMR spectrum of PLGA15K-[E]-A, shows the same basic correlations seen in non endcapped PLGA scans. However, coupling interactions between the methyl protons of the amide endcap with the

methylene proton of the same unit appear highlighting the intra-three bond coupling of protons, thereby confirming the configurational structure of polymer chain (Figure 2.29).

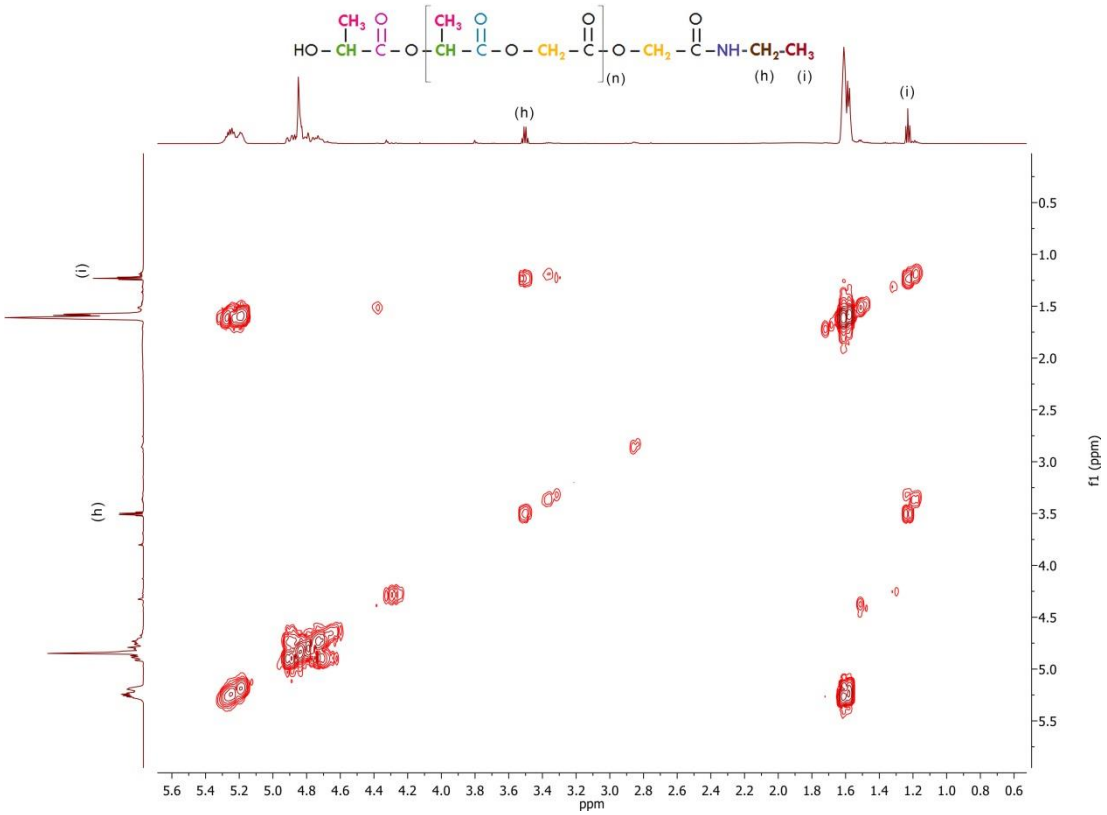

Figure 2.29: 2D COSY ^{1}H-^{1}H correlation NMR spectrum for PLGA-15K-[E]-A in $CDCl_3$.

The analysis of the NMR spectra provided comprehensive data regarding the microstructure of the PLGA copolymers and enabled distinguishing of their endcaps.

(v) Quantitative Analysis

The composition of the PLGAs (the ratio of lactic to glycolic acid moiety in the polymers) was determined by ^{1}H-NMR. Based on the behaviour of the two different hydrogens in the lactic and glycolic acid moieties in a magnetic field the ratio of absorbencies of the methine to the methylene hydrogen was assessed using the following equation.(Nuo *et al*., 2000)

$$\%\ D,L-Lactide\ monomer = \frac{(CH_3)intergral\ area\ /_3}{(CH_3)integral\ area\ /_3 + (CH_2)integral\ area\ /_2} \times 100$$

An example of a typical ^{1}HNMR spectrum is shown in Figure 2.30 illustrating the chemical shift ranges of the CH_3, CH_2 and CH functional groups. The determined composition of the synthesized polymers is shown in Table 2.4. The results of the composition of the synthesized polymers correlated well to the feeding composition of the lactide and glycolide.

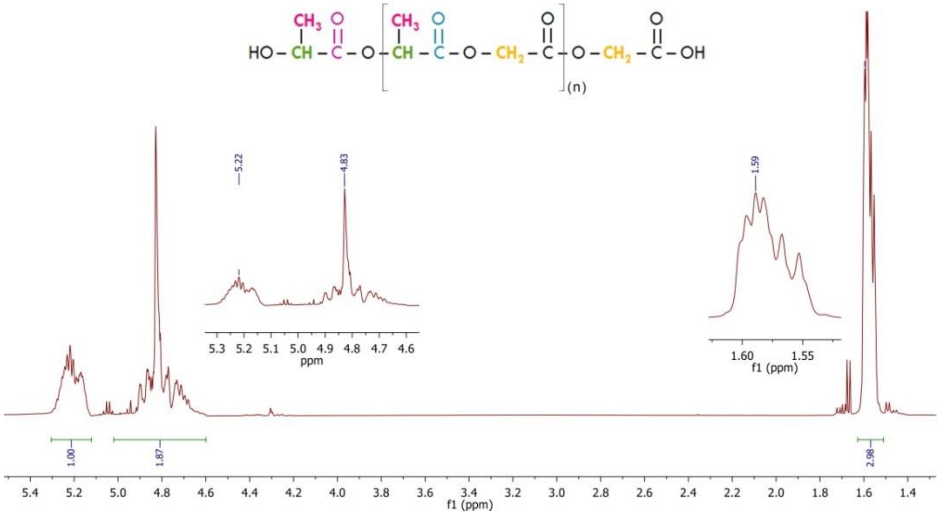

Figure 2.30: ^{1}HNMR spectrum of PLGA15K-[OH] showing 50/50 monomer ratio

Table 2.4: Comparison of the results determined for the composition of PLGA copolymers

Sample Label	Molecular Weight (g/mol)		NMR Determined Composition
	M_n (GPC)[a]	M_n (NMR)[b]	(L/G)[c]
PLGA-15K-[OH]	13790	11864	51/49
PLGA-15K-[E]-E	12127	11047	47/53
PLGA-15K-[Dd]-E	11217	10255	50/50
PLGA-15K-[C]-E	17849	16788	48/52
PLGA-15K-[E]-A	12703	12001	49/51
PLGA-15K-[Bu]-A	12667	11950	48/52
PLGA-15K-[Dd]-A	12095	10595	50/50
PLGA-15K-[Φ]-A	12351	11023	52/48
PLGA-15K-[Bn]-A	11168	11001	46/54

a THF was used as a solvent at 25 ºC. Polystyrene standard was used to determine Mn
b $CDCl_3$ was used as a solvent at ambient temperature.
c Molar ratio of lactic to glycolic units calculated from integration of 1H NMR data.

A slight difference in the molar composition between the initial monomer and the final product was observed, but it seems reasonable to conclude that the Lactide monomer is quantitatively reacted with glycolide. The result is consistent with those reported previously in the literature.(Zhou *et al*., 2004) Analysis of the amide modified PLGA series indicated that the ratio of the peak intensity of the methylene (CH_2) in glycolic acid at 4.83 ppm, and the methine groups (CH) of the D,L-Lactic acid repeated units at 5.22, remained 1:1 indicating the monomer ratio was not affected by endcapping.

Number-average molecular weight (M_n) of each polymer was estimated by integrating appropriate signals in the ^{1}H NMR spectrum due to main-chain lactoyl and glycol units (methyl, methine and methylene signals in the main chain) versus the terminating methyl protons at the lactide hydroxyl end. (Ping Lan and Wang, 2009, Qian *et al*., 2011) The peaks at 5.25 ppm, (methine protons in Lactide repeat units), 4.77 ppm (methylene protons of glycolide blocks), 1.59 and 1.51 ppm (CH_3 of Lactide) were used. There were six and three protons in each D,L-lactide-*co*-glycolide and terminal methyl group. The relationship between NMR peak area and molecular weight can be expressed as *6n : 3 = peak area of a+b+c : peak area of d* (n is the degree of polymerization). Figure 2.31 shows an example of the typical ^{1}H-NMR spectra obtained from PLGA15K-[Dd]-A.

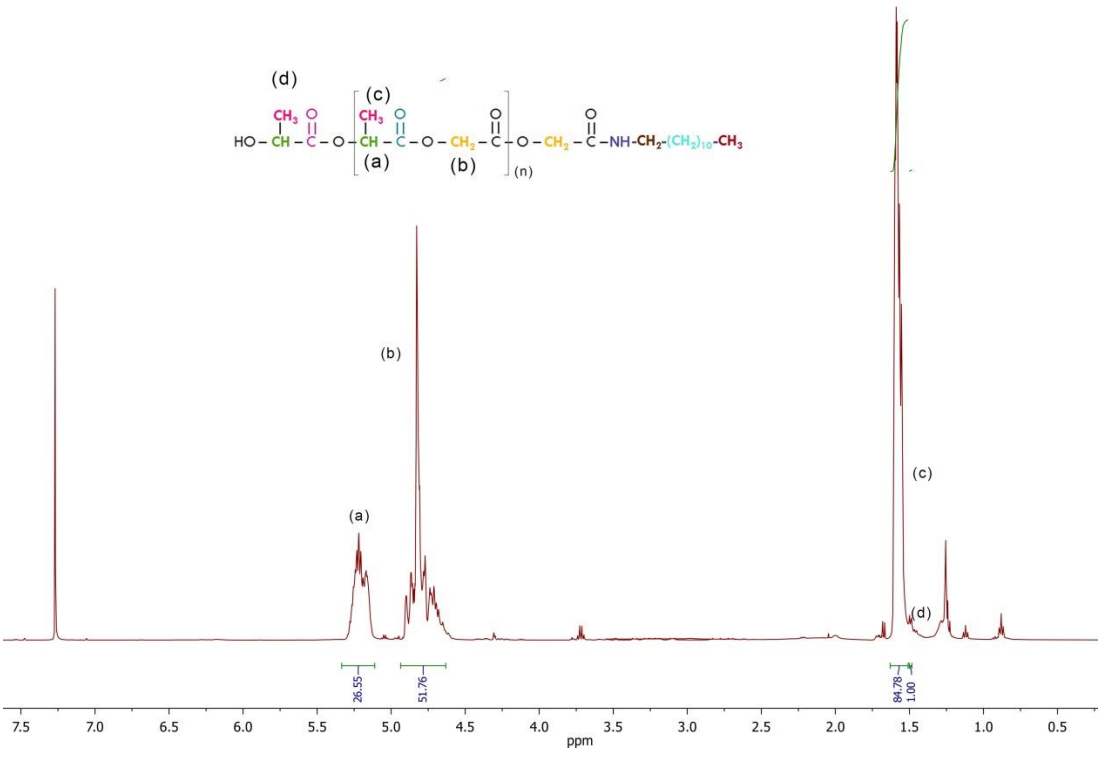

Figure 2.31: ^{1}H-NMR of PLGA15K-[Dd]-A showing estimated number average molecular weight.

Alternatively the methine proton at the hydroxyl end could be used as the reference when the methyl terminal group is not clearly separated from residual lactide monomer peaks.(Kobori *et al*., 2004) The results are summarized in Table 2.4. The molecular weights calculated from ^{1}H-NMR were systematically lower than those determined by GPC, but the order was the same. It has been reported that molecular weights determined by NMR analysis were lower than those determined by GPC. (Hiltunen *et al*., 1997)

A comparison of the integration of the resonance “d” of the methyl protons at the hydroxyl-end of the lactide at 1.5 ppm with integrations for resonance “h” assigned to the methyl protons of the dodecyl amide at 0.99 ppm indicated the percent functionalization. The extent of functionalization typically obtained was 98-99% concluding that the majority of the carboxylic acid chain ends of the PLGA backbones were substituted by the dodecyl ester group as shown in Figure 2.32. (Liu and Lin, 2012)

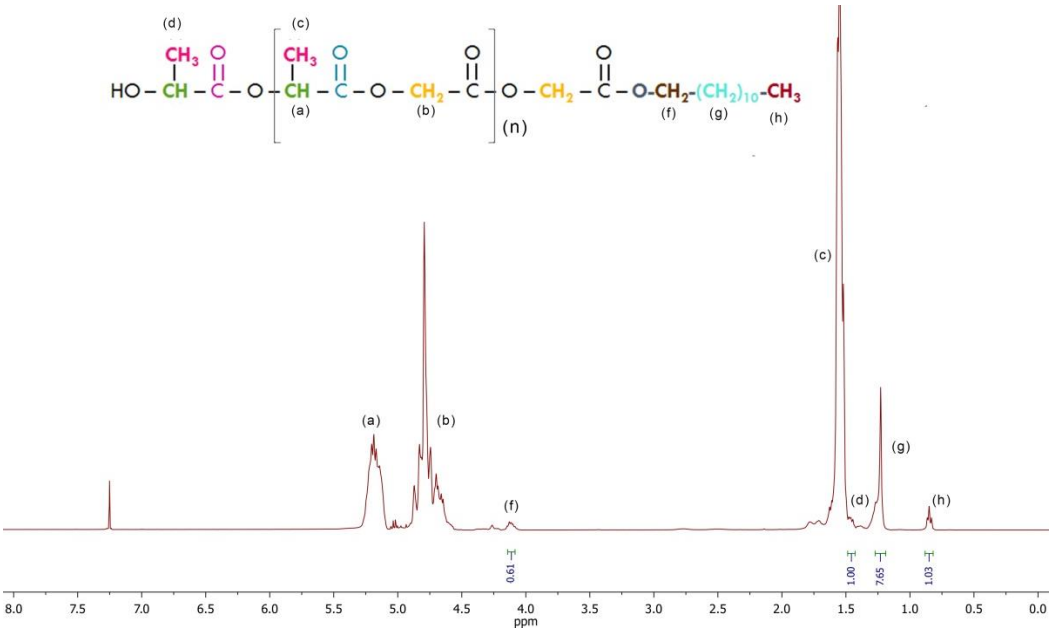

Figure 2.32: ^{1}H-NMR of PLGA15K-[Dd]-E illustrating functionalisation extent

2.3.4. Thermal Behaviour Studies

2.3.4.1. Modulated Differential scanning calorimetry (MDSC)

DSC curves of glycolide and D,L-Lactide are shown in Figure 2.33. The DSC curves show how heat (mW) varies as a function of temperature. Both curves present two sharp endothermic events; the first thermal event on the DSC curves represents the melting of the monomers (84°C for glycolide and 125°C for D,L-lactide). For D,L-lactide, the second endothermic peak (at 257°C) characterizes the evaporation of this monomer. In the case of glycolide, the second peak (at 273°C) relates to the degradation of the monomer, since glycolide does not have a boiling point.(Erbetta *et al*., 2012)

Comparing the DSC curves of a sample of non-endcapped copolymers with the monomers in Figure 2.34, it can be seen that there is no indication of residual monomers copolymers, since no endothermic event characteristic of these monomers melting is observed on the respective DSC curves. The glass-transition temperatures (T_g), of the tested PLGA samples were evaluated by considering the inflection point in the second heating scan of the MDSC thermograms. Glass temperature (T_g) of the tested PLGAs varied from 38.91 to a maximum of 47.58 ^oC as depicted in Table 2.5 and degraded at temperatures above 200 ^oC.

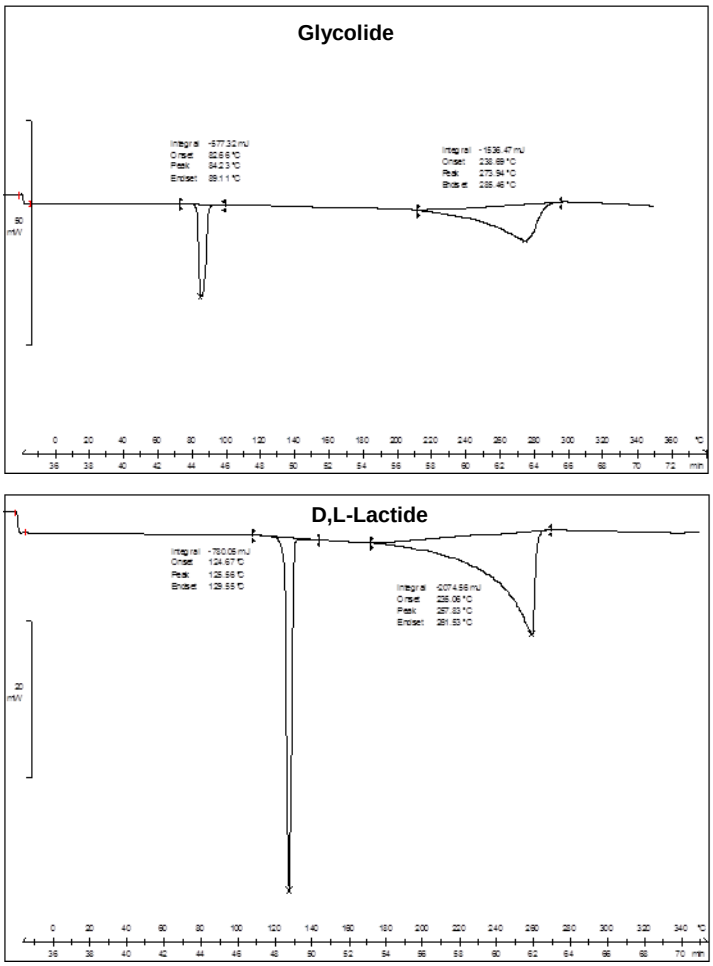

Figure 2.33: DSC curves of glycolide and D,L-Lactide monomers (2nd heating) curve. Heating rate of 10°C.min^{-1} to 300°C

Table 2.5: Thermal properties of PLGA copolymers by MDSC

Sample Label	Tg[a] (°C)		Sample Label
PLGA-5K-[OH]	39.31	40.90	PLGA-15K-[E]-E
PLGA-7K-[OH]	40.35	36.30	PLGA-15K-[Dd]-E
PLGA-10K-[OH]	42.70	44.97	PLGA-15K-[C]-E
PLGA-15K-[OH]	42.68	44.26	PLGA-15K-[E]-A
PLGA-20K-[OH]	43.19	40.22	PLGA-15K-[Bu]-A
PLGA-25K-[OH]	45.16	37.18	PLGA-15K-[Dd]-A
PLGA-30K-[OH]	47.42	44.76	PLGA-15K-[Φ]-A
PLGA-35K-[OH]	47.58	38.91	PLGA-15K-[Bn]-A

[a] Data are the average of triplicate runs from second scan

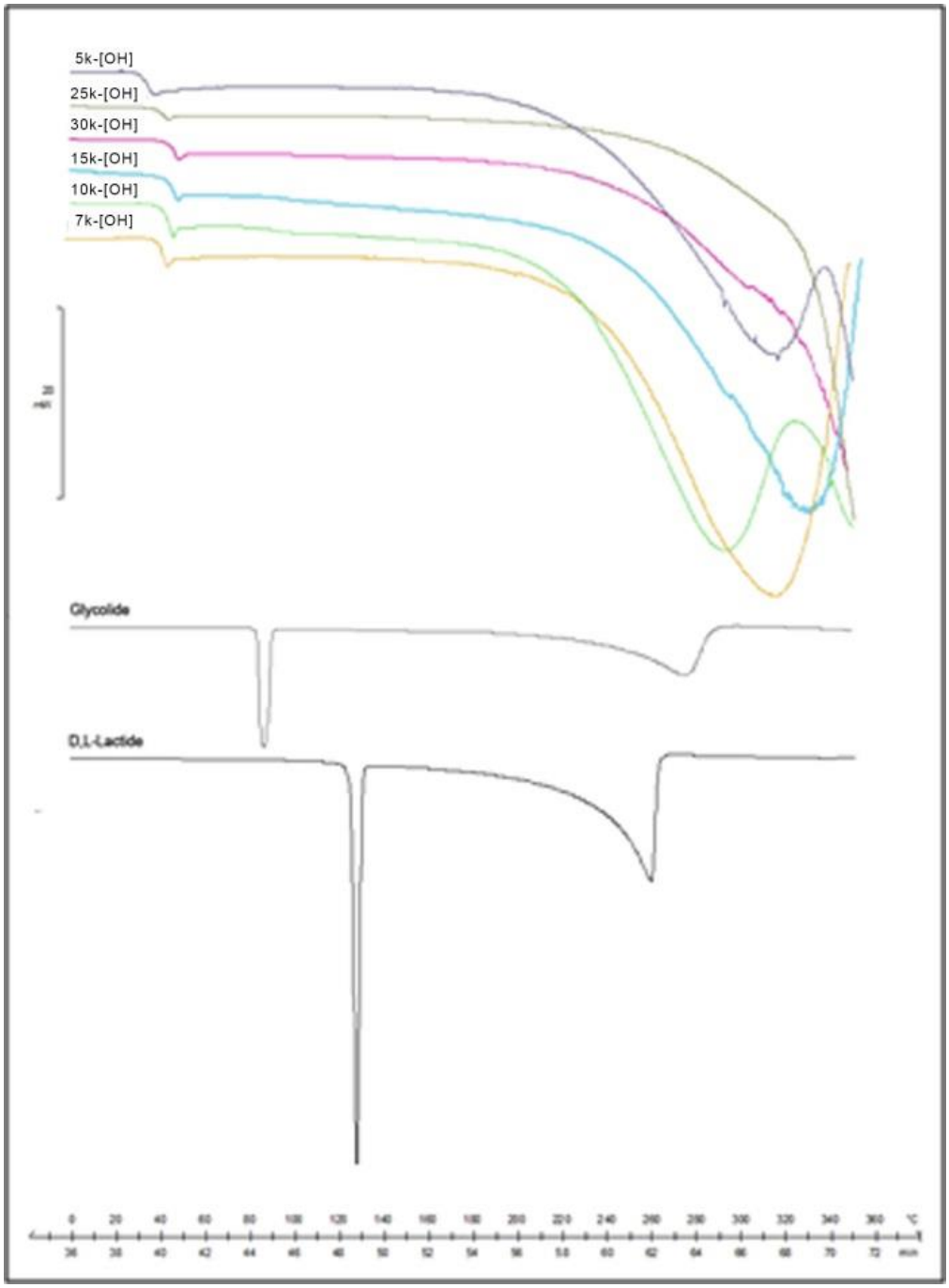

Figure 2.34: DSC curves of the non endcapped PLGA copolymers compared with their respective monomers

Amorphous polymers are characterized by a unique glass transition temperature (T_g), this describes the transition point between a highly viscous brittle structure known as the “glassy state” compared to a less viscous, more elastic, “rubbery state”. The rubbery state (at temperatures above the T_g), represents a liquid like structure with high molecular mobility and is thus more prone to physical and chemical changes than the glassy state.

Figure 2.35 shows the MDSC curves for the first and second heating in the thermal study of PLGA-20K-[OH]. The endothermic peak (enthalpic relaxation) superimposed on the Tg (evident in Figure 2.35A) was attributed to polymer aging, and was separated by the modulated DSC. This endothermic peak is often confused with an endotherm corresponding to the fusion temperature, but, crucially, the distinguishing feature is that the baseline does not return to its original level. As the polymer is heated past the Tg, then quench cooled below its Tg at a faster rate than that used for heating, any history of the polymer can be eliminated. When the thermal behaviour of the polymer analysed over a second identical cycle, the overheating peak almost disappeared, given the minimal potential for relaxation (Figure 2.35B). (Bouissou *et al*., 2006, Hausberger and DeLuca, 1995)

The absence of a melting transition phase event and appearance of a second order transition at 43.73^{o}C (Tg) confirmed the amorphous nature of the PLGA. The results are in agreement with the literature where PLGAs

containing less than 70% glycolide are amorphous compounds with glass temperatures of 40-50°C. (Bendix, 1998, Erbetta *et al*., 2012)

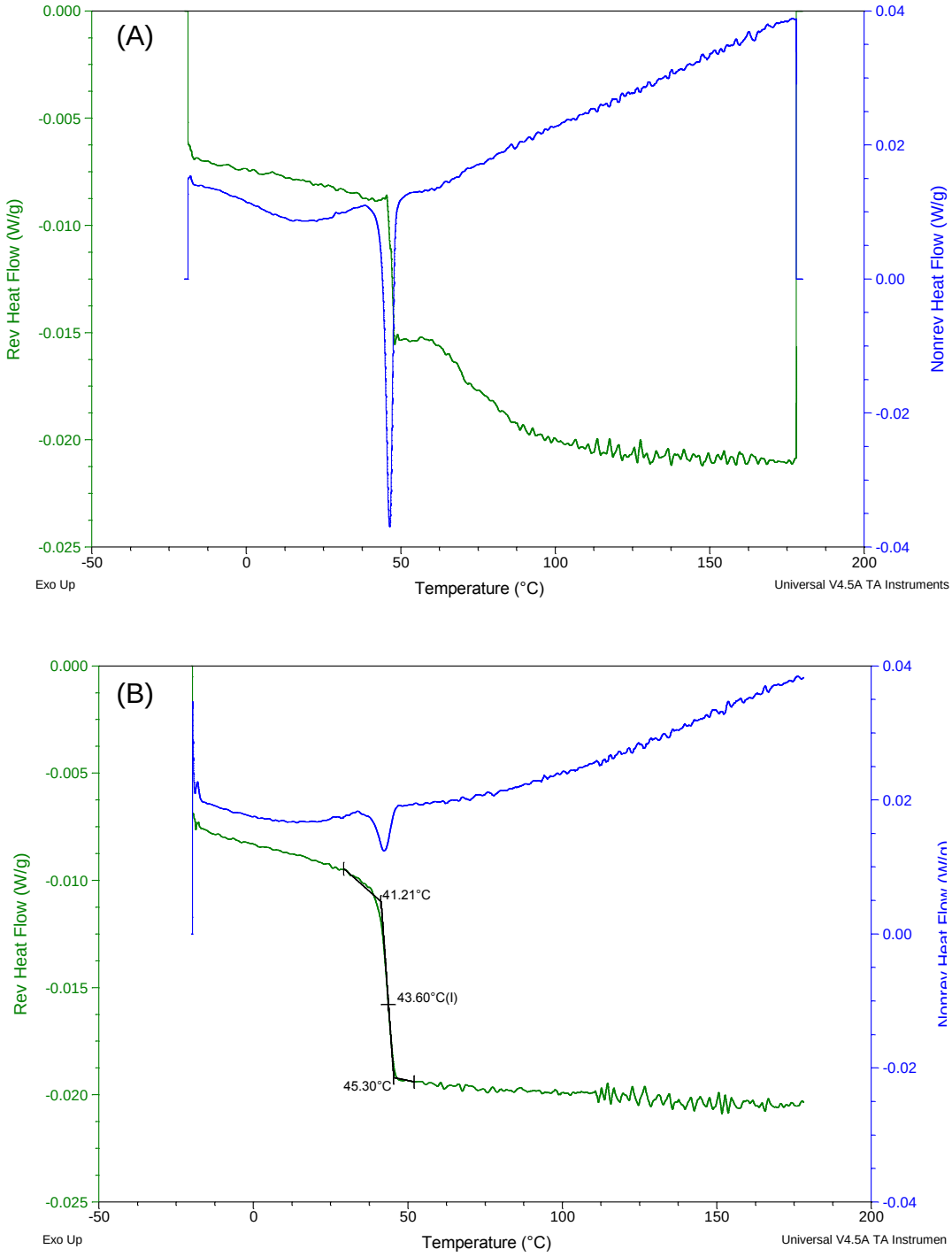

Figure 2.35: DSC curves of PLGA-20K-[OH] 1st (A) and 2nd (B) heating curves. Heating rate of 5°C.min^{-1} and 1°C.min respectively to 200°C

Effect of Molecular weight on Tg

The effect of molecular weight and the chain end on the glass transition temperature, Tg, of a polymer is an old subject of research interest and is usually explained by the idea of excess free volume of the chain ends over that of a similar unit within the chain (Lin, 1990). Studying the non-endcapped PLGA series, Tg increased as the molecular weight of the polymers increased but levelled off when the molecular weight of the polymers reached a certain value.

The relationship between the Tg of the PLGA polymers and the corresponding molecular weights is shown in Figure 2.36. At lower molecular weights, major changes in Tg are witnessed as molecular weight increases however the changes become less at higher molecular weights. Similar results have been observed by other researchers (Nuo *et al*., 2000).

The increase in Tg with molecular weight is attributed to reduced chain mobility. As the polymer chain length increases possible intra- and inter-polymer chain interactions are enhanced which decreases the polymer chain mobility, free volume and consequently increases Tg. (Nuo *et al*., 2000) Free volume depends on the number of polymer chain ends present in the system. End chain units exhibit greater free volume than units within the chain. Therefore as molecular weight increases fewer chain ends per total units exist and hence less free volume than polymers consisting of short chains.

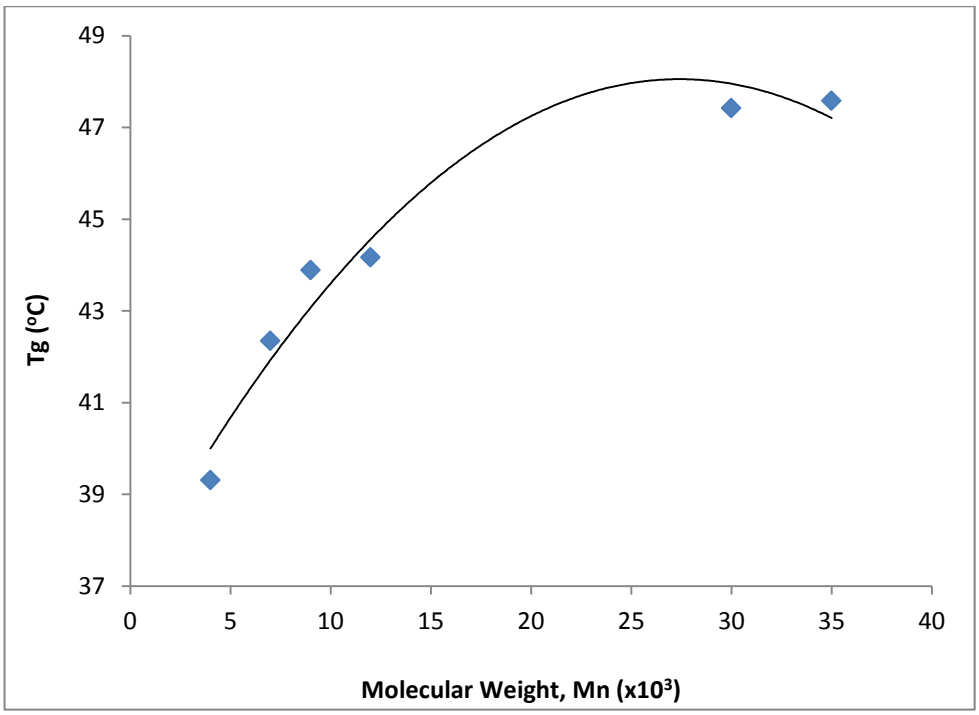

Figure 2.36: Glass transition temperature as a function of the molecular weight of non-endcapped PLGA

In 1950, Fox and Flory reported that the glass transition temperature (T_g) varies with molecular weight (M_n) according to $T_g = T_{g\infty} - k/M_n$ where Tg, is the glass transition temperature (in ^{O}K) observed with a polymer of molecular weight M, $T_{g\infty}$ is the maximum glass transition temperature that can be achieved at a theoretical infinite molecular weight and K is an empirical constant that is related to the free volume present in the polymer sample whose units are ^{o}K mol g^{-l}. (Singh *et al*., 2011b)

Plotting M_n^{-1} against T_g as shown in Figure 2.37 reflects the linear decrease in Tg with the increase in concentration of polymer chain ends. The complete set of molecular weight data and Tg presented in Table 2.5 plotted in Figure 2.37 results in three intersecting straight-line sections having different K's for

different molecular weights. Where K from one region cannot predict Tg in another since K is a function of free volume. This could be attributed to the transition from entangled coils to isolated coils to rod like systems. (Takeuchi *et al*., 2017)

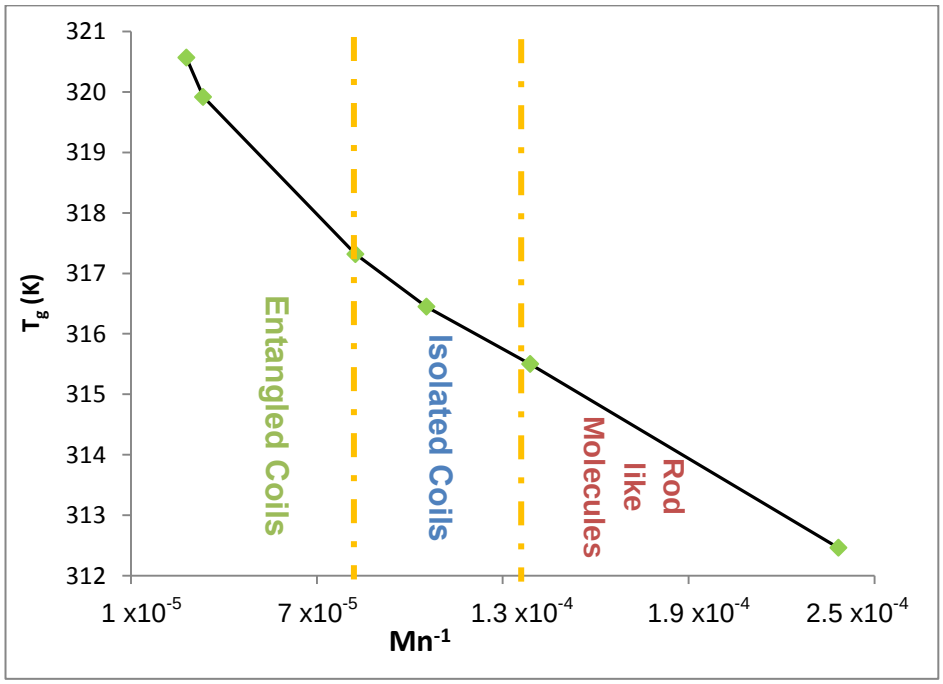

Figure 2.37: Glass transition temperature as a function of $1/M_n$

In other words, Tg is related to the friction constant of the polymer chain segment. Chain entanglement imposes a topological constraint effect on the motion of the polymer chain; namely, the polymer chain follows a reptation process. Thus, it would not be surprising to see that entanglement has an effect on the molecular weight dependence of Tg**.** Where molecular weight of entanglement is considered the point at which Tg starts to be sensitive to the change of Molecular weight. (Lin, 1990)

Effect of Endcapping on Tg

The effect of PLGA endcapping on its thermal properties has been controversial and seems to depend predominantly on the nature of the end group. Several researchers have shown that the change in Tg arises from the ends of the polymer chains, which have more free volume than the same number of atoms in the middle of the chain.(Boyer, 1974, Cown, 1975)

Enhancing the flexibility of the polymer chain was facilitated by introducing ester oxygen into its chain end. It was noted that the recorded Tg of the ethyl ester endcapped PLGA-15K-[E]-E was lower than its non-endcapped counterpart (Figure 2.38.A). As the length of the end groups of the polymer chain increased in length only, for example from an ethyl ester to a dodecyl ester (PLGA-15K-[E]-E to PLGA-15K-[Dd]-E), Tg generally decreases. This occurs because the linear end groups increase the fractional free volume between the chains. (Plazek and Ngai, 2007)

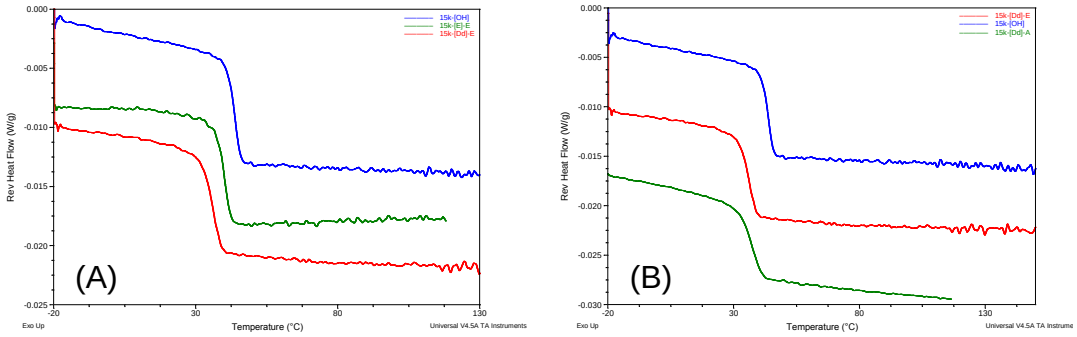

Figure 2.38: DSC curves of (A) PLGA-15K-[E]-E and PLGA-15K-[Dd]-E 2nd heating curve showing the plasticizing effect of the alkyl endcap in comparison to the non-endcapped PLGA-15k-[OH]. (B) PLGA-15K-[Dd]-E and PLGA-15K-[Dd]-A 2nd heating curve. Heating rate of 5°C.min^{-1} to 200°C

From the generated data, both the dodecyl ester and amide end cap of PLGA-15K-[Dd]-E and PLGA-15K-[Dd]-A resulted in an appreciably lower Tg (Figure 2.38.B). This suggested that the dodecyl ester groups at the chain ends are miscible with the PLGA main chain and acts as a plasticizer. The flexible side groups hold chains apart; increase free volume thus lowers T_g, similar results have been previously reported in the literature.(Kobori *et al*., 2004, Samadi *et al*., 2013)

Conversely, increasing the diameter of the end group has the reverse effect as seen with PLGA-15K-[C]-E and PLGA-15K-[Φ]-A (Table 2.5). The positive shift in Tg is attributed to the bulky group added which increases steric barriers to rotation, decreasing chain rotation and thus raising chain stiffness and Tg significantly.(Plazek and Ngai, 2007) In the previous examples qualitatively free volume concepts provided a rationale for observed behaviour. However it does not provide a comprehensive understanding as it dismisses possible interactions between neighbouring polymer chains.(Shen *et al*., 2017)

The stronger the interactions, the greater the thermal kinetic energy must be to create holes of sufficient size to allow a diffusive jump of a chain segment to occur and therefore the Tg will be higher. For example PLGA-15K-[E]-A had a Tg of 44.26 ^{o}C a possible explanation could be the intermolecular interactions between the amide end groups via hydrogen bonding which pull chains together: decreasing free volume and in turn raise Tg. (Pozuelo and

Baselga, 2002) Increasing the polarity or the opportunity for hydrogen bonding between neighbouring chain segments increases Tg. The effects of such variations are illustrated in Table 2.6 where the coupling units are varied in a family of otherwise similar polymers.(Plazek and Ngai, 2007)

Table 2.6: Effect of hydrogen bonding on Tg (Plazek and Ngai, 2007)

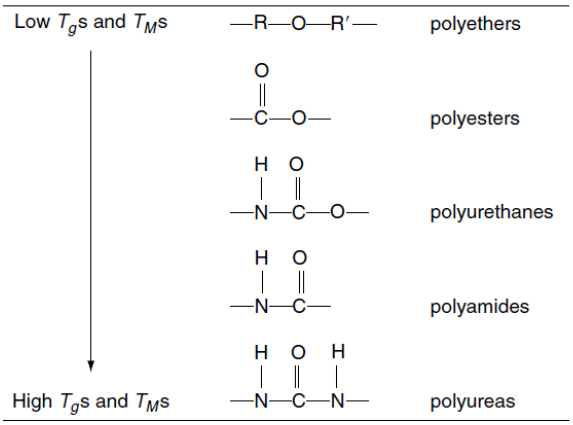

2.3.4.2. Thermogravimetric analysis (TGA)

The results from the TG analyses of the monomers and their respective copolymers are presented in Table 2.7. The T_{onset} , T_{endset} and T_{degmax} values (respectively, the temperatures at which mass loss begins and ends, and maximum degradation temperature) were obtained from the TG and derived TG curves. All of the TG curves presented in Figures 2.39 and 2.40 show mass loss events related to the degradation process, except for the D,L-lactide monomer, in which this thermal event related to its evaporation is observed. Figure 2.39 shows the TGA and DrTGA thermograms of Glycolide [A] and D,L-Lactide [B] over the temperature range from 20 ~ 400^{o}C at a heating rate of 10^{o}C/min under a N_2 purge.

Table 2.7: Thermal properties of monomers and copolymers by TGA.

Sample	T_{onset} (^oC)	T_{deg} (^oC)	T_{endset} (^oC)	Mass Loss (%)
Glycolide	116	189	244	100
D,L- Lactide	111	204*	236	100
PLGA-5K-[OH]	196	341	374	96
PLGA-7K-[OH]	193	290	319	97
PLGA-10K-[OH]	199	296	329	97
PLGA-15K-[OH]	197	291	318	98
PLGA-20K-[OH]	197	294	334	97
PLGA-30K-[OH]	237	339	373	98
PLGA-35K-[OH]	249	379	401	98
PLGA-15K-[E]-E	215	311	390	100
PLGA-15K-[Dd]-E	220	355	368	96
PLGA-15K-[C]-E	236	362	402	98
PLGA-15K-[E]-A	220	328	352	99
PLGA-15K-[Bu]-A	258	371	382	98
PLGA-15K-[Dd]-A	203	373	401	97
PLGA-15K-[Φ]-A	221	335	350	99
PLGA-15K-[Bn]-A	210	295	323	97

*relates to evaporation

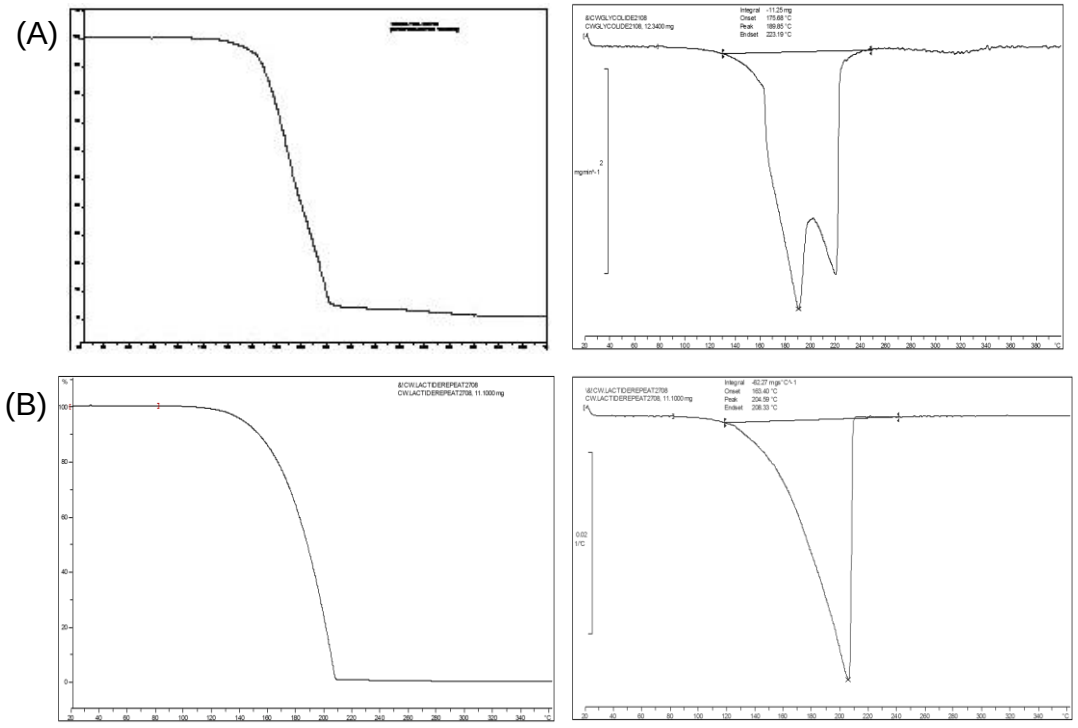

Figure 2.39: TG and DrTG curves of PLGA monomers; Glycolide (A) and D,L-Lactide (B) heating rate 10 $^oC.min^{-1}$ from room temperature to 400^oC.

Figure 2.40 shows TG and DrTG curves for a representative sample of non-endcapped, ester and amide endcapped copolymers. The weight loss versus temperature produced sigmoidal curves with a single mass loss event, suggesting no residual monomer since no mass loss events characteristic of the monomers were observed. The weight of polymers significantly changed when the temperature of analysis reached ~200^{o}C. With weight loss mainly occurring in the range of 200-400^{o}C reaching 100% percentage mass loss (hence compete degradation) in most cases followed by negligible change at temperature higher than 400^{o}C. The existence of only one mass loss stage for the copolymers is confirmed by the single peak observed in the DrTG curves. These TG results corroborate the DSC, FTIR, and NMR results and indicate that the PLGA copolymers have successfully been obtained.

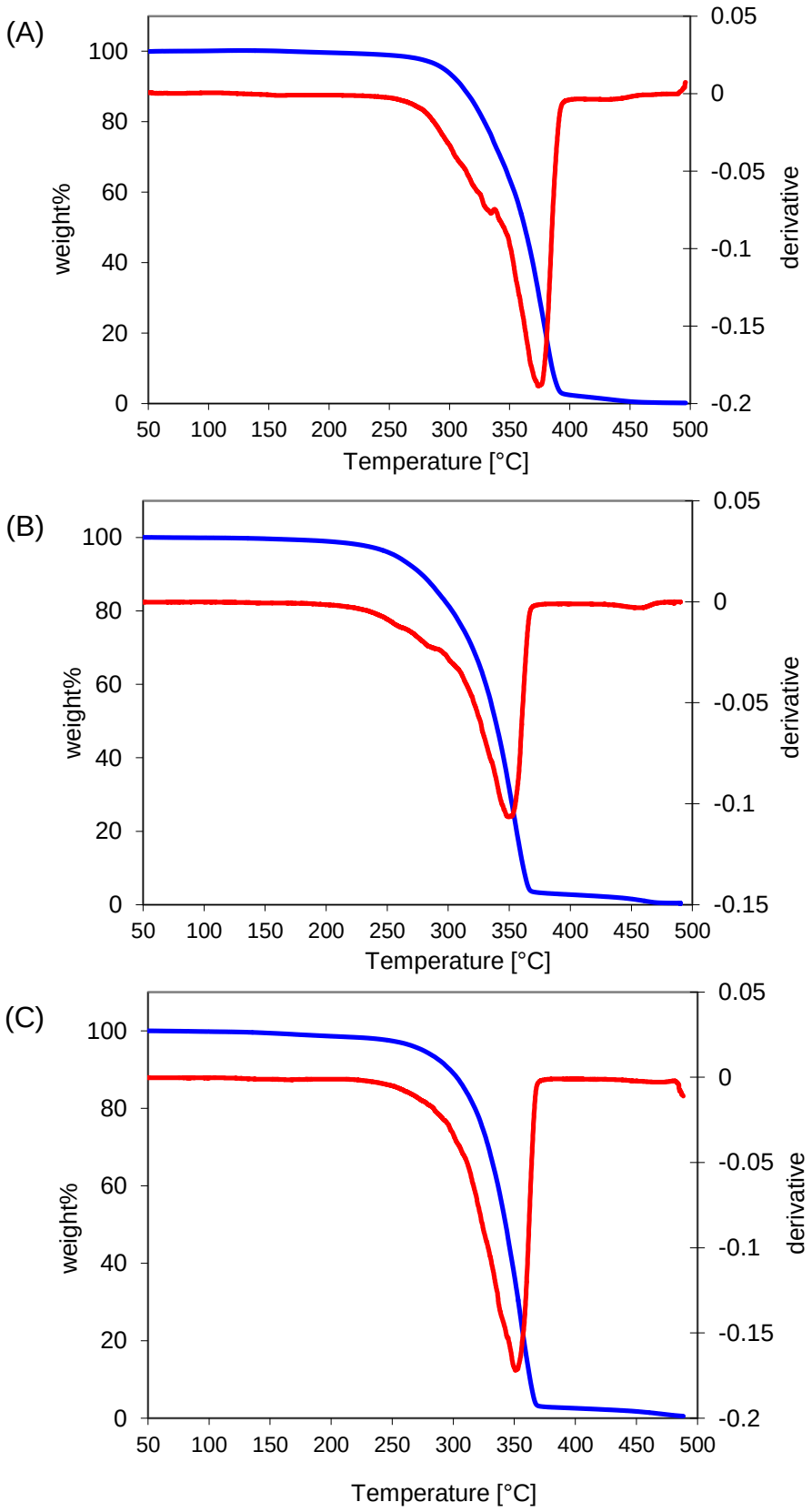

Figure 2.40: TG and DrTG curves of PLGA copolymers; (A) PLGA-30K-[OH], (B) PLGA-15K-[Dd]-E, (C) PLGA-15K-[E]-A heating rate 10 $^{o}C.min^{-1}$ from room temperature to 500^{o}C.

2.4. Conclusion

Three groups of PLGA copolymers have been successfully synthesized. Ring open polymerization was used to synthesis non-endcapped and ester endcapped PLGA. The composition of the synthesized polymers correlated very well to the feeding ratio of lactide to glycolide. The control of the molecular weight was achieved by addition of alcohols. Non-endcapped PLGA was functionalized with amide endcaps using NHS/EDC coupling. GPC measurements showed that the experimental degree of polymerization coincides well with the theoretical degree of polymerization. The NMR spectra of the synthesised copolymers showed chemical shifts in accordance with those anticipated in the literature and confirmed successful endcapping. FTIR analysis of the copolymer spectra showed reference functional groups in agreement with the literature. XRPD indicated all synthesized polymers were amorphous. The glass transition temperatures ranged from 38.91 to 47.58 ^{o}C, depending on the polymer composition and the molecular weight in accordance with the Flory–Fox theory. It can be concluded that the synthesis routes adapted for PLGA copolymers were successful and the copolymers can be fully characterised by FTIR, NMR, DSC, and TG analysis. The next section discusses the essential characterization protocols adapted in an attempt to correlate the different physical and chemical properties of a polymer to its *in vitro* behaviour and thus setting a platform for synthesis of end function oriented, i.e. working with the end in mind.

CHAPTER 3: THE EFFECT OF ENDCAPPING ON THE WATER UPTAKE IN POLY(LACTIDE-CO-GLYCOLIDE),

3.1. Introduction and Objectives

PLGAs are among the few polymers approved by the Food and Drug Administration for clinical use. Owing to their superior biocompatibility, biodegradability and mechanical strength PLGAs have found many applications including carriers in drug delivery systems (DDS). When used as drug delivery matrices the polymers must allow transport of water to permit dissolution of the drug substance. This requires wettability and hydration of the polymer itself. Water uptake plays a vital role in mediating both drug delivery, as well as biodegradation. Water permeability is thus a fundamental property that has intrigued considerable interest due to its relationship with the broad range of the polymer's applications.(Blasi *et al*., 2005)

Hydration of PLGA causes the mass to swell and will change the path length for an eluting species. If the polymer undergoes hydrolysis, the shorter chains decrease glass transition temperature, change the polymer chain mobility and markedly alter drug release. These properties may change gradually or precipitously, as in the case of bulk erosion of PLGA. In this regard, hydration represents the initial step in a rather complex and not completely understood release process. PLGA's hydration kinetics are still poorly understood with few published papers discussing possible moisture

transport routes, yet disagreeing on the dominant mechanism involved. Understanding the effects of hydration on plasticity and the generation of acidic fragments within the polymer is crucial.

Despite numerous publications discussing the effect of copolymer composition and molecular weight on water uptake capacity of PLGA, little is known about the effect of endcapping of the polymer. Endcapping refers to the presence of a hydrophobic end group as the terminal group in the polymer instead of the commonly observed hydrophilic functionalities. An in-depth understanding of the relationship between end group composition and water sorption is lacking since the literature has reported contradicting data. While Singh and colleagues reported a decrease in moisture sorption in poly lactic acid (PLA) due to endcapping, Cairncross and colleagues refuted a significant correlation between sorption and endcapping (Singh *et al*., 2011b, Cairncross *et al*., 2007).

PLGA copolymers have a reported glass transition temperature in the range of 40 to 52^{o}C and therefore remain glassy at room temperature. When introduced into the body PLGAs are in their glassy state at body temperature in their unhydrated form, but become plasticized as they get hydrated since water is a known plasticizer of amorphous polymers. Water uptake into the PLGA delivery system will be influenced by the thermodynamics of the mixing interaction, the concentration dependence of the mass transport coefficient, and chain relaxation effects in the polymer. Physicochemical

characterisation of the polymer, at various stages following introduction into water can be carried out using appropriate instrumentation including contact angle measurement, and advanced gravimetric analysis.

The aim of this chapter was to investigate the effects of water, bulk or vapour, on the physicochemical properties of PLGA namely glass transition temperature (Tg) in the early stage of hydration, prior to the onset of degradation. A DVS instrument was utilized for collecting the data needed for determining the bulk moisture diffusion coefficient for a range of PLGAs. The data was used to understand the water transport mechanisms in PLGA to elucidate if chemical modification by endcapping could be used to modulate moisture uptake properties. This is relevant in the context of its application as an intraocular implant where the polymeric system is in contact with ocular tissues.

3.2. Materials and Methods

3.2.1. Materials

Sorption experiments were run on a selection of both non-endcapped PLGAs and polymers with different end groups to cover the entire design space. Polymers were either purchased (Sigma Aldrich, UK, Purac, Gorinchem Netherlands and PolyScitech, West Lafayette, USA) or synthesized in-house as discussed in Chapter 2. Fifteen PLGA samples were used in the sorption experiments. The molecular weight and Tg of which are listed in Table 3.1

Table 3.1: Analysis of candidate PLGA samples used in Chapter 3

	Sample Label	Molecular Weight		Tg
		M_n	M_w	(^oC)
Non Endcapped	PLGA-5K-[OH]	4335	8910	39.31
	PLGA-7K-[OH]	7201	11923	40.35
	PLGA-10K-[OH]	9980	16018	42.70
	PLGA-15K-[OH]	13790	31393	42.68
	PLGA-20K-[OH]	19771	33926	43.19
	PLGA-25K-[OH]	24507	41866	45.16
	PLGA-30K-[OH]	N/A	N/A	47.42
	PLGA-35K-[OH]	35821	60196	47.58
Ester Endcapped	PLGA-15K-[E]-E	12127	21510	40.90
	PLGA-15K-[Dd]-E	12127	21510	36.30
	PLGA-15K-[C]-E	11217	19430	44.97
Amide Endcapped	PLGA-15K-[E]-A	17849	24288	44.26
	PLGA-15K-[Bu]-A	11376	19558	40.22
	PLGA-15K-[Dd]-A	12667	22056	37.18
	PLGA-15K-[Φ]-A	12703	25297	44.76

As previously described in Chapter 2 non-endcapped PLGA indicates both end groups are a hydrophilic; i.e. a hydroxyl group and a carboxylic acid. Samples were labelled according to their endcap. Endcaps varied Ethyl [E], Butyl [Bu], Dodecyl [Dd], Cholesterol [C], Benzyl [Bn], Phenyl [Φ], while hydroxyl [OH] was designated for the free non-endcapped polymers. The amide series was described as the A series whilst the ester series as E. The approximate molecular weight was given in thousands. For example, a 10,000 g/mol molecular weight PLGA sample initiated with Phenyl ester group is symbolized as PLGA10k-[Φ]-E.

Figure 3.1 illustrates an example of the chemical structures of non-endcapped and endcapped PLGAs. In the ester endcapped series, PLGA samples were prepared with alcohol initiators with different long-chain aliphatic fatty alcohols from ethyl (C2) to dodecyl (C12) leading to varying aliphatic content. Moreover, PLGA with a cholesterol endcap was included in the study to investigate effect of steric/bulky groups. Similarly, the amide series consisted of amide endcaps of various aliphatic content using different alkyl/aromatic amines.

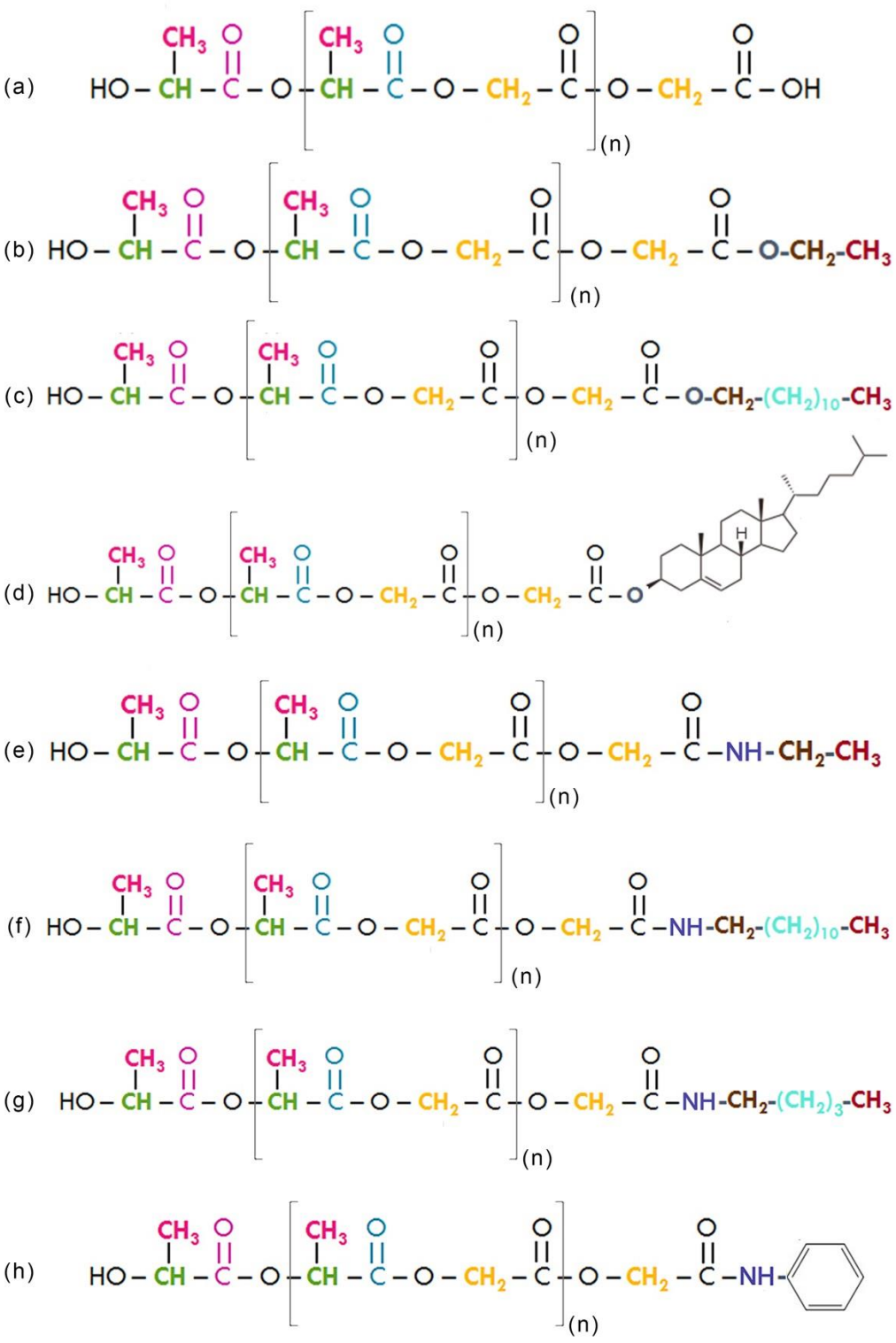

Figure 3.1 Molecular structures of synthesized polymers; standard PLGA-[OH] (a). Ester endcapped PLGAs; PLGA-[E]-E (b), PLGA-[Dd]-E (c), PLGA-[C]-E (d). Amide endcapped PLGAs; PLGA-[E]-A (e), PLGA-[Dd]-A (f), PLGA-[Bu]-A (g), PLGA-[Φ]-A (h).

3.2.2. Instrumentation

Dynamic Vapor Sorption DVS-1 apparatus (Surface Measurement Systems Ltd., London, UK), Digital micrometre (Clarke), Contact angle meter (DataPhysics OCA 15EC), Q5000 SA thermogravimetric analyser (TG-SA)

3.2.2.1. Contact Angle Measurement

The degree of hydrophilicity of PLGA films was investigated using a video-based optical contact angle meter. PLGA/chloroform solutions were prepared by dissolving PLGA pellets in chloroform at 25% w/w and mixing for 2 h to ensure a clear, homogeneous solution. The PLGA/chloroform solution was casted onto a Teflon mould to produce free-standing films (Figure 3.2). The polymer solution was dried at ambient temperature for 24 h, followed by drying at 50^{o}C under vacuum for 24 h.

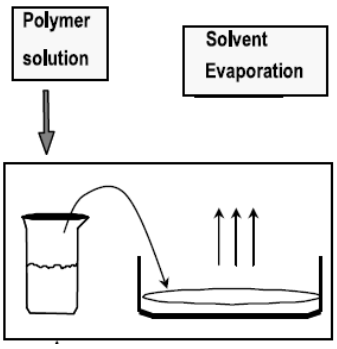

Figure 3.2: Schematic representation of film preparation

Small pieces (4 × 1 cm) of the samples were cut and placed on a glass microscope slide to ensure uniform viewing of the surface. The glass slide

was placed on the stage and a 6μL drop of distilled water was placed on the sample surface. The contact angle on the left and right sides of the drop was measured by the contact angle meter and processed by SCA software. The average of ten angles was reported for each sample.

3.2.2.2. Thermal Gravimetric Sorption Analysis (TG-SA)

Water-uptake properties of the polymers were initially screened using a thermogravimetric analyser from TA Instruments. Figure 3.3 shows a schematic of the Q5000 SA. The analyser is based on a vertical nulling microbalance in which the sample and reference hang-down wires and pans are enclosed in a humidity and temperature-controlled chamber. The balance is thermally isolated from the measurement zone and maintained at a constant 35ºC during experiments to provide the long-term baseline stability required for sorption analysis.

The hang-down wires and sample pan (quartz) are grounded to the balance enclosure to eliminate static effects. A dry nitrogen gas purge at 10 mL/minute assures the dryness of the balance housing. Dried N_2 gas flow (200 mL min^{-1}) was split into two parts. One part was wetted by passing it through a water-saturated chamber, where it is brought to 100 %RH at the temperature of the analysis while the other part remains dry. The desired relative humidity (RH) was obtained by mixing proper proportions (regulated by mass-flow controllers) of dry and wet stream. Capacitance-type sensors

located near the sample and reference pans monitor the %RH to confirm that it is at the desired level. The Q5000 SA can run isothermal experiments in the range of 5-85ºC, and humidity range covered is 0-98 %RH.

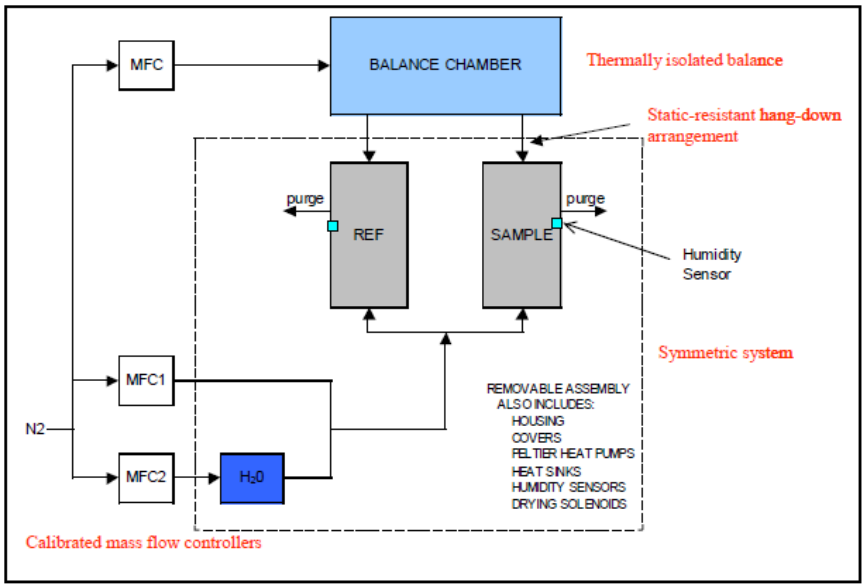

Figure 3.3 TG-SA schematic representation (Hassel, 2006)

The bulk polymer samples were dried prior to analysis by holding the material at 0 %RH for 6 hours at 60ºC and a true “dry weight” obtained. Moisture sorption analyses are usually lengthy because of the time required for the material to reach equilibrium at a specific humidity. Typically, the equilibrium time increases as the %RH increases. With appropriate software, sorption experiments were programmed so that either total elapsed time or the decay of the weight derivative signal, determines when equilibrium at each humidity step has occurred. The latter approach helps reduce the total experimental time, while maintaining the accuracy of the results.

3.2.2.3. Dynamic Vapour Sorption (DVS)

Dynamic vapour sorption is a well-established method for the determination of vapour sorption isotherms. DVS was used to evaluate the effect of endcapping on hydration of PLGA.

(i) Experimental Setup

The DVS-1 instrument (Figure 3.4) used for these studies measured the uptake and loss of vapour gravimetrically using a recording ultra-sensitive microbalance with a mass resolution of ±0.1 µg. The setup consists of two measuring pans (sample and reference) suspended from the arms of a Cahn microbalance. The pans sit in a thermostatically controlled cabinet where the temperature is maintained constant. The relative humidity is controlled by using electronic mass flow controllers to proportionally mix dry carrier gas streams (nitrogen) with moisture-saturated air, at a set flow rate to maintain a selected relative humidity (RH). Thus, in the range 0-95 % RH all levels of RH are possible.

The balance was calibrated with a 100 mg weight and target % RH values were verified using standard salts. In this study, the diffusion of water vapour in amorphous PLGAs was carried out at 25 and 37°C; i.e. below the recorded glass transition and at body temperature. Humidity and temperature probes are located in close proximity to the sample and reference holders providing

direct measurement of these parameters. The temperature and humidity values were very stable during the tests.

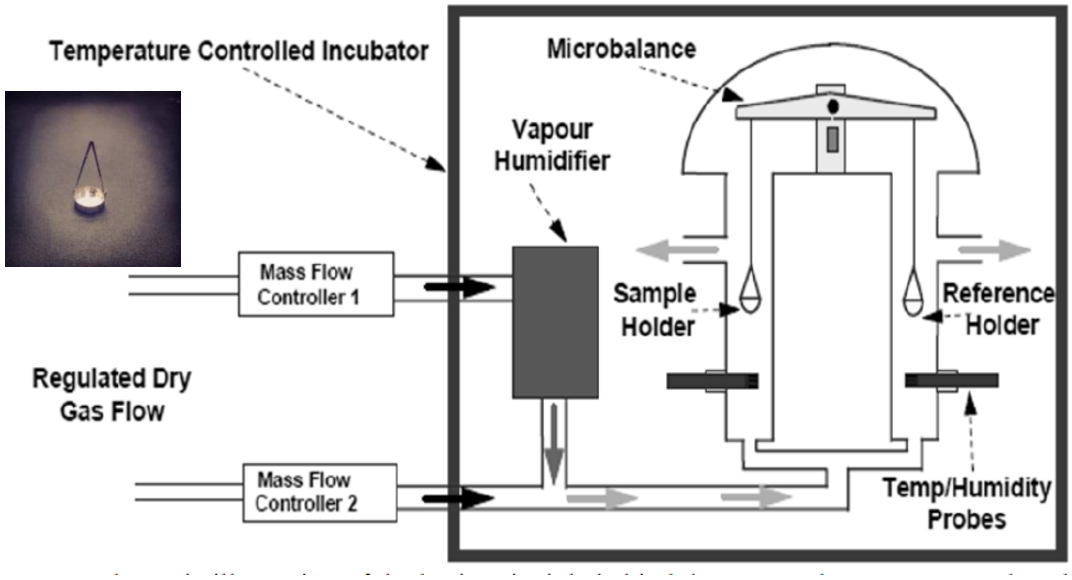

Figure 3.4: Schematic illustration of the basic principle of the DVS. (Engelund *et al*., 2010) DVS pan used (inset)

The DVS sorption automatic operation (SAO) method was used to set both the desired percent relative humidity steps and the equilibrium criterion. According to the experimental design samples were subjected to a controlled cycle of changing relative humidity (RH). Beginning with an initial drying phase, each sample was equilibrated to 0% RH using an equilibrium criterion of a change in mass over time (*dm/dt)* of no greater than 0.0005% per minute, a value that from previous long-term exposure experiments yielded sample moisture content within less than 0.1% of the equilibrium value at extended time. This was done to remove residual moisture.

The instrument produces a ‘‘drying curve’’ with the RH set at zero percent until the sample weight is stable. The total gas flow was parallel to the sample surface and was set at 200 cm^3/min for all experiments. After equilibrium criterion is reached, the relative humidity is ramped to 95% RH as a single step and equilibrated using the same *dm/dt* criterion with a maximum step time of 2000 min. In order to monitor fast diffusion processes, data points were collected every 60s for these experiments. Each sample was run in duplicate.

The data were exported to Microsoft Excel using a DVS Macro. The change in mass of the sample was converted to moisture content by determining the moisture in grams of the initial sample and adding or subtracting it from the weight change measured in the DVS. The total amount of water in grams was then divided by the grams of polymer in the initial sample to calculate the moisture content on dry basis

(ii) Polymer Film Preparation

Polymer cast films were prepared as described previously using 25% w/w PLGA/chloroform solutions. The cast films were dried at ambient temperature for 24 h, followed by drying at 50^oC under vacuum for 24 h. All samples were stored in a desiccator till use to minimise exposure to atmospheric humidity. Prior each experiment, the thickness of the PLGA films was measured using a digital micrometre. Each film thickness was an average of at least three individual measurements at different positions along the length of the film. In

the optimized procedure 10.0 ± 2 mg discs (~9 mm in diameter) of the PLGA films were punched out and placed in a pre-cleaned stainless steel flat sample pan (~10 mm in diameter, Figure 3.4 inset) and carefully placed on the hang down wire connected to the microbalance. The sample chamber was then closed and clamped. The DVS ran at desired temperature and dried at 0% RH to establish a dry mass then a run commenced.

(iii) Determination of the Bulk Moisture Diffusion Coefficient.

When a thin film sample is placed in the DVS, the initial kinetics of sorption for a single step change in humidity can be used to calculate the bulk moisture diffusion coefficient (D). The method used to calculate the diffusion constants for thin films utilizes diffusion equations first employed by Crank and Park. This is done by numerically solving Fick's second law for one dimensional isothermal penetrant diffusion into a thin slab of hydrophilic polymer.(Crank, 1975)

Fickian diffusion is the simplest form of transport of sorbate into substrate where the water concentration gradient is the driving force for the transport phenomena through a defined area. Fick's First Law states that:

$$F = -D\frac{\partial c}{\partial x} \qquad \text{(Equation 3.1)}$$

where *F* the mass flow of water per unit area (kg/s × 1/m^2), is directly proportional to the concentration gradient of the substance in the diffusing medium (dc/dx). *D* is the diffusion coefficient (m^2/s), *C* is the water concentration (kg/m^3), and *x* is the distance (m) in the flow direction.

For the experimental conditions studied here, the following assumptions were made:

(1) *D* is constant for a given sorption experiment,

(2) Swelling (or shrinkage) is negligible, and

(3) Sample is homogeneous.

(4) Diffusion is unidirectional (topside)

The water diffusion coefficient can be obtained from regressing the experimental data (mass versus time) to the solution of Fick's second law. This solution is obtained by solving the one-dimensional continuity equation where the appropriate initial and boundary conditions for the thin slab model used in this study are: initial condition: at $t = 0$, $C = C_0$ for $0 < x < l$, boundary condition: at $t > 0$, $C = C_1$ for $x = l$ and $\partial C/\partial x = 0$ for $x = 0$. Equation 3.1 for the thin slab model may be written as:

$$\frac{\partial C}{\partial t} = D \frac{\partial^2 C}{\partial x^2} \qquad \text{(Equation 3.2)}$$

Where C (kg/m^3) is the concentration of the diffusant (in this case water), *x* is the sample thickness, D is the effective concentration-averaged diffusion coefficient of water in the polymer, and t and x are time and space coordinates, respectively. The initial and boundary conditions specified above correspond to typical conditions found in gravimetric sorption experiments, where the sample is contained in a sample holder and water sorption is occurring via the top surface (one side) of the sample.(Yu *et al*., 2008)

The solution to Fick's second law in the form of a trigonometric series for the above specified conditions is:

$$\frac{M_t}{M_\infty} = 1 - \sum_{n=0}^{\infty} \frac{8}{(2n+1)^2\pi^2}\ exp\left[\frac{-D(2n+1)^2\pi^2\ t}{4x^2}\right] \quad \text{(Equation 3.3)}$$

where M_t and M_∞ denotes the amount of water that diffuses into the polymer at time t, and that at thermodynamic equilibrium as time approaches infinity, respectively.(Crank, 1975) Consequently the gravimetric data can be regressed to Equation 3.4 which is referred to as the slope method for the infinite thin slab model. Equation 3.4 describes the initial kinetics of sorption into the bulk for a one-sided film to determine bulk moisture diffusion coefficient D, which is the only adjustable parameter in this model.(Peppas and Brannon-Peppas, 1994)

$$\frac{\mathrm{M_t}}{\mathrm{M_\infty}} = 2\sqrt{\left(\frac{\mathrm{Dt}}{\pi \mathrm{x}^2}\right)} \quad \text{(Equation 3.4)}$$

When Equation 3.4 is applied for values of $M_t/M_\infty < 0.6$, a plot of M_t/M_∞ against $t^{1/2}$ should be linear. The diffusion constant *D* can then be calculated from the slope of this line where the only input parameter necessary for these calculations is the film thickness.(Burnett *et al*., 2006)

3.3. Results and Discussion

With two hydrophilic end groups; an alcohol initiating end group and a carboxylic acid termination PLGA has relatively high water sorption. The literature review does not provide a solid relationship between end group composition and water sorption. Lee and colleagues reported that longer end groups retarded initial degradation of endcapped PLA.(Lee *et al*., 2001) In similar work Singh and colleagues correlated the increase in aliphatic content via end group modification of PLA to significant decrease in moisture sorption.(Singh *et al*., 2011b) In comparison, Cairncross's work on PLA endcapping indicated insignificant effects of end group on water sorption isotherms.(Cairncross *et al*., 2007)

The current study illustrates how moisture sorption in PLGA is a multifactorial process and is affected by the total polymer composition. In other words, the fraction of the polymer that has the hydrophobic end groups, the fraction that has the hydrophilic end groups, the length of the polyester backbone, and the free volume of the polymer. The effect of molecular weight on moisture barrier properties of standard PLGA was scanned to determine the design space. This was followed by endcapping of PLGA at the selected molecular weight range to investigate the dependence of moisture uptake properties on endcapping.

3.3.1. Effect of Molecular Weight on moisture sorption in PLGA

Preliminary data from contact angle measurements on non-endcapped PLGA-[OH] films indicated dependence of polymer hydrophilicity on molecular weight. Molecular weight was varied systematically to observe the changes in hydrophilicity. Increase in molecular weight inversely correlated to polymer hydrophilicity, demonstrated by the increase in the recorded contact angle as shown in Figure 3.5.

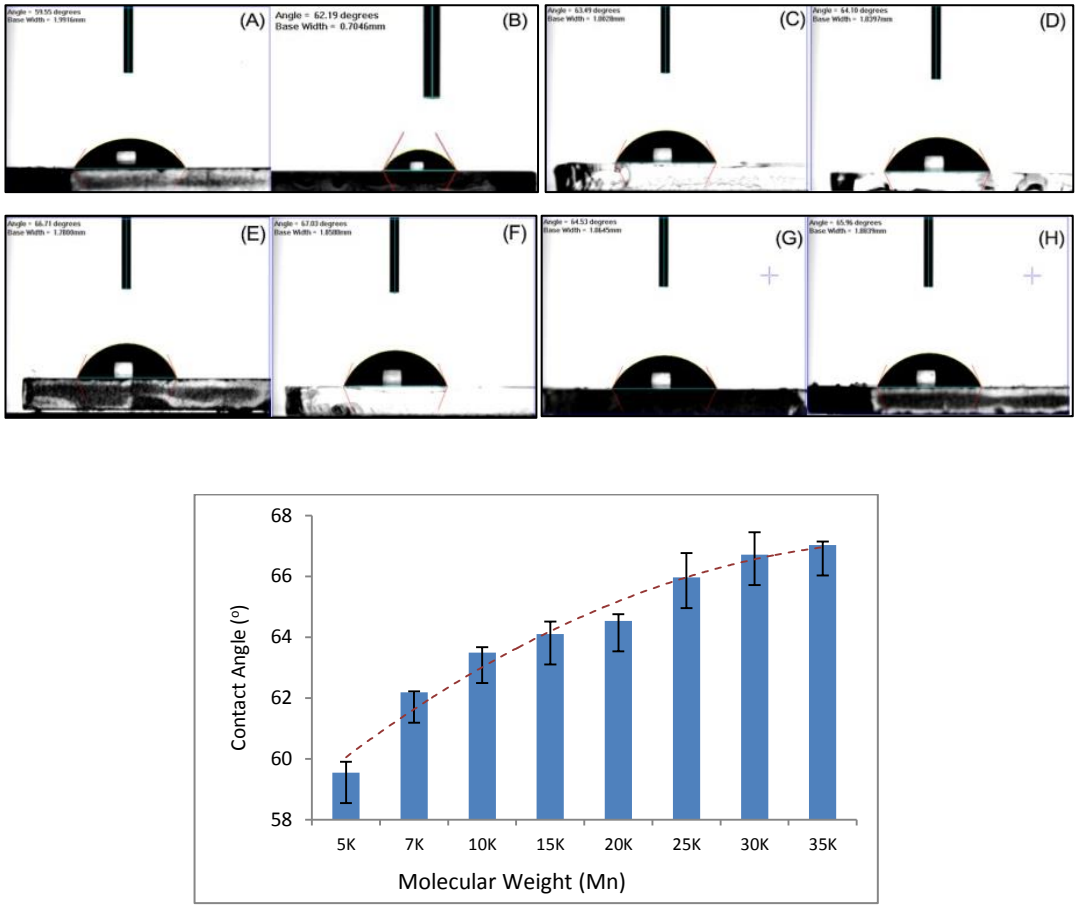

Figure 3.5: **Upper panel**; contact angle images of standard PLGA-[OH] films of increasing molecular weights (M_n) (A) 5K, (B) 7K, (C) 10k, (D) 15K, (E) 20K, (F) 25K, (G) 30K, (H) 35K. **Lower Panel**; Recorded contact angle measurements of standard PLGA-[OH] shows the increase in hydrophobicity of the polymer with increase in molecular weight.

The change in mass of a sample upon moisture uptake is a highly sensitive way of investigating the hydrophilic nature of materials.(Buckton and Darcy, 1996) DVS sorption isotherms were conducted at 25°C on a series of non-endcapped PLGA samples. The average thicknesses of the polymer films were measured by a digital micrometre, varied between 48 – 52 µm. An overlay of all DVS sorption isotherms is shown in Figure 3.6 where the y-axis represents percent change in mass in the films due to moisture sorption. The mass uptake by the polymer film is considered zero at the lowest actual relative humidity.

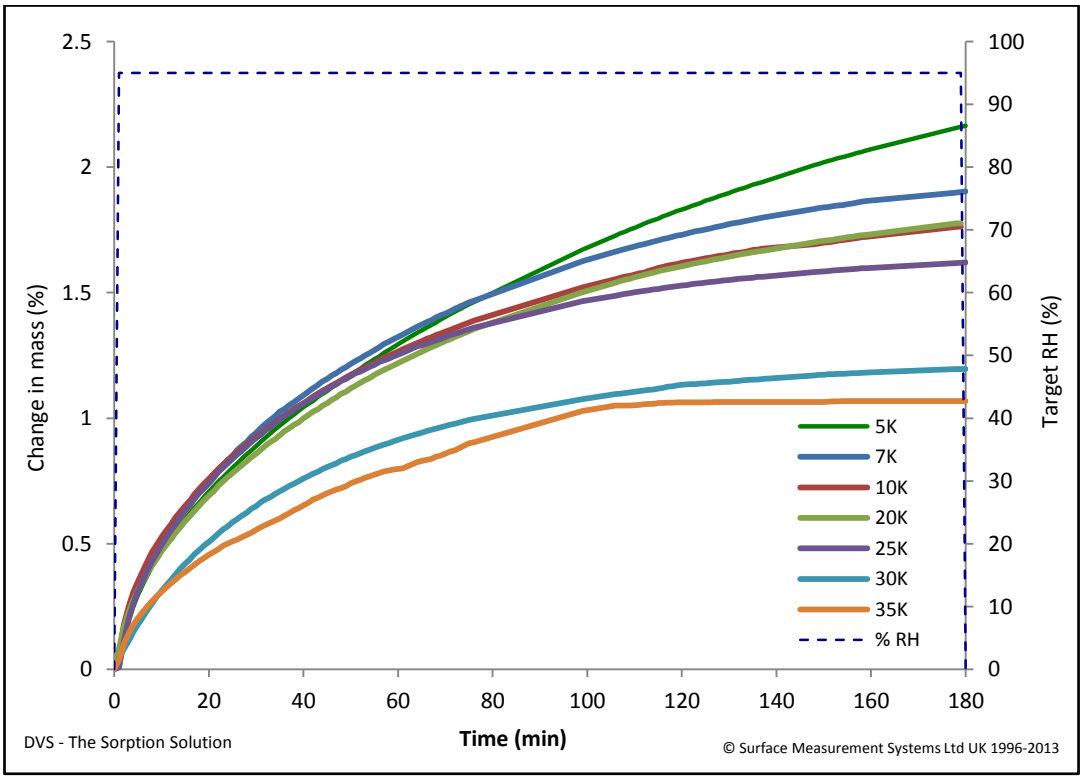

Figure 3.6: The effect of molecular weight (M_n) on DVS sorption isotherms of non-endcapped PLGA-[OH] samples at 95% Relative Humidity for 3 hours at 25^{o}C after 2 hours of drying. Percentage change in mass (left y-axis) decreases with increasing molecular weight.

Moisture sorption decreased monotonically with increasing molecular weight. The percentage of moisture sorption ranged from 1.07 to 2.16% (w/w) recorded at the highest and lowest molecular weight; PLGA-35K-[OH] and PLGA-5K-[OH], respectively. Although the percentage change in mass seems small (up to 2%), this is consistent with work reported by Bouissou and colleagues on PLA, where DVS data for PLA with molecular weight of 12,500-136,500, showed percent weight changes between 1.1 and 1.3% respectively.(Bouissou *et al*., 2006) Figure 3.7 illustrates the trend in sorption with increasing molecular weight. Hydrophilicity of the end group domains of the polymer chains is a major driving force. As molecular weight increases the concentration of hydrophilic hydroxyl and carboxylic acid end groups decreases, hence the inverse correlation of molecular weight to moisture sorption. For example, increasing molecular weight from PLGA-20K-[OH] to PLGA-35K-[OH] resulted in a 50.67% decrease in moisture uptake.

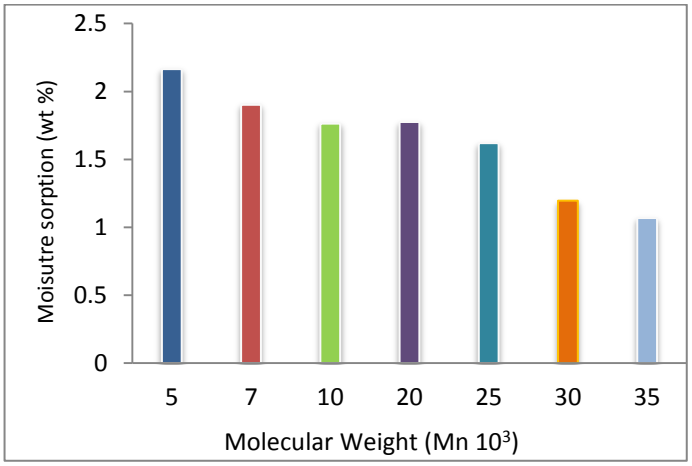

Figure 3.7: Effect of molecular weight of non-endcapped PLGA on total moisture sorption at 25^{o}C. Moisture uptake (%) decreases with increasing molecular weight

Within the accuracy of the experimental data, the sorption isotherms were nearly identical in samples of molecular weight (10 and 20K) without discernible difference (Figure 3.7). Taking the lowest molecular weight polymer as reference, a plateau was observed in Figure 3.8 indicating that the sorption isotherms at moderate molecular weights (10 –20 K), were not sensitive to the change of molecular weight. Hence, moisture sorption was considered independent of molecular weight in that range and the contributions of both aliphatic and hydrophilic end groups can affect sorption in logical ways. The T_g of the studied polymers followed a similar trend plateauing in the molecular weight range of 10 – 20 K. Accordingly recorded changes in moisture sorption could be solely correlated to endcap modifications.

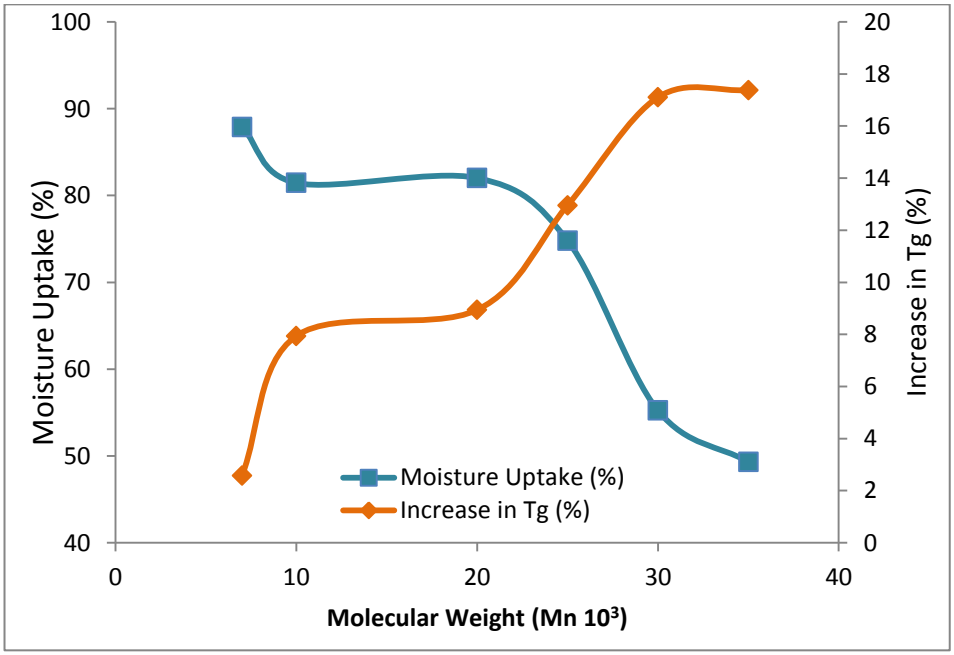

Figure 3.8: The effect of increasing Molecular weight on change in moisture uptake and T_g of PLGA-[OH] samples relative to the lowest molecular weight in the series (PLGA-5K-[OH]), n =3.

At low molecular weight, the high concentration of the hydroxyl end group imparts hydrophilicity and increases free volume leading to higher water sorption. As the molecular weight increases concentration of the hydroxyl groups decrease and water sorption decreases approaching a limiting value close to 1.7 w/w% moisture uptake, at moderate molecular weights.

This suggests that sorption may be more effectively modified by varying aliphatic content than by varying molecular weight.(Singh *et al*., 2011b) At relatively higher molecular weights increase in molecular weight approaching molecular weight of entanglement radically decreases moisture uptake due to decrease in polymer flexibly and chain mobility.(Lin, 1990)

Based on the previous findings to probe the relationship between moisture sorption and endcapping, sorption of PLGA samples having different terminating end groups but fixed molecular weights (~15k) at 95% relative humidity were studied. PLGA-15K-[OH] was set as the control. Figure 3.9 displays the typical moisture sorption kinetic results obtained at 25 ˚C. The solid trace displays the percentage change in mass, referenced to the dry mass, versus time on the left axis while the dashed trace shows the chamber RH as a function of time on the right axis.

The DVS sorption automatic operation (SAO) method was used to set both the desired percent relative humidity steps and equilibrium criterion. The sample was equilibrated to 0% RH using an equilibrium criterion of a change

in mass 0.0005% for 5 consecutive minutes. After this equilibrium criterion was reached, the relative humidity was increased automatically to the target value (95% RH) and equilibrated using the same d_m/d_t criterion. The calculated change in mass for the PLGA-15K-[OH] sample was 1.7% which is in accord with the mass change recorded for the selected molecular weight range (10-20K).

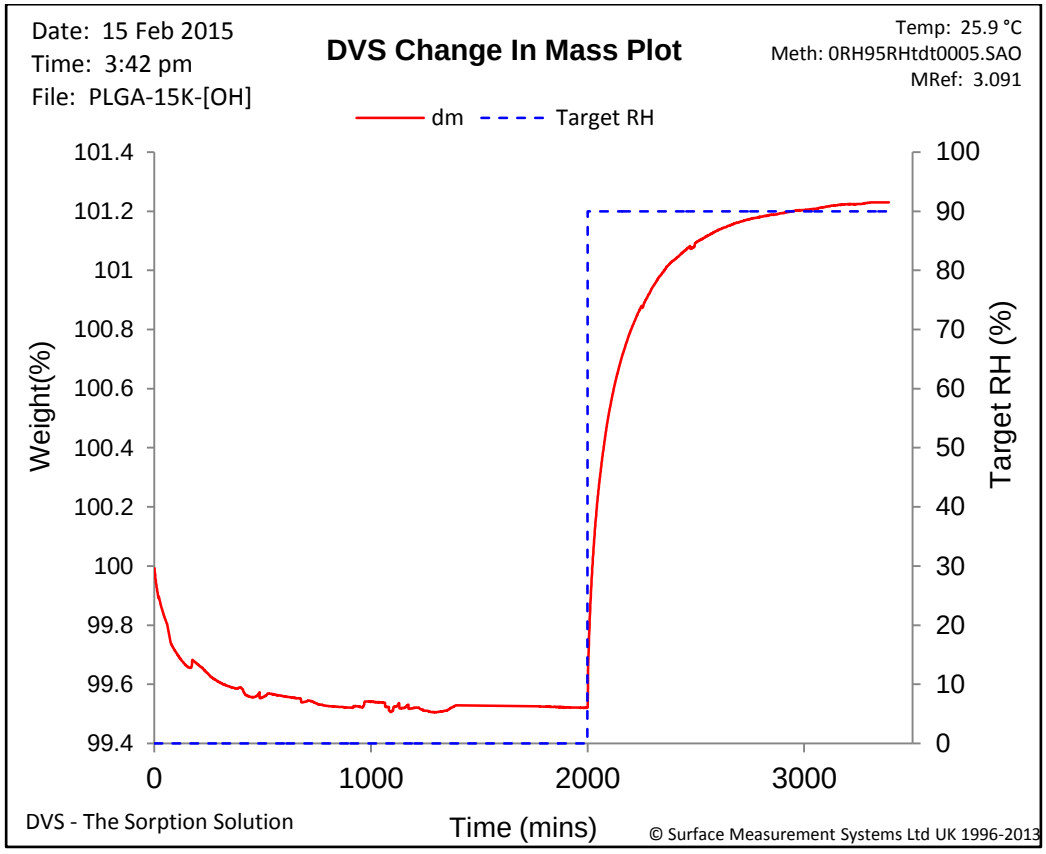

Figure 3.9: Kinetic water sorption profile for PLGA-15K-[OH] sample. The as is PLGA sample was first equilibrated to 0% RH (initial sample equilibration to a moisture content close to zero) then equilibrated to 90% RH (sorption step) with both steps being carried out at 25^{o}C.

3.3.2. Effect of Endcapping on moisture sorption in PLGA

The following section focused on the effect of two functional groups namely; ester and amide on moisture uptake profiles of PLGA. These investigations were followed by the determination of the effect of the chain length on the water-uptake ability. TG-SA, and DVS techniques were used to fully explore the effect of endcapping on moisture uptake properties.

3.3.2.1. Effect of Modified Endcapping

Studying the effect of the nature of the endcap, dodecyl ester PLGA-15K-[Dd]-E and amide endcapped PLGA-15K-[Dd]-A showed different sorption dependency due to different morphologies when compared to the non-endcapped PLGA-15K-[OH], control. Figure 3.10 displays the TG-SA water vapour sorption isotherms for the three polymeric films studied at 25°C.

One way ANOVA statistical test was performed to compare the mean of moisture sorption achieved in triplicate TG-SA runs of the following group PLGA-15K-[OH], PLGA-15K-[Dd]-A and PLGA-15K-[Dd]-E. It was found that the difference in the sample means was statistically significant at 95% confidence level. The introduction of a hydrophobic dodecyl ester endcap in PLGA-15K-[Dd]-E resulted in a significant decrease (31.08%) in moisture sorption when compared to PLGA-15K-[OH] as a control (Figure 3.10 inset).

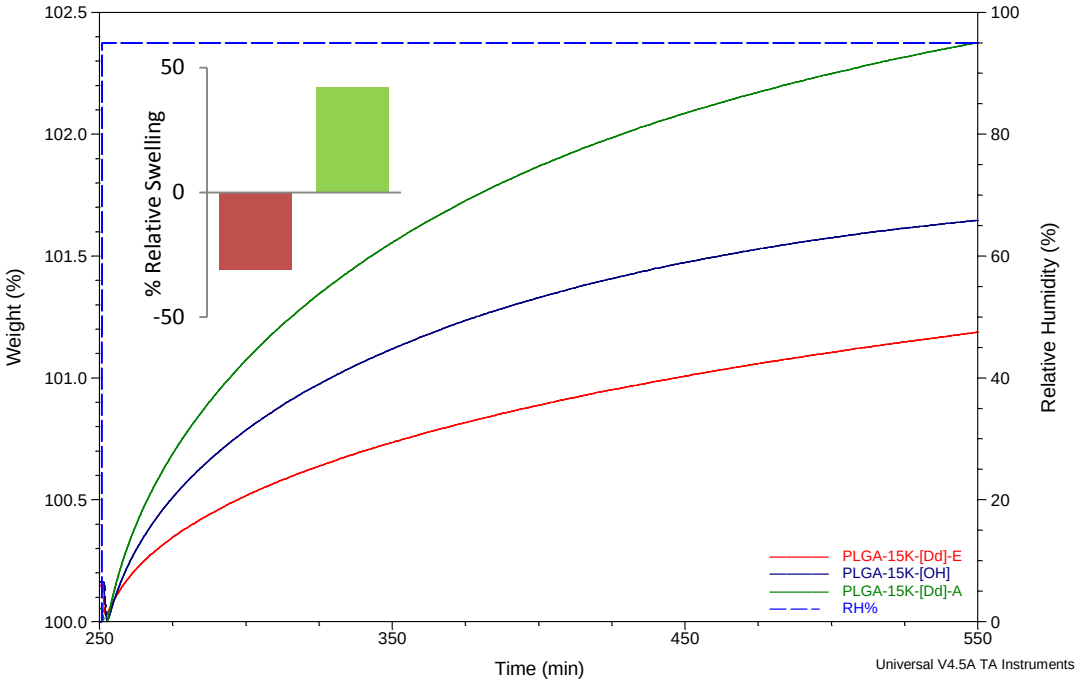

Figure 3.10: TG-SA isotherms of PLGA-15K-[OH], the ester endcapped PLGA-15K-[Dd]-E and amide endcapped PLGA-15K-[Dd]-A demonstrating the weight change (%) as a function of the relative humidity (%) the humidity was increased from 0% up to 95% RH at 25^{o}C after an initial drying phase. Moisture uptake varied with nature of endcap. Ester endcap (red line) decreased moisture uptake whereas amide endcap (green line) increased it, in comparison to the non-endcapped control (blue line).

On the contrary, the dodecyl endcap did not impart similar moisture sorption reduction in the amide endcapped series. In fact, PLGA-15K-[Dd]-A moisture sorption was significantly higher than the control; PLGA-15K-[OH]. Figure 3.10 inset revealed that PLGA-15K-[Dd]-A sorbs 42.06% and 73.14% more than PLGA-15K-[OH] and PLGA-15K-[Dd]-E respectively. One hypothesis for PLGA-15K-[Dd]-A superseding the moisture sorption capacity of PLGA-15K-[OH] in spite of the dodecyl endcap, is the presence of amino groups that have the ability to interact with water molecules.(Aburahma and Mahmoud, 2011)

The hydrogen bond formed with water at the amide conjugate lead to a drop in T_g. Water is known to act as plasticizer reducing the T_g of amorphous polymers and alters their elastic modulus.(Blasi *et al*., 2005) Pragmatically, two processes are progressing upon hydration. First the polymer absorbs water according to its diffusion coefficient. Then water induced plasticity of the chains leads to polymer relaxation and enhanced water mobility which has been described as the diffusion relaxation phenomena.

In fact Berens and Hopfenberg used a two-stage diffusion-relaxation model to describe the transport mechanisms of water in PLGA over the entire experimental time scale.(Berens and Hopfenberg, 1978) Their work concluded that the total mass of penetrant uptake in a polymer is divided into two parts, one for the Fickian process and the other for the relaxation process described by their model:

$$M_t = M_{t,F} + M_{t,R} \qquad \text{(Equation 3.5)}$$

Where M_t is the total mass uptake at time t and $M_{t,F}$ and $M_{t,R}$ are the contributions of the Fickian and relaxation processes, respectively, at time t. Therefore, in gravimetric experiments for a thin slab model, the first part describing the Fickian solution can be inserted in for $M_{t,F}$, while the second part describing a first-order relaxation can be inserted into $M_{t,R}$.(Davis *et al*., 2013)

Berens and Hopfenberg suggest that when segmental relaxation is slow then one should observe a rapid Fickian first stage followed by a slower discernible separate second relaxation-controlled sorption stage, however when diffusion and relaxation proceed at the same rate as in the case of PLGA-15K-[Dd]-A the two stages are additive and not clearly separable.(Berens and Hopfenberg, 1978) It now becomes evident that great care must be taken for each experiment to extend the experimental time for the film thickness used to appropriately observe the non-Fickian diffusion−relaxation phenomena.

From the previous findings, the nature of the endcap contributes significantly toward sorption properties. Therefore, in the following section the effect of the aliphatic content on moisture sorption on the ester and amide endcapped series will be discussed separately.

3.3.2.2. Effect of Ester Endcapping

A selection of ester endcapped PLGAs was used to investigate the effect of increasing the hydrophobic content via end group modification on moisture sorption. Contact angle measurements in Figure 3.11 demonstrate the increase in overall polymer hydrophobicity with increase in endgroups' chain length when samples with the same molecular weight but varying aliphatic content are compared.

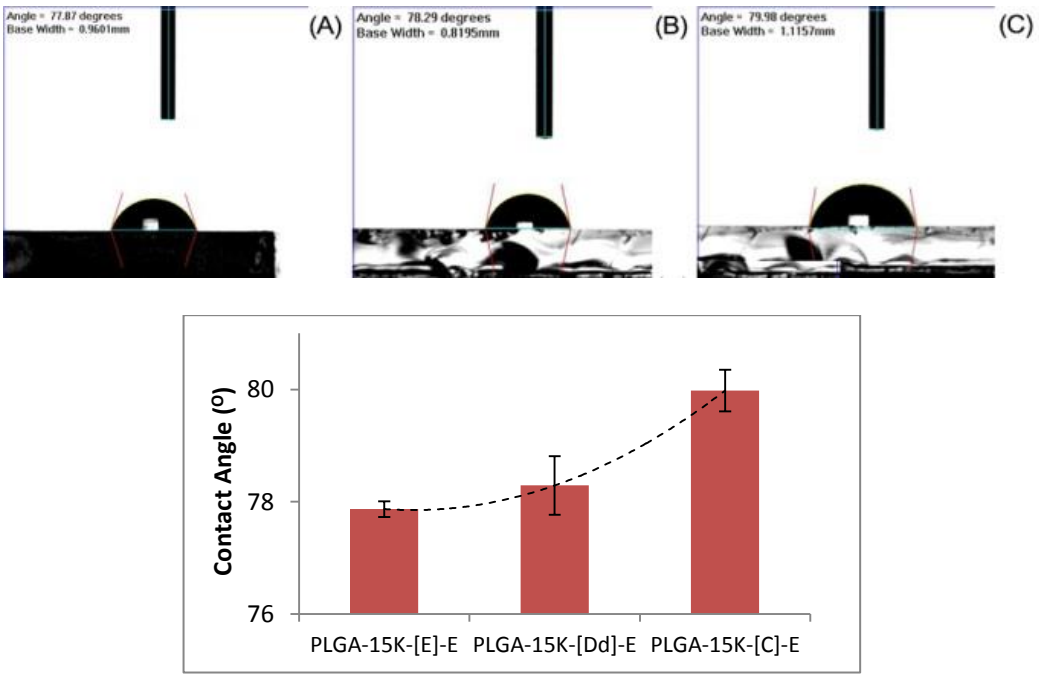

Figure 3.11: Effect of increasing hydrophobic content of ester endcap on contact angle measurements, a) PLGA-15K-[E]-E, b) PLGA-15K-[Dd]-E and c) PLGA-15K-[C]-E. Hydrophobicity of the polymer films increased with increasing hydrophobic content of the end group

Comparing samples with approximately the same molecular weight and with increasing hydrophobic content of endcap improves insight about the effect of end groups on sorption properties. A consistent decrease in water sorption seen in the TG-SA moisture sorption isotherms in Figure 3.12 was observed. The highest water sorption value was observed for PLGA-15K-[E]-E, which has a short aliphatic group on the initiating end and a hydrophilic hydroxyl group on the terminating end. The larger relative mass uptake suggests a lessened impact of the endcap (7.31% moisture uptake reduction). Water sorption decreased as the aliphatic content in the endcap increased, reaching a minimum in the isotherms of the PLGA-15K-[C]-E samples (39.63% moisture uptake reduction).

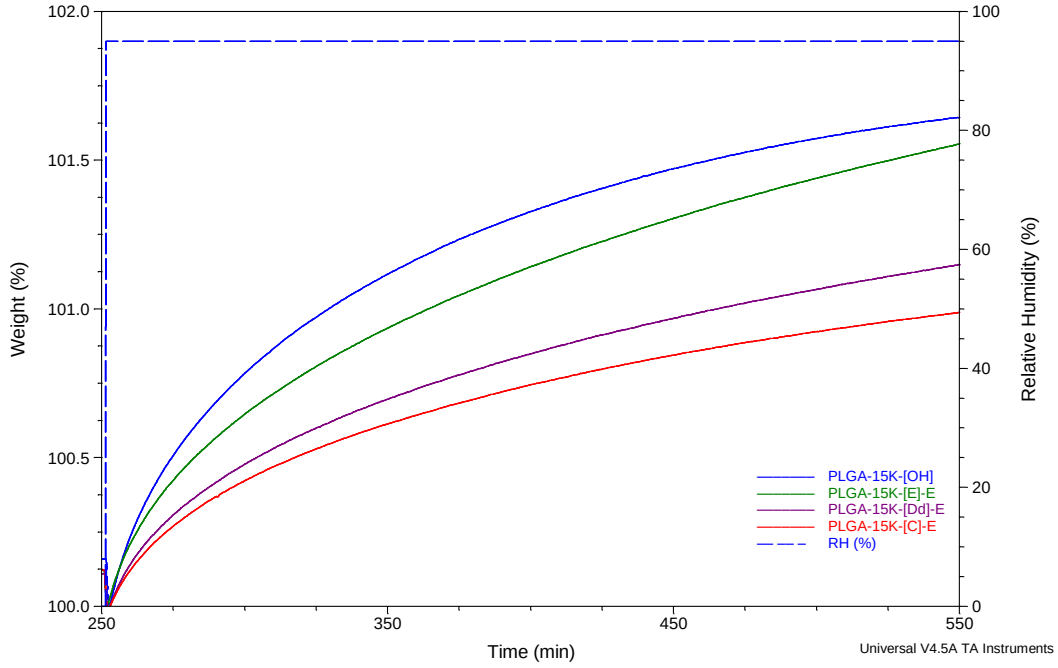

Figure 3.12: TG-SA isotherms of non-endcapped PLGA-15K-[OH], and the ester endcapped series demonstrating the weight change (%) as a function of the relative humidity (%) the humidity was increased from 0% up to 95% RH at 25^{o}C after an initial drying phase. Increasing the hydrophobic content of the ester endcap decreased moisture uptake of the polymers.

Singh and colleagues found that an increase in mass percentage of endcap aliphatic content from 0.6% (butyl polylactide) to 2.3% (palmityl polylactide), resulted in a 14 wt.% decrease in a moisture sorption.(Singh *et al*., 2011b) DVS sorption isotherms performed on cast films of the ester endcapped series corroborated TG-SA results (Figure 3.13). A comparison of PLGA endcapped with ethyl ester end groups with varying molecular weights (PLGA-5K-[E]-E and PLGA-25K-[E]-E) is shown in Figure 3.14-3.15. As molecular weight decreases from 25K to 5K, the mass fraction of the ethyl end group relative to the main polymer chain increases.

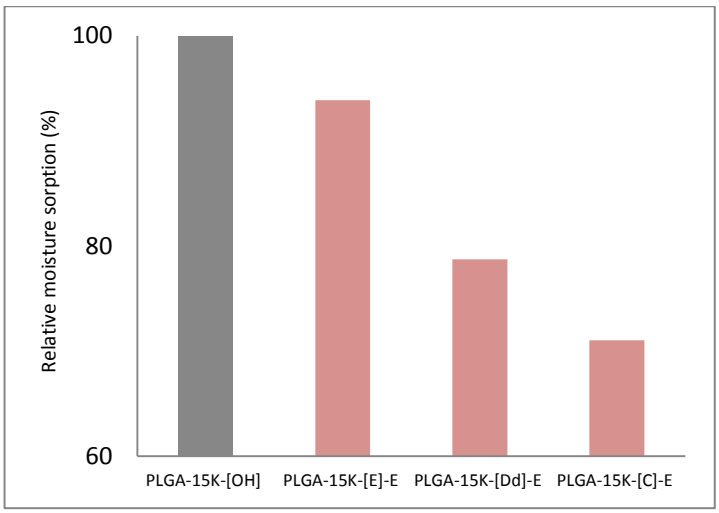

Figure 3.13: Summary of total moisture uptake of ester endcapped PLGA films (n =3) relative to standard nonendcapped PLGA derived from DVS sorption isotherms carried out at 25^{o}C and 95% RH. A decrease in total moisture uptake corelated with increase in hydrophobic conent of end group.

Thus total moisture sorption decreases as the hydrophobic content in the polymer chain increases. On the contrary with the increase of the molecular weight, the number of end groups decrease, and their effect is phased out. It is noteworthy to point out that both molecular weight and mass fraction of end group relative to polymer chain contribute towards sorption properties. Although the increased polymer hydrophobicity imparted by ester endcapping resulted in a more pronounced reduction in the sorption properties of the samples at the lower molecular weight. Simultaneously in a counteracting manner water uptake is enhanced due to increased free volume as molecular weight decreases. This explains the higher relative decrease in water sorption between PLGA-5K-[E]-E and PLGA-25K-[E]-E when compared to their non-endcapped control polymers shown in Figure 3.14-3.15. (Singh, 2008)

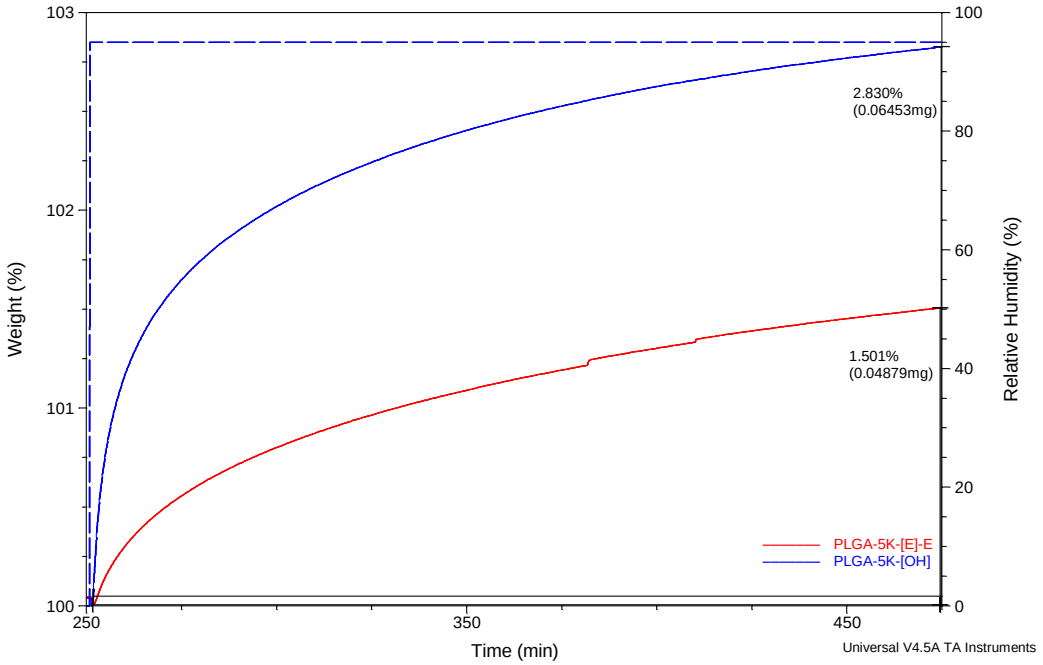

Figure 3.14: The effect of Ethyl ester endcapping at 5K measured by TG-SA at 25^{o}C.

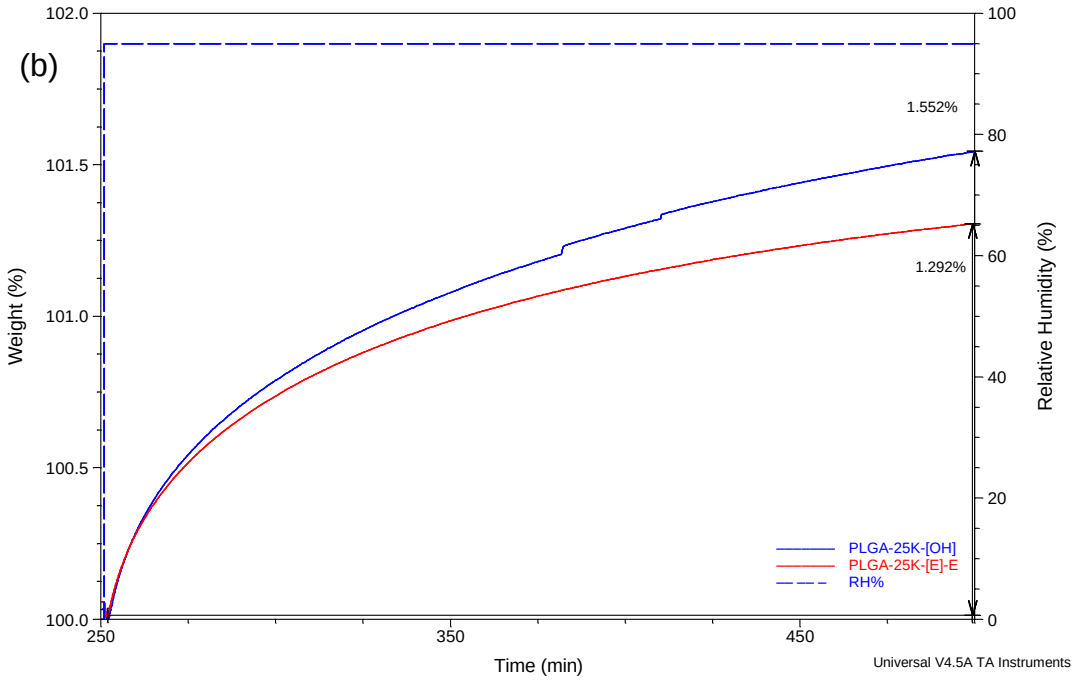

Figure 3.15 The effect of Ethyl ester endcapping at 25K measured by TG-SA carried out at 25^{o}C.

All the previous moisture sorption studies were conducted at 25^{o}C which is significantly below the glass transition of all the test polymers. The Tg of a polymer determines the physical state of the polymer at a given temperature. Running the tests at 25^{o}C mimics temperatures encountered during storage of a DDS. However, since the polymers are intended for biological purposes the reference temperature will be the physiological temperature of 37^{o}C.

If the Tg of a polymer is below the body temperature, the polymer is in a rubbery state. In contrast, if the Tg of a polymer is above the body temperature, the polymer is in a glassy state. A rubbery polymer matrix has a higher permeability to water than a glassy polymer, which results in faster polymer hydration, degradation, and drug release. A glassy polymer will gradually become a rubbery polymer due to the Tg decrease caused by hydration. Thus, it was necessary to run sorption studies at 37^{o}C which is close to the glass transition temperature of some polymers (refer to Table 3.1) and would therefore mimic their performance *in vivo*. Figure 3.16b illustrates that the polymers' moisture uptake profiles followed the previously discussed trend where percentage mass change is inversely correlated to the hydrophobic content of the end groups.

However, the sorption isotherms at 37^{o}C revealed two important observations. First, both total mass uptake and rate of moisture uptake increased in all samples at 37^{o}C in comparison to 25^{o}C as shown in Figure 3.16.

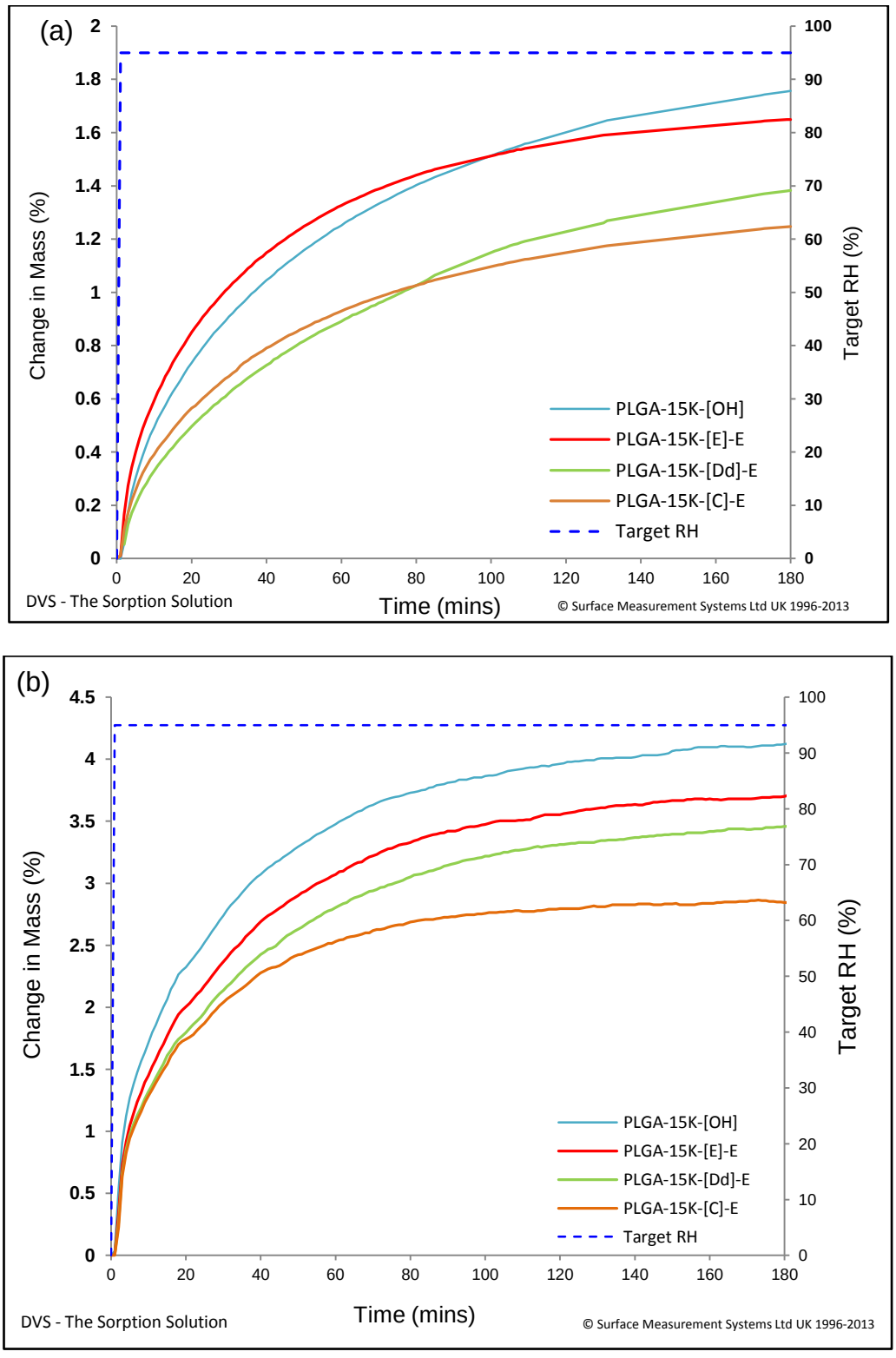

Figure 3.16: DVS isotherm overlay of showing PLGA ester endcapped series; PLGA-15K-[E]-E, PLGA-15K-[Dd]-E and PLGA-15K-[C]-E run at (a) 25^{o}C and (b) 37^{o}C and 95% RH. Polymers moisture uptake increases at elevated temperatures for all studied end groups

This could be attributed to increase in diffusion kinetics as the water mobility increases due to more available energy. In addition to the increase in moisture uptake due to increase in the mobility of polymer chains as temperature increases approaching T_g. Second, the highest increase in moisture uptake was recorded for the dodecyl endcapped polymer, PLGA-15K-[Dd]-E where the samples sorbed approximately 61% more at 37^{o}C than at 25^{o}C unlike the other two test samples PLGA-15K-[E]-E and PLGA-15K-[C]-E where increase in moisture uptake was limited to 56% as seen in Figure 3.17.

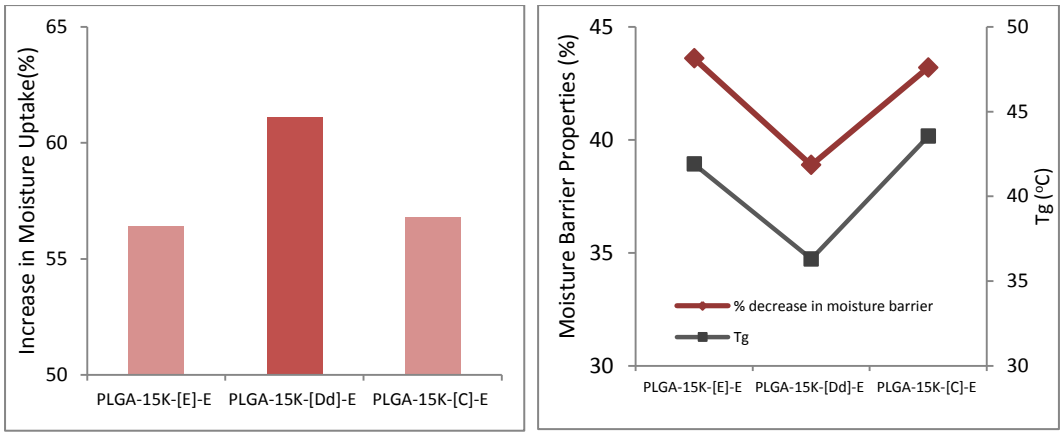

Figure 3.17 Effect of ester endcapping on DVS sorption isotherms at 37^{o}C which demonstrate the effect of Tg on polymer chain mobility influencing water sorption

When the decrease in moisture barrier properties is compared to the polymers' T_g post endcapping (Figure 3.17) it becomes evident that T_g plays a critical role as diffusion is coupled with increased chain mobility at elevated temperatures. The properties of PLGA-15K-[Dd]-E significantly change as the operating temperature approaches polymer's Tg (36.3^{o}C). Once in a

rubbery state, the polymer chains become more mobile. With higher molecular mobility, there is greater propensity for the polymer to undergo physical and chemical changes which explains the unexpected behaviour of the mass uptake. The effect of water on the Tg of polymers has been well established in the literature and will be further discussed in Chapter 5

3.3.2.3. Amide Endcapping

The amorphous PLGA-15K amide series terminated by ethyl, butyl, phenyl and dodecyl amide endgroups, followed the expected trend in hydrophilicity determined by contact angle measurements as seen in Figure 3.18. Data of the moisture sorption experiments of both the amide endcapped polymers conducted using TG-SA at 25^{o}C and DVS at 37^{o}C are depicted in Figures 3.19 and 3.20 respectively. Both isotherm overlays indicate that amide endcapping resulted in different moisture uptake behaviour in comparison to the ester endcaps. A possible explanation is the preferential hydrogen bonding of water at the amide endcaps acting as a plasticizer resulting in a significant drop in Tg and hence increased polymer chain mobility.(Blasi *et al*., 2005) The significantly higher moisture uptake by the dodecyl endcapped polymer suggests that the dodecyl groups at the chain ends are miscible with the PLGA main chain and acts as a plasticizer, similar results have been previously referred in the literature as an in situ plasticizer.(Kobori *et al*., 2004, Samadi *et al*., 2013)

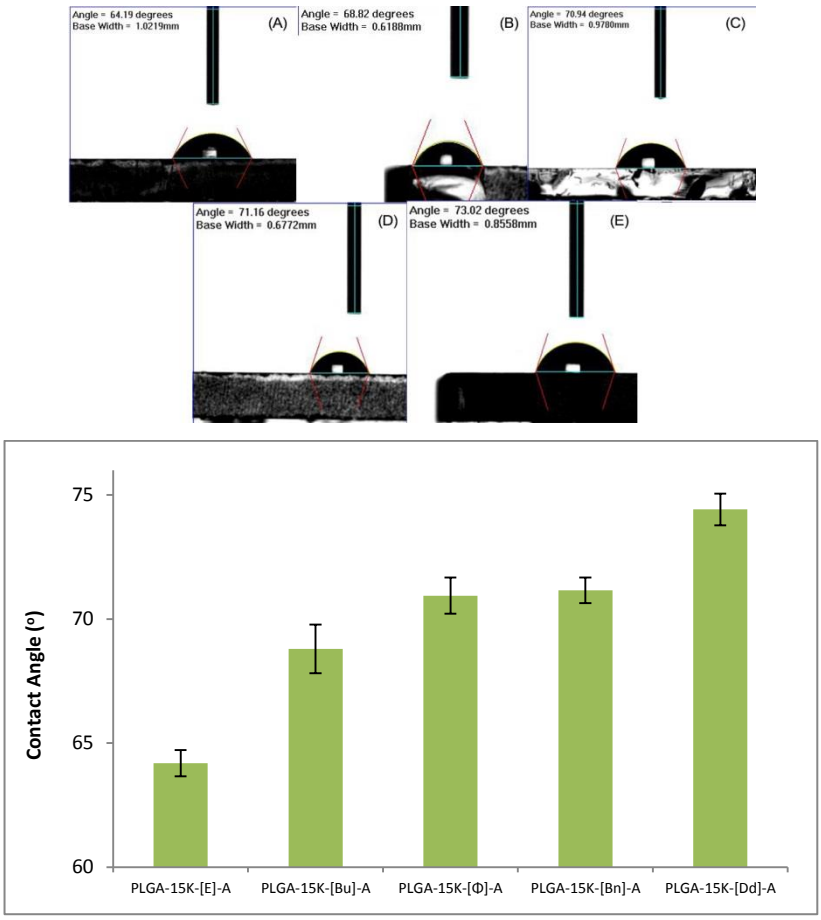

Figure 3.18: Effect of increasing hydrophobic content of amide endcap on contact angle measurements, a) PLGA-15K-[E]-A, b) PLGA-15K-[Bu]-A, c) PLGA-15K-[Φ]-A, d) PLGA-15K-[Bn]-A, and e) PLGA-15K-[Dd]-A. Increased contact angle indicate increased hydrophobicity of the polymer films, n =3.

The presented data illustrates that not only does the aliphatic content of the end chain affect polymer's hydrophilicity but also the nature of the end group and its interaction with water. Plasticization occurs when a small molecule blended with a glassy polymer results in a decrease of its T_g and hence the elastic modulus. Such plasticization normally increases polymer flexibility and chain mobility (Sperling, 2001). Thus the properties of a polymer can be modified in the presence of another substance depending on the nature of the association between the two phases (Blasi *et al*., 2005).

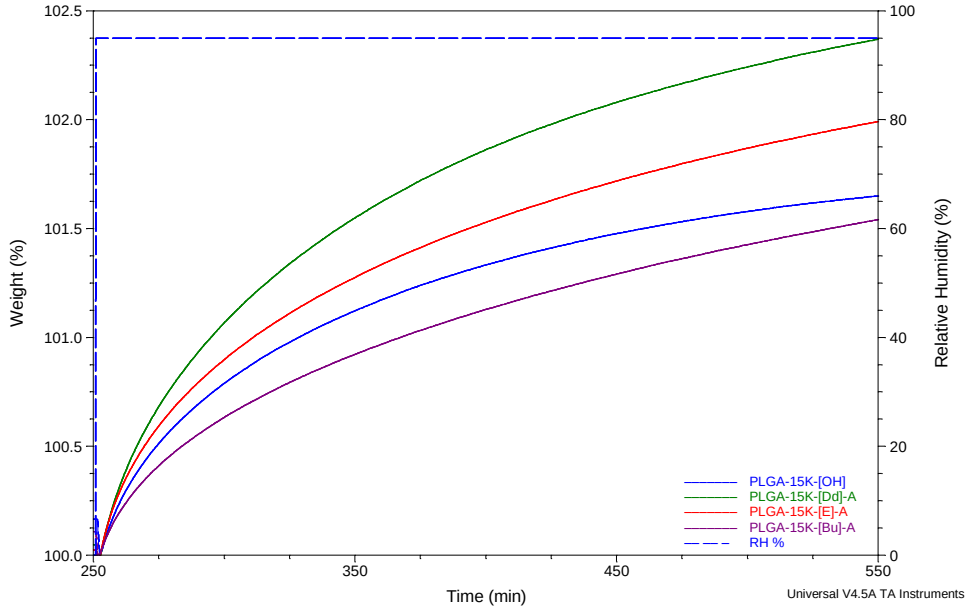

Figure 3.19: TG-SA isotherms of the amide endcapped series demonstrating the weight change (%) as a function of the relative humidity, the humidity was increased from 0% up to 95% RH at 25^{o}C after an initial drying phase

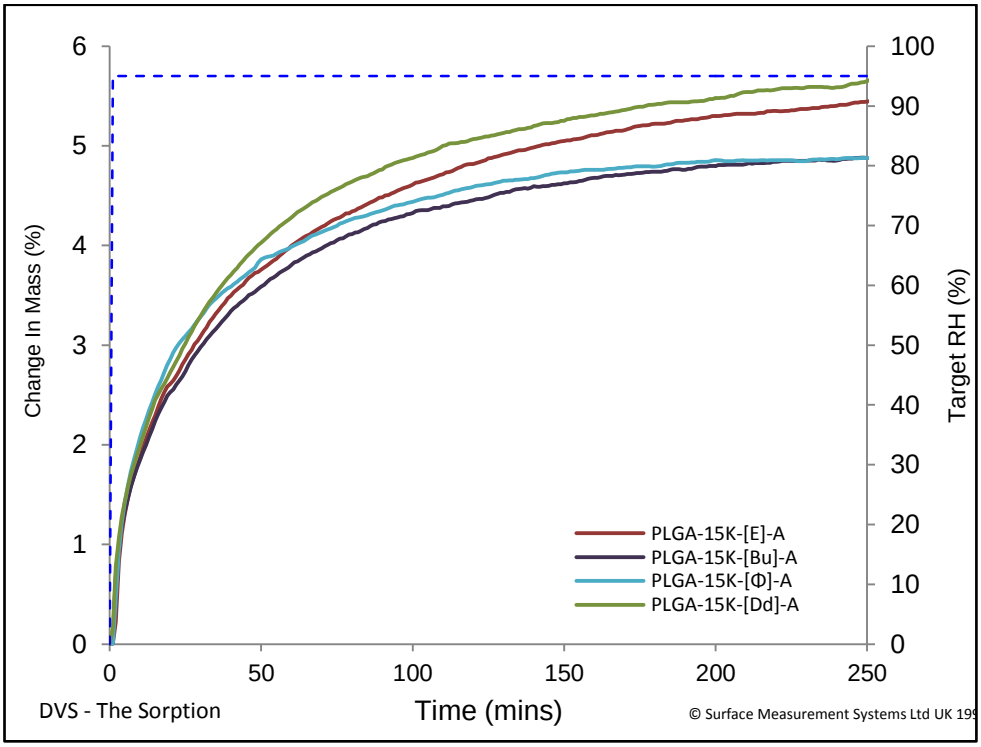

Figure 3.20: DVS isotherm overlay of PLGA amide endcapped series at 37^{o}C and 95% RH.

It is worth noting that the thicker substrates used in TG-SA runs explain the lower total moisture uptake by the samples in comparison to those used in the DVS study. Substrate thickness and structure may impede water from fully penetrating the bulk, thus causing a lower percentage weight gain. The thinner substrates had a greater surface to bulk ratio, thus the surface layers were able to sorb more water vapour comparatively than the bulk (Burnett *et al*., 2006).

The change in mass of a sample upon water uptake is a highly sensitive way of investigating the hydrophilic nature of materials (Bouissou *et al*., 2006). However the rate of water uptake is a crucial parameter in determining polymer performance. In all studied polymers non-Fickian behaviour was observed, where two phenomena occur over two distinct time periods in the same experimental time scale; diffusion driven by a water concentration gradient for the first stage and diffusion driven by a slower (relative to the first stage) polymer relaxation for the second stage (Del Nobile *et al*., 2002).

Since water diffusion varies due to several factors, particularly the plasticization of the polymer chains upon moisture sorption an in depth understanding of the underlying mechanism of transport in the polymer films will be discussed in the next section.

3.3.3. Understanding the underlying mechanism of transport and calculations of diffusion coefficient

In this section, the effect of endcapping on the diffusivity of water molecules in the PLGA copolymers was investigated gravimetrically. The weighing method has been employed by several authors to determine water diffusion coefficients in substrates (Yoon *et al*., 2000, Peppas and Brannon-Peppas, 1994, Yu *et al*., 2008). The water diffusion coefficient of the polymers was calculated from the weight variation of film type specimens of known shape and size kept in an atmosphere of constant diffusant vapour pressure measured at regular intervals. An example of diffusion coefficient calculation is given below using the DVS kinetic water sorption profile of PLGA-15K-[OH] at 37^{o}C and 95% RH (Figure 3.21).

PLGA-15K-[OH] Sample Diffusion Coefficient (D) Calculations

To compute the diffusion coefficient the polymer film sample was first equilibrated to 0% RH (initial sample equilibration to a moisture content near zero), then equilibrated to 95% RH (sorption step) with both steps being carried out at 37°C. As shown in Figure 3.21, once the sample was exposed to 95% RH, the sample mass began increasing due to moisture sorption. At the beginning of sorption (time = t_0) mass of water uptake = 0 was assigned when the relative humidity of the sample chamber was initially switched from 0% RH to the target relative humidity (95% RH).

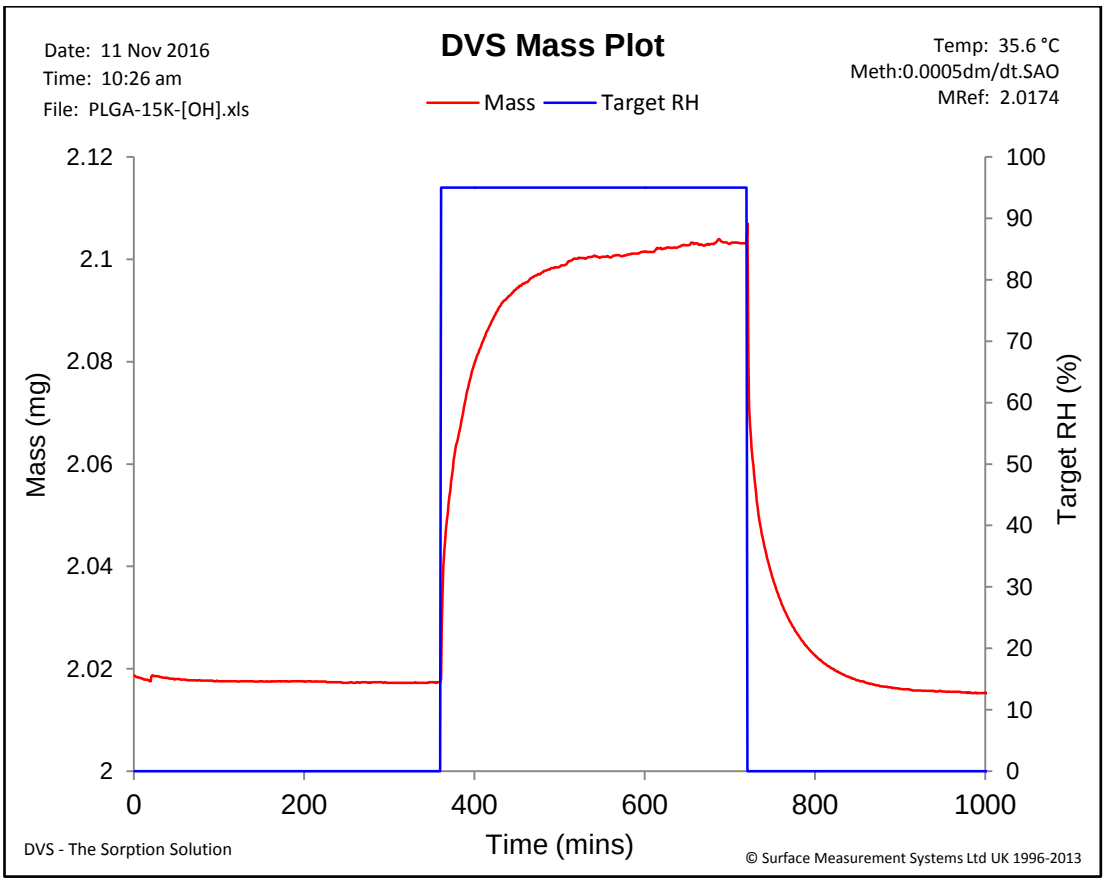

Figure 3.21: Example showing the kinetic water sorption profile for the PLGA-15K-[OH] sample initially equilibrated at 0% RH (drying step) then equilibrated to 95% RH (sorption step) followed by a desorption step equilibrated at 0% RH, with all steps being carried out at 37^{o}C

On average, it took approximately 2 min for the system to reach 97.5% of the target relative humidity and each polymer film sorption experiment lasted 18 hours. Taking the example shown in Figure 3.21 t_0 began at 360 min (marked as sorption time = 0 s), the initial mass of the sample (weight of the dry PLGA film) was 2.02 mg (with 0 g of water uptake and 0 moisture content), the final equilibrium mass of the sample was 2.13 mg reached at 720 min ($\sim t_\infty$) when dm/dt was <0.0005% for 5 min with M_∞ equal to 0.11 mg of water uptake. M_t/M_∞ was plotted as function of time as shown in Figure 3.22

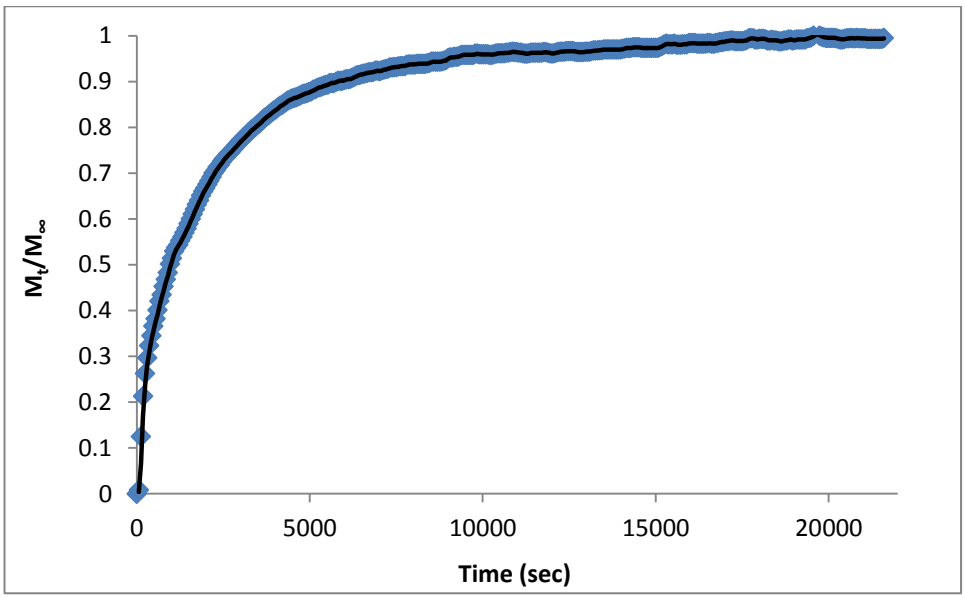

Figure 3.22: M_t/M_∞ moisture sorption values plotted as a function of time in seconds for PLGA-15K-[OH] from 0 to 95% RH at 37°C.

Experimental values of M_t/M_∞ < 0.6 were then plotted as a function of the square root of time in seconds as shown in Figure 3.23, along with the linear fit and resultant equation from which the diffusion coefficient was calculated.

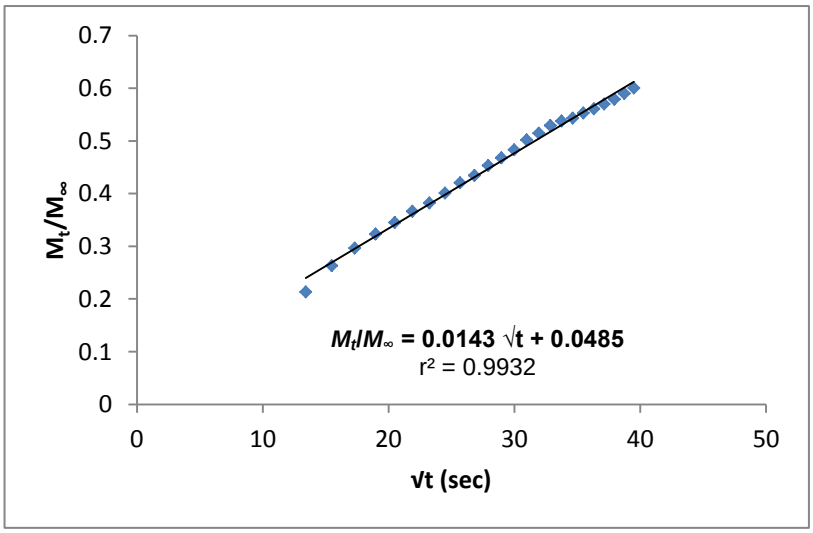

Figure 3.23: M_t/M_∞<0.60 moisture sorption values plotted as a function of the square root of time in seconds for PLGA-15K-[OH] from 0 to 95 RH at 37°C.

The mass uptake was fitted to a simple Fickian, concentration-independent diffusion model. Substituting the value of the slope from Figure 3.23 into equation 3.4 and solving for D yields $D = (0.0143)^2 \pi x^2/4$. The diffusion coefficient was found to be 3.39 x 10^{-11} m^2/s with x = 0.00046 m. This value is consistent with vapour diffusion values published by Sharp and colleagues. (Sharp *et al*., 2001)

Studying the effect of molecular weight on polymer diffusivity, Figure 3.24 illustrates that not only does molecular weight affect the extent of moisture sorption but also the rate of sorption. This suggests that at lower molecular weights the PLGA matrices are more hydrophilic and readily hydrated.

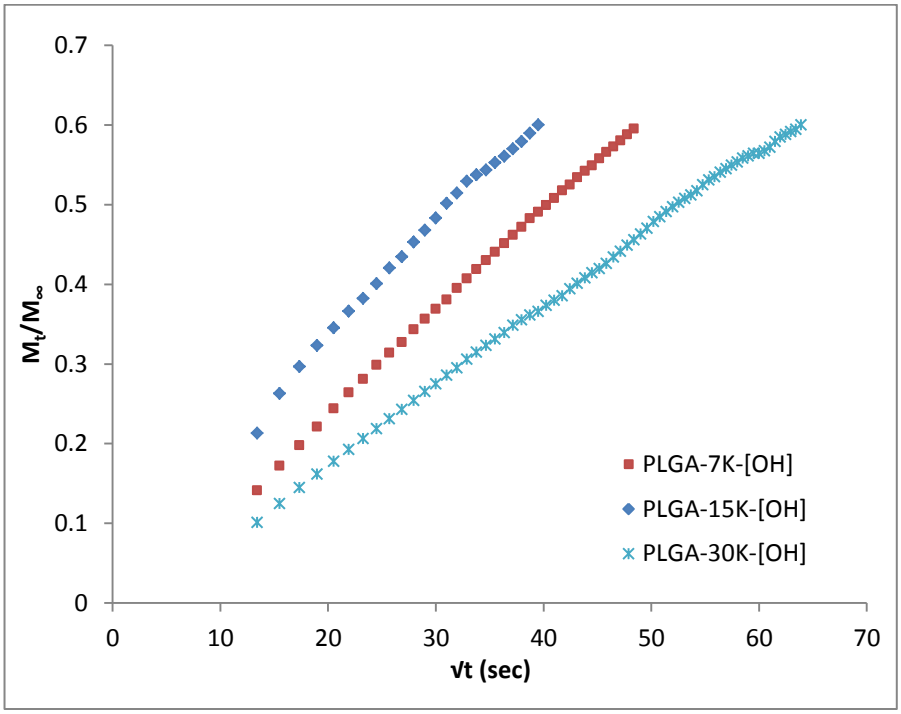

Figure 3.24: M_t/M_∞ values < 0.60 plotted as a function of the square root of time in seconds for non-endcapped PLGA of varying molecular weight (7, 15 and 30K) moisture sorption from 0 to 95% RH at 37^{o}C.

It is worth stressing at this point that the slope method calculates the average diffusion coefficient for the first 60% of the moisture absorption, which normally occurs over the first 10% of the experimental time frame during which the driving force remains large (Yu *et al*., 2008). In addition the diffusion coefficient of water is likely to be highly concentration dependent, and as the polymer is plasticized, it will vary by orders of magnitude.

The current model suffers several limitations and caution should be taken during data analysis. In reality, the polymer film thickness is expected to change as a function of temperature and humidity due to different degrees of swelling which is not accounted for.

Moreover, the mathematical model is based on the assumption that the surface concentration is instantaneously increased to the constant penetrant concentration, at the start of the experiment. Although the relative humidity in the DVS does increase rapidly, it is not instantaneous. Peppas and Brannon investigated this boundary problem by considering a system in which the water concentration was initially zero and the water concentration at the surface approached an equilibrium concentration exponentially, which they say represents the conditions encountered in a dynamic sorption experiment.(Peppas and Brannon-Peppas, 1994)

In addition, the uptake of water by the studied films is not governed by the simple diffusive processes that occur during water transport in bulk swelling

where the samples directly uptake water and display bulk polymer properties. Instead in the DVS setup water uptake is limited by transport of the water through air. Therefore the kinetics of water uptake obtained in the thin film experiments are much slower than those expected for a bulk system.(Sharp *et al*., 2001)

Effect of Endcapping on Diffusion Coefficient (D)

To investigate the effect of different endcaps on PLGA's moisture uptake rates, the sorption moisture diffusion coefficients of PLGA thin films at relative humidity values 95% at 37 °C was calculated using the slope method (Equations 3.1-3.4) using the absorption data. Thickness was determined as previously described in section 3.2. Thickness of all the samples varied from 45 to 53 μm and the average *D* for $M_t/M_\infty < 0.60$ values for the sorption relative humidity study at 37°C were calculated and listed in Table 3.2. The r^2 values obtained for the slope method were all >0.990, ranging from 0.991 to 0.997. This indicates that the thin slab model was a good fit to the data.

Table 3.2: Moisture diffusion rates measurements in PLGA films measured at 37^{o}C and 95% RH

Polymer	Diffusion Coefficient (m^2s^{-1})	r^2
PLGA-15K-[OH]	3.84×10^{-11}	0.995
PLGA-15K-[Dd]-E	2.54×10^{-10}	0.996
PLGA-15K-[E]-E	5.66×10^{-11}	0.992
PLGA-15K-[C]-E	4.86×10^{-11}	0.993
PLGA-15K-[Dd]-A	7.08×10^{-10}	0.991
PLGA-15K-[Bu]-A	3.11×10^{-11}	0.997
PLGA-15K-[Φ]-A	2.17×10^{-11}	0.996
PLGA-15K-[E]-A	2.08×10^{-11}	0.996

Comparing the non-endcapped PLGA-15K-[OH] film with the endcapped PLGA-15K-[Dd]-E sample we found experimentally that despite its lower total moisture uptake the rate of uptake was initially faster in the endcapped specimen, hence reaching equilibrium faster (Figure 3.25). The water diffusivity in the PLGA-15K-[OH] film was almost 2 orders of magnitude lower than that of its endcapped counterpart.

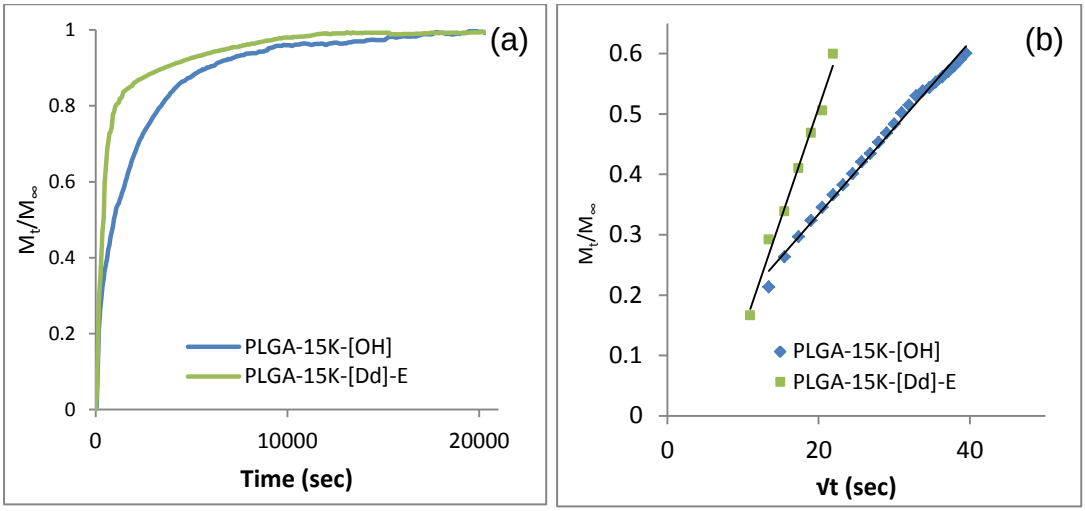

Figure 3.25: (a) water sorption kinetics in PLGA films at 37°C in response to relative humidity step change of 0 to 95 %. (b) Regression of M_t/M_∞ values < 0.60 to the solution of Fick's Second Law where the diffusion coefficient is the only adjustable parameter.

The longer time witnessed in the PLGA-15K-[OH] sample could be interpreted as follows. Water molecules sorbed on the surface of the film associate with each other and form clusters through preferential binding to each other by hydrogen bonding. This behaviour is less evident for the hydrophobic endcapped polymers surface therefore a larger driving force for water uptake originates from the larger chemical potential difference across

the water vapour/polymer interface. Since according to the solution– diffusion model, water molecules are not necessarily soluble in the polymer and permeate through the polymer in the cluster form in response to a concentration gradient.(Yoon *et al*., 2000)

Moreover, build-up of osmotic stresses in the non-endcapped films are expected to be larger since the polymer takes longer to completely relax as the operating temperature is below its Tg. So, at the increased humidity, the osmotic stresses introduced in the early stages of swelling slow down the subsequent rate of water uptake and give rise to longer equilibration times, as previously reported by Sharp and colleagues who studied moisture uptake in PLGA and PLA.(Sharp *et al*., 2001)

Thus, measurement of moisture uptake by the polymer during the initial stages of hydration is crucial to the understanding of water ingress which leads to series of notable events that eventually lead to drug release and degradation of the PLGA polymer.(D'Souza *et al*., 2014)

Understanding the underlying mechanism of transport

The water sorption kinetics of the PLGA shown in Figure 3.26 illustrates anomalous diffusion which arises due to the non-equilibrium nature of the glassy polymer as reported by several investigators studying the diffusion of small molecules in glassy polymers. Initially diffusion is driven by the

concentration gradient of the diffusant and at longer times it is driven by polymer relaxation or swelling, which occurs in response to the stress imposed by the diffusant owing to the non-equilibrium state of the polymer. (Berens and Hopfenberg, 1978)

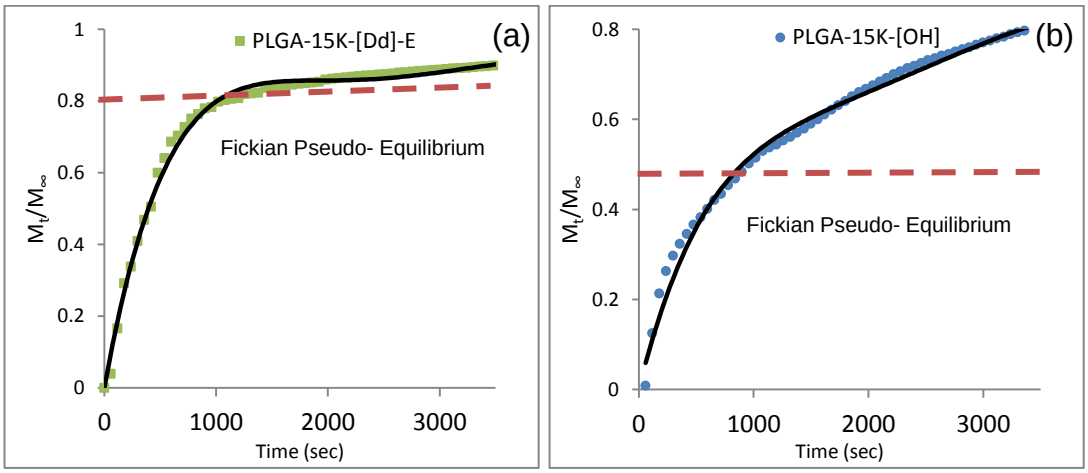

Figure 3.26: Water sorption kinetics in PLGA films; (a) endcapped PLGA-15K-[Dd]-E and (b) non-endcapped PLGA-15K-[OH] at 37^{o}C in response to relative humidity step change of 0 to 95 %. The solid black line represents a regression of the experimental data to the solution of Fick's second law.

Previous reports assume sorption kinetics in PLGA to be Fickian. Recent results by Davis and co-workers on the diffusion of liquid water in PLA, however, show non-Fickian diffusion behaviour. It was suggested that two phenomena are observed on the same experimental time scale, one due to diffusion driven by the penetrant concentration gradient, while the other is due to additional slow ingress of the penetrant driven by stress-induced polymer relaxation or swelling. (Davis *et al*., 2013)

Since the experiments were conducted at a temperature (37^{o}C) above the Tg of the endcapped PLGA-15K-[Dd]-E polymer, the polymer is in an equilibrium

state and would respond instantaneously (elastic) to the stress imposed by water ingress and therefore this relaxation phenomena would not be observed over this experimental time scale (Figure 3.26(a)). In this case, the rate-limiting step is no longer the adsorption of material at the polymer/vapour interface but the diffusion of water through the film. A pure Fickian kinetics also called case I diffusion was observed throughout the experimental time frame, where the water mobility is much slower than the segmental relaxation rate.(Sharp *et al*., 2001, Yu *et al*., 2008)

On the contrary for the non-endcapped PLGA-15K-[OH] films (Figure 3.26(b)) the experimental temperatures are below the Tg of the polymer. Therefore, the polymer is at a non-equilibrium state and polymer relaxation occurs over a much slower time scale (viscoelastic) and can be captured over observable experimental time scales. Figure 3.26(b) illustrates two distinct time periods (two-stage sorption kinetics) over the entire experimental time. The first stage shows a Fickian-like or pseudo-Fickian behaviour whereas the second stage shows the relaxation of the glassy polymer which allows more water into the polymer over the observed time scale.

It is important to note that if the experimental times were shorter, as those analysed for diffusion coefficient calculations, the diffusion of water would appear Fickian. Therefore, the time scale of the experiment is an important feature as it relates to the measurement of diffusivity and solubility and great care must be taken for each experiment to extend the experimental time to

appropriately observe the non-Fickian diffusion−relaxation phenomena. (Davis *et al*., 2013)

Several academicians argue that deviation from Fickian behaviour must be considered for systems where polymer relaxation happens at a much slower pace than the diffusion of the penetrant.(Singh, 2008) According to the Berens and Hopenberg model, the total mass uptake is divided into two parts one for the Fickian process and another for the relaxation process. When both processes operate simultaneously the two stages would not be clearly separable as in the case of PLGA-15K-[OH] films. These findings corroborate with the separable and distinguishable two-stage diffusion-relaxation phenomena observed by Davis and colleagues.(Davis *et al*., 2013) However when the polymer relaxes instantaneously then one should observe a rapid Fickian first stage followed by a slower discernible separate second relaxation-controlled sorption stage, such as that of PLGA-15K-[Dd]-E films.

Figure 3.27 reflects the regressed diffusion slopes for the first 60% of the moisture sorption step of the ester endcapped series. In this initial short time scale the diffusion coefficients were calculated by the solution of Fick's Second Law (equations 3.2-3.5). The high r^2 values obtained indicate that the type of diffusion observed was Fickian (Table 3.2). Remarkably the same Fickian diffusivity was obtained (ca. 5×10^{-11} m^2/s) within experimental errors for both PLGA-15K-[C]-E and PLGA-15K-[E]-E, this could be attributed to free volume considerations which rely on molecular weight and the degree of

plasticization of the polymer. This is an expected result for the diffusion of small molecules in a glassy polymer (at an experimental temperature below the glass transition temperature of the polymer).

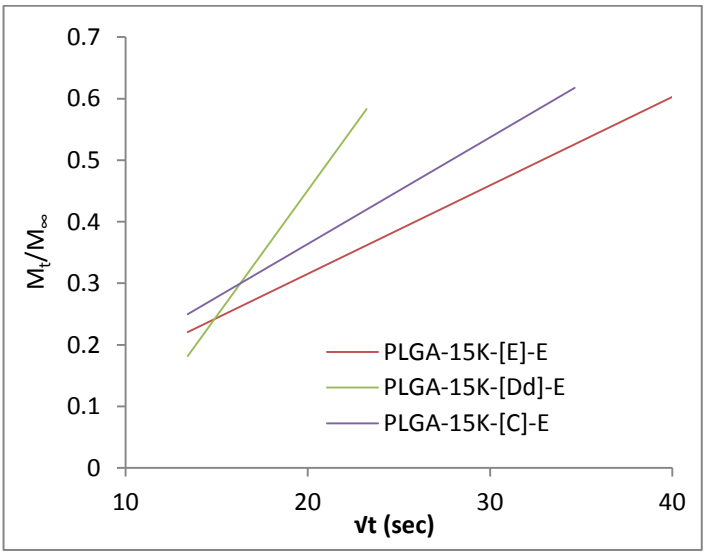

Figure 3.27: The regression of the experimental data of the ester endcapped PLGA films to the solution of Fick's second law in response to relative humidity step change of 0 to 95 % at 37^{o}C.

The anomalous moisture uptake observed in Figure 3.28 for all the amide endcapped polymers suggest that deviation from the Fickian process is because the diffusion coefficient is a strong function of external factors such as relative humidity gradient as well as the temperature, which is explained by the free volume theory.(Yoon *et al*., 2000) However at the shorter time scale moisture transfer in the pseudo-Fickian range is rather determined by the internal properties of the sample itself.(Yu *et al*., 2008) This is clearly seen in Figure 3.29 where decrease in polymer Tg is coupled with increase in diffusion coefficient.

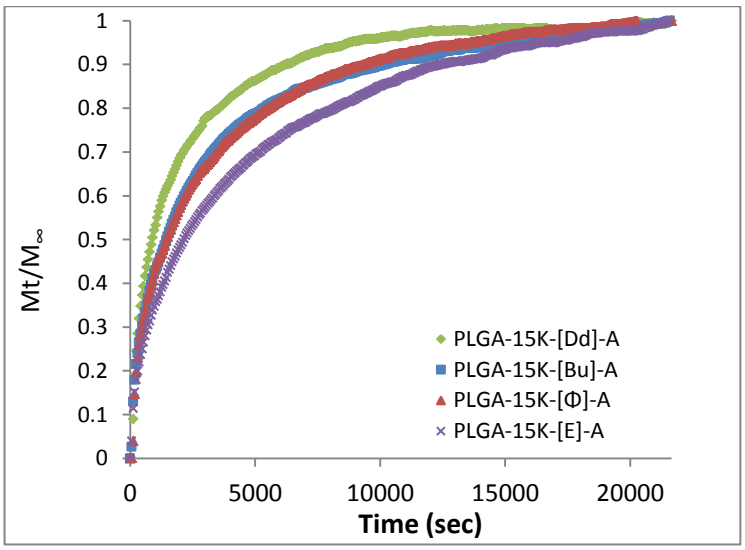

Figure 3.28: water sorption kinetics in amide endcapped PLGA films in response to relative humidity step change of 0 to 95 % at 37^{o}C.

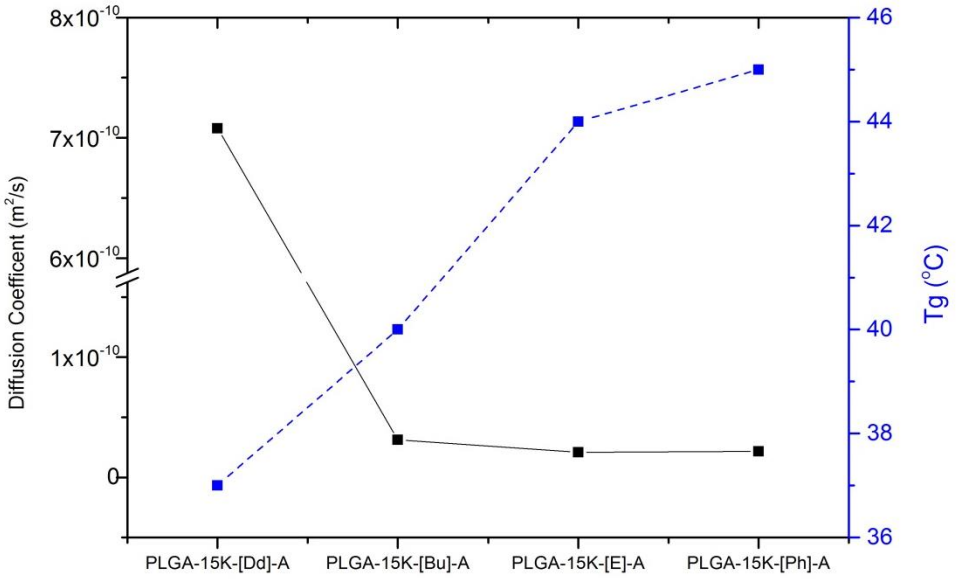

Figure 3.29: The effect of composition of the polymer samples (Tg, dotted line) on its moisture transfer capacity (solid line) at the shorter time scales in the pseudo-Fickian range.

One possible explanation is that the polymer is swollen by the solvent, and stresses are introduced which prevent further uptake of material. Only when these stresses have been dissipated by viscous flow of the stressed polymer chains can further uptake occur. As a result, the solvent concentration in the swollen region of the polymer rapidly reaches the equilibrium value, and a swelling front is produced that propagates through the polymer at uniform velocity. The polymer ahead of the front is glassy, but the material behind it is highly plasticized. This front is responsible for the linear mass uptake kinetics.(Sharp *et al*., 2001) Data based on this strict representation of the glassy structure of penetrant-exposed PLGA have not been reported before.

3.3.4. Nature of sorbed water

The dynamic vapour sorption apparatus regulates the temperature and humidity of the environment surrounding a sample, allowing any weight changes in a sample due to sorption or desorption to be accurately measured. The weight change of the sample was stabilized after each step (in steps of 10% RH) until it was smaller than 0.05% for a time period of 60 minutes. The reverse isotherm was also measured. In this case the humidity was decreased down to 0% and the samples were allowed to stabilize after each step. In order to finalize the isotherm and to compare the results with the initial weight of the sample, an additional drying step was included (60^{o}C at 0% RH). Data on mass change was acquired every 20 seconds and hysteresis was calculated by subtracting the adsorption moisture content

(MC) from the desorption MC at a given RH. Figure 3.30 shows the second moisture sorption-desorption profile of the non-endcapped PLGA-15K-[OH] (a) and the dodecyl endcapped PLGA-15K-[Dd]-E specimens (b). In the non-endcapped PLGA isotherms the desorption branch of the isotherm did not follow sorption curve. Despite the 12-hour drying step at the end of the run, the desorption curve failed to reach the zero point. The asymmetry between sorption and desorption shown in the PLGA-15K-[OH] films, is commonly referred to as hysteresis

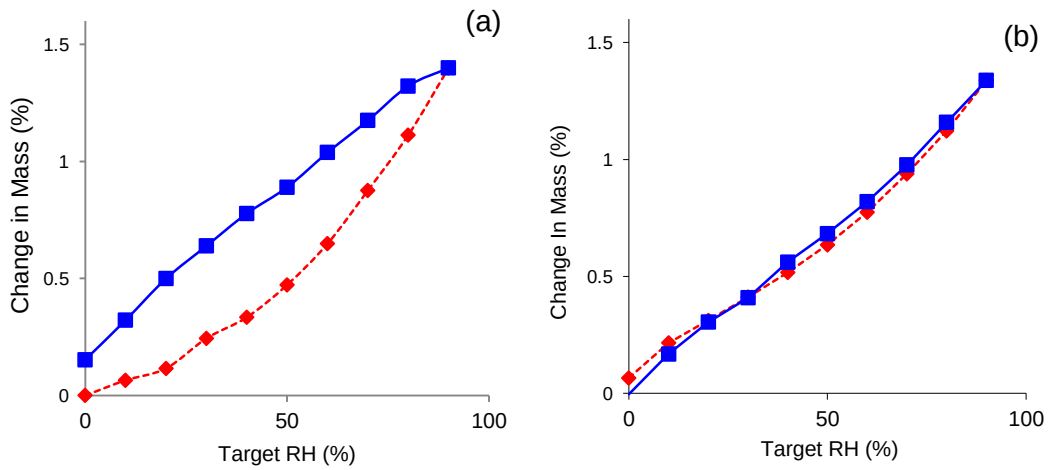

Figure 3.30: Sorption-Desorption curves illustrating change in mass of PLGA films a) PLGA-15K-[OH], b) PLGA-15K-[Dd]-E over increasing relative humidity. Moisture uptake was recorded during sorption (dotted line) and the water loss was inversely sampled during desorption (solid lines).

On the contrary, reversibility of the water uptake at a constant temperature was clearly seen in the case of PLGA-15K-[Dd]-E indicating endcapping influenced water uptake in the polymer and the swelling behaviour. The reversibility (lack of hysteresis) may be indicative that the moisture is adsorbed on the surface of the material rather than being absorbed into its structure. There are several hypothesis to the hysteresis observed in the

non-endcapped PLGA films. One explanation is the changing hygroscopicity of the samples during adsorption and desorption. Hygroscopicity, being a measure of the number of available sorption sites in the material, suggesting possible hydrogen bound water in the bulk phase rather than on the surface (Engelund *et al*., 2010). Another explanation is that the changes might be related to intra-chain hydrogen bonding that also causes hysteresis.

Hysteresis is often discussed as the swelling/deformation phenomenon. From a polymer science point of view, swelling can occur if a polymer is subjected to a thermodynamically reasonably good solvent. Where polymer/polymer interactions can be overcome by a sufficiently strong polymer solvent interaction.(Jeromenok and Weber, 2013) Water sorption also differs from desorption because the polymer must swell to accommodate water molecules but does not necessarily shrink for the water to desorb. In desorption water moves by diffusion from the bulk of the membrane to the membrane/gas interface and then must be transported across the membrane/gas interface (Majsztrik *et al*., 2007). However, if diffusion and interfacial mass transport were the only factors controlling water sorption then water uptake and water desorption should have similar rate constants. It is clear from the data presented in Figure 3.32.a that is not the case. Several theories described by Kapsalis, such as the inkbottle neck theory and the domain theory, are often used to explain hysteresis. Studying the shape of the hysteresis further explains the possible mechanisms involved in the water/polymer interaction (Yu *et al*., 2008)

3.4. Conclusion

This chapter discussed the effect of endcapping on the moisture uptake properties of PLGA polymers with the aim of elucidating structure–property relationships and subsequently designing new polymers with tailor-made moisture uptake properties. In non-endcapped polymer samples the percentage of moisture sorption ranged from 1.07 to 2.16% (w/w) recorded at the highest and lowest molecular weight; PLGA-35K-[OH] and PLGA-5K-[OH], respectively. This was explained by the decrease in hydrophilic end group concentration and reduced polymer chain mobility. The nature of the endcap and the length of the chain end both influenced moisture sorption evident in TG-SA and DVS isotherms. The introduction of a hydrophobic dodecyl ester endcap decreased moisture sorption by 31.08% whereas, the dodecyl amide endcap increased moisture sorption by 42.06% when compared to the non-endcapped control PLGA-15K-[OH]. This was attributed to potential hydrogen bonding at the amide end group. In the ester endcapped series sorption decreased as the aliphatic content in the endcap increased, reaching a minimum in the isotherms of the PLGA-15K-[C]-E samples (39.63% moisture uptake reduction). The moisture sorption properties of the PLGA samples significantly changed as the operating temperature approached polymer's Tg. Once in a rubbery state, the polymer chains become more mobile with greater propensity for mass uptake. Calculation of the moisture sorption diffusion coefficient in the polymer films revealed that water diffusivity in the PLGA-15K-[OH] film was almost 2 orders

of magnitude lower than that of its endcapped counterpart. Two processes were identified to be progressing upon hydration. First the polymer absorbs water according to its diffusion coefficient. Then water induced plasticity of the chains leads to polymer relaxation and enhanced water mobility which has been described as the diffusion relaxation phenomena. This explains why despite its lower total moisture uptake the rate of uptake was initially faster in the endcapped specimen, hence reaching equilibrium faster.

CHAPTER 4: FABRICATION AND CHARACTERIZATION OF DRUG LOADED INTRAOCULAR IMPLANTS

4.1. Introduction and Objectives

Within the intraocular drug delivery field, biodegradable implants of PLGA are currently under investigation by many pharmaceutical companies as potential products for treating disease a typical example being Posurdex©.(Tamaddon *et al*., 2015) Intraocular polymeric implants offer long‑term exposure at the desired location offering local drug delivery advantages. Intensive research on the use of PLGA as a polymeric matrix began in the 1970's, however the number of products that appeared on the market were relatively low. This is attributed to the complexity in modulating drug release and polymer erosion profiles (Allison, 2008). Drug release describes the way in which drug molecules are transported across the carrier matrix. In PLGA-based systems drug release is a function of molecular weights, lactide: glycolide ratios, end-group, etc. New insights into processes that modifying drug release are continuously being presented (Fredenberg *et al*., 2011).

The two mechanisms associated with drug release from PLGA-based systems are an initial phase of drug diffusion followed by degradation/erosion of the bulk polymer during the later stages leading to a shortened drug diffusion path and 'burst'.(Mollo and Corrigan, 2003) The release profile is often used as the basis for mechanistic evaluation. A bi-phasic or tri-phasic

release profile is most common in PLGA systems. A generalised explanation for the different phases is not always feasible due to the complexity of the different factors that influence drug release as illustrated in Figure 4.1. In addition the dynamic nature of PLGA, as its properties and behaviour change with degradation adding to the complexity.(Park, 1994)

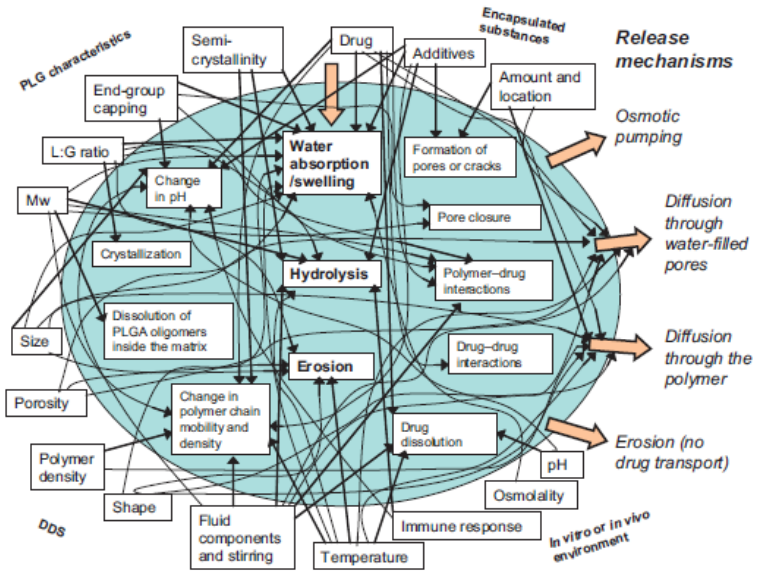

Figure 4.1: The complex picture of the different factors that influence drug release from PLGA matrices. The effect of the properties of the DDS and the surrounding environment on the process that in turn influence drug release. (Fredenberg *et al*., 2011)

The following work focused on the production of a controlled-release intraocular implant of Brimonidine free base using hot melt extrusion. The implants were fabricated to deliver the drug load over a period of 3 months. The effects of endcapping and drug type/loading on the release mechanism and related kinetic parameters of the implants were evaluated. The dissolution data obtained, was fitted to various mathematical models corresponding to possible release mechanisms.

4.2. Materials and Methods

4.2.1. Materials

A range of non-endcapped PLGAs and polymers with different modified end groups were either purchased (Sigma Aldrich, UK, Purac, Gorinchem Netherlands and PolyScitech, West Lafayette, USA) or synthesized in-house as discussed in Chapter 2. Detailed specifications of endcap and molecular weight of each polymer are depicted in Tables 2.1 to 2.5.

Acetonitrile, and Phosphate buffer saline tablets pH 7.2 were purchased (Sigma Aldrich, Dorset, UK). Brimonidine Free Base (BFB) and Brimonidine Tartrate (BT) were kindly provided by Allergan, Inc., Irvine, CA, USA

Sample Labelling

Samples were labelled according to their endcap and drug loading. Endcaps varied Ethyl [E], Butyl [Bu], Dodecyl [Dd], Cholesterol [C], Benzyl [Bn], Phenyl [Φ], while hydroxyl [OH] was designated for the free non-endcapped polymers. The amide series was described as the A series whilst the ester series as E. The nominal molecular weight was given in thousands. The percentage drug loading was followed by the form of the loaded drug; Brimonidine Free Base as (BFB) and Brimonidine Tartrate as (BT). Figure 4.2 shows an overview of implant labelling scheme and the design space is depicted in Table 4.1

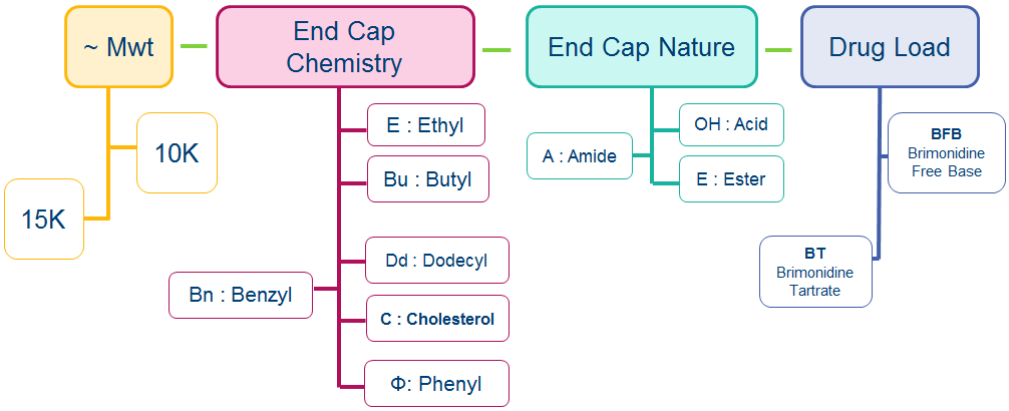

Figure 4.2: Scheme showing labelling system for Brimonidine loaded PLGA implants

Table 4.1: Overview of a design space for the extruded implants

Effect of Endcap: Ester Series	**Effect of Drug loading: 1 - 20 %**	
	15k-[E]-E-1%BFB 15k-[Dd]-E-1%BFB 15k-[Dd]-E-10%BFB 15k-[C]-E-1%BFB	15k-[OH]-1%BFB 15k-[OH]-10%BFB 15k-[OH] 20%BFB
Effect of Endcap: Amide Series	15K-[E]-A-1%BFB 15K-[Bu]-A-1%BFB 15K-[Dd]-A-1%BFB 15K-[Bn]-A-1%BFB 15K-[Φ]-A-1%BFB	15K-[E]-A-1%BT 15K-[Bu]-A-1%BT 15K-[Dd]-A-1%BT 15K-[Bn]-A-1%BT 15K-[Φ]-A-1%BT
	Effect of Drug Type: Free Base vs Tartrate Salt	

4.2.2. Implant Extrusion

Prior to extrusion the copolymers were ground using a ball mill (Stoneware) at 100 rpm and sieved in a 24-mesh sieve. Brimonidine Tartrate (BT) or Brimonidine Free Base (BFB) and ground PLGA, with different ratios were mixed to form a homogenous drug/polymer mixture. The implants were extruded by hot melt extrusion (HME) using a laboratory scale piston extruder. Figure 4.3 shows the schematic presentation of the apparatus.

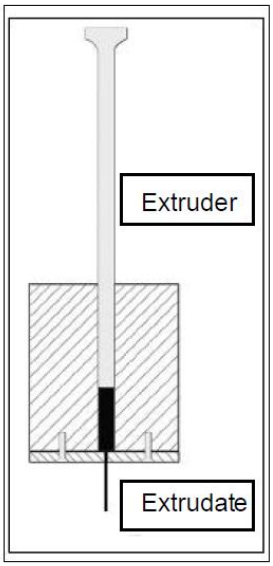

Figure 4.3: Schematic representation of the implant extrusion (Tamaddon *et al*., 2015)

Approximately 300 mg of the obtained powder mixture was fed manually, into the barrel of the extruder. The barrel was heated using a digitally controlled heater. In order to determine the processability of various formulations, preliminary experiments were carried out at different temperatures. On the basis of these preliminary trials, the temperature range of 50 - 80°C, allowed

for successful production of extrudates with uniform shape and satisfactory smooth surface. The obtained semi-solid mass was extruded through a nozzle of 360 µm in diameter. The different prepared formulations and their processing conditions are shown in Table 4.2. Once the samples had cooled to ambient temperature, the rod-shaped solid extrudates were cut into segments with approximately 6 mm in length.

Table 4.2: PLGA-Brimonidine Implants' Formulation and Extrusion Parameters

	Polymer	Drug Composition		Extrusion Temperature (^{o}C)
		Drug	Concentration (w/w%)	
Acid Endcap	PLGA15K-[OH]	BFB	1	80
			10	80
			20	75
Ester Endcap	PLGA15K-[E]-E	BFB	1	80
	PLGA15K-[Dd]-E	BFB	1	73
			10	75
	PLGA15K-[C]-E	BFB	1	75
Amide Endcap	PLGA15K-[E]-A	BT	1	55
		BFB	1	55
	PLGA15K-[Bu]-A	BT	1	73
		BFB	1	65
	PLGA15K-[Dd]-A	BT	1	73
		BFB	1	75
			10	80
	PLGA15K-[Φ]-A	BT	1	75
		BFB	1	73

*The polymers with Benzylamine end groups degraded significantly during extrusion and were excluded from the study

4.2.3. Extrudate Characterization

Analytical Balance (Mettler Toledo, Leicester, UK), Modulated Differential Scanning Calorimetry (DSC 822^{e}, Mettler Toledo, Leicester, UK), Gel Permeation Chromatography (Waters® 515 GPC), X-Ray Powder Diffractometer, (Bruker D8 Advance II diffractometer, GmbH, Germany), Scanning Electron Microscopy (SEM, Seron Technology, model AIS‑2300), and High performance liquid chromatography (HPLC).

4.2.3.1. *Scanning electron* microscopy (SEM)

The morphological appearances of the implants were investigated using scanning electron microscopy to determine the presence/absence of pores/cracks in the implants and monitor the integral and morphological changes during the degradation studies. The implants were mounted on aluminium specimen holders with a conductive adhesive sheet and sputter-coated with gold for imaging.

4.2.3.2. X-ray powder diffraction (XRDP)

XRPD analysis was conducted using a high-resolution X-ray powder diffractometer to study the physical state of the drug-loaded implants. The PLGA samples were scanned at room temperature in Symmetrical reflection mode with CuKα radiation (λ=1.54 Å) with Göbel mirror bent multilayer optics

at a step width of 1 degree per minute in the angular range of 4–35° (2θ). The measuring time was of 1 s per step. The samples were compressed into the sample holder to provide a smooth surface. Each experiment was conducted in triplicate. All diffraction patterns were normalized to the peak of highest intensity.

4.2.3.3. Modulated Differential Scanning Calorimetry (MDSC)

Glass-transition temperatures were determined by modulated differential scanning calorimeter (MDSC). Approximately 2 mg of implants were crimped in aluminium pans (40µl). The lid was pierced before the measurement. An empty pin-holed aluminium pan was used as a reference under a nitrogen purge. Both the reference pan and the sample pan were allowed to equilibrate isothermally for 10 min at -20 ^{o}C. The pans were heated from -20 ºC to 200 ºC at 1 ºC/min, with modulation amplitude of +/- 0.16 ºC/min and a period of 60 s, quench cooled to -20 ^{o}C (to eliminate any sample thermal history), and then heated again to 400 ^{o}C at 1 ^{o}C /min with modulation amplitude of +/- 0.16 ºC/min and a period of 60 s. The results were analysed using TA universal analysis software. The second run DSC curve was the reference for determining the glass transition temperature (T_g), and phase transition temperature (T_m). Each experiment was conducted in triplicate. Data was compared to that of pure polymer, physical mixture of drug and polymer and placebo implants to investigate drug-polymer interaction as well as effect of HME on polymer physical properties.

4.2.3.4. Content Uniformity Test

For the evaluation of content uniformity of BT or BFB in the implants, three implants of each batch were selected and weighed. Each implant was dissolved in a mixture of acetonitrile and PBS (10:90) (5ml). After filtration and appropriate dilution, the amount of the drug was determined by high-performance liquid chromatography, according to the procedure described further in 4.2.3.5. The amounts of drug in each implant (µg) were estimated and the results were expressed as mean and relative standard deviation.

4.2.3.5. High performance liquid chromatography

The reverse-phase HPLC method was developed and validated for *in-vitro* release medium. The instrument was a waters system composed Waters 515 pump and Waters 2487 dual absorbance detector (Waters, USA). The stationary phase was CN-RP column (250 × 4.6 mm, 5 µm particle size) from Macherey-Nagel (Germany), and a mixture of acetonitrile and PBS pH 7.2 (10:90) was used as a mobile phase. All the chromatograms were recorded at 252 nm with mobile flow rate of 0.25 ml/min. Solutions of the pure drug with different concentration were injected for generating a calibration curve.

4.2.3.6. Swelling Studies

The swelling of individual implants was monitored to investigate the bulk hydrophilicity of polymers as it affects drug release from polymeric matrix. To

test the swelling of BFB-loaded implants 16-well standard microplates were used. A 6mm implant in length was introduced into each well, filled with 250 µL phosphate buffer pH 7.2. The well plates were placed on a horizontal shaker (Model 1083, GLF Corp., Burgwedel, Germany) set at a speed of 25 strokes/min in a thermostatically controlled temperature room at 37°C± 0.5°C. To minimize water evaporation, the well plates were closed and sealed with Parafilm. At specific time intervals, the implants were removed, blotted with lint-free tissue to remove excess surface PBS, dried till constant weight then weighed. The degree of fluid uptake was calculated as swelling index using the following equation:

$$Swelling\ index = \left[\frac{W_t - W_0}{W_0}\right] \times 100 \qquad \text{(Equation 4.1)}$$

where W_0 is the initial weight of the sample and W_t its weight at t time.

4.2.3.7. In-vitro dissolution studies

The *in-vitro* release studies were performed under sink conditions over 3 months. Aiming to simulate the pH conditions of intracameral aqueous fluid; three implants of each batch belonging to a formulation were placed in three 300 µl glass inserts containing 250 µl of phosphate buffer saline PBS (pH 7.2) and secured in 2 ml glass vials shown in Figure 4.4. The vials were placed on a batch shaker (Model 1083, GLF Corp., Burgwedel, Germany) set at a speed of 25 strokes/min in a thermostatically controlled temperature room at 37°C± 0.5°C (Figure 4.4).

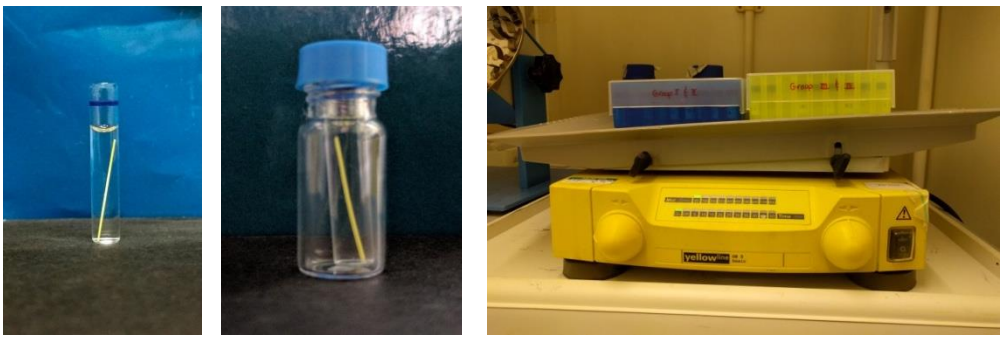

Figure 4.4: *In vitro* drug release setup showing the implants suspended in PBS in a glass insert. The inserts are placed in glass vials on batch shaker in a thermostatically controlled temperature room at 37^{o}c

At predetermined intervals, 100 µl aliquots of the release medium were collected and samples were replenished with equal volumes of fresh release medium to keep the release volume constant throughout the experiment. The aliquots were withdrawn through Millipore® membrane filter of 0.45 µm pore size. The amount of drug released from the collected samples was measured by high-performance liquid chromatography (HPLC) using the method described in Section 4.2.3.5. The release profile was expressed as the cumulative percentage of Brimonidine Tartrate or Brimonidine free base released in the medium over time.

4.2.3.8. *Kinetic Model analysis*

The *in-vitro* release data was fitted to various kinetic models corresponding to possible release mechanisms. Approximately the first 60% of the total drug released was fitted into the equations 4.2-4.5. These equations are commonly used in the drug release kinetic studies, because of their simplicity

and applicability.(Li *et al*., 2006, Peppas and Sahlin, 1989, Ritger and Peppas, 1987)

$$\frac{M_t}{M_\infty} = K_o t \quad \text{(Equation 4.2)}$$

$$\frac{M_t}{M_\infty} = K_H t^{1/2} \quad \text{(Equation 4.3)}$$

$$\ln\left(\frac{M_t}{M_\infty}\right) = -K_1 t \quad \text{(Equation 4.4)}$$

$$\frac{M_t}{M_\infty} = K t^n \quad \text{(Equation 4.5)}$$

Equation 4.2, the zero‑order model equation; Equation 4.3, Higuchi's square ‑root equation; Equation 4.4 the first order and the 4.5 is the Korsmeyer‑Peppas empirical equation. Where, M_t/M_∞ is the fraction of drug released at any time t; and K_0, K_H, K_1 and K are release rate constants for Equations 4.2, 4.3, 4.4 and 4.5, respectively. In Korsmeyer-Peppas power model, Equation 4.5, *n* is the diffusional exponent. The *n* value is indicative of the mechanism of drug release as shown in Table 4.3 for cylindrical‑shaped matrices.(Tamaddon *et al*., 2015, Korsmeyer *et al*., 1983)

Table 4.3: Diffusion exponent and release mechanism for cylindrical shapes

Exponent (n)	**Overall solute diffusion mechanism**
≤ 0.45	Fickian Diffusion
$0.45 < n < 0.89$	Anomalous (Non-Fickian) Diffusion
0.89	0.89 Case-II Transport
$n > 0.89$	Super Case-II Transport

4.2.3.9. *Degradation Studies*

In vitro degradation of the rods placed in phosphate buffer solution (PBS) (pH 7.2) was carried out. The decrease in polymer molecular weight (Mn) of PLGA during drug release was measured by gel permeation chromatography (Separation Modules e2695 and e2695D, 2414 RI Detector; Waters, Guyancourt, France) (column: PLgel 5 µm MIXED-D, 7.5 × 300 mm, Polymer Laboratories, Varian, Les Ulis, France). Tetrahydrofuran was used as mobile phase at a flow rate of 1 mL/min. Samples were treated as described for the *in vitro* drug release studies. At predetermined time points, implants were withdrawn, and dissolved in tetrahydrofuran (3 mg/ml). Fifty microliter samples were injected. Molecular weights were calculated using the Empower GPC software and polystyrene standards (Polymer Laboratories).

4.3. Results and Discussion

The fabricated implants were designed to be easily injected intraocularly once during the course of a 3 months treatment period, providing an alternative to conventional dosage forms. Many reports have recorded the successful applications of intraocular implants containing wide range of drugs such as antimicrobial, antiviral and anti‑inflammatory agents.(Bourges *et al*., 2006, Choonara *et al*., 2009, Eljarrat-Binstock *et al*., 2010, Thrimawithana *et al*., 2011)

Attempts to design controlled release dosage forms of Brimonidine have been previously discussed in the literature. Ibrahim and colleagues prepared and characterized Brimonidine loaded bioadhesive nanoparticles for topical application.(Ibrahim *et al*., 2015, Ibrahim *et al*., 2013) Several authors investigated the controlled release of Brimonidine from topical ocular insert such as Patel *et al*., Gupta *et al*. and others (Sauraabh Gupta and Gilhotra, 2011, Dipti Patel *et al*., 2009, Aburahma and Mahmoud, 2011). The literature is scarce on the intraocular controlled release of Brimonidine, one example is the work of Deokule and colleagues on intravitreal Brimonidine implants.(Deokule *et al*., 2012)

Hot Melt Extrusion (HME) is becoming a widely used method by pharmaceutical industries. With less process steps compared to other methods the process converts raw materials into extrudates of uniform

density and predefined shape and size, by forcing them through a nozzle at controlled conditions such as temperature and pressure. HME is currently applied in the pharmaceutical industries for the manufacture of a variety of dosage forms such as tablets, granules, suppositories and implants.(Breitenbach, 2002, Verhoeven *et al*., 2009)

Brimonidine the drug of choice is available in two chemical forms that differ in their solubility. Brimonidine tartrate, the water-soluble drug (34 mg/ml) and its sparingly soluble free base (1.5 mg/ml) were extruded using HME into rod shaped, sustained release intraocular PLGA implants without requiring any additional excipients for improving shape or compressibility.

4.3.1. Extrudate Characterization

The extruded implants were characterized to fully understand the factors that have significant impact on the implants' performance evaluated by its drug release profile.

4.3.1.1. Evaluation of Implant Morphology

The appearance of the implants was evaluated after extrusion. Macroscopically, the rods were smooth and showed colour uniformity; yellow and white for BFB and BT loaded implants respectively compared to the transparent placebo implants, Figure 4.5. Implant diameter was controlled by nozzle size (360 µm) and mean diameter recorded in Table 4.4.

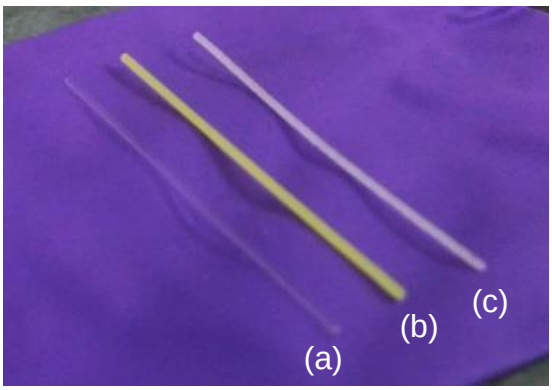

Figure 4.5: Macroscopic evaluation of extruded PLGA implants a) Placebo b) BFB loaded c) BT loaded PLGA-15k-OH.

Table 4.4: Performance of extruded implants; Physical characterization (weight, diameter) and measured drug content (± SD, n = 3)

Formulation	Implant Weight (mg ± SD)	Drug Content (µg ± SD)	Average Diameter n =3 (µm ± SD)
15k-[OH]-1%BFB	3.0 ± 0.1	29 ± 4	382 ± 15
15k-[OH]-10%BFB	2.9 ± 0.4	292 ± 5	354 ± 29
15k-[OH]-20%BFB	3.5 ± 0.2	713 ± 14	355 ± 11
15k-[E]-E-1%BFB	3.6 ± 0.8	35 ± 9	337 ± 9
15k-[Dd]-E-1%BFB	3.1 ± 0.3	30 ± 5	364 ± 17
15k-[Dd]-E-10%BFB	3.5 ± 0.4	359 ± 18	396 ± 28
15k-[C]-E-1%BFB	3.2 ± 0.6	30 ± 10	347 ± 11
15K-[E]-A-1%BFB	3.0 ± 0.8	28 ± 5	352 ± 18
15K-[E]-A-1%BT	3.1 ± 0.5	31 ± 5	334 ± 14
15K-[Bu]-A-1%BFB	3.6 ± 0.7	34 ± 8	367± 26
15K-[Bu]-A-1%BT	3.6 ± 0.6	33 ± 5	387± 17
15K-[Dd]-A-1%BFB	2.7 ± 0.5	26 ± 7	363 ± 22
15K-[Dd]-A-10%BFB	2.7 ± 0.1	25 ± 8	364 ± 15
15K-[Dd]-A-1%BT	3.2 ± 0.3	31 ± 6	396 ± 31
15K-[Φ]-A-1%BFB	3.5 ± 0.3	34 ± 4	377 ± 13
15K-[Φ]-A-1%BT	3.5 ± 0.4	37 ± 7	395 ± 12

The surface of the heat extruded cylinders appeared smooth and dense as seen in the SEM micrographs of PLGA-15k-[OH]-1%BFB implants (Figure 4.6). Figure 4.7 shows a representative sample of SE micrographs of the series of BFB loaded implants with their average diameter recorded in Table 4.4

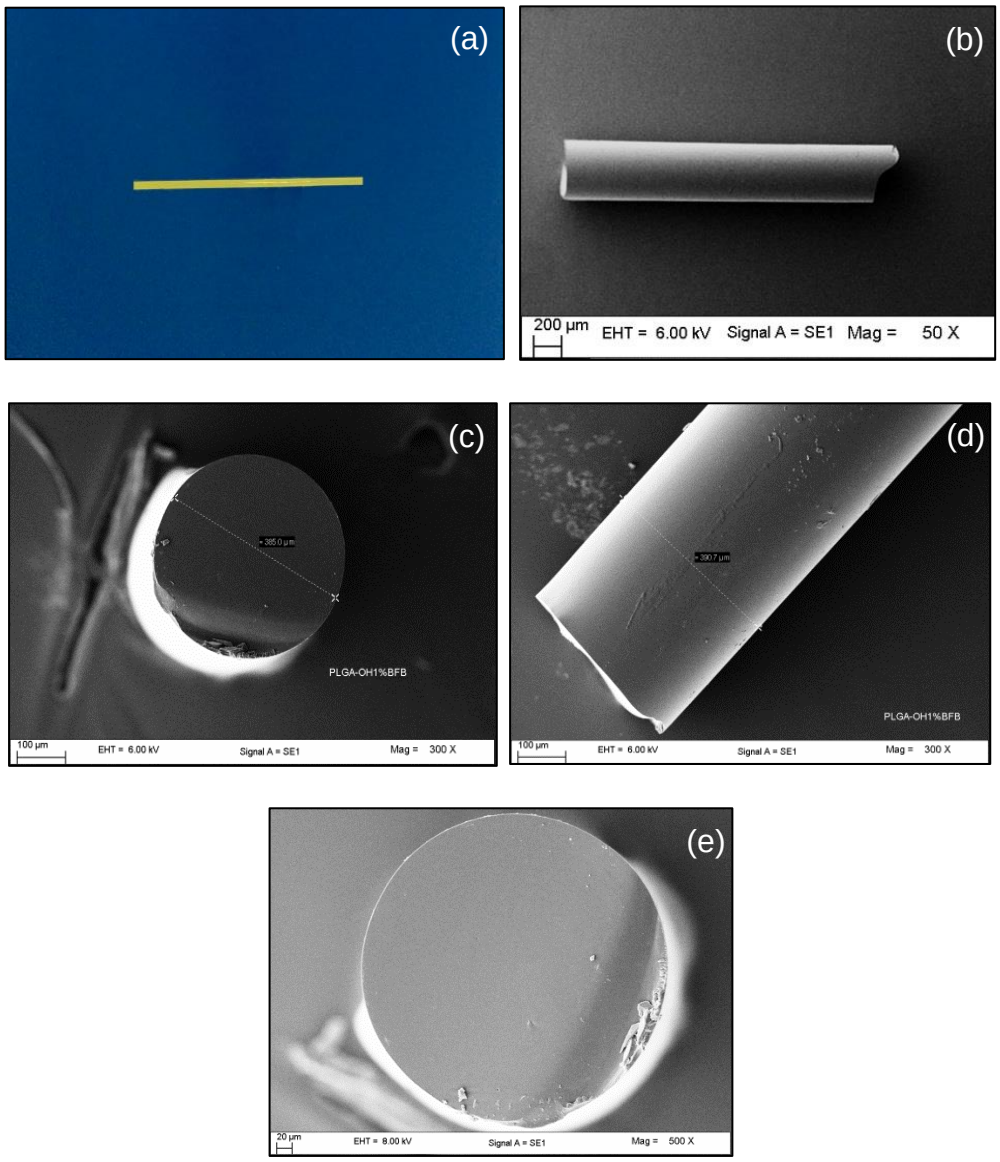

Figure 4.6: a) Macroscopic Image of 1% BFB loaded PLG-15k-[OH] implants. SE micrographs of 1% BFB loaded PLG-15k-[OH] implants;b) magnified at x50 c) cross-section of the implants magnified at x 300 d) longitudinal surface view magnified at x 300, e) cross-section of the implants magnified at x 500

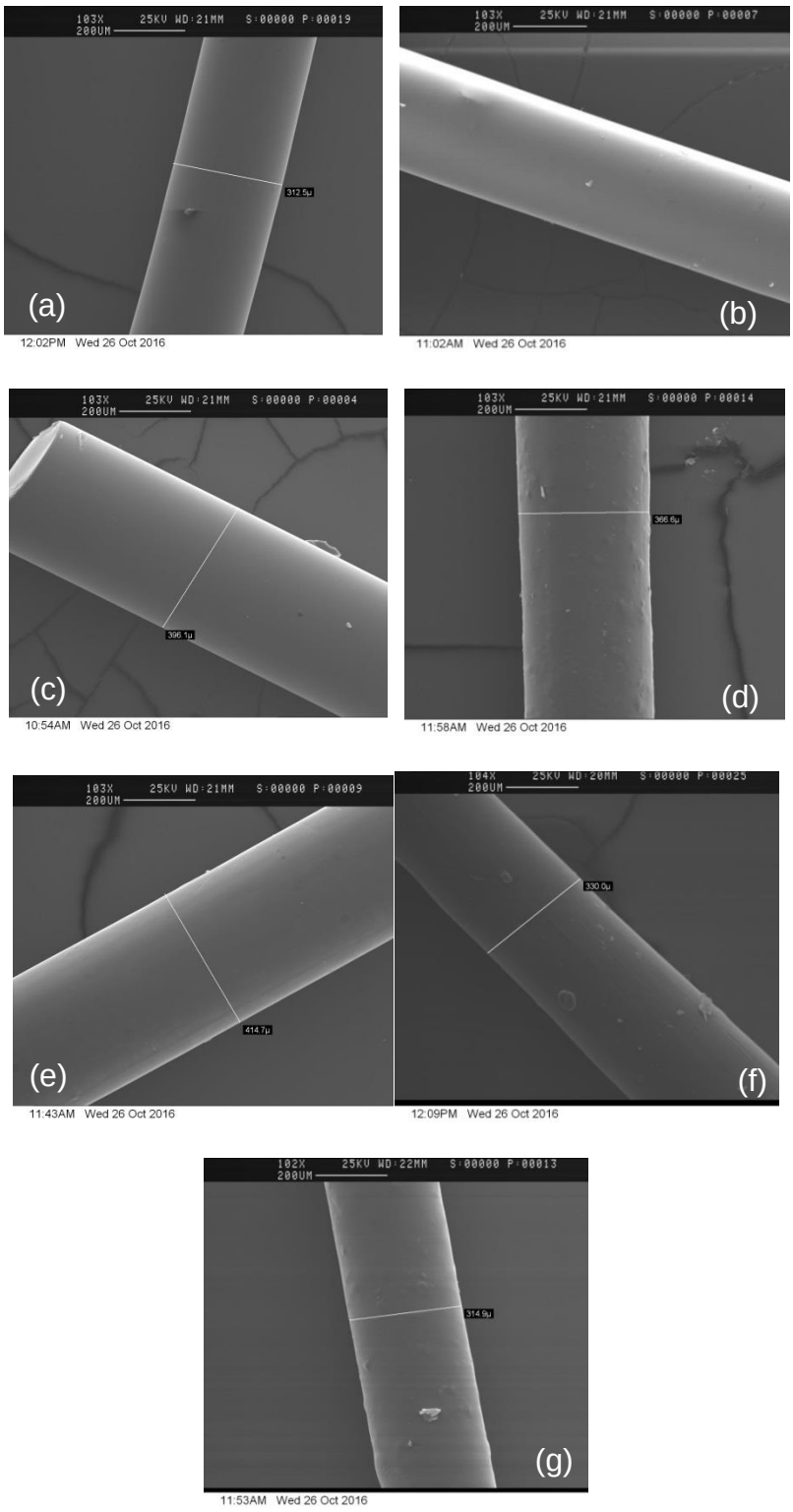

Figure 4.7: SE micrographs of 1% BFB loaded PLGA implants; a) 15k-[E]-E-1%BFB, b) 15k-[Dd]-E-1%BFB, c) 15k-[C]-E-1%BFB, d) 15K-[E]-A-1%BFB, e) 15K-[Bu]-A-1%BFB, f) 15K-[Dd]-A-1%BFB, g) 15K-[Φ]-A-1%BFB, (Table 4.4) magnified at x 100

4.3.1.2. Content uniformity test

The drug content uniformity values for the prepared ocular implants depicted in Table 4.4 indicated that using mixing followed by compression at the appropriate heat and pressure was a suitable technique for development of implants of uniform drug content. The mean measured drug loading values were found satisfactorily within limits and consistent in all batches varying from 92 to 106% of pre-indicated amount of Brimonidine. This confirmed that the adopted method of preparation gave reproducible results and that the drug was uniformly distributed in the polymeric matrix.

4.3.1.3. Effect of Extrusion and Drug loading on Polymer's Thermal Properties

MDSC scans were performed on pure as received Brimonidine, individual polymers, physical drug/polymer mixtures, placebo and medicated implants in order to evaluate the thermal properties of the polymer as well as the physical state of the drug in the implant. Table 4.5 shows that HME did not significantly affect the polymer's glass transition temperature as the placebo extruded implants exhibited glass transition temperatures similar to those of their composing polymers. The DSC thermogram of pure drug powder was typical of a crystalline substance, exhibiting a sharp endothermic peak at 201.15°C (Figure 4.8) corresponding to its melting. All MDSC measurements were performed on the dry implants, since water is an efficient plasticizer for PLGA as previously discussed in Chapter 3. (Faisant *et al*., 2002)

Table 4.5: Thermal properties of PLGA copolymers, drug/copolymer physical mixture, placebo and drug loaded implants by MDSC.

	Formulation	Glass Transition Temperature (T_g °C)			
		Polymer	Placebo Implant	Physical Mixture	Loaded Implant
Acid EndCap	15K-[OH]-1%BFB	41.94	42.05	43.20	42.49
	15K-[OH]-10%BFB				43.54
	15K-[OH]-20%BFB				47.15
Ester Endcap	15K-[E]-E-1%BFB	40.90	39.99	41.11	41.90
	15K-[Dd]-E-1%BFB	36.30	36.06	36.42	36.31
	15K-[Dd]-E-10%BFB				36.58
	15K-[C]-E-1%BFB	44.97	43.49	45.65	43.55
Amide Endcap	15K-[E]-A-1%BFB	44.26	42.44	43.97	44.56
	15K-[E]-A-1%BT			41.04	44.06
	15K-[Bu]-A-1%BFB	40.22	39.86	41.01	40.32
	15K-[Bu]-A-1%BT			40.53	39.40
	15K-[Dd]-A-1%BFB	37.18	38.90	37.02	37.39
	15K-[Dd]-A-10%BFB				39.55
	15K-[Dd]-A-1%BT			37.40	38.94
	15K-[Φ]-A-1%BFB	44.76	42.68	43.50	45.14
	15K-[Φ]-A-1%BT			44.46	42.07

Results depicted in Table 4.5 indicate Brimonidine loading at the tested concentrations 1 and 10% w/w did not significantly affect the Tg of the polymer. Examples are shown in the thermogram in Figures 4.9 and 4.10. However, in the formulation 15k-[OH]-20%BFB (Figure 4.9) increasing the concentration of BFB to 20%w/w, the drug appears to have an anti-plasticizing effect increasing the implant's Tg, suggesting drug/polymer interaction at higher drug loading.(Gasmi *et al*., 2015) This could be due to possible hydrogen bonding between the free base and the free carboxylic acid groups on the PLGA chains.(Aburahma and Mahmoud, 2011)

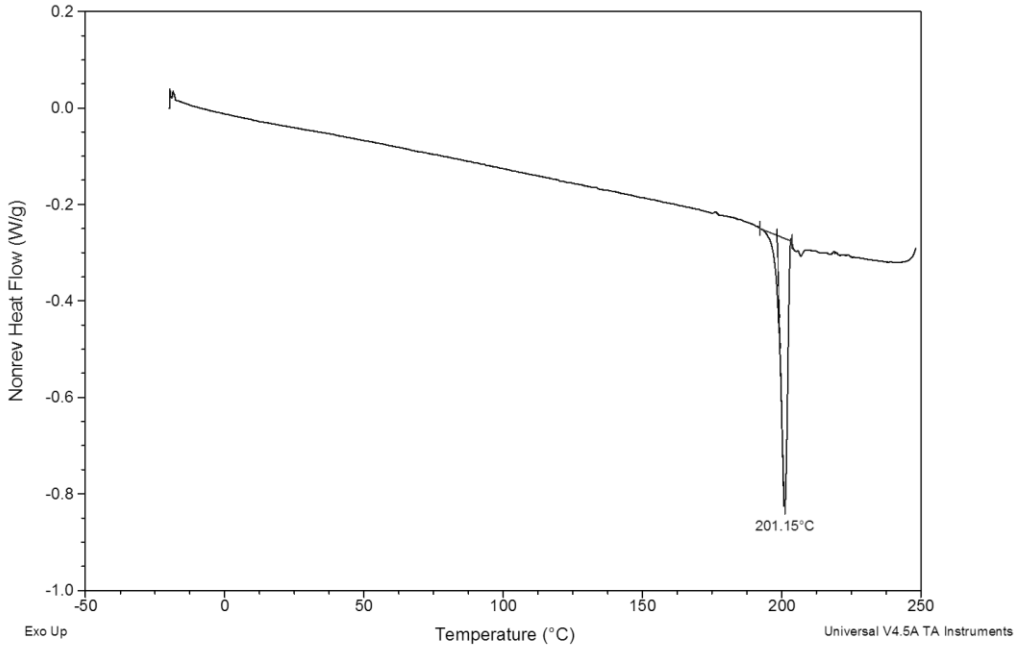

Figure 4.8: DSC curve of second heat curve of Brimonidine Tartrate. Heating rate of 5^{o}C.min^{-1} to 250^{o}C

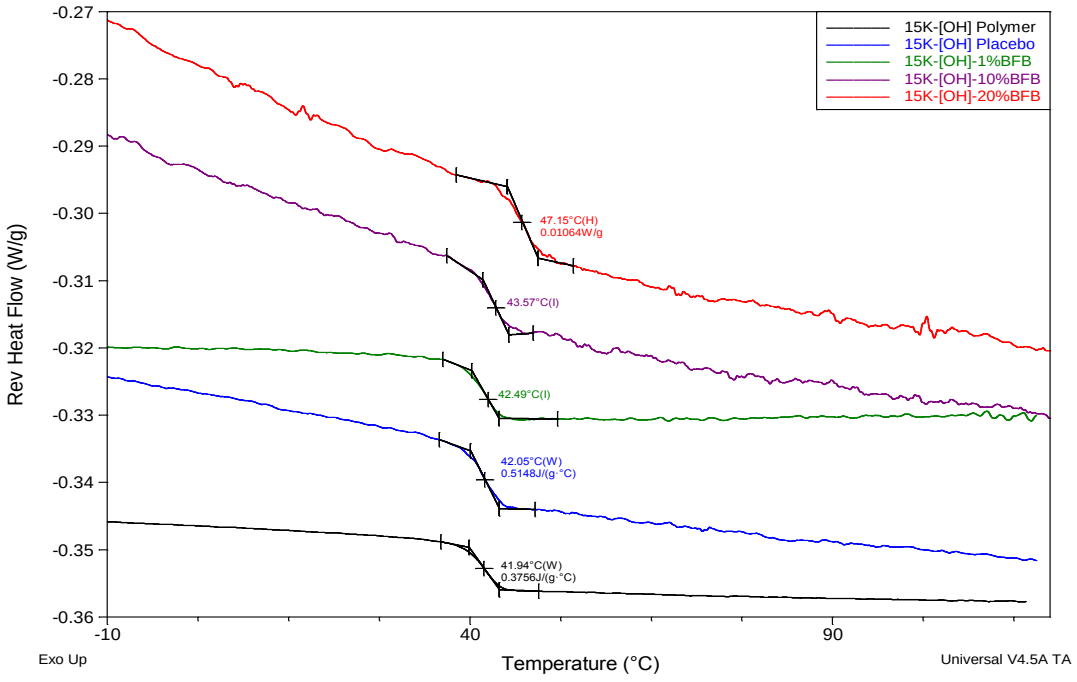

Figure 4.9: MDSC scans showing the effect of extrusion and percentage drug loading on PLGA-15-[OH]'s thermal properties. Drug loading at 1-10% did not affect the recorded Tg significantly, nor did the extrusion process. However drug loading at 20% increased the recorded Tg.

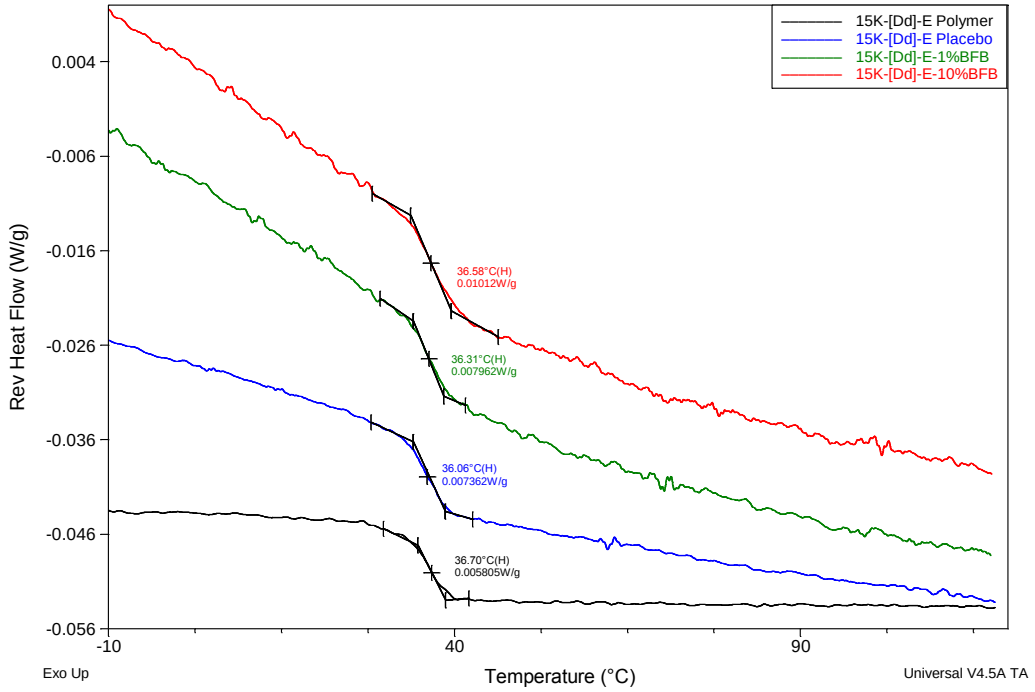

Figure 4.10: MDSC scans showing the effect of extrusion and percentage drug loading on PLGA-15-[Dd]-E's thermal properties. Drug loading at 1-10% did not affect the recorded Tg significantly.

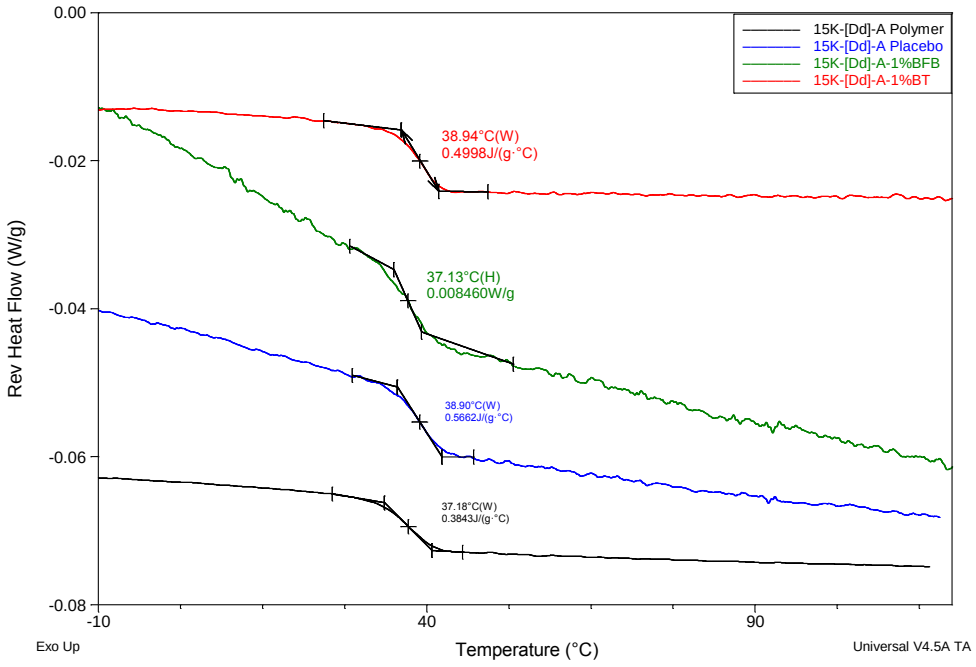

Figure 4.11: MDSC scans showing the effect of drug type loading on PLGA-15K-[Dd]-A thermal properties.

Figure 4.11 illustrates that regardless of the drug form whether as a free base or tartrate salt, at 1% w/w loading the polymer's Tg was not significantly affected. An example of the thermograms of the physical mixtures of Brimonidine free base with the butyl amide endcapped PLGA copolymer is shown in Figure 4.12. The existence of Brimonidine endothermic peak but with marked reduction in its intensity could be attributed to the low drug to polymer ratio.

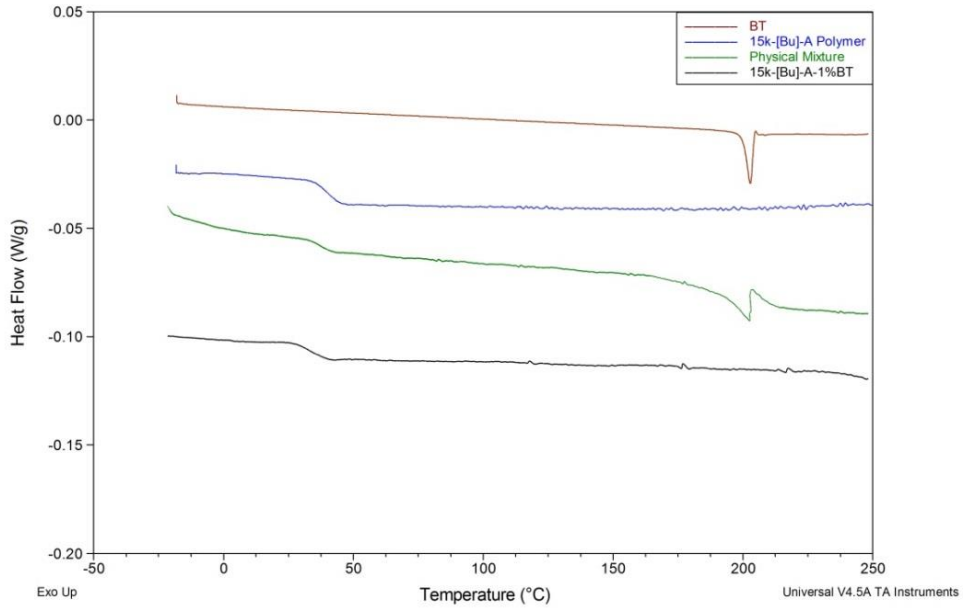

Figure 4.12: MDSC analysis of second heat curve of Brimonidine tartrate (BT), PLGA-15k-[Bu]-A, physical mixture of drug and polymer, drug loaded implant 15k-[Bu]-A-1%BT. Heating rate of $5^{o}C.min^{-1}$ to $250^{o}C$

On the contrary, the investigated Brimonidine-loaded PLGA implants showed no thermal event in this temperature range. The drug sharp characteristic peak was completely broadened and hardly detected in the DSC thermograms of the implants when compared to that of the physical mixture (Figure 4.12). These findings suggest the suppression of the drug crystallinity indicating complete drug amorphization and/or good distribution of

Brimonidine in the polymer matrices.(Aburahma and Mahmoud, 2011) X-ray powder diffractometry was considered in conjunction with MDSC analysis to reach a definite conclusion.

4.3.1.4. Effect of Extrusion and Drug loading on Polymer Crystallinity

The diffraction pattern of Brimonidine free base powder in Figure 4.13 revealed several sharp high intensity peaks at diffraction angles 2θ of 12.8°, 17.7°, 19.2°, 24.0°, 24.4°, 26.6°, and 34.3°, as previously recorded suggesting that it existed as a crystalline material.(Aburahma and Mahmoud, 2011)

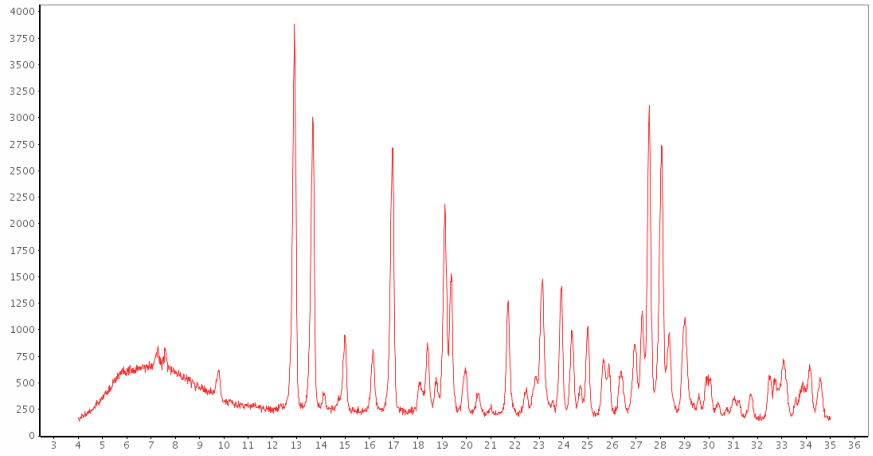

Figure 4.13: XRD diffractometry of Brimonidine free base

Figure 4.14 presents the XRPD of a representative example of the investigated implants, showing the polymer, placebo and 1% drug loaded implants. Both PLGA-15k-[Bu]-A polymer and its placebo implant recorded superimposable halo patterns indicating their amorphous nature was not affected by extrusion.(Park and Kang, 2013)

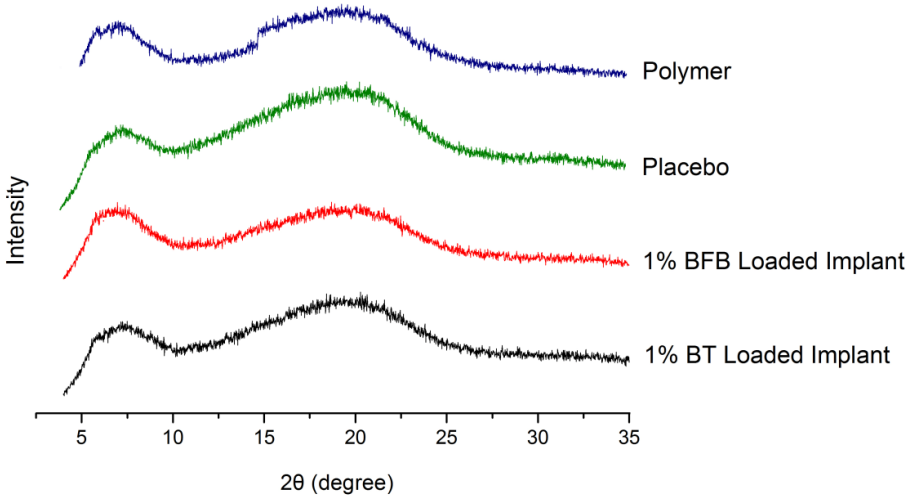

Figure 4.14: XRPD diffractometry PLGA-15k-[Bu]-A (powder), PLGA-15k-[Bu]-A Placebo implant, and drug-loaded PLGA-15k-[Bu]-A; 1% w/w Brimonidine free base and Brimonidine tartrate showing overlapping hallow indicating amorphous PLGA structure and possible uniform distribution of the drug load in the implant

Moreover, the diffraction pattern of the investigated 1% loaded implants did not differ from the placebo implant diffractogram showing a typical diffuse pattern which may be indicative of the complete conversion of Brimonidine to an amorphous form and/or its uniform distribution in the implant, supporting the results of DSC analysis presented earlier. The absence of sharp peaks associated with crystalline drug molecules has been previously used to verify that the drug is either molecularly dispersed or present in an amorphous state within the polymeric matrix. (Chandak and Verma, 2008)

This observation however, was not apparent at the higher drug loading concentration (10% w/w). Where the diffraction pattern of the 10% BFB loaded implants in PLGA-15k-[OH], PLGA-15k-[Dd]-E, and PLGA-15k-[Dd]-A

corresponded to the superposition of its individual components therefore Brimonidine was present in a crystalline state, as evident by the presence of its diffraction lines in Figure 4.15.

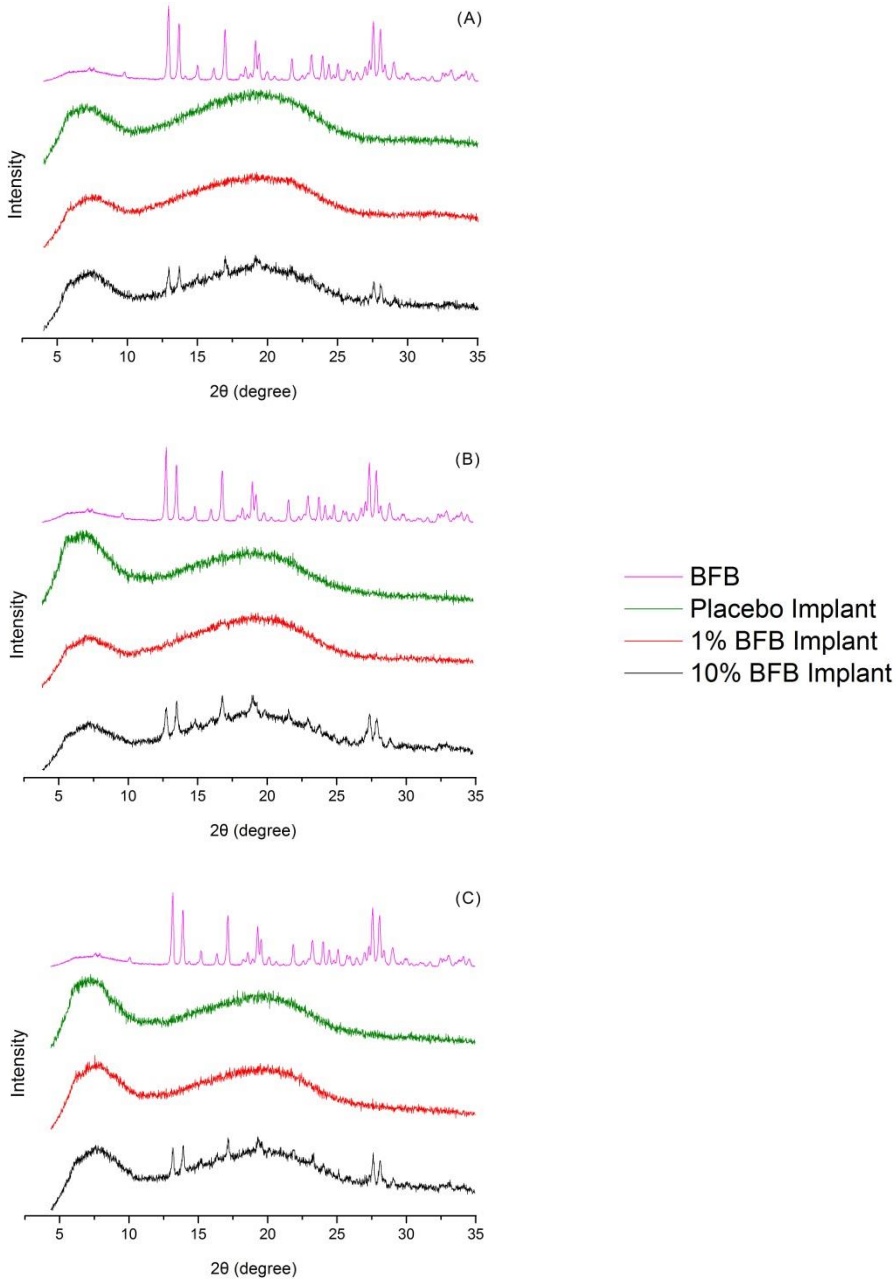

Figure 4.15: XRD diffractometry of (A) PLGA-15k-[OH], (B) PLGA-15k-[Dd]-E, and (C) PLGA-15k-[Dd]-A. showing the appearance of the crystalline Brimonidine free base peaks at higher drug loadings (10%w/w) compared to placebo and low drug loading implants (1%w/w)

4.3.2. In-Vitro drug release kinetics

The extruded implants were characterized for their *in vitro* release kinetics and effects of the end group and drug loading on drug release were evaluated. Plots of cumulative Brimonidine released (%) versus time for the controlled release of BFB/BT loaded implants are presented in Figures 4.16 to 4.30. These release profiles followed either a bi-phasic or tri-phasic release pattern previously reported for PLGA controlled release systems.(Berchane *et al*., 2007, Fredenberg, 2011) However several discrepancies appear which cannot be explained by a single theory. Therefore the formulations were divided into 4 subgroups for ease of comparison and discussion. Group I investigated the effect of drug loading concentration. The effect of ester and amide endcapping was studied in Group II and III respectively using non-endcapped PLGA as the control. Finally, Group IV studied the effect of using the salt form of the drug compared to the free base.

4.3.2.1. Group I: Effect of Drug Loading

The impact of the initial drug loading (1, 10 and 20%) on the resulting release kinetics in phosphate buffer pH 7.2 from PLGA-15K-[OH] implants is shown in Figure 4.16. Interestingly, although the initial drug loading substantially affected the resulting drug release rate (in other words the slope of the curves), it did not affect the shape of the drug release profiles (drug release patterns). The three plots showed a biphasic release pattern.

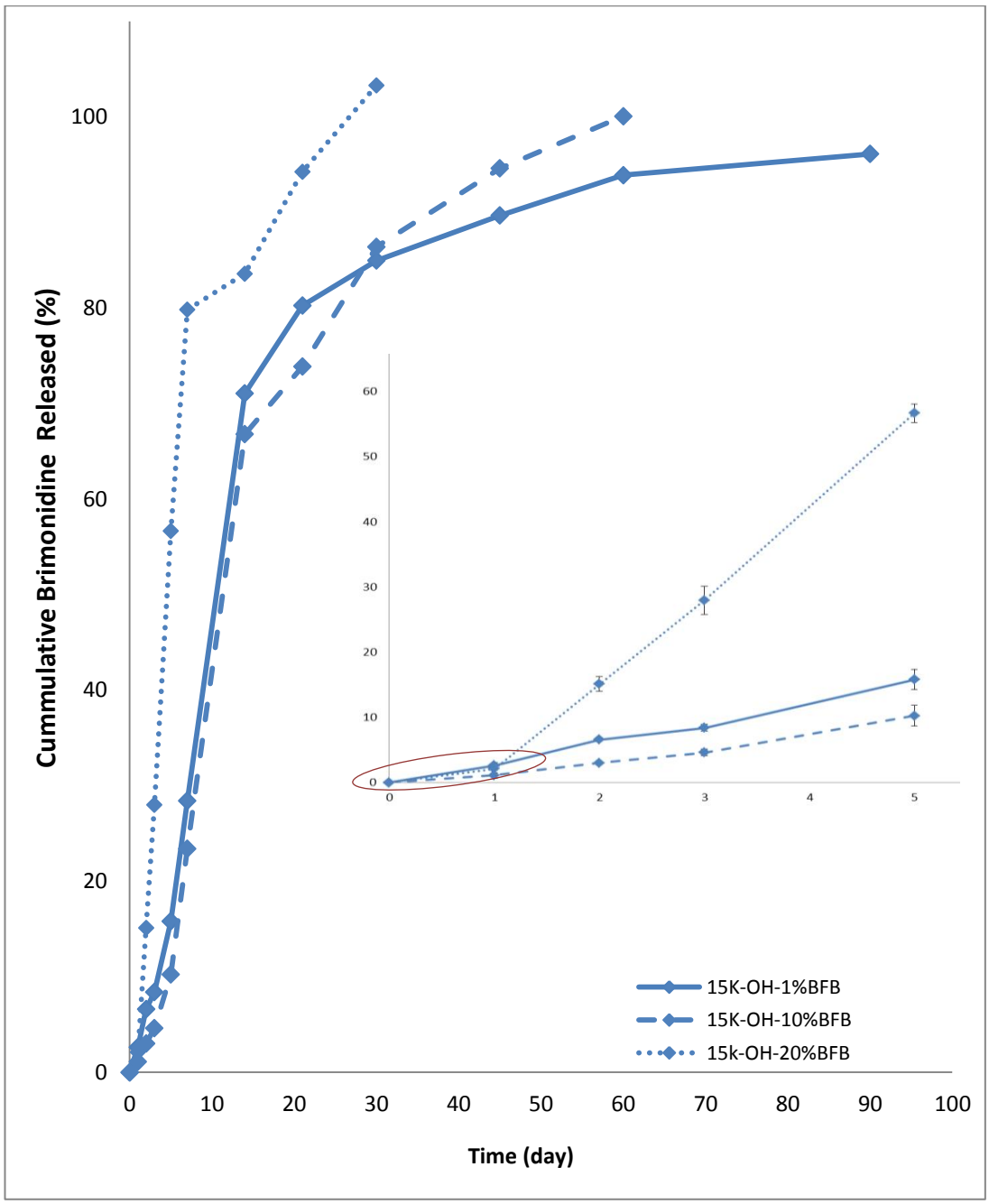

Figure 4.16: Effect of drug loading on Brimonidine free base release from non-endcapped PLGA implants upon exposure to the phosphate buffer pH 7.2 (Group I) in a 3-month release study. Each data point represents the average of three samples with SD. A biphasic release is evident at all drug loadings with depletion time of implant accelerated as drug loading increases.

When exposed to the release medium, an initial lag phase at all drug loadings illustrated by the red ellipse in Figure 4.15 inset was witnessed, unlike the typical burst release common in PLGA DDS. Pan *et al*. similarly reported that the release profile of curcumin from PLGA stents did not exhibit any burst release.(Pan Ch *et al*., 2006) One possible explanation is that significant water penetration and polymer relaxation has not been achieved yet. Therefore drug release is controlled by the diffusion of the drug with limited mobility through the glassy polymer matrix. Although transport through the polymer phase does occur when the drug is small and hydrophobic, the drug needs to enter the water phase, either at the surface or in the pores inside the DDS, since only the dissolved drug is available for diffusion.(Raman *et al*., 2005) Transport through water-filled pores by diffusion is concentration gradient dependant. For a sparingly soluble drug such as Brimonidine free base the rate limiting step then becomes drug dissolution - where the drug's solubility in water is 1.5 mg/ml, and this process could decrease the overall release rate.

Figure 4.17 schematically describes all the physical phenomena which are involved in the control of drug release from a swellable delivery system and will be used to explain the underlying mechanisms involved in the release of Brimonidine from the PLGA implants. As shown, the inner core of the implant is in the dry and glassy state (non-swollen). Upon contact with the release medium, water imbibes into the PLGA implant, the polymer concentration as well as polymer entanglement decreases.

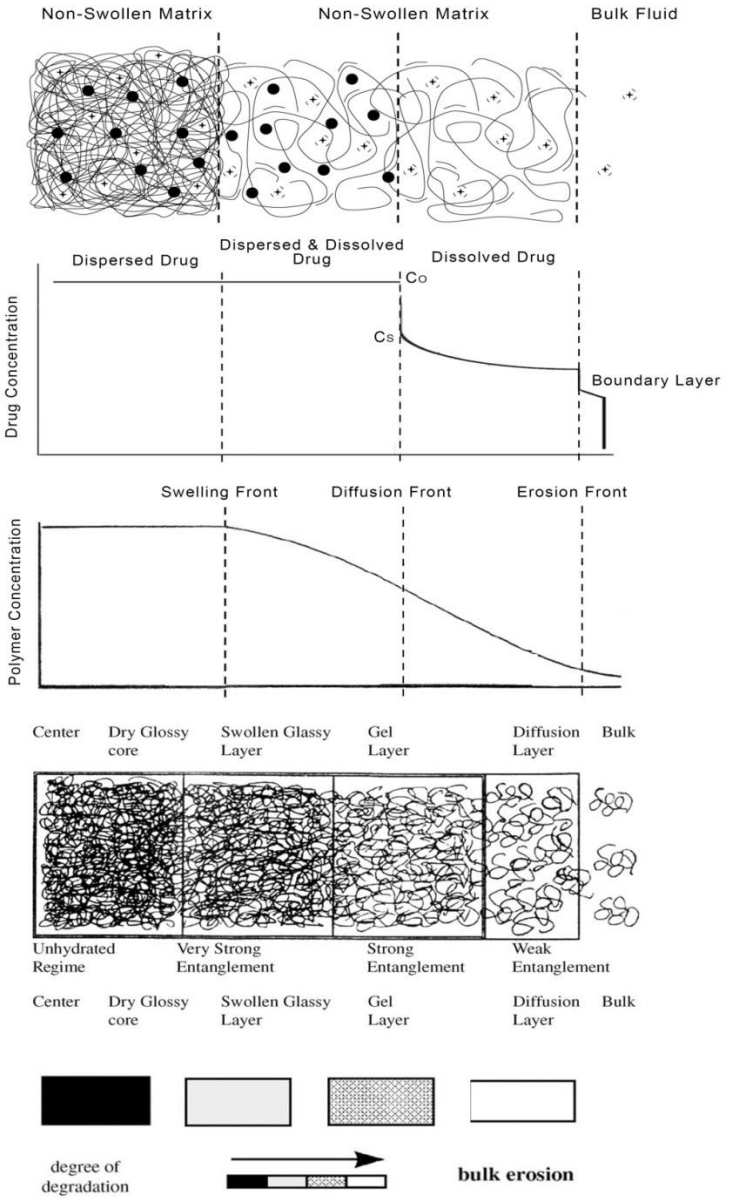

Figure 4.17: Schematic presentation of a swelling controlled drug delivery system containing dissolved and dispersed drug (stars and black circles, respectively). The system exhibits three moving boundaries: an erosion, a diffusion, and a swelling front. The level of polymer matrix disentanglement is shown as a function of the polymer concentration, where the disentanglement is due to the imbibing of water into the system that results in polymer concentration changes in the matrix. The drug concentration profile shows the drug concentration at the matrix surface (Cs) and the initial drug loading (Co). Finally, bulk degradation proceeds throughout the DDS. (Fredenberg *et al*., 2011),(Siepmann and Siepmann, 2008)

As soon as certain, polymer-specific water concentration is reached, the macromolecular mobility steeply increases. This phenomenon is called “polymer chain relaxation”.(Fredenberg *et al*., 2011) The transition from the glassy (less mobile) to the rubbery (more mobile) state leads to implant swelling and the front at which this process takes place is called “swelling front”. Importantly, this is not a *stationary* boundary, but rather a *moving* one. The described phenomenon has to be accounted for when studying the release profiles of controlled delivery systems, as it can either increase or decrease drug release rates depending on the type of polymer and drug delivery system.(Siepmann and Siepmann, 2008)

At the three studied drug loadings in the PLGA implants as the rubbery front proceeds the mobility of the polymer chains significantly increases, resulting in increased drug mobility and, thus, potentially increasing drug release rates. In fact in a fully swollen polymer matrix the diffusion coefficient of the drug has been reported to be of the same order of magnitude as in an aqueous solution.(Arifin *et al*., 2006)

At 1 and 10% w/w Brimonidine free base drug loadings both formulations showed overlapping slopes hence similar release rates. This may also be caused by possible ionic polymer–drug interactions with the free carboxylic groups. Miyajima and colleagues reported that basic drugs remained dissolved in PLGA matrices throughout the release study due to strong polymer-drug interaction. This suggests that based on their physicochemical

properties, basic drugs would undergo a diffusion-controlled release from polymer cylinders including an initial Fickian phase followed by a second faster stage associated with diffusion of the drug through aqueous pores formed in the polymer.(Miyajima *et al*., 1998)

In practice, doubling the initial drug loading from 10 to 20% w/w significantly increased the resulting drug release rate, indicating the loading threshold of the implants. This might be attributable to the distribution of the drug inside the implant as well as the volume ratio of drug to polymer. Drug molecules trapped on the surface of the polymer matrix during the manufacturing process, are rapidly released. The amount of drug encapsulated, i.e. the load, and location are of paramount importance as the space left vacant after drug release will result in pore and channel formation thus penetration of substantial amount of water into the system upon activation in a release medium. This further accelerates the release rate.(Gasmi *et al*., 2015, Tamaddon *et al*., 2015)

The enhanced diffusion phase was followed by a second slower release rate as the polymer starts to dissolve and erode at the interface where the entanglement is weak which is known as the erosion front which is also moving. Erosion starts when the dissolved polymer degradation products are able to diffuse into the release medium. PLGA normally undergoes bulk erosion as it is relatively rapidly hydrated.(Fredenberg *et al*., 2011) With increasing drug load the implant was depleted earlier. As shown in the Figure

4.16 complete drug release observed at earlier time points, for example from 90 to 60 and 30 days as drug loading increased from 1 to 10 and 20 %w/w respectively. The explanation may be as follows. As the initial drug concentration in the delivery system exceeds solubility in the drug matrix, dissolved and drug as a particulate co-exist within the matrix. During the swelling of the matrix, the dissolved drug moves to the exterior, the establishment of a diffusion front. In which a sharp gradient of drug concentration occurs. At high drug loadings, the undissolved drug particulates are released as the integrity of the swollen zone fails. Drug dissolving from the particulates creates pore and channels which allows solvent to the interior accelerating the release rate. As long as a non-dissolved excess of drug exists, the concentration of dissolved drug is constant (drug molecules that are released are replaced by dissolution of solid drug, providing a continuous saturated solution). Once the excess drug is dissolved, the concentration within the swollen matrix and the release rate decrease.(Siepmann and Siepmann, 2008)

The superimposition of the various physical phenomena occurring at the same time (illustrated in Figure 4.17) adds to the complexity of modelling drug release from the system. Therefore, caution should be exercised when drawing conclusions merely from the release profile. The release studies were carried out for the complete intended therapeutic duration (3 months), however significant difference appear in the first month of the study and thus will be the focus of analysis in the following text.

4.3.2.2. Effect of Endcapping:

Group II: Effect of Ester endcapping

At low molecular weight non-capped PLGA result in a less hydrophobic polymer with increased rates of water absorption, hydrolysis and erosion. The amount of water absorbed and the duration of drug release is highly dependent on these properties. The initial Tg is also dependent on these properties. Therefore, modification of PLGA end groups is perhaps one of the effective ways to modulate drug release.(Fredenberg *et al*., 2011) The effect of ester endcapping on the initial rapid release phase witnessed in the non-endcapped PLGA implants is illustrated in Figure 4.18.

In the control implant PLGA-15K-[OH] (blue line) the polymer absorbed a significant amount of water, which plasticised the polymer chains and led to increased chain mobility. This resulted in accelerated initial drug release. On the other hand, ester endcapping with ethyl, dodecyl and cholesterol end groups resulted in the introduction of a prolonged lag phase, recognized in the first 7 days of the study. Consequently, shifting the enhanced diffusion mediated phase to later time points, thus producing a rather distinct overall triphasic profile. The lag phase is primarily attributed to increased implant hydrophobicity and consequent depression of the initial water penetration into the system governing the dissolution and diffusion mediated part of the release profile. Results confirm the effect of endcapping previously discussed in Chapter 3 Figure 3.16 where endcapping resulted in significant decrease

in polymer moisture uptake properties. The reduced water uptake was coupled with the structural relaxation of amorphous PLGA which results in increased polymer density and reduced porosity.

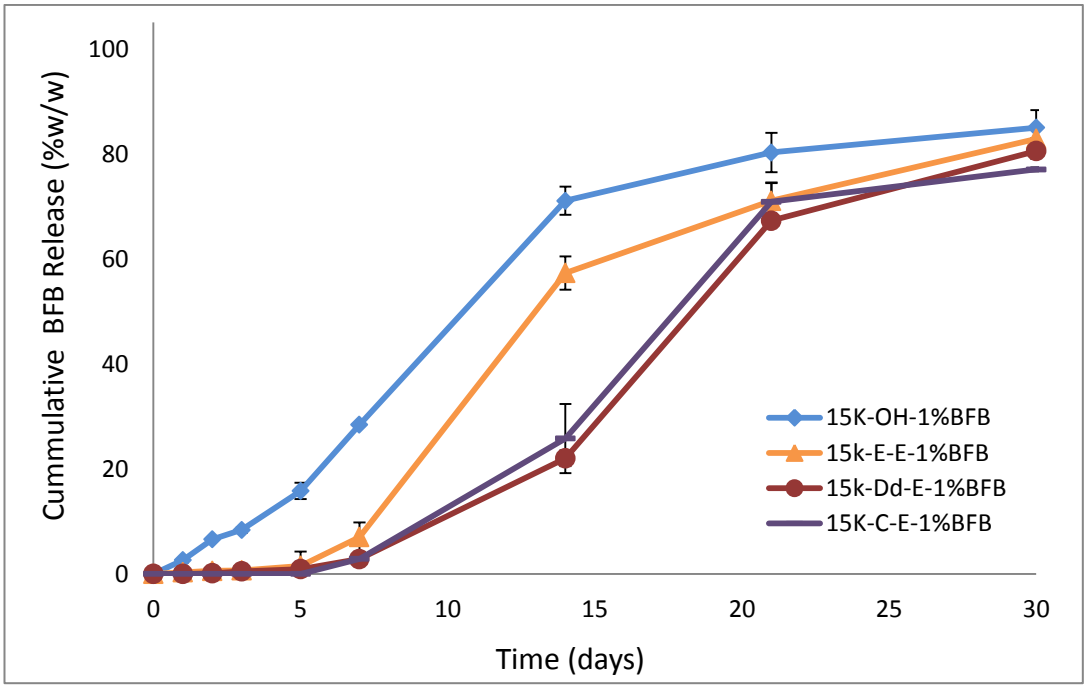

Figure 4.18: Comparative release profiles of PLGA implants with ethyl, dodecyl and cholesterol ester endcapping (Group II) at 1% Brimonidine loading in a 3 months' release study. The first month of the release profiles indicate an initial lag phase attributed to increased polymer hydrophobicity when compared to the non-endcapped PLGA implant (control). Each data point represents the average of three samples with SD.

The initial lag phase was followed by a second more rapid diffusion controlled drug release phase as the implant swells and pores/channels form resulting in accessibility of new surfaces (days 7 - 21). Consequently, around day 21 the release profiles converged and started to overlap as they enter a third relatively slower release phase which is primarily governed by erosion.

Figure 4.19 illustrates how the nature of the ester endcap influences the implants' ability to reduce the initial rapid release phase. As the hydrophobic content of the endcap increases so does the polymer's hydrophobicity (as thoroughly discussed in Chapter 3).

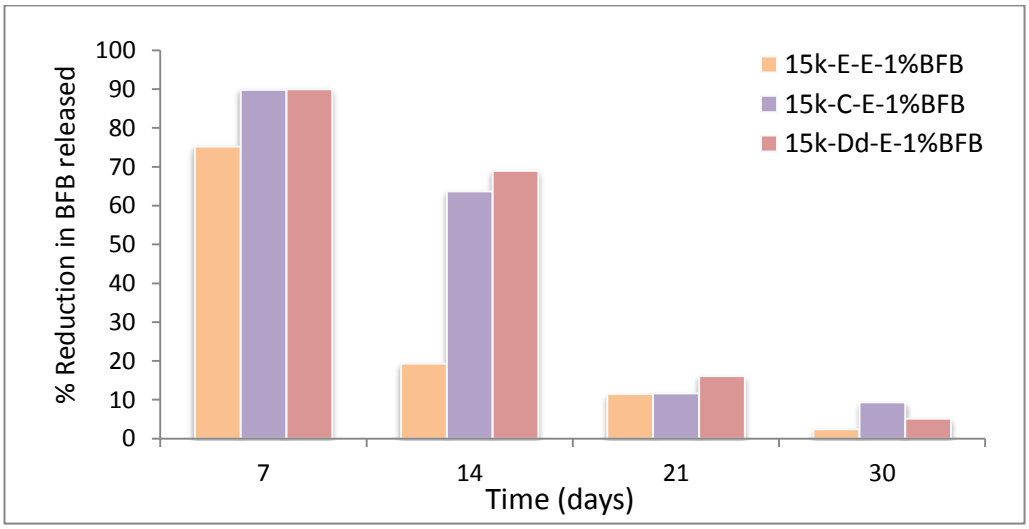

Figure 4.19: Effect of Ester endcap hydrophobic content on reduction in Brimonidine release relative to non-endcapped PLGA implants at 1 %w/w drug loading. Increased hydrophobicity imparted by the endcap retarded initial drug release in the diffusion mediated phase (up to day 14). As erosion of the implants is initiated (day 21) endcapping has no significant effect on drug release rates.

The reduced water uptake capacity explains the significant reduction in cumulative drug released in comparison with the non-endcapped implants. The dodecyl ester and cholesterol endcap recorded the highest percentage reduction of 90% during the first week of the release study. Whereas the ethyl ester endcap resulted in a lower overall reduction in Brimonidine released (75% reduction) after day 7.

The role of endcapping in decreasing the drug release rate subsides after the initial two weeks as seen in Figure 4.19 since the governing rate limiting step is no longer swelling and dissolution but rather correlated with erosion and/ or deformation of the implant. The reduced release rate in the last phase may also be attributed to the decreasing concentration gradient and increasing diffusion distance, leading to a decrease in the rate of transport.

Group III: Effect of Amide endcapping

Similar to previous findings in Chapter 3, amide endcapping imparted different properties to the polymer than ester endcapping. The Brimonidine release profile from the amide endcapped PLGA implants followed one of two trends as seen in Figure 4.20. Taking the non-endcapped PLGA implant as the control, endcapping with the short chain ethyl amide and the relatively longer dodecyl amide resulted in release profiles comparable to that of the control. Meanwhile endcapping with butyl and phenyl amide introduced an initial lag phase similar to that seen in the ester endcapped series.

The onset of rapid drug release was found to be correlated with rate and extent of swelling, erosion and deformation of the DDS. The increase in release rate was ascribed to the accessibility of new surfaces. There is a difference between erosion leading to drug release without drug transport, and erosion that increases the rate of drug transport. The latter has been reported as a release mechanism countless times, at least after a lag period,

which is often described as diffusion-controlled release. (Fredenberg *et al*., 2011) The observed drug release profile results confirmed the dependence of drug release on the dynamic physical properties of the polymer illustrated in Table 4.6

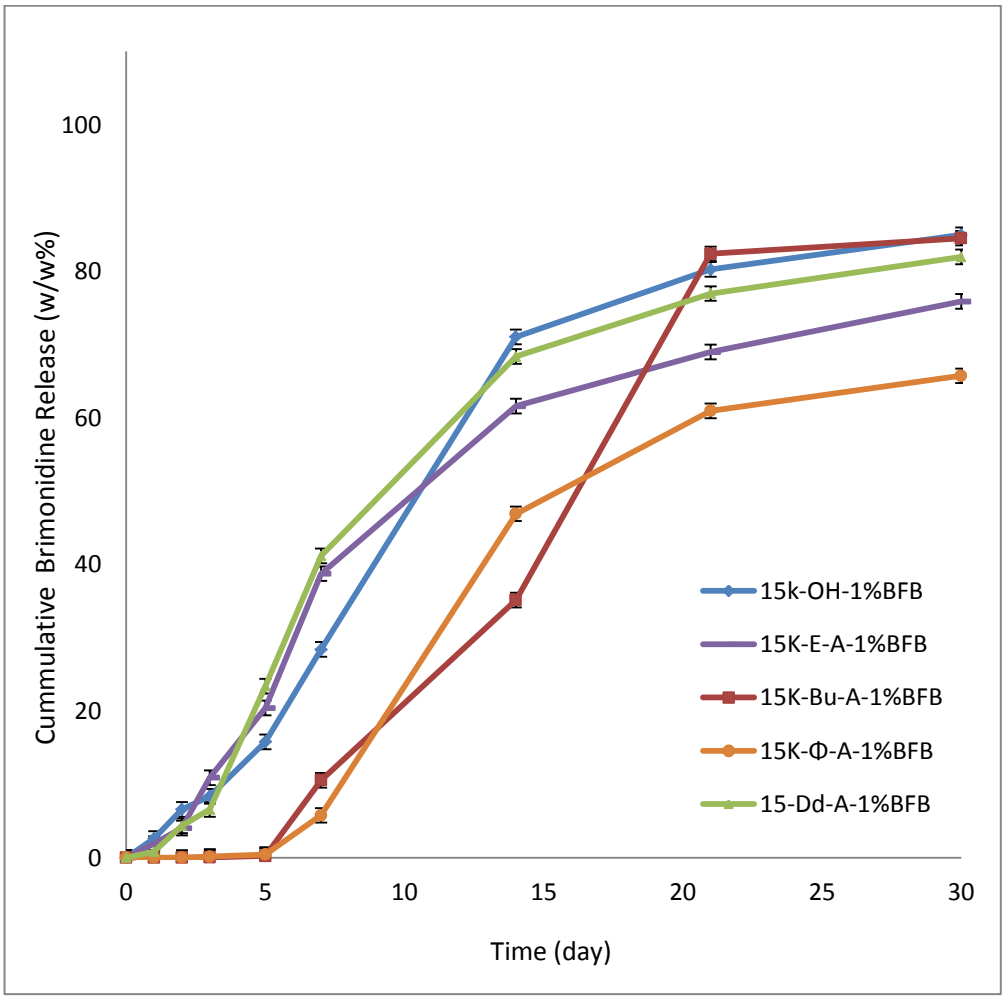

Figure 4.20: Comparative release profile of Brimonidine free base from 1% w/w loaded controlled release matrix implants prepared using PLGA with different amide endcapping (Group III) in a 3 months' release study. The ethyl and dodecyl amide endcapped PLGA samples (15k-[Dd]-A and 15k-[E]-A) showed drug release rates similar to the control. Endcapping with butyl and phenyl amide (15k-[Bu]-A and 15k-[Φ]-A) resulted in impeded drug release evident by the lag phase up to day 7. Each data point represents the average of three samples with SD

Table 4.6: Implant analysis showing the effect of sorption on glass transition and the properties of different PLGA polymers after 7 days' exposure to PBS pH 7.2 at 37^{o}C

Polymer	Tg (^{o}C)*		Molecular Weight at day 7 (%)	Cumulative Brimonidine Released at day 7(%)
	before exposure	after exposure		
15k-[E]-A	44.26	38.41	53.51	38.72
15K- [Bu]-A	40.22	39.37	59.18	10.57
15K-[Φ]-A	44.76	43.74	67.73	5.78
15K-[Dd]-A	37.18	35.23	58.10	41.17

*Tg measured before and after sorption in DVS (data adapted from Chapter 3)

Since the diffusivity of Brimonidine in the polymer is low, the two main release mechanisms associated with its release from the PLGA-based implants are swelling and degradation/erosion. At significant water uptake and swelling the transition from the glassy to the rubbery state has to be accounted for in the model.(Siepmann and Göpferich, 2001, Arifin *et al*., 2006)

In the case of the 15K-[Dd]-A-1%BFB implants the starting T_g was 37.18^{o}C, therefore PLGA was in the rubbery state during the entire drug release period which increases drug mobility. Coupled with the relative significant drop in molecular weight (22.2% decrease, Figure 4.21) after the first 24 hrs and the water uptake capacity of the amide species in the polymer backbone, 15K-[Dd]-A-1%BFB implants witnessed the highest release rate profiles.

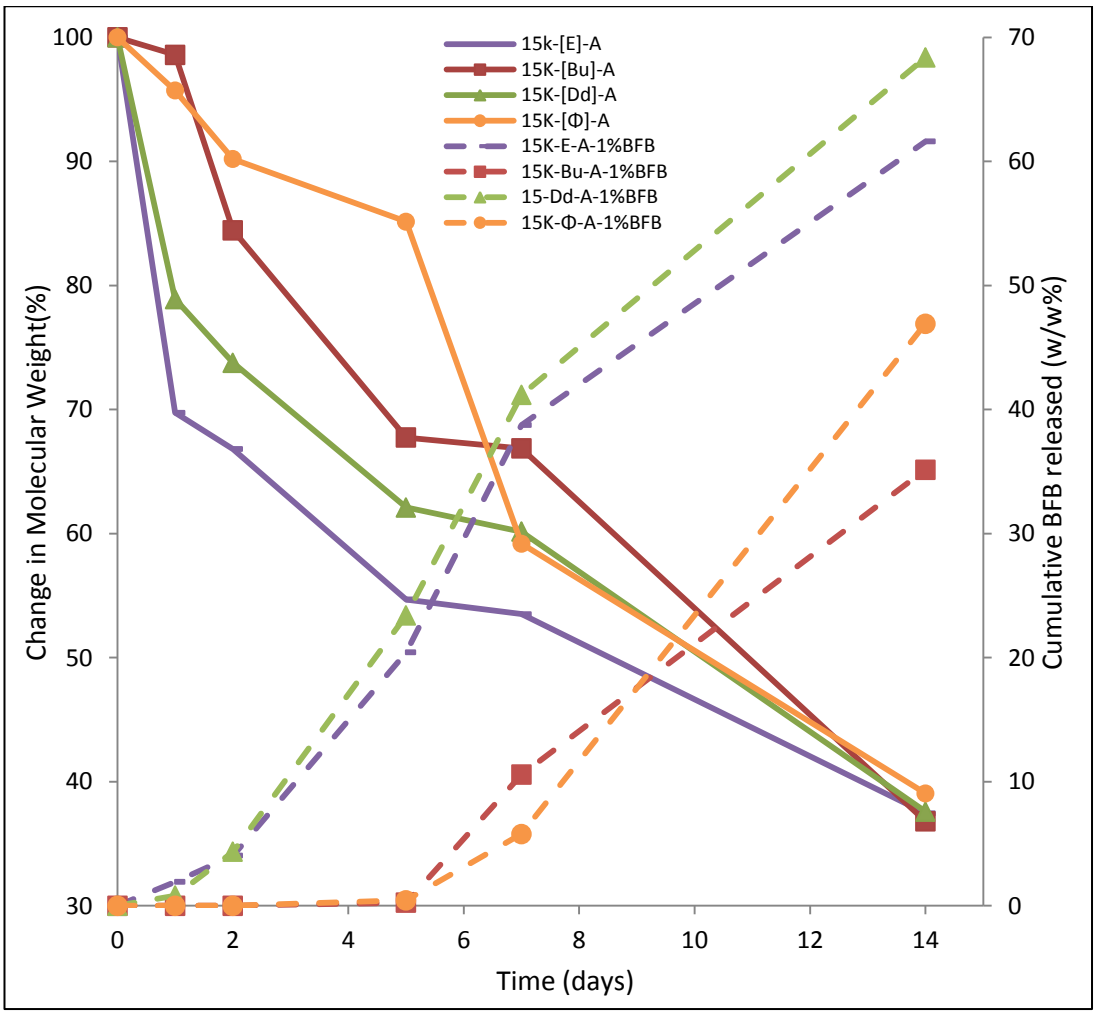

Figure 4.21: Time-dependent molecular weight changes in PLGA polymers incubated in PBS pH 7.2 at 37^{o}C and the corresponding drug release rate for the respective Brimonidine loaded implants. Cumulative Brimonidine released was found to correlate with percentage degradation of the polymer matrix, a slower degradation rate in 15k-[Bu]-A and 15k-[Φ]-A (solid lines) was mirrored in a lag phase in the release profile of 15k-[Bu]-A-1%BFB and 15k-[Φ]-A-1%BFB (dotted lines).

Although the rest of the implants had T_g values above 37˚C for the original polymer upon immersion in water at 37˚C, they behaved differently. The high water uptake capacity of 15K-[E]-A-1%BFB implants magnified the plasticizing effect of water which transfers the polymer into the rubbery state

as seen in the drop in T_g recorded in Table 4.6. Since the rate of diffusion through the PLGA matrix is very dependent on its the physical state it increases by several orders of magnitude at the transition from the vitreous to the rubbery state.(Fredenberg *et al*., 2011)

In addition, the enhanced water uptake of the system resulted in accelerated polymer erosion and degradation as seen in Figure 4.21. Erosion creates pores, further increasing the rate of diffusion. While a high concentration of drug near the surface of the implant is the most common cause of burst release. Both surface-associated and internally located drug may contribute to an initial rapid release rate. Where early loss of implant integrity results in an initial rapid release rate even in implants containing a uniform distribution of drug.(Allison, 2008)

Unlike the 15K-[E]-A-1%BFB and 15K-[Dd]-A-1%BFB, the degradation of 15K-[Bu]-A-1%BFB and 15K-[Φ]-A-1%BFB was slower, leading to less decrease in their Tg upon contact with water. The mobility of polymer chains depends on the glass transition temperature (Tg). The transport resistance is higher for PLGAs in the vitreous state, and water absorption and hydrolysis proceed more slowly. This explains the delay in their degradation and erosion kinetics (Figure 4.21). This was confirmed by their ability to maintain their physical integrity for longer durations as shown in Figure 4.22. Whereas 15K-[E]-A-1%BFB and 15K-[Dd]-A-1%BFB, experienced a collapse in structure

which is often the result of degradation and the decrease in Tg as explained by Park Et al.(Park *et al*., 1995)

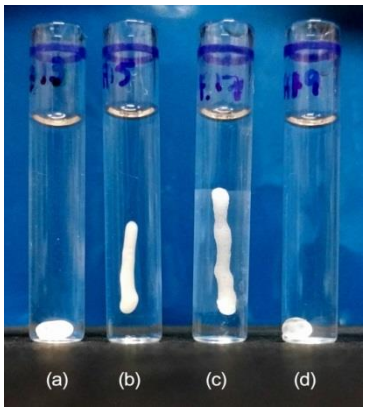

Figure 4.22: Macroscopic evaluation of Amide endcapped PLGA series after 7 days of incubation at 37^{o}C. Implants 15K-[Bu]-A-1%BFB (b) and 15K-[Φ]-A-1%BFB (c) maintain integrity meanwhile 15K-[E]-A-1%BFB (a) and 15K-[Dd]-A-1%BFB (d) show complete collapse of structure

In other words, once in contact with water, scission of ester bonds and subsequent decrease in molecular weight started immediately influencing the degradation rate of the polymers, their swelling behaviours and overall integrity. Hydrolysis creates acids, which further catalyse hydrolysis. The polymer becomes less hydrophobic with decreasing Molecular weight. The polymer molecular weight thus becomes a potentially decisive factor for key properties of the implant such as their mechanical stability and swelling behaviour, consequently drug release profile. (Gasmi *et al*., 2015) This is depicted in Figure 4.21 where the delay in polymer degradation in 15K-[Bu]-A-1%BFB and 15K-[Φ]-A-1%BFB resulted in a lag phase in their initial drug release.

Although hydrolysis leads to erosion and pore formation and small pores consequently grow, eventually coalescing with neighbouring ones to form fewer, larger pores thus increasing the rate of drug release. Erosion may also lead to a drop in Tg, with possible rearrangement of polymer chains, and

pore closure, and thus possibly a decrease in drug release, another explanation for the impeded release rates. As seen in the previous example several process take place at different locations in the matrix which may result in regions with different characteristics, affecting drug release in more than one way.(Fredenberg *et al*., 2011)

4.3.2.3. Effect of Drug form

Group IV: Effect of using the Brimonidine free base versus tartrate salt

Generally, controlling the release rate of a hydrophilic drug is more challenging, especially if the matrix swells in the release medium. Consequently, the drug diffuses rapidly through the swollen regions and ‘‘dumps’’ into the solution.(Tamaddon *et al*., 2015)

The use of Brimonidine free base in the solid implant formulations has several advantages over its tartrate salt, where the lower solubility of the free base lowers burst effect, and the free base drug equivalent dose per implant can be higher at the same weight. Therefore, the controlled delivery of hydrophilic drugs such as Brimonidine tartrate is preferably done in relatively hydrophobic polymeric matrices where the drug has negligible release through the hydrophobic matrices. However, the setback with using hydrophobic polymers is longer degradation profiles.

The amide endcapped PLGA implants successfully controlled the release of the salt form of Brimonidine following similar release profiles of its base

counterpart – with the exception of 15K-[E]-A implants. Although the 15K-[E]-A based implants released 38.07% and 41.08% Brimonidine free base and Brimonidine tartrate respectively after 6 days, the Brimonidine tartrate loaded implant showed an initial fast release rate this could be attributed to the fact that 15K-[E]-A has the highest degradation rate accelerating drug release (Figure 4.23).

The previous findings indicate that in the studied implants drug dissolution is not the rate limiting step and the release was controlled by diffusion through water channels. Therefore, the events governing pore formation and closure play a crucial role in drug release. However, the different factors that influence these processes, sometimes in more than one way, add to the complexity of the system which means that there are many possible explanations for a given release profile. For example, a soluble basic salt may decrease the rate of hydrolysis by neutralizing acids or create pores due to water absorption caused by increased osmolality, and act as a porogen enhancing drug release.(Fredenberg *et al*., 2011)

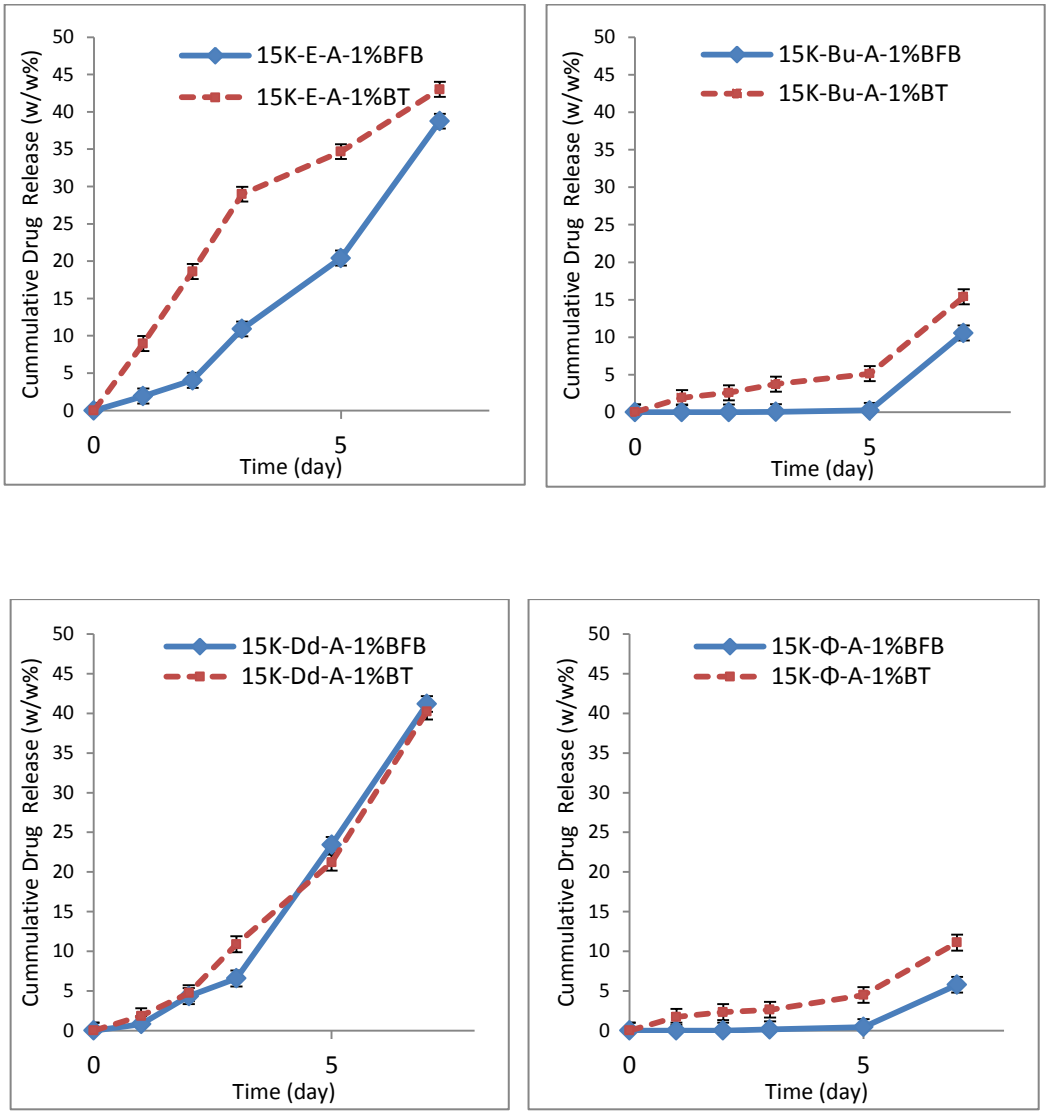

Figure 4.23: Comparative release profile of 1% w/w loaded Brimonidine free base (solid line) or Brimonidine Tartrate (dotted line) from controlled release matrix implants prepared using PLGA with different amide endcapping (Group IV) in a 3 months release study. Graphs showing the first week of the study. Each data point represents the average of three samples with SD.

4.3.3. Understanding underlying release mechanisms

As discussed in the previous section visual analysis of the release profile does not provide a distinct start and end-point of each phase, phases may have their origin as additive processes or events that counteract each other. Consequently, there are many possible explanations of the different phases. The complexity of the processes or events that enhance or inhibit drug release makes it difficult to draw any conclusions merely from the release profile. A slow second phase, or lag-phase, may not necessarily be caused by a dense polymer with low porosity, which is the common explanation. It may also be caused by pore closure or polymer–drug interactions that inhibit the release of the drug.(Fredenberg *et al*., 2011)

In attempt to understand the effect of endcapping on the underlying release mechanism from PLGA implants, the dodecyl ester and amide endcaps where chosen as representatives of the ester and amide endcap series respectively in the following study. The primary effect of drug loading on the initial release phase (14 days) of the release profiles was further investigated. Figure 4.24 shows the drug release profiles of the two studied drug loadings (1 and 10%) on the different endcap chemistry (ester and amide) with the same aliphatic content (dodecyl) compared to the non-endcapped polymer.

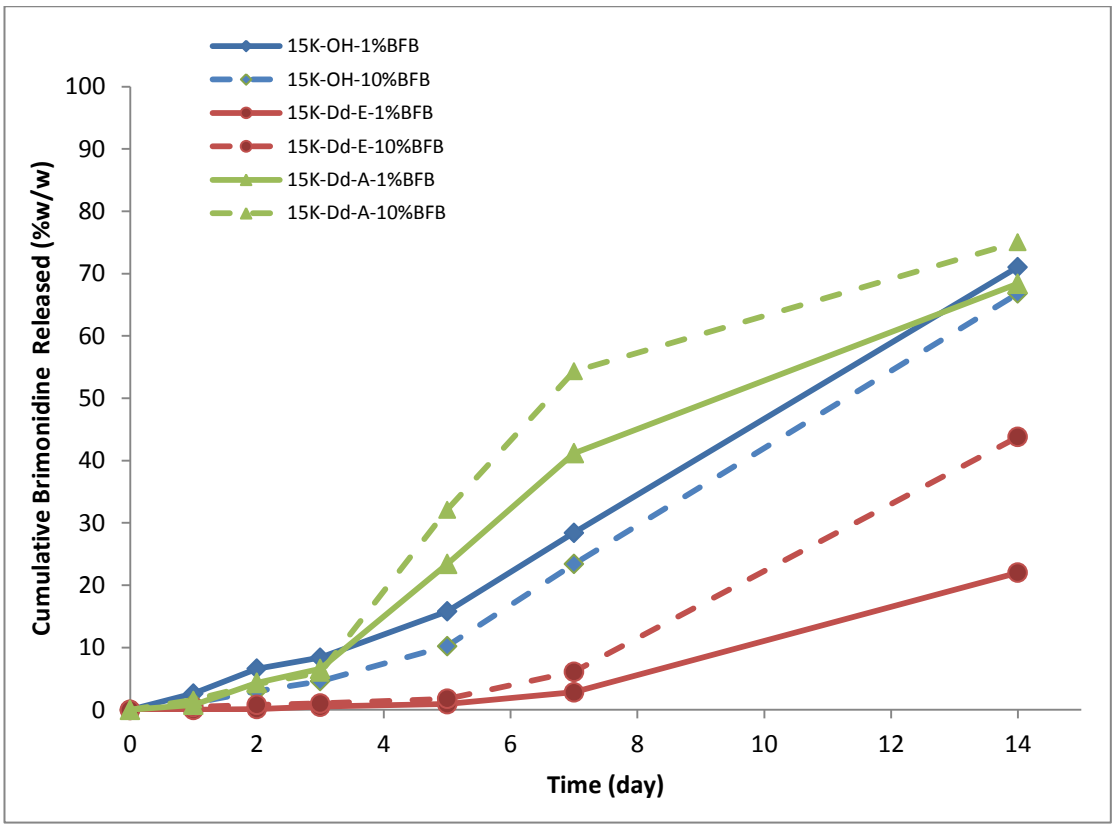

Figure 4.24: Effect of drug loading; 1 and 10% w/w BFB loaded dodecyl ester and amide endcapped PLGA implants with non-endcapped PLGA implants as the control. Results indicate that at 1-10% w/w drug loading critical loading threshold was not exceed and hence release mechanism unchanged.

The increase in drug loading in the non-endcapped polymeric implants (15k-OH-1%BFB and 15k-OH-10%BFB) did not result in a significant change in the release profile. Brimonidine is a base with a pka of 7.8. Thus, it is protonated at the pH values which can be expected within the PLGA-based implants during drug release.

The non-endcapped PLGA as well as its degradation products exhibit free carboxylic end groups. Consequently, ionic attractive interactions are highly likely between these carboxylic end groups and the positively charged

Brimonidine. Such attractive forces can be expected to hinder drug diffusion within the polymeric network and, thus, explain the overall of the release profiles. Similar suggestions were adopted by Klose *et al* for the release of lidocaine from PLGA based DDS. (Klose *et al*., 2008)

In contrast, no attractive ionic interactions can be expected between Brimonidine free base and the endcapped PLGAs. This is evident as increasing drug loading in both dodecyl ester and amide endcaps lead to a significant increase in cumulative Brimonidine released at 14 days (98.79 and 9.79% increase respectively). Another possible polymer–drug interaction that may influence the release rate is hydrogen binding of Brimonidine with the dodecyl amide endcap. This was found to plasticize PLGA which may enhance drug release as reported by Blasi and colleagues.

As the environment inside PLGA matrices is dynamic so is the degree of polymer–drug interactions. Consequently these interactions may be responsible for the release of only a certain proportion of the drug molecules or play a role only in part of the release period.(Fredenberg *et al*., 2011)

X-ray scans of the 10% loaded implants were performed to provide a better understanding of the drug distribution with in the matrix system an example of which is illustrated in Figure 4.25 and 4.26 (left pane). The scans revealed that the implants were monolithic, having the therapeutic agent homogenously distributed through the biodegradable polymer matrix.

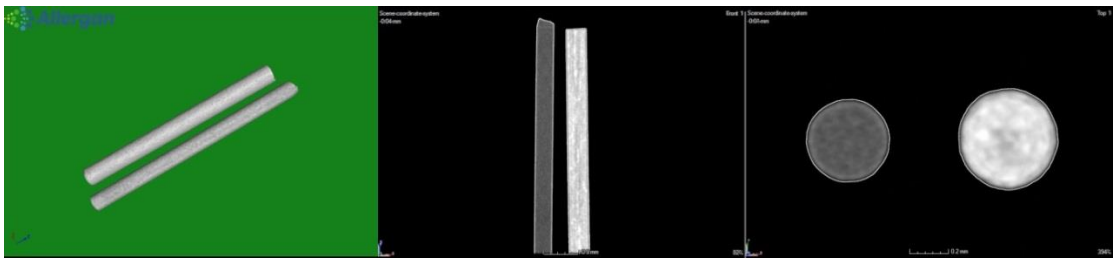

Figure 4.25: X-ray micro-CT images of placebo and 15k-OH-10%BFB PLGA implants showing uniform distribution of Brimonidine throughout the implant.

Figure 4.26 shows how the integrity of the 10% loaded implants changes with time and how that is reflected in their respective release profiles. To elucidate the underlying mass transport mechanisms controlling release from endcapped PLGA implants 1% w/w drug loading was selected for further analysis

4.3.3.1. Swelling kinetics and correlation with drug release

Endcapping with either a dodecyl ester or amide decreased the polymer's glass transition as recorded in Table 4.7. Therefore, PLGA in both implants was expected to be in the rubbery state during virtually the entire time periods of drug release, allowing for similar release profiles and change in implant shape pattern.(Gasmi *et al*., 2015) However that was not the case because although PLGA-based systems are mostly considered diffusion or erosion-controlled possible swelling often is ignored. The amount of water absorbed is highly dependent on the properties of the PLGA which significantly controls drug release rates. (Fredenberg *et al*., 2011)

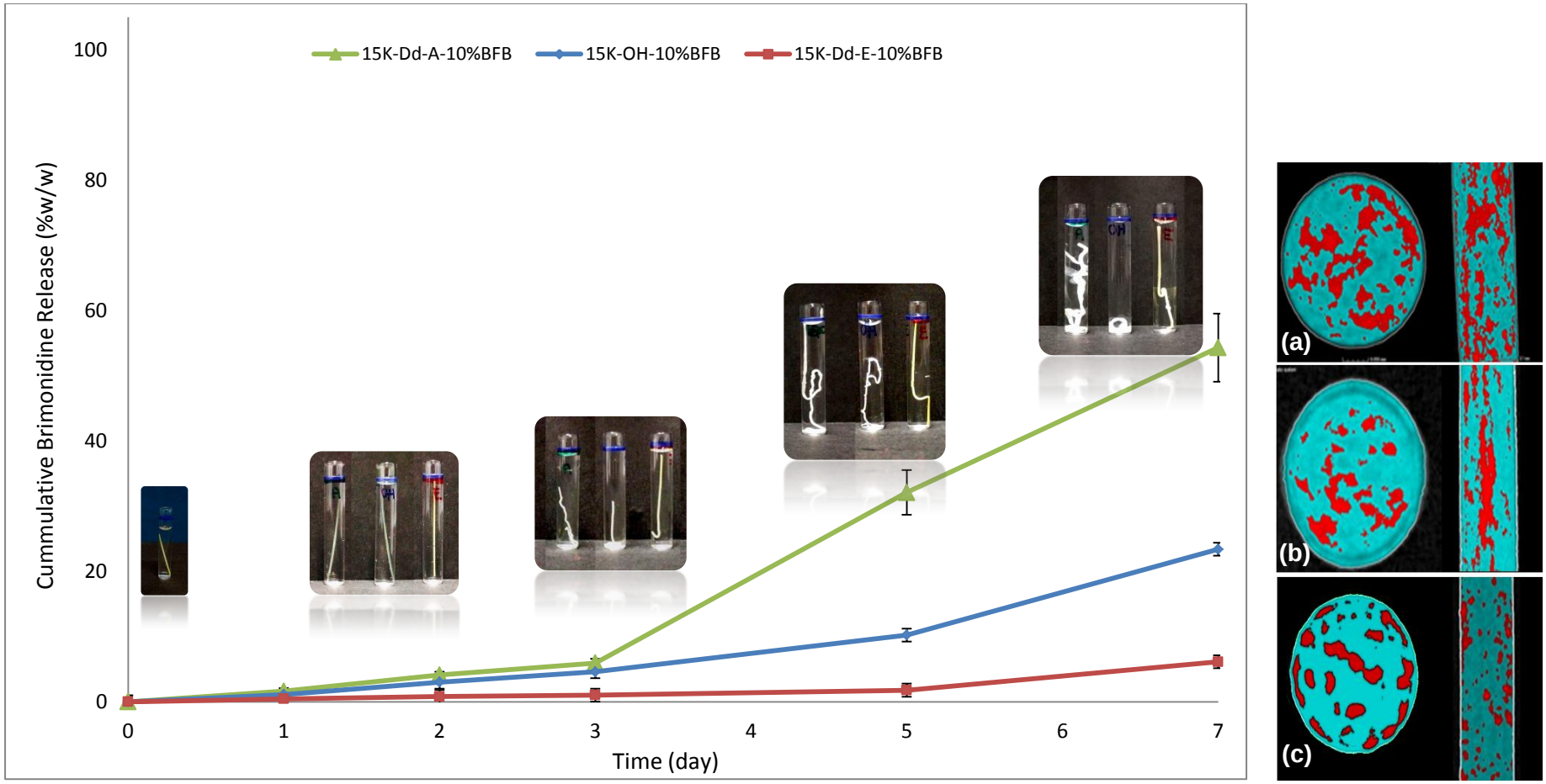

Figure 4.26: Comparing 10% w/w Brimonidine loaded implants of different endcaps. The X-ray micro-CT images of 15k-[Dd]-A-10%BFB (a), 15k-OH-10%BFB (b), and 15k-[Dd]-E-10%BFB (c) indicate homogenous distribution in drug in matrix (left pane). The cumulative release profiles indicate that after 5 days of incubation significant morphological changes in the implants occur which coincide with significant drug release.

Table 4.7: Implant analysis after 7 days' exposure to PBS pH 7.2 at 37^{o}C

Polymer Sample	TG-SA data* Moisture Sorption (%w/w)	Water uptake after 7 days (%w/w)	Tg (^{o}C)		Cumulative Brimonidine Released at day 7(%)
			before swelling	after 7 days of swelling	
15K-[OH]	1.5	55.56	42.49	17.75	28.41
15K-[Dd]-E	0.9	37.5	36.31	21.41	2.84
15K-[Dd]-A	2.3	126.19	37.39	19.59	41.17

*TG-SA data adapted from Chapter 3

Taking the non-endcapped 15k-[OH]-1%BFB PLGA implants as reference, the control implants showed a cumulative release of 28.41% at day 7. Endcapping the polymer with a dodecyl amide further increased the initial release by 44.95% reaching 41.17% cumulative Brimonidine released from the 15K-[Dd]-A-1%BFB implants. On the contrary adding a dodecyl ester end group in 15K-[Dd]-E-1%BFB significantly impeded the initial release to 2.84%, thereby causing 90.00% reduction.

This confirms the previous discussion, that drug release from the implants is dependent on both the relaxation of the polymer, based on its Tg, as well as its degree of hydrophilicity and capacity to uptake water creating channels thus enhancing drug dissolution and diffusion.

Figure 4.27 illustrates both the *in vitro* drug release kinetics (upper panel) and the swelling kinetics (lower panel) of PLGA implants loaded with 1% Brimonidine upon exposure to phosphate buffer pH 7.2. Clearly, the onset of

implant swelling precedes the onset of the drug release phase as water penetration into the implants is generally much more rapid than subsequent drug release. (Siepmann and Siepmann, 2008) Thus, the swelling of the PLGA significantly regulates the resulting drug release rate as the mobility of dissolved Brimonidine molecules increased with the onset of significant swelling. (Gasmi *et al*., 2015) This is further evidence for the hypothesis that PLGA implant swelling plays a dominant role in the control of Brimonidine release from the investigated systems.

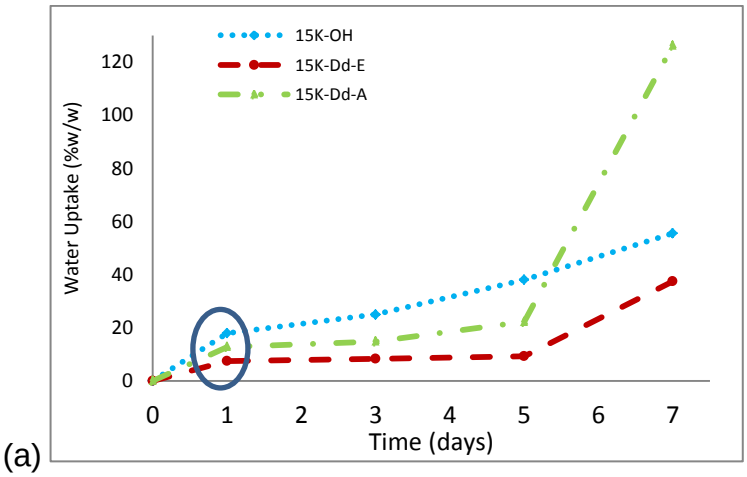

(a)

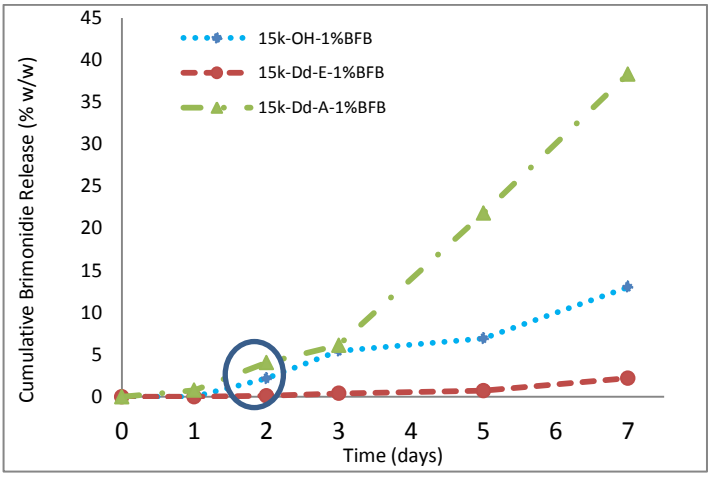

(b)

Figure 4.27: Swelling of (a) and drug release from (b) PLGA implants loaded with 1% Brimonidine in phosphate buffer pH 7.2 at 37 ^{o}C

On the first day, the highest swelling capacity was observed in the 15K-[OH]-1%BFB implants followed by 15K-[Dd]-A-1%BFB implants, where rapid increase in their swelling index was accompanied by great expansion in size. This can be attributed to the hydrophilic nature of the end groups as a consequence of the presence of hydroxy and amino groups in their respective structures that have the ability to interact with water molecules.(Aburahma and Mahmoud, 2011) At day 5 of the study 15K-[Dd]-A-1%BFB implants swelling rate significantly increases overriding 15K-[OH]-1%BFB implants' water uptake capacity. Findings from TG-SA sorption studies carried out in Chapter 3 and replicated in Table 4.7 support the discussion.

This parameter is of paramount importance not only for drug release prediction but also for prediction of potential irritability caused by the implant due to possible change in geometry and orientation post injection. Visual observation indicated different endcapped polymers undergo different change in shape pattern. Both 15K-[OH]-1%BFB and 15K-[Dd]-A-1%BFB implants swelled rapidly and expanded in their size, failing to preserve their integrity as seen in Figure 4.28. Whereas, 15K-[Dd]-E-1%BFB implants maintained their integrity throughout the swelling study and their swelling index did not reach the values of the other tested implants. This observation was logically ascribed to the increased hydrophobic nature of the polymer due to endcapping, which prevented water from rapidly penetrating into the ocular implant.

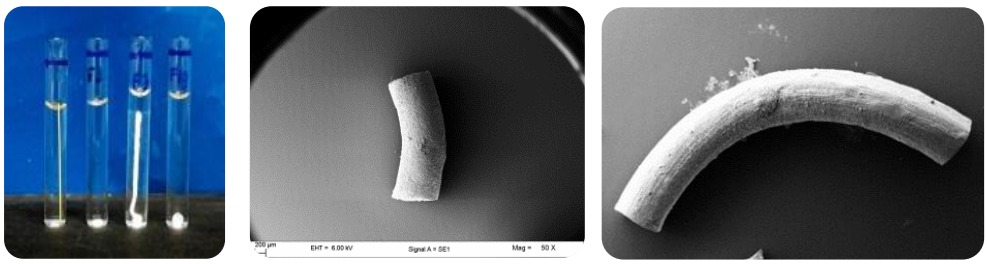

Figure 4.28: Macroscopic images comparing 15k-OH-1%BFB, 15k-[Dd]-A-1%BFB and 15k-[Dd]-E-1%BFB show that 15k-OH-1%BFB, 15k-[Dd]-A-1%BFB implants failed to preserve their integrity, while 15k-[Dd]-E-1%BFB witnessed the least change, evident in SE micrographs on sectioned implants after swelling.

Thus the reduction in the initial drug release rate could be attributed to the depression in the rate and extent of initial water penetration into the system governing the dissolution mediated part of the release profile. (Aburahma and Mahmoud, 2011), where enhanced polymer relaxation due to the plasticizing effect of the endcaps leads to polymer closure and increased diffusion path length.

4.3.3.2. Implant Degradation and Impact on Drug Release

For the underlying drug release mechanisms not only the physical states of the drug and polymer are of utmost importance but also the dynamic changes in the polymer molecular weight upon exposure to the release medium can be decisive.(Siepmann and Göpferich, 2001)

Once in contact with water, the ester bonds of the macromolecules are randomly cleaved influencing the degradation rate of the polymer. The

polymer molecular weight thus becomes a determinant factor for key properties of the implant.(Gasmi *et al*., 2015) The term degradation is used with slightly different meanings in different studies: i.e. both hydrolysis and erosion of the polymer, or the combination of the two processes. In this study degradation refers to the molecular weight decrease caused by hydrolysis.

In order to verify the *in-vitro* release data and gain more insight regarding the degradation characteristics of the implants in the release medium, the implants were evaluated microscopically (Figure 4.29 and 4.30). Implants' surfaces were compared before exposure to the release medium and after 3, 7 and 14 days of exposure. Figures 4.29 shows the polymer degradation kinetics, swelling behaviour and examples of microscopic pictures of PLGA implants loaded with 1 % Brimonidine upon exposure to phosphate buffer pH 7.2 at 37^{o}C. The implants' changes in shape due to water uptake was accompanied by substantial morphological changes as seen in the cross-sectional view of the implants under the SEM at 3, 7 and 14 days of incubation.

Monitoring the dynamic changes in the diameter of the implants during the first 14 days of the drug release period offered valuable insight into the possible underlying drug release mechanisms. The diagrams in Figure 4.29 show that the diameter remained almost constant and then substantially increased. This is explained by the initial high degree of polymer chain entanglement that effectively prevents substantial swelling.

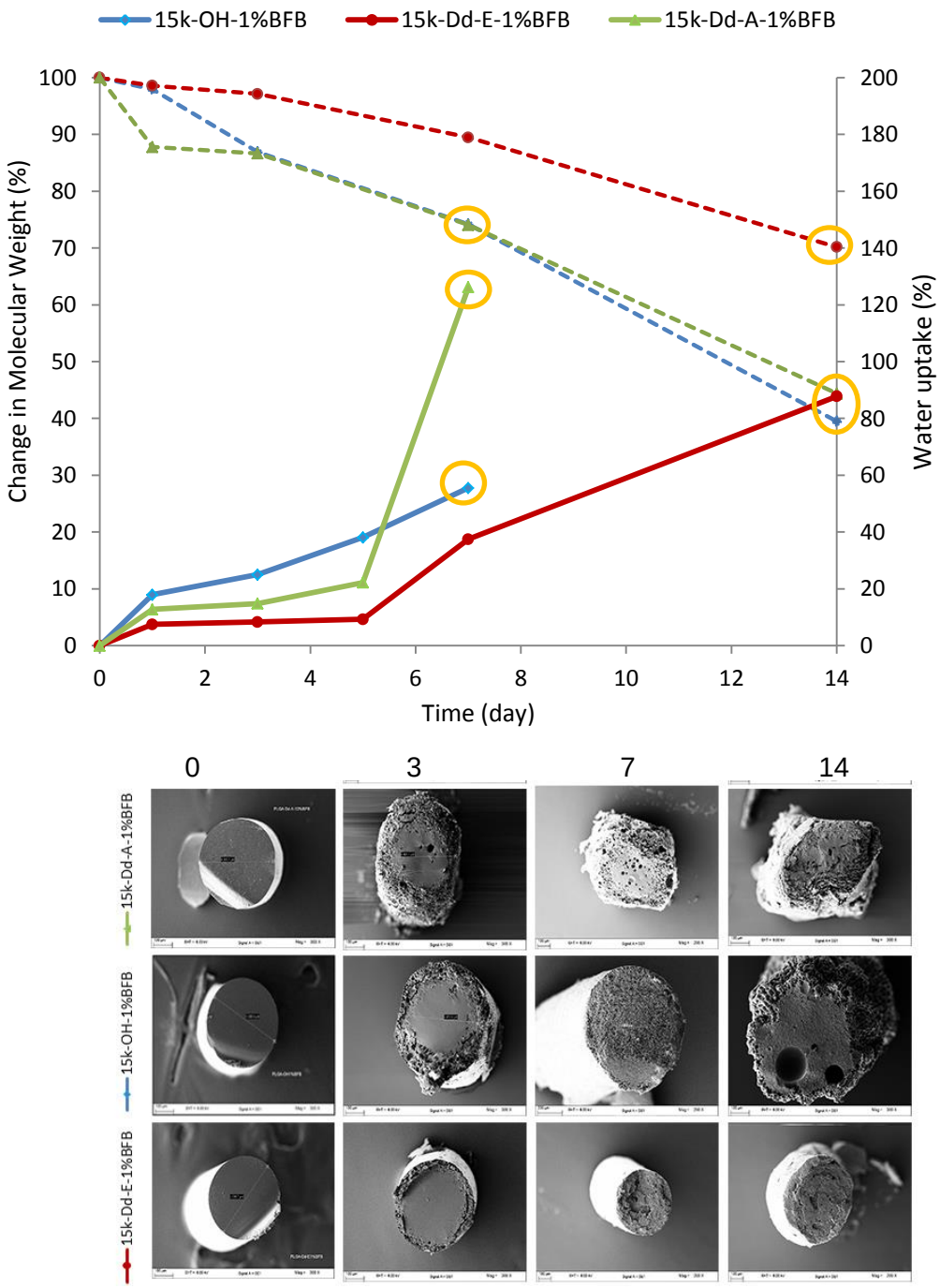

Figure 4.29: Change in molecular weight (left y-axis) and the swelling kinetics (right y-axis) of PLGA loaded with 1% Brimonidine upon exposure to phosphate buffer pH 7.2. The ellipses indicate the periods for the onset of substantial swelling (upper Figure). SEM images of the cross-sectional surfaces of PLGA implants containing 1% w/w Brimonidine base showing the Dynamic changes in the diameter before incubation in release medium, and after 3, 7, 14 days of incubation (lower image).

Upon contact with water, the polyester chains are plasticized and cleaved by hydrolysis and as soon as the degree of macromolecular entanglement becomes insufficient to prevent substantial particle swelling, the PLGA matrix can increase in volume. This is illustrated by a certain lag-time seen in Figure 4.29 till the critical PLGA molecular weight is reached, at which polymer swelling is less hindered. This was defined by GPC analysis, as 75% of starting Molecular weight.

As it can be seen, the critical PLGA molecular threshold value seems to be roughly around 7 days for 15K-[OH]-1%BFB and 15K-[Dd]-A-1%BFB implants, which coincides with the onset of swelling. The ellipses in Figure 4.29 illustrate the approximate onset time points for substantial swelling observed in this study. However, this was shifted to later time points in the case of the hydrophobic 15K-[Dd]-E-1%BFB implants. Thus, the decrease in the polymer molecular weight of the PLGA is more rapid with increasing polymer hydrophilicity. Where the critical macromolecular chain length, allowing for substantial particle swelling, is more rapidly reached and drug release phase sets at earlier time points. Moreover, the swollen ocular implants failed to preserve their integrity and were easily fragmented upon removal from the swelling medium. Accordingly, they were discontinued from the swelling study.

Figure 4.30 shows the polymer degradation, drug release kinetics and microscopic pictures of PLGA implants initially loaded with 1% Brimonidine.

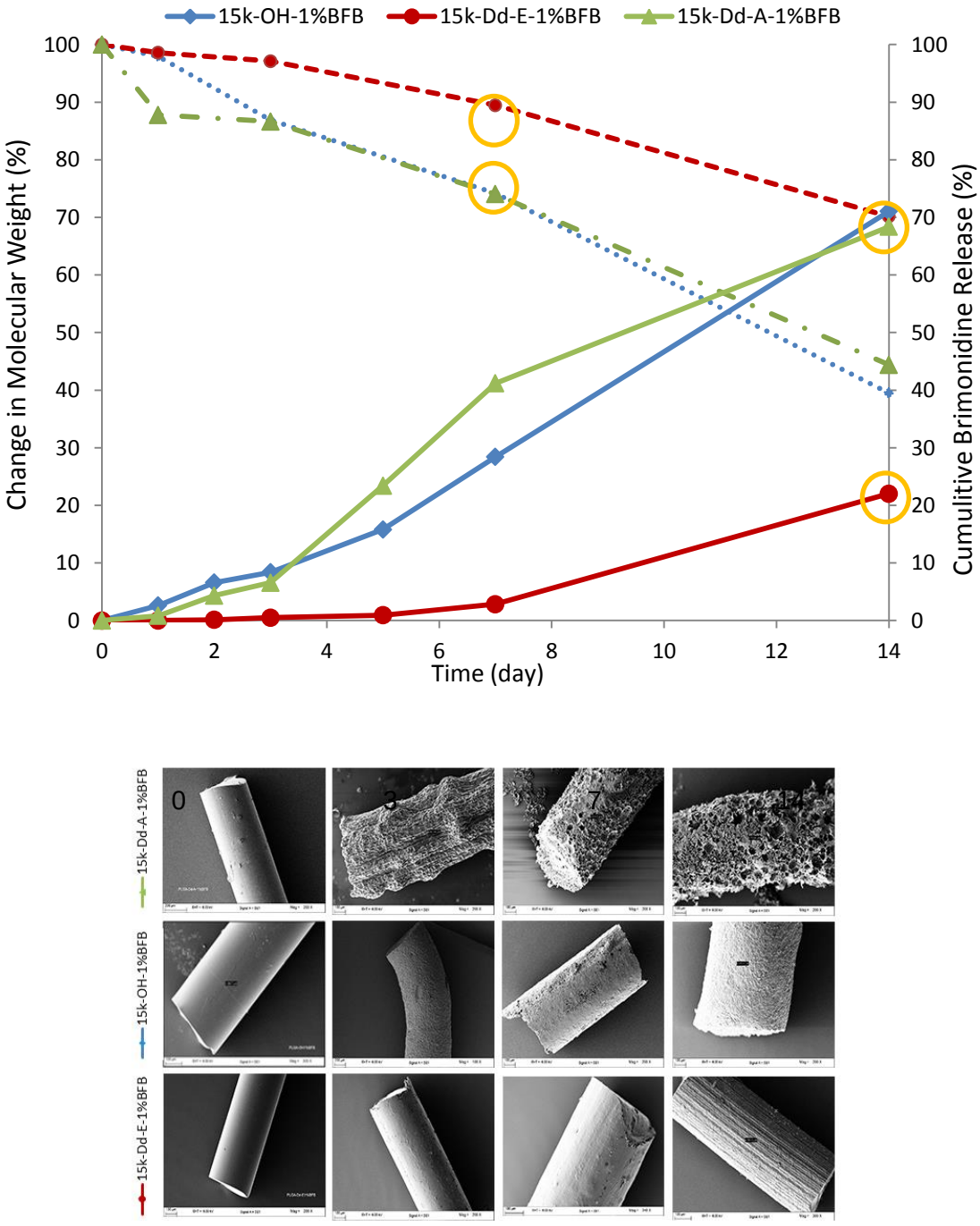

Figure 4.30: Change in molecular weight (left y-axis) and cumulative Brimonidine released (right y-axis) of PLGA loaded with 1% Brimonidine upon exposure to phosphate buffer pH 7.2 The ellipses indicate the time points for the onset of substantial degradation is followed by significant drug release (upper Figure). SEM images of showing the surfaces of PLGA implants illustrate pore formation and deformation in the implants upon incubation after 3, 7, 14 days (lower image).

Once again, upon exposure to phosphate buffer pH 7.2, the right y-axis shows the drug release kinetics, whereas the left y-axis illustrates the dynamic changes in molecular weight. The images at the bottom of Figure 4.30 show examples of microscopic pictures of implants' surface after 3, 7 and 14 days of exposure to the release medium.

As it can be seen, the implants' surface was initially smooth, but progressively became irregular with time. Negligible cracks appeared on the implants before incubation. However, as the random cleavage of the ester bonds of the polymer continues the degradation products steadily create an increasing osmotic pressure within the system, attracting more and more water into the implant. When the polymer degradation products become water-soluble, they diffuse out into the surrounding bulk fluid. Consequently, the local pH in the systems can significantly drop which then leads to autocatalytic effects, since PLGA degradation is catalysed by protons in the systems. (Gasmi *et al*., 2015)

As the pH and other micro-environmental characteristics change with time, the conditions causing the slow release are altered and the observed dynamic changes in the implants' size result in tremendous changes in the systems' composition and hence drug release. More fractures develop and a highly porous surface of the systems becomes obvious drug depletion accelerates, as the process of pore formation dominates over pore closure.(Fredenberg *et al*., 2011) This is particularly evident in the highly

porous structure of the 15K-[Dd]-A-1%BFB implants coupled with a 70% cumulative release after 14 days.

Langer and Peppas described two types of erosion; *surface* or *bulk erosion.* This was dependent on the relative rates of water penetration and polymer chain cleavage.(Langer and Peppas, 1983) In surface erosion, polymer chain cleavage is faster than water penetration. Consequently, the degradation process is mostly restricted to the outermost polymer layers and the erosion predominantly affects the surface, and not the inner parts of the device. In contrast, if water penetration is much more rapid than polymer chain cleavage, the entire system is rapidly wetted and degradation occurs throughout the device (bulk erosion). PLGA copolymers tend to be bulk eroding due to their water uptake capacity and less reactive functional groups as evident in the 15K-[Dd]-A-1%BFB and 15K-[OH]-1%BFB implants.(Siepmann and Siepmann, 2008)

However, the SE micrographs of the 15K-[Dd]-E-1%BFB implants indicate that the structure of the PLGA implants witnessed little erosion and degradation during the treatment period. Endapping PLGA with a hydrophobic ester resulted in segmental relaxation overriding the rate of water uptake. This lead to pore closure and thus a rather decelerated degradation rate, as a matter of fact referring to Figure 4.29 the cross-sectional SEM images of the implant show a dense core coupled with porous outer shell which has been previously reported for PLGA systems where a

collapse in the polymer structure results in decreased porosity hence retarded drug release. This may explain the delay in the onset of the rapid release phase commonly attributed to the onset of polymer degradation, as Friess and Schlapp reported that the onset of could be phase in II or III depending on the type of PLGA.(Friess and Schlapp, 2002)

It is possible from the previous discussion to visualize three steps which govern the drug release from PLGA implants; penetration of the dissolution medium into the polymeric matrix, dissolution and diffusion of dispersed drug particles through the polymeric matrix, erosion and degradation of the polymer matrix. The slowest step will control the release rate. Describing the process controlling the release rate is more informative than describing the way of drug release, when it comes to how drug release can be modified. However, due to the complexity of the system it is not always clear which of the processes is dominating, and in a chain of processes that leads to drug release it is not obvious which one is the rate-determining process. This will be further examined in Section 4.3.4

4.3.4. Kinetics of Release from Implants.

In order to understand the mechanism and kinetics of drug release, the results of the *in vitro* drug release study for the first 60% cumulative drug released were fitted into various kinetic models (Equations 4.2-4.5). Namely, zero order (cumulative percent drug released versus time), first order (log cumulative percent drug retained versus time), Higuchi (cumulative percent released versus √t), and Peppas (log of cumulative percent drug released versus log time) as depicted in Table 4.8.

These models best describe the process of drug release and help determine whether the release is due to a simple diffusion phenomenon, or there is a rate-limiting step, governing the drug-release process.(Costa and Sousa Lobo, 2001) The coefficient of determination (r^2) values for the various kinetic models was evaluated. The selection of the model that best fits the dissolution data was based on the highest recorded r^2

In general, in a monolithic system such as the extruded PLGA implants, where there is no local separation between a drug reservoir and a release rate controlling barrier the system's geometry significantly affects the resulting drug release rate. At the selected low drug loading (1 %w/w) the drug molecules form a monolithic solution within the carrier matrix in contrast to a monolithic dispersion formed at higher drug concentrations.

Table 4.8: Kinetic values for the formulations in phosphate buffer pH 7.2 at 37^{o}C

Formulation	Kinetics Model								
	Zero order		First Order		Higuchi Model		Korsmeyer-Peppas		
	k_o (mg.h^{-1})	r^2	k_1 (h^{-1})	r^2	k_H (mg.cm^2.h$^{-1/2}$)	r^2	k	n	r^2
15K-[OH]-1%BFB	**0.17**	**0.96**	-1.40 x 10^{-03}	0.95	3.86	0.75	-0.57	0.83	0.94
15K-[E]-E-1%BFB	0.12	0.91	**-1.00 x 10^{-03}**	**0.94**	3.31	0.67	1.82	0.55	0.93
15K-[Dd]-E-1%BFB	0.13	0.88	**-8.65 x 10^{-04}**	**0.93**	3.53	0.92	2.01	0.46	0.99
15K-[C]-E-1%BFB	0.14	0.75	-9.65 x 10^{-04}	0.83	**3.79**	**0.85**	2.01	0.45	0.95
15K-[E]-A-1%BFB	0.11	0.89	**-9.41 x 10^{-04}**	**0.96**	4.79	0.93	1.08	0.92	0.93
15K-[Bu]-A-1%BFB	0.14	0.97	-1.28 x 10^{-03}	0.88	**5.18**	**0.91**	2.23	0.93	0.89
15K-[Φ]-A-1%BFB	0.06	0.81	**-6.00 x 10^{-04}**	**0.94**	4.75	0.92	2.15	0.49	0.94
15K-[Dd]-A-1%BFB	0.13	0.88	**-1.19 x 10^{-03}**	**0.96**	6.17	0.92	0.90	0.69	0.86
15K-[E]-A-1%BT	0.08	0.85	**-7.09 x 10^{-04}**	**0.97**	3.78	0.94	-0.36	1.65	0.92
15K-[Bu]-A-1%BT	0.09	0.95	**-8.03 x 10^{-04}**	**0.99**	4.35	0.87	2.15	0.85	0.96
15K-[Φ]-A-1%BT	0.12	0.96	**-9.87 x 10^{-04}**	**0.97**	4.42	0.83	1.42	0.75	0.94
15K-[Dd]-A-1%BT	0.10	0.78	**-8.11 x 10^{-04}**	**0.92**	4.50	0.92	1.07	0.86	0.92

In a *monolithic solution* and in the absence of significant changes in the carrier matrix during drug release such as constant porosity, no swelling, time-independent permeability of the drug and perfect sink conditions, drug release is primarily controlled by diffusion through the carrier matrix, and the resulting release can be calculated based on Fick's law of diffusion.(Siepmann and Siepmann, 2008) However, in practice deviations from Fick's law is commonly observed in PLGA delivery systems where the drug release is not only controlled by the diffusion of the drug inside the matrix, but also by the polymer matrix disentanglement and dissolution process.(Arifin *et al*., 2006)

Results of the kinetic analysis of drug release (Table 4.8) indicate that a single kinetic model could not account for all the release profiles of Brimonidine, suggesting the influence of endcapping on drug release kinetics. The non-endcapped PLGA implant's release data was best described by zero order kinetics. On the other hand, upon endcapping the most predominant release mechanism however was first order with a few exceptions (15K-[C]-E-1%BFB and 15K-[Bu]-A-1%BFB following Higuchi and zero order release kinetics respectively). This is usually the case when drug transport is modelled by a varying diffusion coefficient that depends strongly on polymer concentration and a polymer dissolution that follows first order kinetics at the interface with release medium. Similar findings have been reported by Tamaddon and colleagues who studied the release of clindamycin from PLGA intracameral implants.(Tamaddon *et al*., 2015)

In the simplest manner, zero order kinetics often suggests that dissolution of the drug is the rate limiting step. Whereas high correlation values for first order kinetics or the Higuchi model usually suggest concentration dependent release rates or that the diffusion of the drug is the rate limiting step, respectively.(Costa and Sousa Lobo, 2001, Fu and Kao, 2010)

Although these empirical models may give an indication for the underlying drug release mechanism, caution has to be taken and violation of model assumptions must carefully be verified. For instance, the superposition of various physicochemical phenomena (such as polymer swelling, time and position dependent changes in the diffusion coefficients of water and drug) might result in an apparent square root of time kinetics.(Siepmann and Siepmann, 2008) Meanwhile, a zero-order release pattern may be modelled by the rate of polymer degradation/erosion rather than drug dissolution.(Fredenberg *et al*., 2011) Therefore although these mathematical models can be useful for comparison of different drug release profiles several possible explanations cannot be ruled out.

The previous discussion suggests that although the physical states of the drug and polymer aid in explaining drug release mechanisms a crucial often less tackled parameter is the dynamic nature of the polymer and the changes it encounters upon exposure to the release medium which can be rather decisive. (Siepmann and Göpferich, 2001) Korsmeyer and colleagues developed a mechanistic semi-empirical equation based on a power-law

expression. It allows for the *simultaneous* consideration of the diffusion of water into the device and drug out of the system as well as of polymer swelling (Equation 4.5).(Korsmeyer *et al*., 1983)

Brimonidine release data was fitted to Peppas model and the parameters k and n where computed. *k* is a constant incorporating structural and geometric characteristics of the system, and n is the release exponent, which might be indicative of the mechanism of drug release.(Frank *et al*., 2005, Albers *et al*., 2009)

The recorded *n* values ranged from 0.45 to 1.65 (Table 4.8). Based on the implant's geometry "n" values of 0.45 indicate Fickian diffusion, where diffusion across the matrix is the rate limiting step. In contrast, if polymer relaxation is rate-limiting (e.g., all other phenomena, such as diffusion and dissolution are much faster) and in the case of a cylindrical geometry a release exponent of *n* = 0.89 is observed and corresponds to zero-order release kinetics (case II transport).(Siepmann and Siepmann, 2008) An anomalous (non-Fickian) diffusion release model is characterized by 0.45 < n < 0.89 and n >0.89 indicates a super case II transport relaxational release.(Ritger and Peppas, 1987)

The release exponent for the majority of the formulations ranged from 0.45 to 0.89, indicating anomalous mechanism, which is the combination of drug diffusion and polymer relaxation, hence a non-Fickian mechanism. For

example the non-endcapped PLGA (15K-[OH]-1%BFB) formulation exhibited an n value of 0.83 indicating anomalous transport, where both diffusion and dissolution overlap and are quite indistinguishable.(Siepmann and Siepmann, 2008) Upon contact with water as water penetrates the implant, swelling takes place to achieve thermodynamics equilibrium due to the water concentration gradient. A transformation of polymer from a glassy to rubbery state occurs at the same time and the dimension of the matrix increases. The drug dissolves due to a concentration difference at two interfaces. First at the glassy rubbery phase then diffuses out through rubbery solvent phase according to its concentration gradient. The high n value indicates that water mobility dominates nearing a “Case-II transport” of drug release takes which is characterized by the existence of a sharp interface advancing at constant velocity.

In this case the drug release exhibits a zero-order kinetic profile as depicted in Table 4.8 which is controlled by the polymer dissolution process at the moving interface known as the “erosion front”. (Arifin *et al*., 2006) Although zero-order release is the favourable kinetics due to its ability to deliver drug at a constant rate, and providing a predictable bioavailability status in controlled release it is often not the case in matrix systems. This is usually attributed to the time-dependant changes in the drug depleted matrix surface area and diffusional path length.(Ofokansi and Kenechukwu, 2013) Therefore caution must be taken when drawing conclusions regarding apparent zero order kinetics.

Hopfenberg proposed that zero order process might result from the superposition of several processes, such as dissolution, swelling and/or polymer chain cleavage. In fact, a previous study on the release of leuprolide acetate from PLGA microparticles reported that the zero-order release could be indicative of possible pore closure at a rate that counteracts the effect of pore formation resulting in a denser polymer and thus drug release relies on polymer degradation in this stage (Berens and Hopfenberg, 1978). The Hopfenberg model (Equation 4.6) allows for a better quantitative description of drug release from degradable drug delivery systems exhibiting a release rate which is proportional to the (time-dependent) surface area of the device for polymer matrices, where a zero order surface detachment of the drug is the rate limiting release step (Fredenberg *et al*., 2011). A more detailed analysis for cylinders undergoing surface erosion was also presented by Cooney (1972).(Siepmann and Siepmann, 2008)

$$\frac{M_t}{M_\infty} = 1 - \left(1 - \frac{k_o\ t}{c_o\ a}\right)^n \qquad \text{(Equation 4.6)}$$

Based on the implant geometry, a release exponent of n ≤ 0.45 serves as an indication for diffusion controlled drug release. This was evident in two ester endcapped PLGA formulations 15K-[Dd]-E-1%BFB and 15K-[C]-E-1%BFB. This data clearly confirms previous findings regarding the effect of endcapping on decreasing polymer hydrophilicity, and hence polymer swelling. Thus, the rate-limiting step for drug release is diffusion of Brimonidine through the polymeric matrix, satisfying the classical Higuchi equation. The Higuchi equation therefore represents a special case of the Peppas equation where the drug is entrapped in systems in which matrix

swelling and dissolution are negligible. Similarly, the lower n value exhibited by the amide endcapped formulation 15K-[Φ]-A-1%BFB with relative higher Tg (45.15 ^{o}C), can be attributed to the decreasing polymer relaxation role in drug release and closing the release to a Fickian one. This confirms the crucial impact of endcapping on modulating drug release from the different PLGA implants

Another exception to the predominance of first order kinetics in most amide end capped formulations is 15K-[Bu]-A-1%BFB formulation which was fitted best to a zero-order kinetic profile. This was corroborated by its Peppas "n" values of 0.93 which implies super case II release kinetics (a strong indication of zero order).(Ofokansi and Kenechukwu, 2013) A rather helpful modification the semi-empirical model was performed by Peppas and Sahlin (Peppas and Sahlin, 1989) by decoupling diffusion and Case II transport with the following expression

$$\frac{M_t}{M_\infty} = K_1 t^m + K_2 t^n \qquad \text{(Equation 4.7)}$$

where k_1, k_2, m and n are constants. The first term of the right-hand side is the diffusional contribution, whereas the second term is the "Case-II transport" contribution. Since chemical reactions, mass transfer and other kinds of processes are concurrently influencing drug release, it is crucial to choose an appropriate model for each DDS. The models described above are a simplification of the real system, and their applicability and suitability are restricted where conclusions can only be drawn if the assumptions associated with the equations are fulfilled.(Fredenberg *et al*., 2011)

4.4. Conclusion

Cylindrical extrudates were produced using HME to develop Brimonidine loaded PLGA intraocular implants. The implants were characterized to understand the effect of endcapping on the implants performance as evaluated by drug release profile and degradation properties. The control implant PLGA-15K-[OH] absorbed a significant amount of water, which plasticised the polymer chains and led to increased chain mobility. This resulted in accelerated initial drug release. In contrast, ester endcapping with ethyl, dodecyl and cholesterol end groups resulted in a prolonged lag phase, in the first 7 days of the study, producing overall triphasic profile rather than the biphasic profile. The dodecyl and cholesterol ester endcaps showed 90% reduction during the first week of the release study owing to the imparted hydrophobicity. In the amide endcapped implants, endcapping with ethyl and dodecyl amide resulted in release profiles comparable to that of the control. This was explained by the low starting T_g of the implants. Therefore PLGA was in the rubbery state during the entire drug release period which increases drug mobility. This was coupled with a drop in molecular weight (22.2%) after the first 24 hrs. Endcapping with butyl and phenyl amide behaved similarly to the esters due to the higher initial Tg. Polymer endcapping significantly modified hydrophilicity and glass transition temperature. These parameters in turn affected polymer swelling and segmental relaxation. Depending on the composition of the polymer one of two these phenomena potentially dominates resulting in decreasing or increasing drug release rates.

CHAPTER 5: FUNDAMENTAL UNDERSTANDING OF ENDCAPPING STRUCTURE-PROPERTY RELATIONSHIP OF PLGA POLYMERS

5.1. Introduction and Objective

In the classically applied one variable at a time (OVAT) approach, where only one factor at a time is varied, the attainment of the true understanding of the influence of one parameter is never guaranteed. The application of the OVAT approach in understanding structure property relationships suffers from several pitfalls like being strenuous and inept to reveal interactions. It results in “just satisfactory” solutions as one cannot establish a true “cause and effect”, it becomes futile when all variables are changed simultaneously. (Singh *et al*., 2011a, Dejaegher and Vander Heyden, 2010)

Design of experiment (DOE) is a structured and organized method to determine the relationship among critical structural variable and properties, as well as defining the sources of variability.(Yu, 2008) A factorial experiment is an experimental strategy in which design variables are varied together, instead of one at a time.(Montgomery, 2009)This relationship is known as “design space”. DoE helps in identifying the “important” and “unimportant” variables. One can simulate the product behaviour using model equation(s) and thus save a significant amount of resources. The remarkable feature of DoE is that once a true relationship between factor and output is established it can predict as well as detect and estimate the possible interactions and synergies among variables.(Singh *et al*., 2011a)

The selection of the experimental design depends upon the amount of resources available, the degree of control over making wrong decisions that the experimenter desires, and whether linear or nonlinear responses are detected We often find, however, that real-world problems involve restrictions or constraints on the experimental region. Based on this fact and given our need to build models that accurately describe the system's behaviour, it is imperative that we incorporate the limitations of the system within in our experimental plan. A D-optimal design is an efficient design when the studied response varies nonlinearly.(Myers *et al*., 2009) Once a minimum design is analysed, further points can be added to refine knowledge of the system.(Hibbert, 2012) Due to the computational intensity involved in creating optimal designs, sophisticated computer search algorithms have been developed to determine the optimal set of points at which to take observations, which are frequently available in statistical software packages.(Kovach and Cho, 2009)

The previous chapters have highlighted the significance of ocular delivery systems possessing a certain quality profile particularly efficient drug loading, temporal drug release and reproducible, defect-free morphology. Optimization of drug delivery profile of extruded ocular implants whilst maintaining acceptable implant mechanical properties has been the scope of this research. However, each critical quality attribute was studied as a single parameter. In this chapter, we investigate the influence of the underlying physical properties of the polymers and their interaction on the Brimonidine release from PLGA based matrices.

5.2. Materials and Methods

5.2.1. Materials

PLGA samples were selected according to the design space. For drug release studies Acetonitrile, and Phosphate buffer saline tablets pH 7.2 were purchased (Sigma Aldrich, Dorset, UK). Brimonidine Free Base (BFB) was kindly provided by Allergan, Inc., Irvine, CA, USA

5.2.2. Factorial Design (D-optimal solution)

Before the selection of an experimental design, it is essential to demarcate the experimental domain within the factor space. While selecting the levels, one must see that the increments between them should be realistic. Too wide increments may miss finding the useful information between the levels, while a too narrow range may not yield accurate results.

According to the results obtained from the *in vitro* release studies conducted in Chapter 4 the cumulative drug released from the implant was significantly reliant on the polymers' endcapping and varied as a function of time. It was also concluded that polymer endcapping directly affected polymer hydrophobicity, and Tg (as previously discussed in Chapters 2 and 3). Therefore polymer hydrophobicity, Tg and in-vitro release time were selected to define the experimental field.

When a response is known to be a linear function of a factor, two levels (−1,+1) would be sufficient to define it. However, preliminary data showed the response to be non-linear requiring at least three levels (−1, 0, +1) of each quantitative factor to characterize the response. This is because in a nonlinear function the effects between (−1, 0) differ from those between (0,+1). (Myers *et al*., 2009 , Dejaegher and Vander Heyden, 2010) Table 5.1 lists the selected levels for each of the variables; Polymer hydrophobicity (X_1), T_g (X_2) and *in vitro* release time (X_3) on the, % cumulative drug release (Y) as the selected response.

Table 5.1: The selected independent variables and their respective levels

Coded Variable	Variable	Level			Response (Y)
		-1	0	+1	
X_1	Hydrophobicity (CAG, ^{o})	65	72	79	% Cumulative Drug Release
X_2	Tg (MDSC, ^{o}C)	35	40	45	
X_3	In-vitro release time (hour)	72	120	168	

The codes (-1), (0) and (+1) stand for low, medium and high variable levels respectively.

In a full factorial experimental design one experiment is required at all possible combinations between three levels of each variable considered. In general, the necessary number of experiments is 3^k, where *k* is the number of factors. A factorial design evaluating 3 factors at all possible combinations for each factor would result in a full factorial design consisting of $3^3 = 27$ runs (Figure 5.1).(Mathew *et al*., 2007, Elkheshen *et al*., 1996)

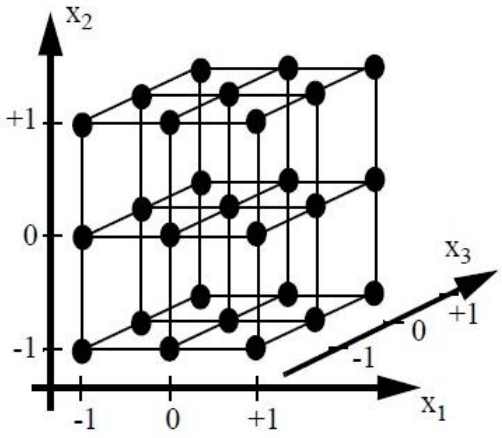

Figure 5.1: Illustration of 3^3 full factorial design (Montgomery, 2009)

However, a full 3^3 factorial design was not possible since combinations of some polymer physical properties were practically unattainable creating constraint points. For example, constraint point (1) listed in Table 5.2 necessitates low level of hydrophobicity i.e. those witnessed in non-endcapped polymers at the selected molecular weight coupled with low level Tg which is essentially characteristic to endcapped PLGAs due to the plasticizing effect of the endcap.

Optimal designs are particularly useful in such design spaces, when the factor space is not uniformly accessible. They allow shifting of the factor space away from the constraint area to find the optimum levels of the variables. Another useful aspect is that the number of experiments is specified. However, a minimum number of experiments are required to calculate the coefficients of the effects model (the number of effects plus a constant term). The D-optimal solution answers the question given a number of design points to choose from a total number, what is the optimal

distribution of the points (i.e. to select a number of design points from a larger set of candidate points).The optimality criterion enables a more efficient construction of a quadratic model (Hibbert, 2012, Montgomery, 2009)

A D-Optimal factorial design was selected to understand and optimize the individual effects of hydrophobicity (X_1), T_g (X_2) and *in vitro* release time (X_3) on the % cumulative drug release (Y). After identifying the constraint points (Table 5.2) the software selected a set of candidate points as a base design. These included factorial points (high and low level from the constraints on each factor, vertices, constraint plane centroids, and an overall centre point).

Table 5.2: Level for constraint points of different formulae

Constraint points	Levels		
	X_1	X_2	X_3
1	-1	-1	-1
2	-1	-1	0
3	-1	-1	1
4	1	1	-1
5	1	1	0

Accordingly, the base design consisted of 20 runs (19 formulations and one overall centre point replicate). The experiment at the centre point is replicated to determine an estimate of the experimental error and to check for linearity of the factor effects. The base design runs are shown in Table 5.3 in coded form. Since the factor values are changed in a systematic way, it is important that the order of experiments is randomized. This negates any spurious

systematic effect that would be manifested with the non-random order in time of the experiments, and ensures that the estimates of repeatability variance properly reflect the random aspects of the process.(Hibbert, 2012) Table 5.4 shows the actual composition of the formulations in randomized run order.

Table 5.3: Composition of the extruded PLGA implants (coded values)

Run Order	Formula	Variable levels in coded form		
		Hydrophobicity (CAG, ^{o}C)	Tg (^{o}C)	Time (hour)
20	F1	0.0	1.0	1.0
3	F2	-0.5	1.0	-1.0
10	F3	1.0	-1.0	0.0
8	F4*	0.0	-0.1	-0.1
4	F5	-0.4	-0.7	-0.8
16	F6	-0.6	-0.5	1.0
11	F7	-1.0	0.5	0.0
9	F8	0.0	-0.1	-0.1
6	F9	0.0	-0.1	-0.1
19	F10	-1.0	0.5	1.0
2	F11	0.5	0.5	-1.0
5	F12	-0.4	-0.7	-0.8
14	F13	-0.2	-1.0	0.3
7	F14	0.0	-0.1	-0.1
13	F15	0.5	1.0	0.0
15	F16	0.4	-1.0	1.0
17	F17	1.0	0.0	1.0
12	F18	-0.2	1.0	0.0
18	F19	1.0	0.0	1.0
1	F20	1.0	-0.5	-1.0

*F4 matrix centre point will be replicated

Table 5.4: Composition of the extruded PLGA implants (actual values) in randomized run order

Run Order	Formula	Variable levels in actual values		
		Hydrophobicity (CAG, ^{o}C)	Tg (^{o}C)	Time (hour)
16	F1	71.5	45	168
7	F2	68.5	45	72
15	F3	78	35	120
6	F4*	71.3	39.58	114.28
12	F5	69	36.67	81.14
5	F6	67.5	37.5	168
4	F7	65	42.5	120
1	F8	71.3	39.58	114.28
18	F9	71.3	39.58	114.28
11	F10	65	42.5	168
9	F11	75	42.5	72
2	F12	69	36.67	81.14
17	F13	70	35	133.71
10	F14	71.3	39.58	114.28
20	F15	75	45	120
8	F16	74	35	168
3	F17	78	40	168
19	F18	70	45	120
14	F19	78	40	168
13	F20	78	37.5	72

*F4 matrix centre point will be replicated

5.2.2.1. Factorial Analysis

After acquiring the drug release data related to each experimental point of the design, it was necessary to fit a mathematical equation to describe the behaviour of the response according to the levels of values studied.(Bezerra *et al*., 2008) For the studied responses, an interactive statistical second-order polynomial complete model (Equation 5.1) was fitted to correlate the relationship between the 3 variables and the studied response. Analysis of variance (ANOVA) was carried out to determine the significance of the fitted equation, using the Design Expert software. For the studied response (% cumulative dug released):

$$y = \beta_0 + \sum_{i=1}^{m} \beta_i x_i + \sum_{i=1}^{m} \beta_{ii} x_i^2 + \sum_{i=1}^{m=1} \sum_{j=2}^{m} \beta_{ij} x_i x_j + \varepsilon$$

(Equation 5.1)

Where x_1, x_2,…,x_i are the independent variables which influence the predicted response y. β_o is the model constant (intercept), β_1, β_2 and β_3 are linear coefficients; β_{12}, β_{13} and β_{23} are cross (1^{st} order interaction) product coefficients and β_{11}, β_{22} and β_{33} are the quadratic coefficients. The interaction terms show how the response changes when two or more factors are simultaneously changed. In other words, interaction exists between factors when the effect of one factor depends on the level of other factor(s) at the same time. The β coefficients are obtained by the method of least squares (MLS). MLS is a multiple regression technique used to fit a

mathematical model to a set of experimental data generating the lowest residual possible. The model based on Equation 5.1, if m=3 is:

$$y = \beta_0 + \beta_1 x_1 + \beta_2 x_2 + \beta_3 x_3 + \beta_{11} x_1^2 + \beta_{22} x_2^2 + \beta_{33} x_3^2 + \beta_{12} x_1 x_2 + \beta_{13} x_1 x_3 + \beta_{23} x_2 x_3 + \varepsilon \quad \text{(Equation 5.2)}$$

5.2.2.2. Statistical Design

A commercially available software program (Design Expert, Version 10.0.1, Stat-Ease Inc, Minneapolis, MN) was used to generate the experimental design, fit a model to the data, check the model adequacy, test the fit, as well as calculate the model parameters and model graphs including various one-factor and interaction plots. The experimental design chosen was surface response, 3-factor, 3-level D-Optimal design. Analysis of variance (ANOVA) and all statistical analyses were also performed using the Design Expert software. Calculation of the effects was performed and only the significant effects constituted the model. F test was used to compare the variance among the treatment means with the variance of individuals within the specific treatments (i.e. comparing the treatment variance with the error variance).

The multiple correlation coefficients were calculated; a measure of the amount of variation about the mean, which is explained by the model. All assumptions underlying the ANOVA were checked. The fit of the model to the data was then evaluated statistically by ANOVA or the examination of residuals.(Dejaegher and Vander Heyden, 2010, Montgomery, 2009) The

estimated effects of the individual independent variables and their interactions on the response of the implants were assessed for statistical significance using ANOVA and using P-value significance levels with the aid of the supplied software. This value represents the probability of the effect of a factor being due solely to random error.

Thus, if the P value was less than 5%, the effect of the corresponding factor was considered significant. (Dejaegher and Vander Heyden, 2010, Zougagh *et al*., 2000) Insignificant variables were removed by backward elimination, and the adequacy of the fitted model was checked by ANOVA. F-ratios and correlation coefficients were the criteria used for validation. *P-value* < 0.05 was accepted to denote significance. In short, a model will be well fitted to the experimental data if it presents a significant regression and an insignificant lack of fit.

In other words, the major part of variation observation must be described by the equation of regression, and the remainder of the variation will certainly be due to the residuals. Most variation-related to residuals is due to pure error (random fluctuation of measurements) and not to the lack of fit, which is directly related to the model quality.(Bezerra *et al*., 2008) The quality of fit of the polynomial model equation was expressed by the adjusted coefficient of determination, r^2_{adj}. (Sankalia *et al*., 2007) However, using ANOVA for testing the fit requires that certain assumptions be satisfied. Specifically, these assumptions are that the observations are adequately described by the

model and that the errors are normally and independently distributed with zero mean and constant but unknown variance δ^2.(Mathew *et al*., 2007) It is assumed that errors present a random distribution profile with a zero mean and a common unknown variance and that these errors are mutually independent of each other. (Bezerra *et al*., 2008, Montgomery, 2009)

In practice, however, these assumptions will usually not hold exactly. Consequently, it is usually unwise to rely on the analysis of variance until the validity of these assumptions has been checked.

Violation of these basic assumptions and model adequacy can be investigated by examination of residuals which are the differences between the responses observed at each combination values of the independent variables, and the corresponding prediction of the response computed using the regression function. If the model is adequate, the residuals should be structure-less.(Montgomery, 2009, Myers *et al*., 2009)

Model diagnostic tests include normal probability plot of the residuals to check for normality of residuals, plot of residuals versus fitted (predicted) values to check for constant error and plot of residuals in run sequence of data collection to check for time independency of residuals. Diagnostic tests also include outlier-t plot to look for outliers, i.e., influential values on the model fit which can distort the analysis of variance and residual plot of the predicted versus actual values to show the quality of fit of the model. (Box

and Cox, 1964) In case of non-constant variance, evident from plot of residuals versus predicted values, a variance-stabilizing transformation is applied and then ANOVA is run on the transformed data. Box Cox plot for power transformation indicates that recommended data transformation is essential when its confidence limits do not include the value 1. It provides a guideline for selecting the correct power law transformation. In addition to statistical validation, the reliability of the model was challenged by comparing the predicted values of the responses with the observed ones. In order to validate the agreement between the predicted values and the actual data, the following statistical criteria were examined (Giannakou *et al*., 2002):

1. The ratio between actual and predicted values, should be close to one
2. The standard error (SE) or residual, should be close to zero
3. The % relative standard deviation, should be lower than 15%.

5.2.2.3. Check point analysis (CPA):

A check point analysis was performed to confirm the validity of the generated mathematical model for response prediction, verification of the validity of the reduced model and detection of any curvature in the response.(Sankalia *et al*., 2007, Nasr *et al*., 2011) Actual values for the independent variables used for the preparation of the check point formula are stated in Table 5.5. The release study was run in triplicate and the average responses determined. The actual responses were compared to the predicted ones according to the obtained regression line.

Table 5.5: Formulation variables considered in check point analysis

Run	Hydrophobicity (X_1)	Tg (X_2)	Time (X_3)
1	72	40	168
2	65	40	120
3	65	45	168

5.2.3. Characterization of Extruded Implants

5.2.3.1. *In vitro* release studies

The *in vitro* release studies for the selected formulation were performed under sink conditions as described in Chapter 4. Three implants of each formulation were placed in three 300 µl glass inserts containing 250 µl of phosphate buffer saline (PBS**,** pH 7.2). The vials were placed on a batch shaker set at 25 strokes/min in a thermostatically controlled temperature room (37 °C). The amount of drug released from the collected samples was measured by HPLC using the method in Section 4.2.3.5.

5.2.3.2. PLGA in Aqueous environment and High Humidity

Approximately 50 mg of dried polymer was incubated in deionized water and stored at 37 ◦C in a temperature controlled room. At predetermined intervals, samples were removed, filtered, rinsed with deionized water, and dried under vacuum until constant weight. Similarly, a second set of samples were weighed and placed in DVS flat pans at 95%RH, at 37 ◦C. At predetermined

intervals, samples were removed and vacuum-dried until constant weight. Finally, a set of control samples were exposed to dry heat in an oven at 37 ◦C. Hygrothermal aging of the polymers was also tested by incubation at different temperatures; 25, 37 and 55^{o}C.

5.2.3.3. Determination of Glass transition.

Glass transition temperature (Tg) was determined using a modulated differential scanning calorimetry (MDSC) as described in previous chapters. In summary 2 mg of implants were crimped in aluminium pans that were hermetically sealed and subjected to two cooling and heating cycles from -20 to 200 ºC at 1 ºC/min, with modulation amplitude of +/- 0.16 ºC/min and a period of 60 s, quench cooled to -20^{o}C and then heated again to 100^{o}C at 1^{o}C /min with modulation amplitude of +/- 0.16 ºC/min and a period of 60 s. The results were analysed using TA universal analysis software. The second run DSC curve was the reference for determining the glass transition temperature (T_g). The plasticization of PLGA by water was investigated by hydrating samples and then using MDSC to determine the Tg of the polymers after incubation for designated time periods. Samples were dried under vacuum to constant weight and MDSC rerun to determine Tg recovered

5.3. Results and Discussion

Throughout the discussion in this thesis it has become evident that release of active ingredients from an amorphous polymeric system is a complex process. The release doesn't solely rely on the diffusion of water into the polymer matrix, resulting in the dissolution and diffusion of the ingredient out it. But rather, couples with the time-dependent changes in the polymer properties arising from water diffusion such as hydrolytic degradation and physical plasticization resulting in polymer relaxation.

The reciprocal influence of these changes on water uptake and ingredient release means that the release process cannot be modelled by a straightforward diffusion process emphasizing the need to predict penetrant-induced effects on PLGA.(Sharp *et al*., 2001) Figure 5.2 proposes a summary of several contributing factors that govern the mechanism and kinetics of drug release. Polymer's Tg and hydrophobicity were identified as key parameters and were selected as key variables to be investigated by a factorial design approach

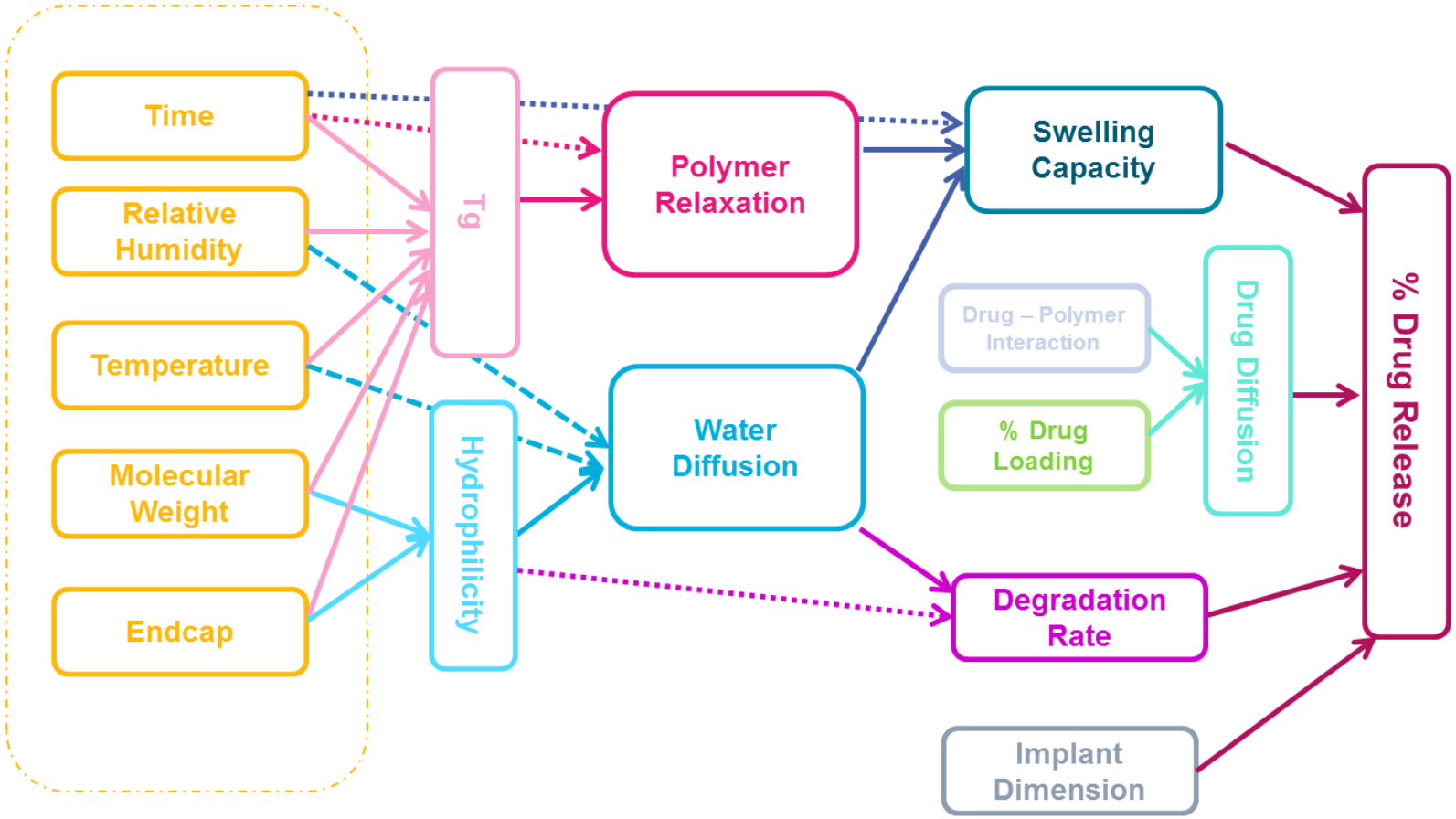

Figure 5.2: An illustration of the complexity of physico-chemical processes that influence drug release from PLGA matrices

5.3.1. Factorial Design

Kiefer and Wolfowitz developed the theory behind optimal experimental designs. The approach refers to creating experiments that are optimum by choosing the points at which to take observations, out of a candidate set, in order to satisfy the specified design criterion.(Kiefer and Wolfowitz, 1959) Optimal experimental designs are particularly useful when; improving an existing design based on a specific design criterion, modifying an existing design due to restrictions placed on the experimental parameters, or developing a design for an irregularly shaped/non-standard experimental region.(Kovach and Cho, 2009) D-optimal designs are created, as shown in Figure 5.3.

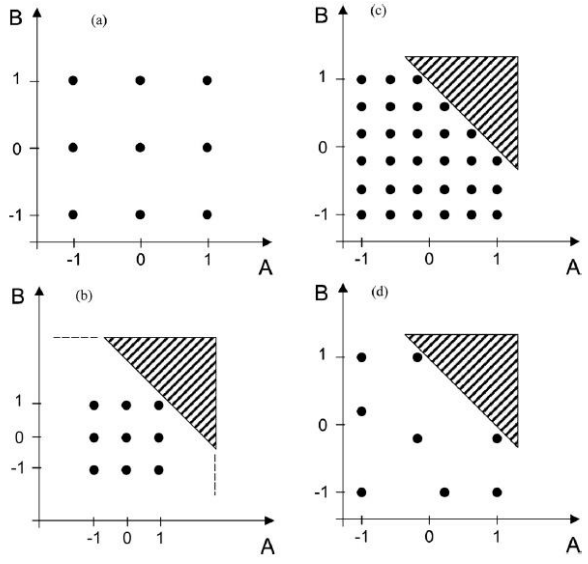

Figure 5.3: (a) A 3^3 full factorial design in a rectangular symmetrical domain (b) a restricted 3^3 full factorial design in an asymmetrical domain (c) the candidate points of the grid in the asymmetrical domain, and (d) the selected points constructing D-optimal design. (Dejaegher and Vander Heyden, 2010)

D-optimal design leads to response surface models for which the maximum variance of the predicted responses is minimized. This means that the points of the experiment will minimize the error in the estimated coefficients of the response model. The advantages of this method are the possibility to use irregular shapes and the possibility to include extra design points. In other words, they offer the best possible design to yield the best possible estimate of the model parameters.(Montgomery, 2009, Mannarswamy *et al*., 2010)

The simple and interactive effects of the selected variables; namely polymer hydrophobicity, Tg and time (Table 5.1) on Cumulative Drug Released (%) were assessed using surface response methodology. Based on the defined constraint points (Table 5.2) the D-optimal design with 4 centre points resulted in a total of 20 runs. Cumulative Drug Released (%) ranged from a minimum of 0.51 to a maximum of 41.75% as listed in Table 5.6.

The experimental runs were randomized so that the environment in which the treatments are applied were as uniform as possible to exclude any bias.(Montgomery, 2009) The responses of all model formulations were treated by Design-Expert® software (version 10.0.6; Stat-Ease, Inc., Minneapolis, MN). The best fitting mathematical model was selected based on the comparisons of several statistical parameters including the multiple correlation coefficient (r^2), the adjusted multiple correlation coefficient (r^2_{adj}) and the predicted residual sum of square (PRESS). Among them, PRESS indicated how well the model fit the data, and for the chosen model it should

be small relative to the other models under consideration. Polynomial models including interaction and quadratic terms were generated for all the response variables using a multiple linear regression analysis approach. In addition, 2-D and 3-D contour plots were constructed, after the fitting of the mathematical model.

Table 5.6: Cumulative Drug Released (%) of the different test formulae

Run Order	Formula	Cumulative Drug Released (%)	Run Order	Formula	Cumulative Drug Released (%)
20	F1	11.10	2	F11	0.69
3	F2	25.51	5	F12	6.57
10	F3	3.93	14	F13	23.41
8	F4	0.24	7	F14	0.31
4	F5	6.57	13	F15	4.49
16	F6	28.41	15	F16	41.17
11	F7	20.42	17	F17	7.03
9	F8	0.29	12	F18	4.49
6	F9	0.34	18	F19	7.03
19	F10	41.75	1	F20	0.51

Before conclusions from ANOVA were adopted, the adequacy of the underlying model was checked. The primary diagnostic tool is residual analysis. A check of the normality assumption is to construct a normal probability plot of the residuals (difference between the actual and predicted values) as in Figure 5.4. The normal probability plot of the residuals was a

straight line, placing more emphasis on the central values of the plot than on the extremes, implying normal distribution of the error.

The tendency of the normal probability plot to bend upward slightly on the right side implied that the tails of the error distribution were somewhat *thinner* than would be anticipated in a normal distribution; that is, the largest residuals are not quite as large (absolute value) as expected. However, this plot was not grossly abnormal.(Montgomery, 2009)

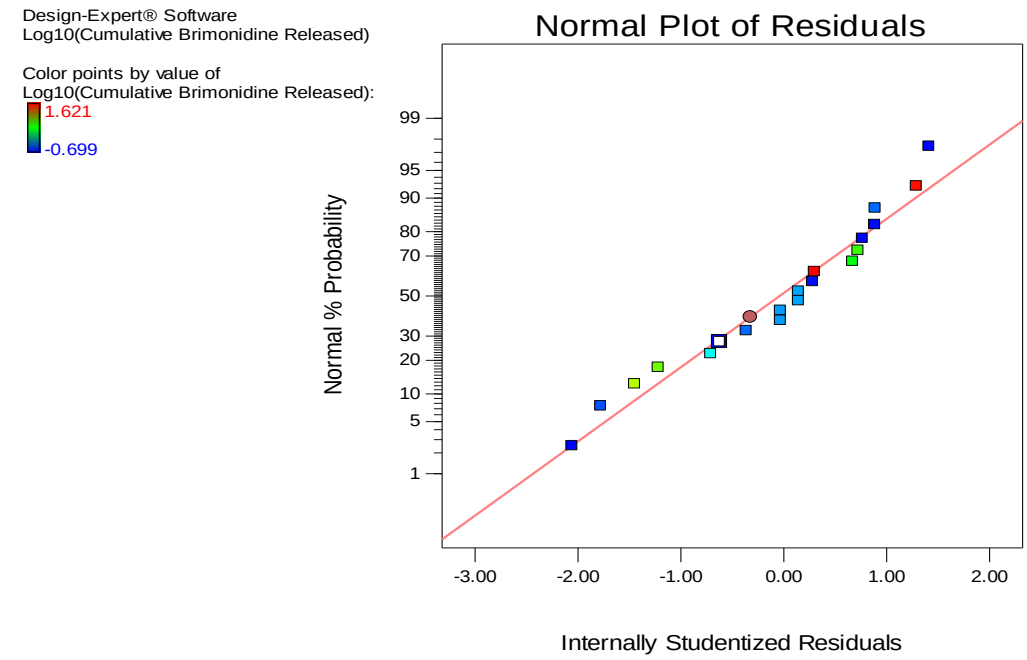

Figure 5.4: Normal probability plot of residuals of the Cumulative Drug Released response forming a straight line with more emphasis central values of the plot than on the extremes, implying normal distribution of the error

According to the assumption that the errors were normally and independently distributed with zero mean and constant but unknown variance, the studentized residuals (the residuals divided by their estimated standard deviation) should be approximately normal with mean zero and unit variance.

Thus, about 68 percent of the standardized residuals should fall within the limits 1, about 95 percent of them should fall within 2, and virtually all of them should fall within 3. A residual bigger than 4 standard deviations from zero, is a potential outlier.(Montgomery, 2009) Figure 5.5 shows that all residuals were within the limit ±3 and hence no outliers were present. Plotting the studentized residuals in run order of data collection (randomized order) also resulted in a structure-less pattern indicating independency of the error. This plot is helpful in detecting correlation between the residuals. For example a tendency to have runs of positive residuals indicates positive correlation. This would imply that the independence assumption on the errors has been violated.(Montgomery, 2009)

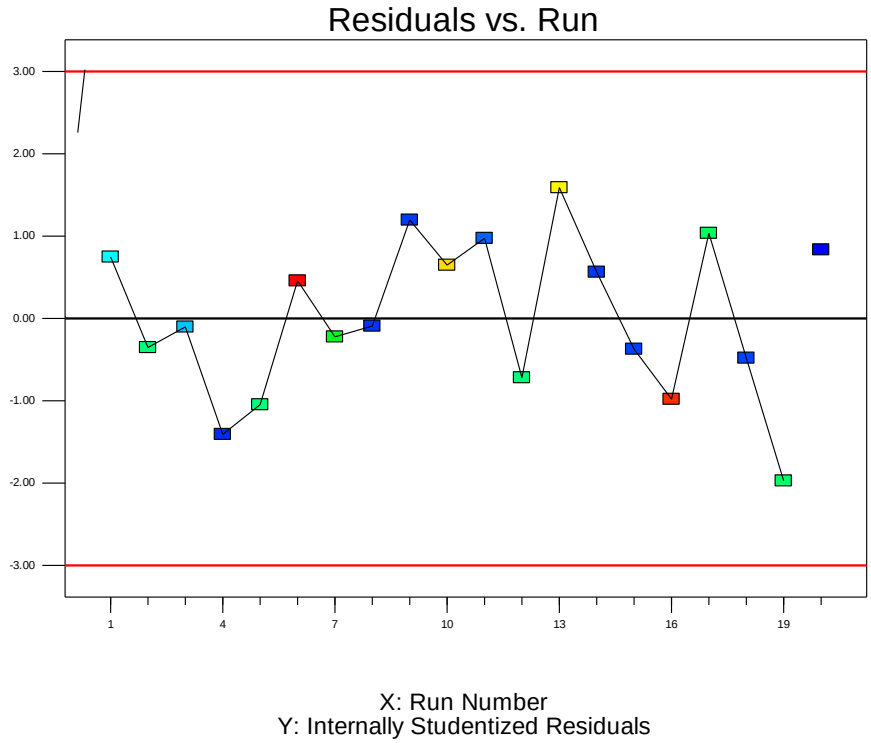

Figure 5.5: Plot of studentized residuals *vs.* run order of the Cumulative Drug Released response

The Box Cox plot of Cumulative Drug Released response showed that the 95% confidence interval did not include the value 1 (Figure 5.6). This necessitated applying data transformation. The software-recommended data transformation was a log transformation. Data transformations are often a very effective way to deal with the problem of abnormal responses and the associated inequality of variance.

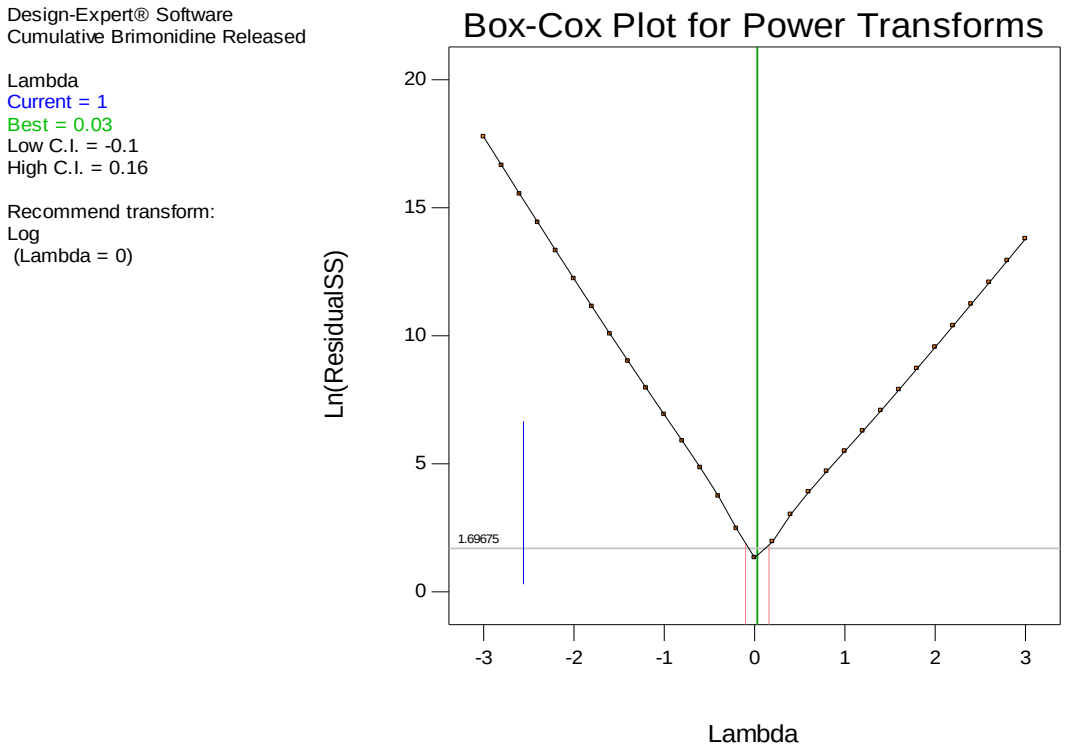

Figure 5.6: Box-Cox Plot before power transformation for Cumulative Drug Released response

Generally, transformations are used for three purposes: stabilizing response variance, making the distribution of the response variable closer to the normal distribution and improving the fit of the model to the data. This last objective could include model simplification, by eliminating interaction terms. Sometimes a transformation will be reasonably effective in simultaneously

accomplishing more than one of these objectives.(Montgomery, 2009) After applying log transformation, the 95% confidence interval included the value 1 (Figure 5.6) which allowed running the ANOVA on the transformed data.

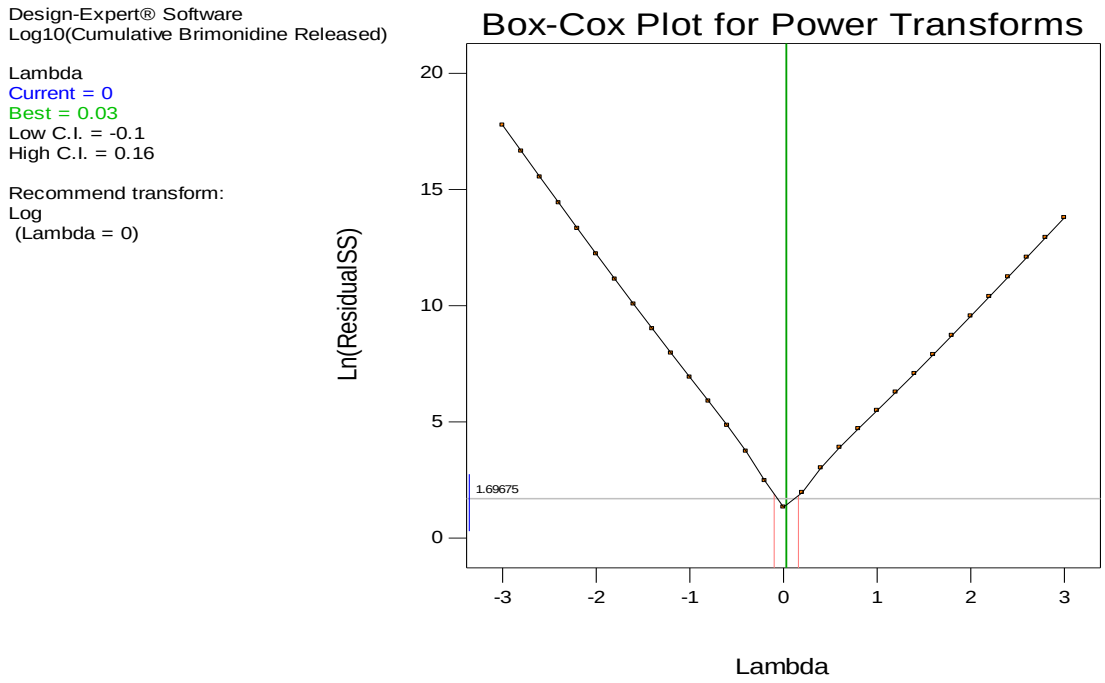

Figure 5.7: Box-Cox Plot after power transformation for Cumulative Drug Released response

The Analysis of variance (ANOVA) applied to the transformed populations could therefore be undertaken for the detection of the main effects. ANOVA was used to analyse the significance of the terms of the complete equation. ANOVA compares the variation due to the treatment (change in the combination of variable levels) with the variation due to random errors inherent to the measurements of the generated responses. This allows for the evaluation of the significance of the regression used to foresee responses considering the sources of experimental variance.(Bezerra *et al*., 2008)

The terms that are not significant were eliminated from the equation in backward successive stages one-by one and in decreasing order of the *P*-value up until the statistic r^2 fitted to the degrees of freedom (r^2 adjusted for d.f.) nears unity. The value of r^2 adjusted for d.f. was chosen as it is more suitable for comparing models with different numbers of independent variables.(Contreras and Sanchez, 2002) In general, the adjusted r^2 statistic will not always increase as variables are added to the model.

In fact, if unnecessary terms are added, the value of r^2_{adj} will often decrease. When r^2 and r^2_{adj} differ dramatically, there is a good chance that insignificant terms have been included in the model. If more than one model was significant ($p < 0.05$) for the response, the adjusted r^2 and PRESS value (prediction error sum of squares) of the model were compared to select the best mathematical model for that response. Focus on maximizing the value of adjusted r^2 and predicted r^2 while low PRESS value indicated adequate fitting of model.(Singh *et al*., 2011)

The adjusted determination coefficient (r^2_{adj} = 0.993) was high indicating model significance. The goodness of fit of the model was also checked by the correlation coefficient r^2 and the prediction r^2. Correlation r^2 is the fraction of variation of the response explained by the model while prediction r^2 is the fraction of variation of the response that can be predicted by the model. The model was found to be statistically excellent for the Cumulative Drug Released with correlation r^2 (0.996) and prediction r^2 (0.984) close to unity. In

this case, the value of correlation coefficient indicates that almost 99% of the total variations is explained by the model while prediction r^2 value indicates an almost 98% predictive ability of the response.

All the above considerations indicated an excellent adequacy of the regression model. Precision is a measure of the signal-to-noise ratio, and a value greater than 4 is required. In this model the ratio was 47.26 indicating an adequate signal and a low PRESS value (0.18). Therefore this model can be used to navigate the design space.

ANOVA revealed that the cumulative drug released was significantly affected by all the three independent variables tested ($p < 0.05$) and was best fitted to a response surface quadratic model as shown in Table 5.7. Fisher F test with low probability value, (*P* model < 0.01), demonstrated significance of the regression model. The Model F-value of 309.70 implied model significance. There is only a 0.01% chance that a "Model F-Value" this large could occur due to noise. The regression equation enabled the study of the effects of each factor and their interactions over the considered response, within the space defined by the upper and lower limits of the independent variables. The regression equation after correcting for insignificant terms is (in coded units):

$$\log(\text{Cumulative Brimonidine Released}) = -0.60 - 0.79\,x_1 - 0.17x_2 + 0.25x_3 + 0.53x_1x_2 + 0.35x_1x_3 - 0.18\,x_2x_3 + 1.12\,x_1^2 + 1.25\,x_2^2 + 0.51\,x_3^2$$

(Equation 5.3)

Table 5.7: ANOVA table of the Cumulative Drug Released response (Y)

Source of variation	Sum of squares	d.f*	Mean square	F value	*p*-value** prob> F
Model	11.96629	9	1.329587	309.7055	< 0.0001
X_1- Hydrophobicity	3.726488	1	3.726488	868.0242	< 0.0001
X_2- Tg	0.247692	1	0.247692	57.69587	< 0.0001
X_3- Time	0.582306	1	0.582306	135.6386	< 0.0001
X_1 X_2	0.430965	1	0.430965	100.3863	< 0.0001
X_1 X_3	0.521357		0.521357	121.4416	< 0.0001
X_2 X_3	0.13522		0.13522	31.49735	0.0002
X_1^2	2.007615	1	2.007615	467.6409	< 0.0001
X_2^2	4.426489	1	4.426489	1031.078	< 0.0001
X_3^2	0.965608		0.965608	224.9225	< 0.0001
Residual	0.042931	10	0.004293		
Lack of Fit	0.019588	5	Not significant		

*df denotes degrees of freedom

** Model terms of of "Prob > F" less than 0.05 indicated that model terms were significant

A high value of the correlation coefficient (r^2 =0.996) signified an excellent correlation between all independent variables (X_1, X_2 and X_3) and the response Y. Coefficients with more than one factor represent the interaction between factors while coefficients with second order terms indicate the quadratic nature of the phenomena.(Bodea and Leucuta, 1997)

It is obvious that the regression coefficient of X_1 was much higher than that of X_2 and X_3. Therefore, the main effect on cumulative drug released was significantly impacted by polymer hydrophobicity. A positive value of a term indicates synergistic, while a negative sign represents an antagonistic effect or inverse effect of the factor on the selected response.(Bodea and Leucuta, 1997, Nagarwal *et al*., 2009)

The one factor plots of the main effects were plotted by changing only one factor over its range, while holding the other factors constant. The plots obtained in Figure 5.8, show a steep curvature indicating that the cumulative drug released is sensitive to the selected factors where it decreases as hydrophobicity and Tg increase as illustrated in the second order curve but increases as a function of time. (Mathew *et al*., 2007)

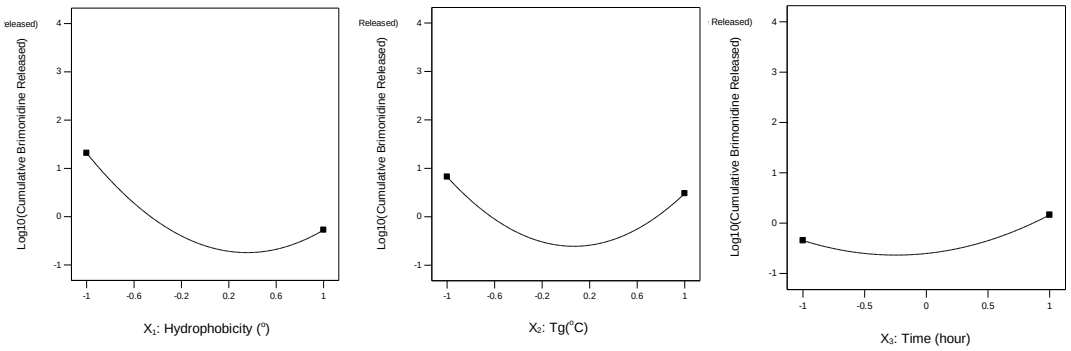

Figure 5.8: One factor plots of the main effects on cumulative drug released

The high negative coefficient of hydrophobicity (X_1) confirms previous findings from Chapter 4 where hydrophobic endcaps were suggested to inversely correlate with drug release. For example, the dodecyl and cholesterol ester endcaps significantly decreased the initial release due to the decreased in total water uptake capacity of the implants and hence retard diffusion of the drug outside the polymer matrix. The one factor plot of Tg (X_2) shows an interesting correlation between Tg and drug release. This could be attributed to the fact that at low Tg the polymer instantaneously relaxes which may facilitate water ingression, as Tg increases the polymer is in a glassy state and takes a longer time to relax as water penetrates acting as an

efficient plasticizer. The amount of drug released increased with increase in Tg after a certain value. This is clearly explained in the interaction plot of Tg and Time. A possible explanation is the interaction of water and polymer endcap this is further discussed in section 5.3.2.

It's worth mentioning that although the one factor plots can be used to account for the main effect of each factor, main effects alone do not have much meaning when they are involved in significant interactions. Those interactions are the key to getting the optimal conditions.(Chuo *et al*., 1996) However one can conclude from the regression equation and pertubation plot seen in Figure 5.9 that polymer hydrophobicty had the highest effect on controlling drug release. Perturbation plots help to compare the effect of all the factors at a particular point in the design space.

Interactions were evident by the ANOVA results (Table 5.7). A significant negative interaction existed between polymer Tg and time as seen from the interaction plots (Figure 5.10). An interaction is the failure of a factor to produce the same effect on the response at the different levels of the other factor.(Montgomery, 2009) For example the antagonistic interaction between Tg (X_2) and time (X_3) illustrates that in order to obtain the highest retardation of drug release at longer exposure times polymers with high Tg would be the best candidates.

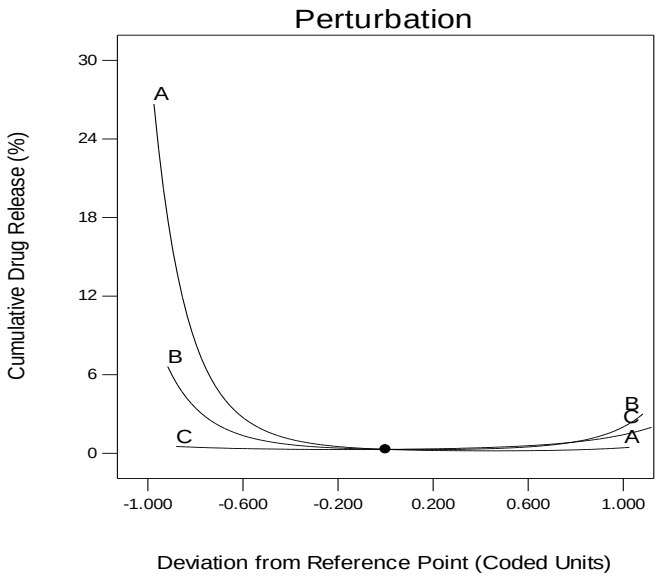

Figure 5.9: Perturbation plot of the main effects on cumulative drug released (%)

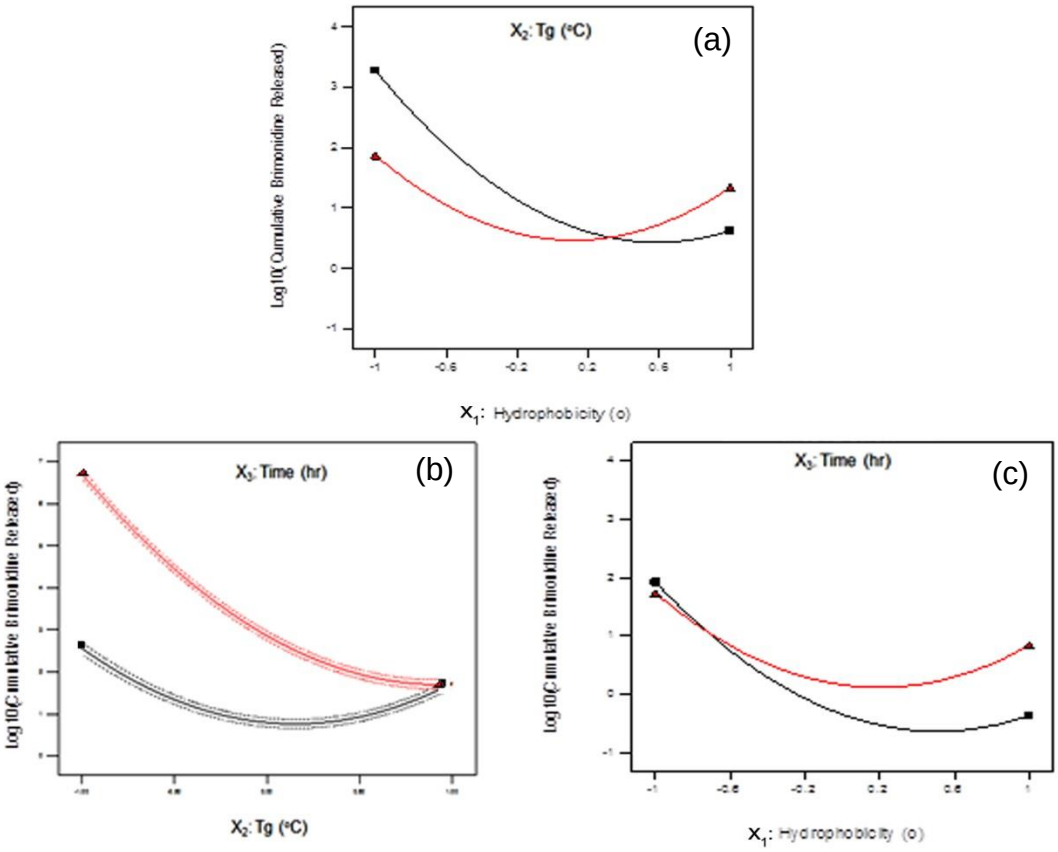

Figure 5.10: Plot of the interaction between a) Hydrophobicity (X_1) and Tg (X_2), b) Hydrophobicity (X_1) and Time (X_3) c) Tg (X_2) and Time (X_3) on cumulative drug released

Contour plots revealed the significance of the interaction between the tested variables. This interaction was reflected by the lack of parallelism between the lines of cumulative drug released (Elkheshen *et al*., 1996)in the 2D contour plots as seen in Figures 5.11. In two-dimensional contour plots, contour lines represent points of equal response. These types of plots show the effect of two factors on the response at a particular time while the third factor is kept at level zero. When non-linear relationships between the factors are seen, this indicates the presence of the strong interaction effects between variables.(Bezerra *et al*., 2008) The interaction was also evident in the 3D plots as the twist in plane (Figure 5.12)

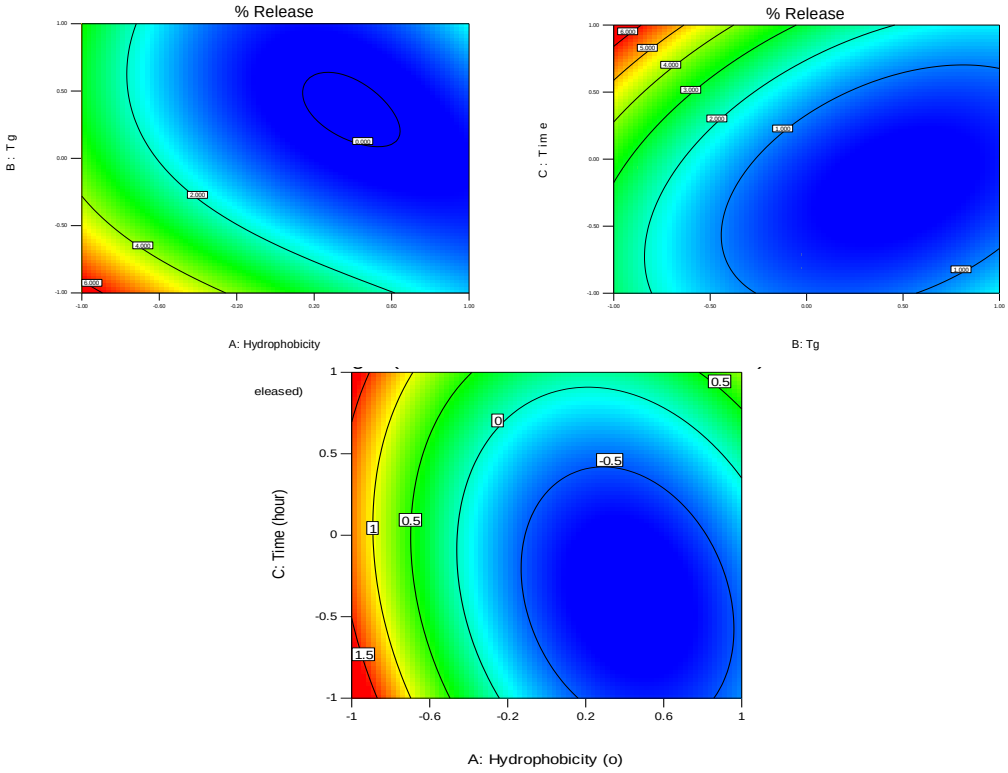

Figure 5.11: Two -dimensional plots for the multifactor effect of the tested variable on cumulative drug released response predicted by the model.

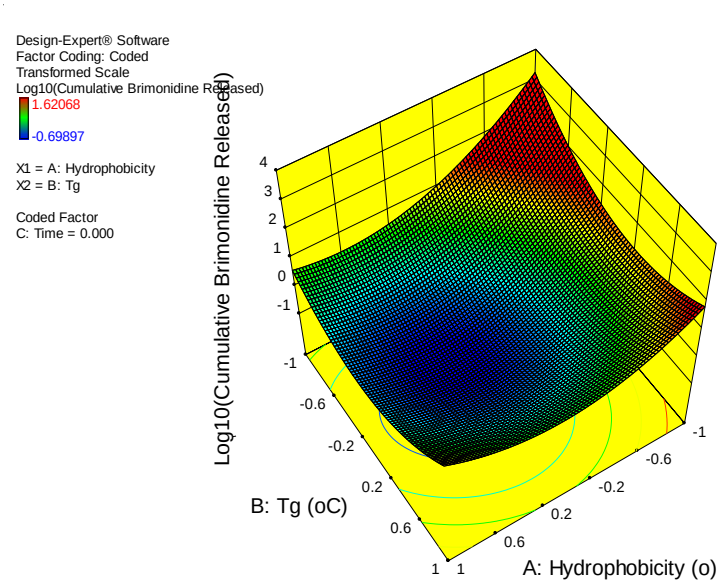

Figure 5.12: Three-dimensional plots for the multifactor effect of Hydrophobicity (X_1), Tg (X_2) and Time (X_3) on cumulative drug released response predicted by the model.

Therefore, as seen from the cube graph (Figure 5.13), in order to attain maximum drug release, polymer Tg and hydrophobicity should be kept at their lowest levels (lower outward left corner).

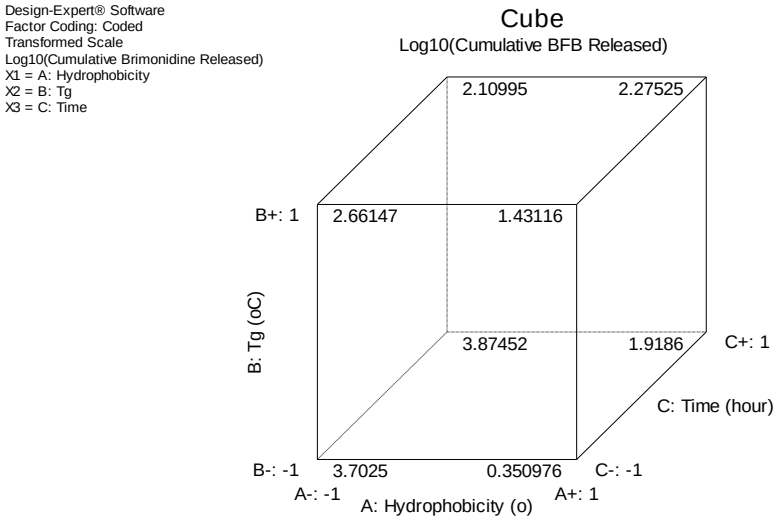

Figure 5.13: Cube graph showing the effect of polymer hydrophobicity, Tg and time on cumulative drug release.

To justify the use of the regression equations, values of X_1, X_2 and X_3 from all experimental runs were substituted in Equation 5.3 to obtain the predicted values. Residual plot of predicated values versus the experimentally determined values in relation to the specific formulations showed that the points were fairly close to the straight line. This indicated good model and fulfilment of the aforementioned requirements for residuals (Figure 5.14).

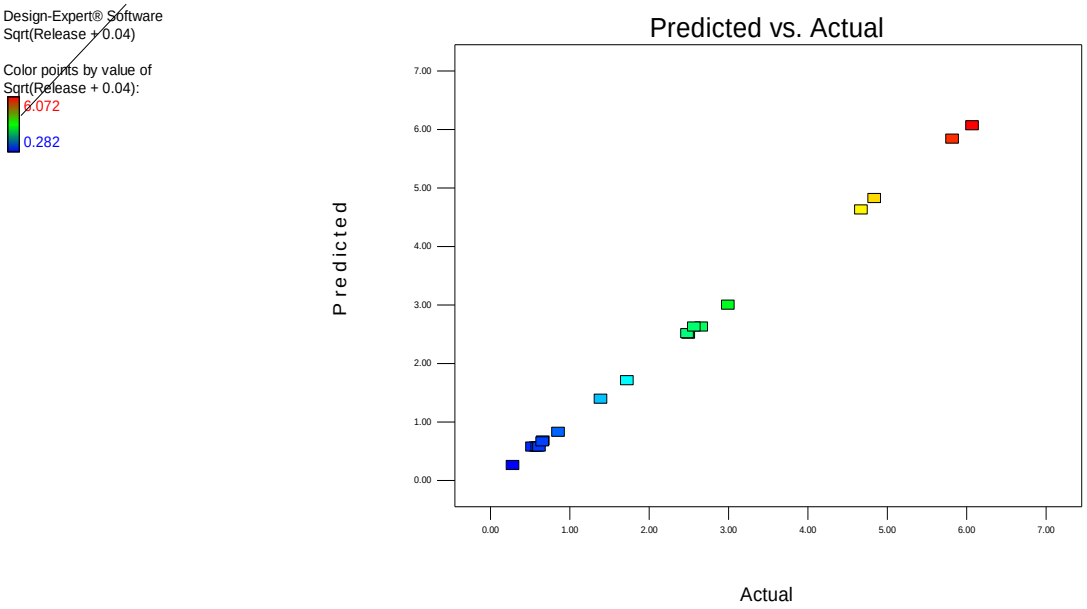

Figure 5.14: Plot of predicted values *vs.* actual values of the Cumulative Drug Released response

As shown in Table 5.8, the ratio between actual and predicted values was close to unity and the % relative standard deviation (RSD) was far below 15%. On the other hand, residual values were close to zero. Small %RSD indicated adequacy of the regression equation to describe the influence of the selected independent variables on a certain response.

It can be seen that in all cases there was a reasonable agreement between the predicted and the experimental values. This was confirmed as the value of the % relative error found was low. It can be concluded that the equation describes adequately the influence of the selected process variables on the response under study.(Sankalia *et al*., 2007)

Table 5.8: Actual and predicted values of cumulative drug release (%)

Run order	Actual value	Predicted value	Residual*	Actual / Predicted	% RSD**
1	1.05	1.07	0.04	0.98	3.29
2	1.41	1.45	0.03	0.97	1.84
3	0.56	0.62	0.01	0.89	2.06
4	-0.70	-0.58	0.09	1.20	-15.89
5	0.82	0.82	0.02	1.00	2.23
6	1.45	1.52	0.01	0.96	0.35
7	1.31	1.28	0.01	1.02	0.65
8	-0.54	-0.58	0.01	0.92	-1.74
9	-0.62	-0.58	0.06	1.06	-10.48
10	1.62	1.61	0.02	1.01	1.02
11	-0.16	-0.17	0.01	0.93	-3.63
12	0.82	0.82	0.02	1.00	2.23
13	1.37	1.33	0.04	1.03	3.35
14	-0.50	-0.58	0.03	0.86	-4.62
15	0.65	0.67	0.02	0.98	2.80
16	1.61	1.56	0.04	1.03	2.50
17	0.85	0.84	0.00	1.01	0.29
18	0.65	0.60	0.05	1.08	7.54
19	0.85	0.84	0.00	1.01	0.29
20	-0.29	-0.32	0.00	0.90	-0.77

*Residual = $|\text{Actual Y} - \text{Predicted Y}|$

**RSD = (Residual / Predicted Y) * 100

The predicted and experimental values for each response parameter shown in Table 5.8 were further correlated by the Cook's distance. This essentially measures the overall influence, potential or actual, of each observation on the regression coefficients, including the intercept. Points with a Cook's distance of 1 or more are considered to merit closer examination in the analysis as they may distort the outcome and accuracy of a regression equation.(Singh *et al*., 2011a) Analysis of Cook's distance revealed that all observations were well below 1 indicating absence of influential observations (Figure 5.15). A check point (Table 5.9) was chosen within the factor space to verify the validity of the reduced model.

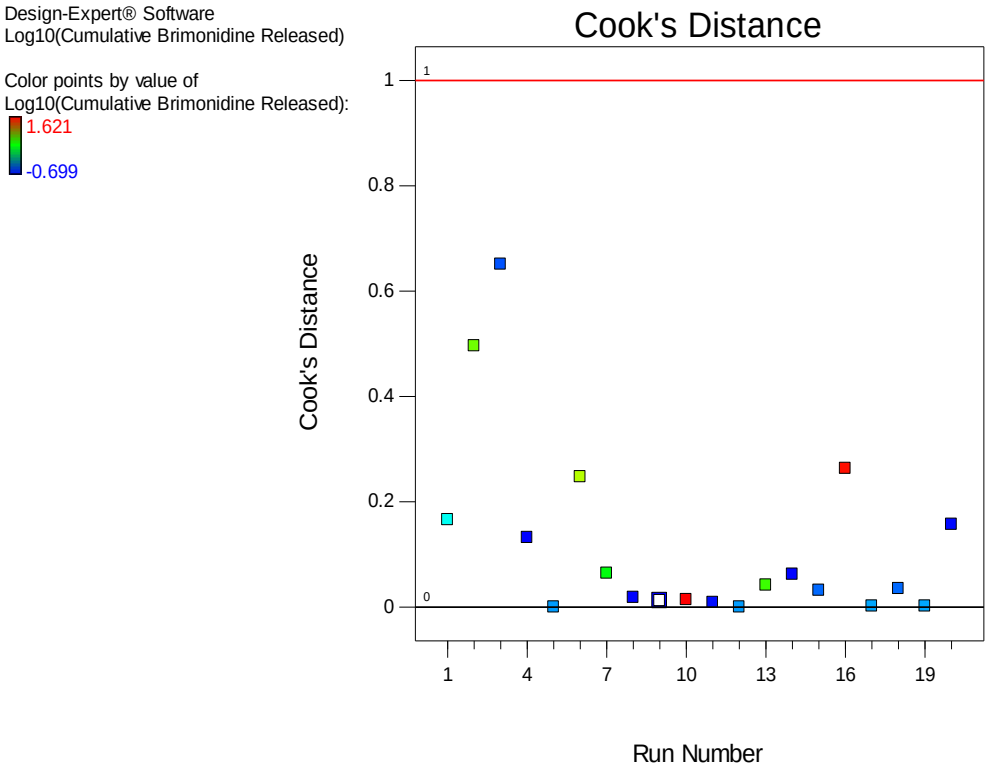

Figure 5.15: Plot of Cook's Distance *vs* run order of the % Release Response

The calculated % cumulative release values for the check points were in agreement with the experimentally determined values. This was seen as giving acceptable residuals, actual/predicted ratios and %RSD below 15% in Table 5.9

Table 5.9: Actual and predicted responses of check point

Run	Actual value	Predicted value	Residual*	Actual / Predicted	% RSD**
1	11.73	10.57	1.16	1.11	10.97
2	14.35	13.01	1.34	1.10	10.30
3	15.02	16.94	1.92	0.89	11.33

*Residual = $|\text{Actual Y} - \text{Predicted Y}|$
**RSD = (Residual / Predicted Y) * 100

5.3.2. Effect of bulk water on polymer Tg

Chapter 3 highlighted the potency of water as a potent plasticizer lowering the polymer's glass transition. This adds additional factors to consider when evaluating implant performance.(Hunter *et al*., 2010, Park and Kang, 2013, Kranz *et al*., 2000) The plasticization of PLGA in bulk water at 37^{o}C was investigated. At designated time periods MDSC was used to determine the Tg after incubation (Wet Tg). This was followed by drying the samples under vacuum to constant weight and rerunning MDSC to determine Tg recovered (Rec Tg). Table 5.10 illustrates the plasticizing effect of water on the studied polymers.

Table 5.10: Glass transition temperatures of dry, hydrated and recovered polymers as determined experimentally using MDSC

Time (days)	15K-OH		15K-Dd-E		15K-Dd-A	
	Wet Tg (^{o}C)	Rec Tg (^{o}C)	Wet Tg (^{o}C)	Rec Tg (^{o}C)	Wet Tg (^{o}C)	Rec Tg (^{o}C)
0	42.23	42.23	36.3	36.3	37.18	37.18
0.25	31.88	41.55	27.42	37.01	27.99	36.95
1	24.57	41.38	26.79	36.78	27.36	37.02
3	23.72	42.02	25.54	36.9	27.32	36.99
5	22.74	42.25	24.01	35.59	27.56	37.23
7	20.95	41.99	24.36	36.01	26.29	37.01
14	17.75	31.56*	21.41	36.23	19.59	22.32*

* Drop in Tg suggests polymer degradation which was confirmed by GPC

Over the 14 day study period the Tg becomes suppressed by 25 °C in the case of PLGA-15K-[OH] and by 15 °C and 11 ^{o}C for PLGA-15K-[Dd]-E and PLGA-15K-[Dd]-A respectively. The effect of water in solution form on the Tg of polymers is illustrated in Figure 5.16. From initial values of 42.23, 36.30, and 37.18 ◦C for PLGA-15K-[OH], PLGA-15K-[Dd]-E and PLGA-15K-[Dd]-A respectively a sudden drop (~11◦C) was observed within a mere 6 hours of exposure to water (Wet Tg). In fact, the value at the 6-hour time point was below the incubation temperature of 37◦C for all studied polymers (dotted line, Figure 5.16). This means that physical properties, such as the viscosity and the storage modulus of the polymer, are changing by orders of magnitude when they are placed in biological environments.(Karlsson *et al*., 2001) Given that the PLGA-15K-[Dd]-E was hydrophobic and end-capped, the sharp initial decrease in glass transition temperature was rather surprising but corroborated with data generated by Souza and colleagues on similar polymers.(D'Souza *et al*., 2014)

After the initial drop in Tg, values appeared to plateau between 24 and 27◦C for the endcapped PLGA-15K-[Dd]-E and PLGA-15K-[Dd]-A. However, the non-endcapped PLGA-15K-[OH] had another sharp decline in Tg before reaching a plateau at 24 hours. For the three specimens, a steady descent in values was noted through the last time point. Thus, the drop in Tg appeared to be triphasic; that is, the first phase was characterized by an initial drop, followed by a plateau, and finally the third phase where a steady decrease in Tg values was observed.

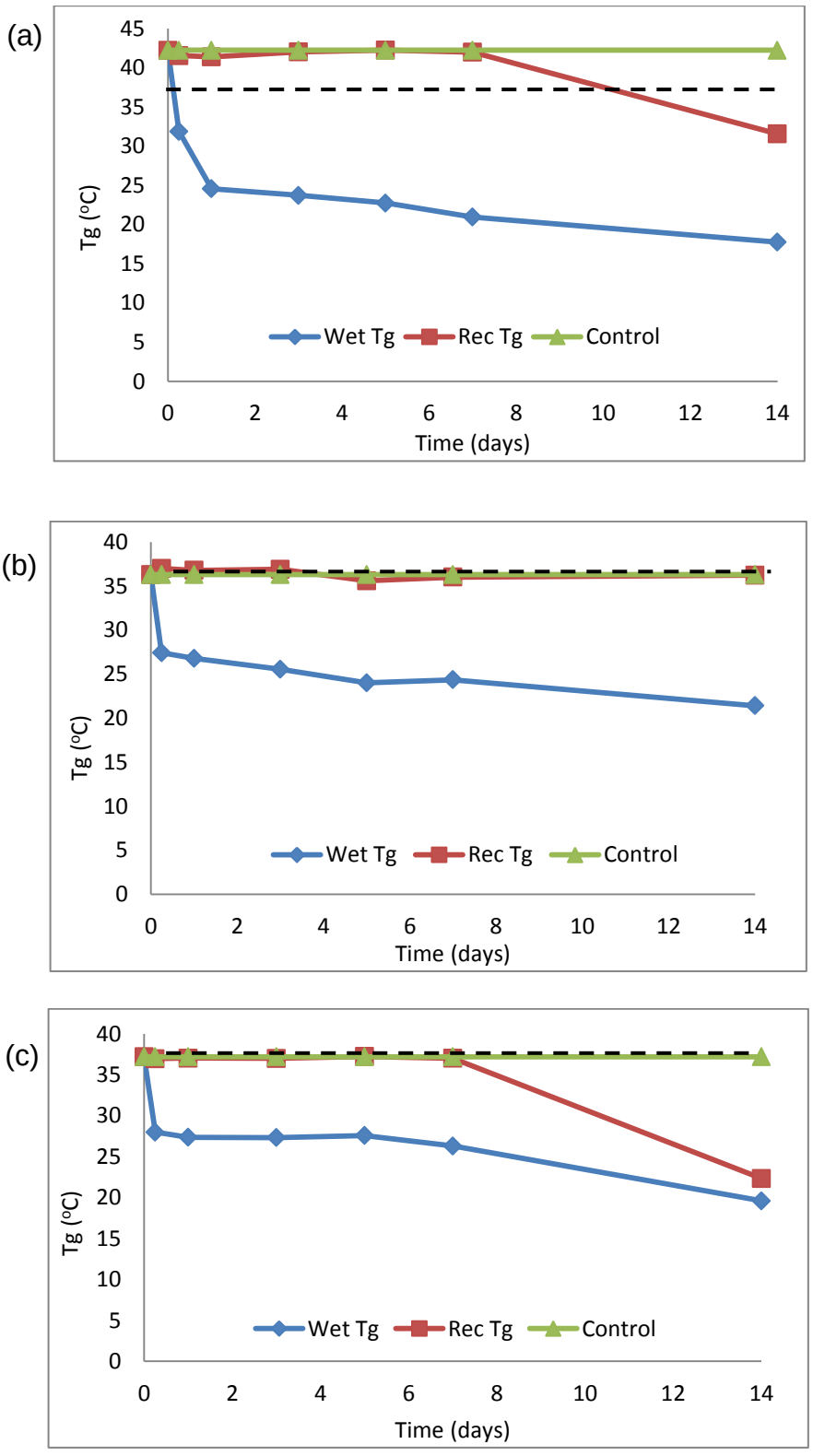

Figure 5.16.: Glass transition temperature of a) PLGA-15K-[OH], b) PLGA-15K-[Dd]-E and c) PLGA-15K-[Dd]-A after incubation at 37°C and after drying. Dotted line represents incubation temperature (37°C).

Sharp and colleagues reported that a reduction in the Tg of 10 °C would cause an increase in the diffusion coefficient by a factor of 2000 at 20 °C which explains the relatively rapid rate of water sorption in the ester endcapped PLGA-15K-[Dd]-E in spite of its hydrophobic nature discussed in Chapter 3 Figure 3.25.(Sharp *et al*., 2001)

Figure 5.16 also describes a third set of control samples (the green line) that were exposed to dry heat (37°C, no moisture). Unlike the polymer exposed to bulk water, the control samples did not exhibit any increase or decrease in Tg during the entire course of the experiment; indicating that, in the absence of moisture, storage of the polymer at a temperature below its Tg did not alter its glass transition temperature.

The decrease in Tg was reversible, at least through a period of 7 days. The dried polymer samples exhibited nearly constant Tg values (red line in Figure 5.16). That is, the polymer appeared to regain its initial Tg value after drying. After 7 days only the PLGA-15K-[Dd]-E specimens retained their initial Tg during the course of the experiment. PLGA-15K-[OH] and PLGA-15K-[Dd]-A no longer appeared to recover their Tg after the first week. This phase was manifested by a consistent drop in polymer Tg after drying and continued through the last measurement (14 days). The irreversible drop in Tg suggests possible change in chain length of the polymer upon degradation which was confirmed by GPC data.

The overall suppression of Tg in the ester end-capped polymer was significantly lower than the non-endcapped polymer. This suggests that although water act as an efficient plasticizer in both polymers, the decrease in Tg depends on the nature of the interaction of water with the functional end groups of the polymer. Interestingly, Figure 5.17 confirms previous findings from the mathematical model derived explaining the effect of interaction between Tg and polymer hydrophobicity which is governed by its endcap. Huang and colleagues reported similar findings where acid-terminated PLGA films incubated in water displayed a lower Tg as compared to the ester-terminated films over time, due to the faster ester cleavage kinetics of the acid-terminated PLGA films.(Huang *et al*., 2013)

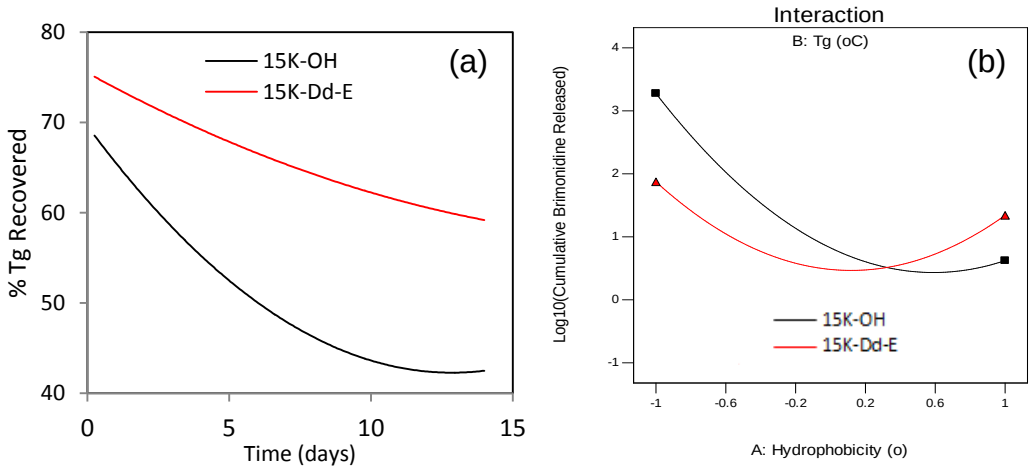

Figure 5.17: a) Interaction Plot between Hydrophobicity and Tg b) Effect of endcap interaction with water on the plasticizing efficacy of bulk water. Interaction plot indicates at low hydrophobicity (black line) Tg sharply decreases upon incubation. Whereas at high hydrophobicity (red line) Tg is maintained with constant levels upon incubation.

5.3.3. Correlation between water uptake and Tg

From the 5 day period data shown in Figure 5.18, a steep drop in Tg to below the incubation temperature was coupled with a sharp increase in water uptake of PLGA-15K-[OH] (24-hour time point, Figure 5.18.a) . After that, the Tg remains virtually unchanged (~22°C) meanwhile the water uptake continued steeply reaching 38%. PLGA-15K-[Dd]-E showed significantly less total water uptake albeit the drop in Tg (6 hour time point) confirming that the nature of endcap influences the interaction between water and polymer (Figure 5.18.b). The relationship between moisture uptake and glass transition temperature in the initial hydration period was linear (Figure 5.19) and an excellent correlation (r^2 >0.99) was obtained for both sets of samples suggesting compliance to the Gordon–Taylor/Kelley–Bueche theory. (Blasi *et al*., 2005) The Gordon-Taylor equation has been used to relate glass transition temperature and water content in PLGA within narrow range of moisture content and limited polymer degradation.(Houchin and Topp, 2009)

The presented data suggests that water incursion into the polymer impacts chain mobility. That is water diffuses through the polymer chains, loosening the rigid glassy structure and increasing mobility transitioning the polymer from a glassy rigid state to a rubbery, more mobile state manifested by a drop in Tg. These findings are in agreement with similar work on PLGA conducted by other authors.(D'Souza *et al*., 2014, Blasi *et al*., 2005)

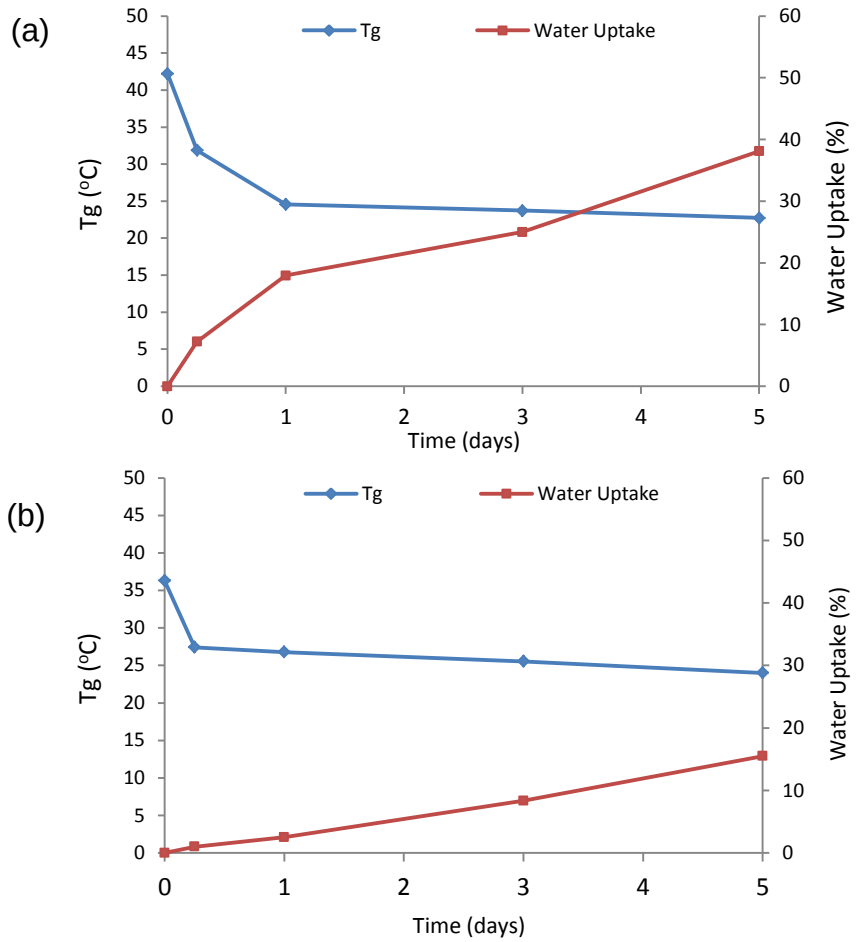

Figure 5.18: Comparison of glass transition temperature of a) PLGA-15K-[OH] and b) PLGA-15K-[Dd]-E and the water content of the samples incubated at 37 ^{o}C in deionized water for 5 days

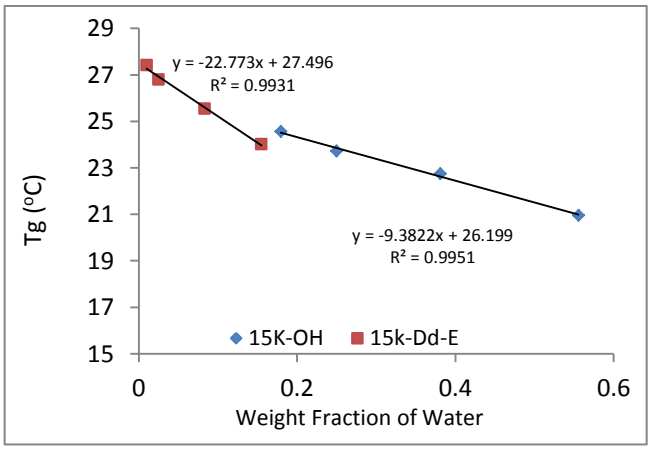

Figure 5.19: Glass transition temperature as a function of weight fraction of water. The plots show the concentration-dependent lowering of Tg due to the plasticizing effect of water

5.3.4. Hygrothermal aging

An evaluation of the effect of endcapping, storage temperature and hydration on the glass transition temperature (Tg) of two samples of PLGA was conducted. The polymers were incubated in deionized water at 25, 37 and 55^{o}C. The thermal properties of the studied polymers reflect the mobility between the PLGA chains. Modification in the structure was detected using DSC.(Pozuelo and Baselga, 2002, Mandal *et al*., 2002, Bouissou *et al*., 2006)The period of storage used in these studies was 1 week, guided by the rapid absorption of water and avoiding the long-term events, dependent on PLGA hydrolysis. The change in Tg upon storage at ambient and elevated temperature revealed an interesting behaviour as summarized in Table 5.11.

Table 5.11: Glass transition Temperature of hydrated PLGAs (Wet Tg) after Incubation in deionized water at 25, 37, 50^{o}C

Time (days)	**15K-OH** Wet Tg			**15K-Dd-E** Wet Tg		
	(25^{o}C)	(37^{o}C)	(50^{o}C)	(25^{o}C)	(37^{o}C)	(50^{o}C)
0	42.23	42.23	42.23	36.3	36.3	36.3
0.041	38.08	37.66	37.11	36.37	35.97	36.21
0.25	32	31.88	30.17	26.77	27.42	23.8
1	28	24.57	16.01	25.54	26.79	24.1
3	24	23.72	10.53	24.36	25.54	23.23
5	23.3	22.74	N/A*	24.18	24.01	N/A*
7	21.87	20.95	N/A*	22.7	24.36	N/A*

*N/A not available because substantial polymer degradation had occurred

When PLGA-15K-[OH] was incubated in bulk water for 1 h (0.041 day), the Tg was depressed from 42 to about 37^{o}C independent of the test temperature (Table 5.11) which is indicative that the polymer was in a hydrated state. Prolonging the incubation time from day one to five days, a moderate decrease in Tg was observed, except in the case of the sample incubated at 55^{o}C were remarkable amount of degradation had occurred. Due to the polymer hydrophobicity, the PLGA-15K-[Dd]-E samples were hydrated after a 6-hour lag period at all incubation temperatures emphasizing the influence of end group interaction with water. Following the 10^{o}C decrease in Tg regardless the incubation conditions, Tg remained constant for 5 days at 25 and 37 but not at 55 ^{o}C suggesting polymer degradation.

Since GPC showed no substantial lowering of molecular weight of samples incubated at 37^{o}C or lower over the initial 5 days, the lowering of Tg due to the change in chain length during the plasticization process was insignificant in comparison to that due to the water absorbed. This result was confirmed also by the observation that after rapid polymer hydration, which leads to Tg depression, no further changes in wet Tg were detected (Table 5.11).

5.3.5. Determination of nature of hydration

The results of the water uptake and Tg experiments can be correlated by understanding the effect of water on the polymer. This section investigated the physical state of water within the hydrated polymer. Since the thermodynamic properties of the water sorbed into a polymer undergo

change with respect to those of bulk water, the nature of the interaction between water and hydrophilic polymers has been investigated in the literature using calorimetric techniques.

Moisture present in hydrophilic polymer has been categorized into three types. Bulk freezable (free) water (Type I) is not strongly associated with the polymer, and shows melting/crystallization temperature with relative enthalpy not different from that of bulk water. Water species exhibiting large differences in transition enthalpies and temperatures, or those for which no phase transition can be observed calorimetrically, are referred to as bound water. Bound freezable water (Type II) is not closely associated with the polymer, and exhibit a melting/crystallization, but often considerable supercooling is observed and the area of the peaks on both, the heating and cooling cycles is significantly smaller than that of bulk water. Bound non freezable water (Type III) which is closely associated with the polymer matrix does not give rise to observable phase transitions by calorimetric analysis.(Hatakeyama and Hatakeyama, 1998, D'Souza *et al*., 2014, Blasi *et al*., 2005)

Figure 5.20 shows the second run of the MDSC data of the PLGA-15K-[OH] wet polymer after incubation in bulk water at 37^{o}C for over a period of 7 days at different time intervals, where the plasticizing effect of water is evident and the endothermic peak of free bulk water is clearly observed.

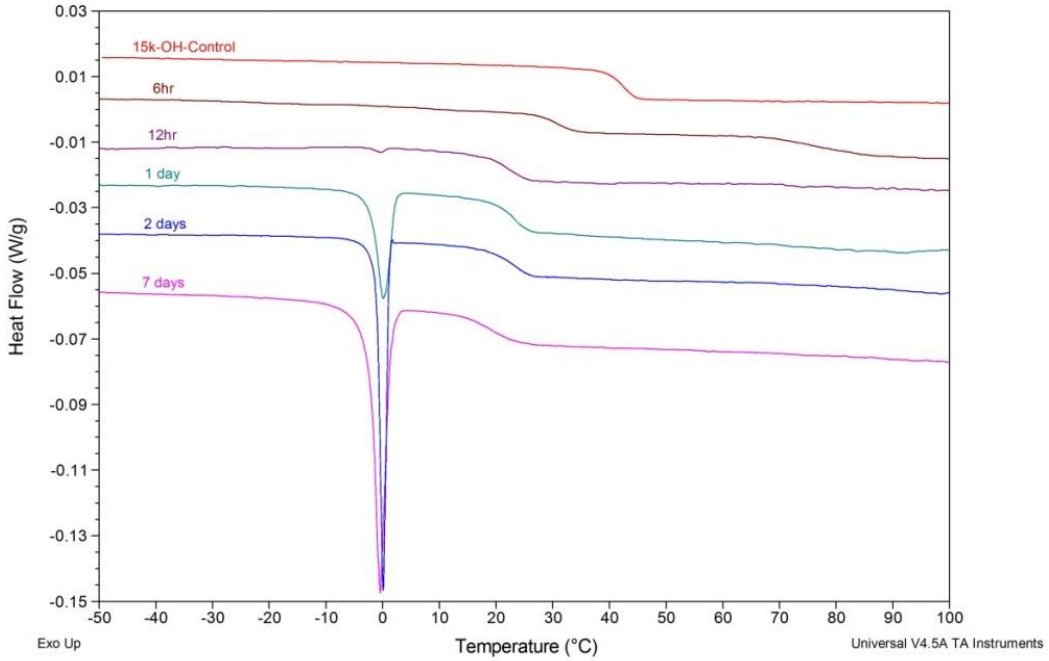

Figure 5.20: MDSC data of PLGA-15K-[OH] incubated in bulk water at 37^{o}C showing the wet Tg of the polymer at preset time intervals where the endothermic peak of free bulk water is clearly observed.

Studying the nature of the water species closely a schematic of the DSC data of PLGA-15K-[OH] is shown in Figure 5.21. Initially after 1 hour of incubation the thermograms display only the glass transition event of the polymer and the first-order transition was not observed until the water content exceeded a critical amount known as the maximum amount of non freezable bound water (Wnf). The maximum Wnf depends on hydrophilicity of polymers and is frequently impossible to observe calorimetrically.(Hatakeyama and Hatakeyama, 1998)

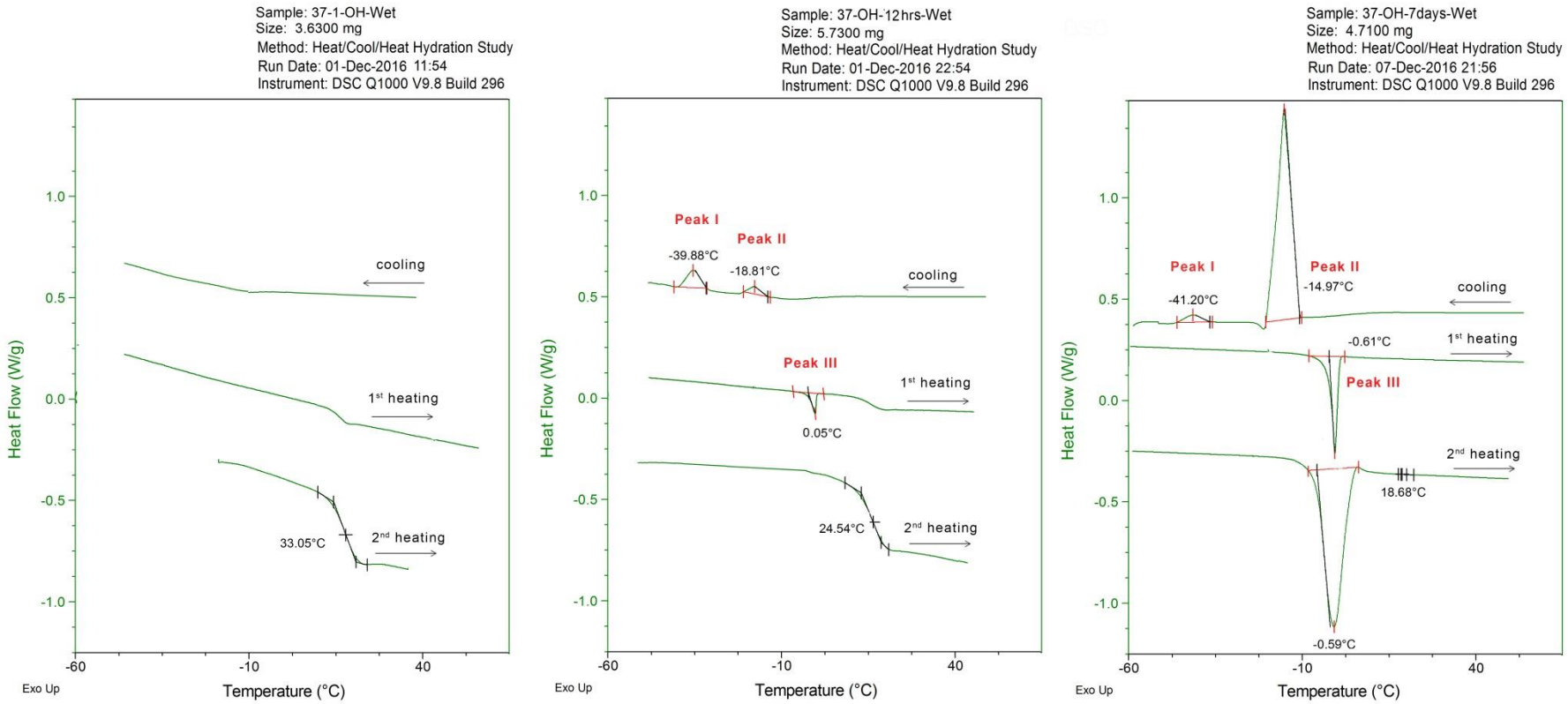

Figure 5.21: MDSC data of PLGA-15K-[OH] incubated in bulk water at 37^{o}C for 1 hour (a), 12 hours (b) and 7 days (c)

When Wnf was surpassed a broad crystallization peak (Peak I) appeared in the cooling ramp at a temperature much lower than the crystallization peak of bulk water. This is categorized as freezing bound water (Wfb). This transition suggests supercooling, which is characterized also by the asymmetric peak shape, as reported by Blasi and colleagues.(Blasi *et al*., 2005) The sum of freezing bound and non-freezing water is the bound water content. When the height of Peak I reached a maximum, a new sharp peak appeared (Peak II). The shape and transition of the second exothermic peak accords well with that of pure water.(Hatakeyama and Hatakeyama, 1998)

A broad endothermic peak was observed around $0^{o}C$ (Peak III) during both heating ramps. The temperature and enthalpy of which was not significantly different from that of bulk water, they were attributed to the freezable free (bulk) water. Direct incubation in water usually provides an excess of water, some of which orients in the matrix as clusters or remains adsorbed on the surface, behaving like bulk water. However, the asymmetry observed was a characteristic pattern of the melting of water adsorbed on the polymer surface of a hydrophilic polymer behaving as bulk water.(Hatakeyama and Hatakeyama, 1998, Hatakeyama *et al*., 2000)

It is hypothesized that only small fractions of non-freezable water absorbed into PLGA matrix, remain in a molecular state in the polymeric matrix. Therefore water molecules could directly interact with groups such as carbonyl and carboxyl by forming hydrogen bonds.(Park and Kang, 2013)

Such interactions may be responsible for Tg depression due to an increase in free volume and a lubrication effect.(Hodge *et al*., 1996) This plasticization effect could generally be described using a simplified form of the Gordon-Taylor/Kelley-Bueche relationships derived from polymer free volume theory.(Hancock and Zografi, 1994)

In fact, the free-volume theory represents one of the three main groups of theories of the glass transition.(Ping *et al*., 2001) Prolonging the incubation time until 5 days did not result in significant changes in Tg which suggests that quantities of water higher than Wnf did not cause further reduction of the Tg. At water concentrations greater than 30%, the water molecules are able to freeze, indicating a saturation of the non-freezing water content in the amorphous region. As the level of free, non-bound water increases polymer degradation in the same manner as bulk water which results in the irreversible drop in Tg.(Blasi *et al*., 2005)

In the thermograms of PLGA-15K-[OH] incubated at 95% RH for 5 days (Figure 5.22) no discernible melting or evaporation events were detected. Therefore, the water sorbed into the matrix, in the range 4.6% w/w, can be classified as non-freezable (bound) water. Since both bulk and vapour water aging caused a decline in Tg. It is proposed that the water responsible for plasticizing the polymer is non-freezable (bound) water.(Blasi *et al*., 2005)

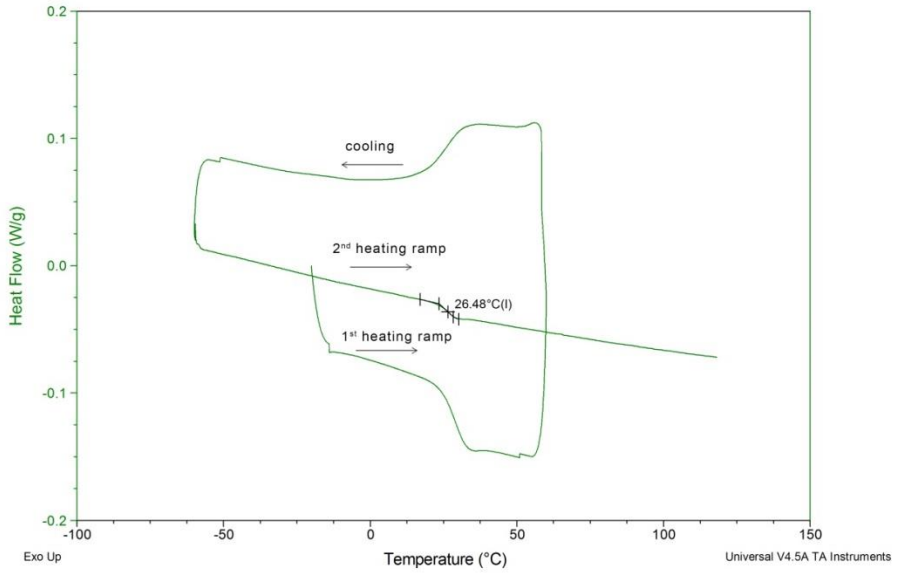

Figure 5.22: MDSC thermogram of PLGA-15K-[OH] at total water uptake content of 4.8% w/w, after equilibration at 95% RH and 37^{o}C for 5 days.

This confirms previous findings that further uptake by samples exposed to deionized water did not impact the Tg significantly where most of it could not diffuse into the polymer matrix and was probably associated with the surface. In fact, the ongoing discussion in the literature regarding the interaction of water with hydrophilic polymers has revealed that the thermodynamic properties of absorbed water are different than those of bulk water.(Maeda *et al*., 1999, Hatakeyama *et al*., 2000)

5.4. Conclusion

Response surface methodology was applied to understand the correlation of three critical factors namely; polymer hydrophobicity, polymer Tg and *in vitro* release time on the cumulative drug release from Brimonidine loaded PLGA implants. The simple and interactive effects of the variables were assessed using a D-optimal design. Analysis indicated significant contribution of the three variables, particularly the polymer hydrophobicity. Cumulative drug release decreased as polymer hydrophobicity and Tg increased this was attributed to impeded water uptake and consequent drug diffusion. The computed regression equation showed a high negative coefficient for hydrophobicity which confirms impact of endcapping on modulating drug release from PLGA matrices where hydrophobic endcaps are suggested to inversely correlate with drug release. Moreover interactions of the variables evident in the regression equation by the ANOVA results were further investigated. A significant negative interaction existed between polymer Tg and time this was further confirmed by hydration studies. Where Tg of the polymer is dynamic and changes as a function of time. Another significant interaction was Tg and hydrophobicity. This clearly identified the effect of the nature of the endcap and its interaction with water. Results complied to the Gordon–Taylor/Kelley–Bueche theory.

CHAPTER 6: SUMMARY AND FUTURE DIRECTIONS

In this work, diversification of the PLGA structure by endcapping allowed for the preparation of a wide variety of polymers with well-defined functionality. The first part of the thesis focused on the synthesis of ester and amide endcapped PLGA. The production of ester endcapped polymers via ring opening polymerization was developed with help from colleagues at Virginia Tech. It was found that control of moisture and vacuum conditions were detrimental for successful endcapping. This was particularly true for the synthesis of the dodecyl ester endcaps. With regard to amide end group substitution, conducted at Strathclyde, milder conditions were required. Overall, amide endcapping proved simpler and went to completion with high yield. In this work, we think that this use of NHS/EDC chemistry is novel as there are no published reports of similar usage.

Characterization of the synthesized endcapped polymers was complex. Nuclear magnetic resonance was used for elucidation of structures. This was a challenging task since very few studies examining the endcapping of PLGA copolymers using NMR have been reported. In addition the ratio of the end group to the polymer chain was low. However, 1D and 2D NMR spectral analysis confirmed successful endcapping and synthesis of PLGA. To determine the presence of residual monomers in the synthesised copolymers, the results of all of the techniques employed were evaluated together. The DSC technique showed that no endothermic event was detected close to the melting temperatures of the monomers. The

thermogravimetry did not present any significant mass loss prior to the onset of copolymer degradation. The NMR analyses did not indicate any significant chemical shift in the spectra for the copolymers that were exactly identical to those in the spectra for the monomers.

The second part of the thesis focused on understanding the effect of endcapping on polymer properties to lay foundation for structure property relationship. The effect of endcapping on polymer thermal behaviour was thoroughly investigated. For the polymers of interest two main temperatures will govern its physical state. The first reference temperature if the polymer is used for drug delivery is the physiological temperature, (37^{o}C). The second being the processing temperature, 60^{o}C for melt extruded implants.

Factors pertinent to the molecular bases of polymer glass formation are usually structurally interdependent. Experimental studies performed on polymers whose microstructures were controlled in a manner that permit systematic assessments of the individual structural contribution to polymer glass formation are scarce, so the relative importance of each factor on the glass formation of real polymers is largely unknown. Undoubtedly, the lack of this experimental information deprives theoreticians of the ability to test a theory's predictive power against the glass-transition behaviours of real polymers. Therefore it was difficult to isolate a single effect when comparing different chemical structures.

In the current work the following factors were found pivotal. First the inherent conformational flexibilities of individual polymer chain backbones. Second the sizes, steric bulk, and the relative flexibility of the side-chains. Third, the possible interactions between the polymer chains such as steric, dipolar, hydrogen-bonding, van der Waals, etc. As it can be seen from the previous discussion it was easier to rationalise Tg rather than predict the effect of endcapping on it.

Another rather important but less discussed implication to endcapping is the effect of the end groups on polymer hydrophilicity. And in turn the effect on properties related to the polymer's water uptake capacity such as degradation, swelling and drug release. Hydrated polymer systems have been widely investigated owing to the effect of water on their performance and the critical role played by water-polymer interactions *in vivo*. Therefore, the effects of moisture cannot be overlooked when designing the dosage form particularly that it will be subjected to a high humidity environment when injected by the intraocular route. The presence of water may exhibit profound effect on a polymer's behaviour due to changes in mechanical, chemical, rheological, and transport properties, which may be either desirable or undesirable. The rate of and mechanism of water uptake is a crucial parameter in determining polymer performance. The work done in Chapter 3 focused on understanding the manipulation of the rate and extent of moisture in a polymer with different endcaps.

In general, the ability of the polymers to absorb water was due to the presence of hydrophilic groups such as –OH,– CONH–, and –COOH. However, an important conclusion was that the endcaps did not only influence the water uptake properties according to their hydrophilicity and ability to hydrogen bond with water molecules. Instead, addition of endcaps imparted two vectors for change within the polymer water uptake dynamics. First the endcaps imparted a significant effect on polymer's Tg. This in turn dictates whether the polymer is in a rubbery state or a glassy one. Once in a rubbery state, the polymer chains become more mobile. With higher molecular mobility, there is greater propensity for the polymer to undergo physical and chemical changes which explains the unexpected behaviour of the mass uptake. Second, although water is a known plasticizer the nature of the interaction between water and the endgroups resulted in varied magnitudes of plasticization.

In all studied polymers non-Fickian behaviour was observed, where two phenomena occur over two distinct time periods in the same experimental time scale; diffusion driven by a water concentration gradient for the first stage and diffusion driven by a slower (relative to the first stage) polymer relaxation for the second stage. Therefore water uptake by the polymers was suspected to be an additive effect relying on both water diffusion and the dependence of Tg on the water-polymer interaction.

Double endcapping could allow further control of the characteristics of the polymer. For example we attempted endcapping both the carboxyl and alcohol end groups of PLA. The constraints of time meant this approach could not be fully developed. In year three prepared PLA endcapped with lauryl, benzyl and acetyl end groups. Moisture uptake properties of the polymer is show in Figure 6.1 shows evidence of further reduction of water uptake. The double endcapped PLA showed radical change in sorption kinetics. It was concluded the mechanisms of water uptake in double capped polymer were significant different from that observed with the amide and ester with a single endcap. This would entail more work to fully characterize and apply for PLGA copolymers.

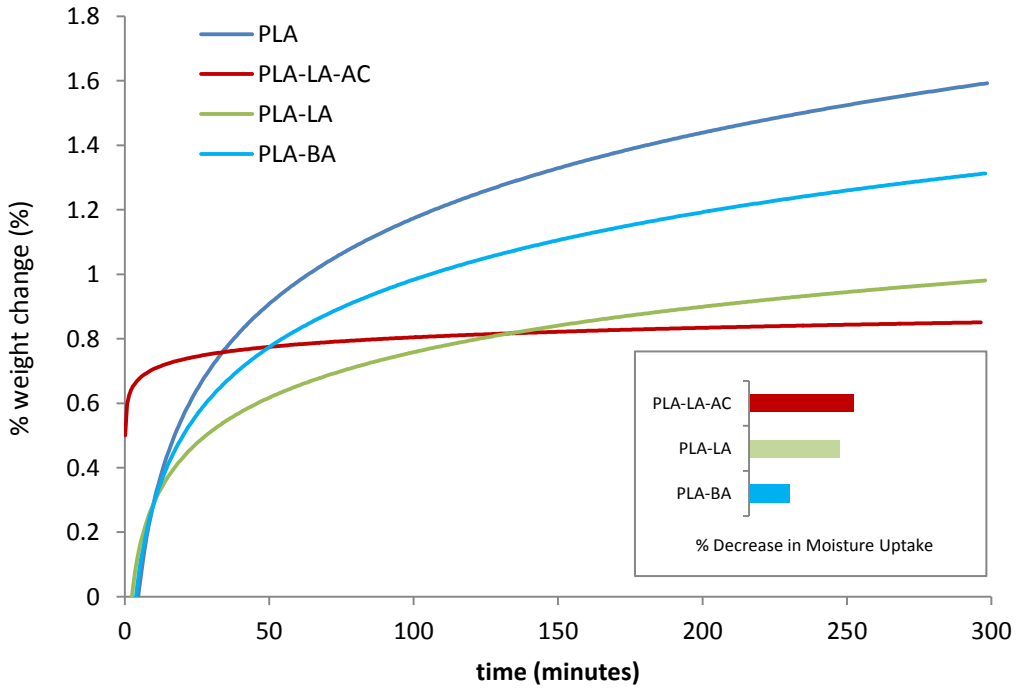

Figure 6.1: Water uptake isotherm of endcapped PLA. A comparison of single endcapped PLAs with a lauryl and benzyl endcap on one end versus a double endcapped PLA that exhibits a lauryl and acetyl end.

The effect of endcapping on drug release properties from PLGA implants was also investigated. The α_2 agonist Brimonidine is among the most promising therapeutic agents for treatment of open-angle glaucoma and ocular hypertension and was selected as the candidate drug. Its ocular hypotensive efficacy is achieved through increasing uveoscleral outflow along with decreasing aqueous humour production.

Although PLGA copolymers are extensively used as drug delivery matrices the underlying release mechanisms in PLGA implants are not fully understood, due to the complexity of overlapping mechanisms involved. Several publications have highlighted the effect of different formulation parameters on drug release kinetics, but only a few have investigated the effect of polymer endcapping. The two main release mechanisms associated with drug release from PLGA-based DDSs were diffusion initially followed by degradation and erosion during the later stages of the release period. In this work we described the overlapping processes controlling the release rate such as water absorption, pore closure, swelling, drug dissolution and rate of drug diffusion or polymer–drug interaction and degradation kinetics to name a few to lay foundation on how drug release can be modified by endcapping. It was concluded that the rate and extent of swelling and structural relaxation, and their effect on the magnitude of drug release, can be significantly manipulated by altering endcaps. Certainly, more work is required to understand this largely overlooked cause of variability in drug release.

All of the practical uses of PLGA involve, at one time or another, their biodegradable character, and thus their decomposition profile had to be precisely matched to the needs of the application. The degradation rate of the polymer depends not only upon external conditions such as pH, temperature, but also on several intrinsic structural parameters such as the polymer composition, its molecular weight and polymer chain ends. The effect of endcapping on polymer degradation and erosion was investigated. It was concluded that both polymer erosion and degradation were a function of the polymer's water uptake capacity. The rate and extent of the swelling governed the rate of erosion and chain scission within the polymer matrix. PLGA of the same molecular weight and copolymer composition but different end caps have elicited different degradation profiles.

The non-endcapped PLGA had half-lives half that of their ester terminated counterparts of the same molecular weight. This is in part because of the higher water penetration into non-endcapped matrices due to their greater hydrophilicity resulting in faster ester bond hydrolysis and thus faster molecular weight decrease. Not only that but also, the non-endcapped polymer degradation is initially faster because the acidic end groups catalyse hydrolysis of the ester bonds resulting in the production of more acidic groups in an autocatalytic cycle. Moreover the nature and length of the alkyl ester end cap can further modulate the degradation rate.

By understanding moisture effects on the Tg of the matrix, chain mobility, and surface structure, it may be possible to controllably modify the bulk properties

of the PLGA for controlled release facilitating the diffusivity of both the escaping drug and the penetrating water while conserving a structural integrity.

To construct an approximation model that can capture interactions between the different effects of endcapping on polymer performance measured as drug release a design of experiment approach was utilised. This enables the investigation of several factors simultaneously to identify possible synergistic or antagonistic interactions on the studied response. A D-optimality criterion was chosen due to the inaccessibility of the complete design space. Analysis revealed dependence of drug release on nature of end cap. This was influenced primarily by the imparted polymer hydrophobicity and Tg. The endcaps modified the segmental relaxation and hydrophilicity of the polymer, and in turn influenced both polymer swelling and degradation rates.

Given the number of motifs generated during the study, we were able to propose a model describing the relationship between drug release and polymer hydrophobicity and Tg as a function of endcap chemistry. It would be interesting to follow these initial investigations with a wider range of drugs, to modulate the molecular weight of the polymers and to change drug loadings in the implants.

References

Aburahma, M. and Mahmoud, A. (2011). Biodegradable Ocular Inserts for Sustained Delivery of Brimonidine Tartarate: Preparation and *In vitro* /*In vivo* Evaluation. *AAPS PharmSciTech,* 12, pp 1335-1347.

Agrawal, R. Fernandez-Sanz, G. Bala, S. and Addison, P. (2014). Desegmentation of Ozurdex implant in vitreous cavity: report of two cases. *British Journal of Ophthalmology,* 98, pp 961-963.

Albers, J. Alles, R. Matthée, K. Knop, K. Nahrup, J. and Kleinebudde, P. (2009). Mechanism of drug release from polymethacrylate-based extrudates and milled strands prepared by hot-melt extrusion. *European Journal of Pharmaceutics and Biopharmaceutics,* 71, pp 387-394.

Allison, S. (2008). Effect of structural relaxation on the preparation and drug release behavior of poly(lactic-co-glycolic) acid microparticle drug delivery systems. *J Pharm Sci,* 97, pp 2022-35.

Arifin, D. Lee, L. and Wang, C. (2006). Mathematical modeling and simulation of drug release from microspheres: Implications to drug delivery systems. *Advanced Drug Delivery Reviews,* 58, pp 1274-1325.

Athanasiou, K. Niederauer, G. and Agrawal, C. 1996. Sterilization, toxicity, biocompatibility and clinical applications of polylactic acid/polyglycolic acid copolymers. *Biomaterials,* 17, pp 93-102.

Batycky, R. Hanes, J. Langer, R. and Edwards, D. (1997). A Theoretical Model of Erosion and Macromolecular Drug Release from Biodegrading Microspheres. *Journal of Pharmaceutical Sciences,* 86, pp 1464-1477.

Bendix, D. (1998). Chemical synthesis of polylactide and its copolymers for medical applications. *Polymer Degradation and Stability,* 59, pp 129-135.

Berchane, N. Carson, K. Rice-Ficht, A. and Andrews, M. (2007). Effect of mean diameter and polydispersity of PLG microspheres on drug release: experiment and theory. *International Journal of Pharmaceutics*, 337, pp 118-26.

Berens, A. and Hopfenberg, H. (1978). Diffusion and relaxation in glassy polymer powders: 2. Separation of diffusion and relaxation parameters. *Polymer,* 19, pp 489-496.

Bezerra, M. Santelli, R. Oliveira, E. Villar, L. and Escaleira, L. (2008). Response surface methodology (RSM) as a tool for optimization in analytical chemistry. *Talanta,* 76, pp 965-977.

Blasi, P. D'souza, S. Selmin, F. and Deluca, P. (2005). Plasticizing effect of water on poly(lactide-co-glycolide). *Journal of Controlled Release,* 108, pp 1-9.

Bodea, A. and Leucuta, S. (1997). Optimization of propranolol hydrochloride sustained release pellets using a factorial design. *International Journal of Pharmaceutics,* 154, pp 49-57.

Bouissou, C. Rouse, J. Price, R. and Van Der Wall, C. (2006). The influence of surfactant on PLGA microsphere glass transition and water sorption: remodeling the surface morphology to attenuate the burst release. *Pharmaceutical Research* , 23, pp 1295-305.

Bourges, J. Bloquel, C. Thomas, A. Froussart, F. Bochot, A. Azan, F. Gurny, R. Benezra, D. and Behar-Cohen, F. (2006). Intraocular implants for extended drug delivery: Therapeutic applications. *Advanced Drug Delivery Reviews,* 58, pp 1182-1202.

Box, G. and Cox, D. (1964). An Analysis of Transformations. *Journal of the Royal Statistical Society. Series B (Methodological),* 26, pp 211-252.

Boyer, R. (1974). Variation of Polymer Glass Temperatures with Molecular Weight. *Macromolecules,* 7, pp 142-143.

Breitenbach, J. 2002. Melt extrusion: from process to drug delivery technology. *European Journal of Pharmaceutics and Biopharmaceutics,* 54, pp 107-117.

Buckton, G. and Darcy, P. (1996). Water mobility in amorphous lactose below and close to the glass transition temperature. *International Journal of Pharmaceutics,* 136, pp 141-146.

Bucolo, C. Salomone, S. Drago, F. Reibaldi, M. Longo, A. and Uva, M. 2013. Pharmacological management of ocular hypertension: current approaches and future prospective. *Current Opinion in Pharmacology,* 13, 50-55.

Burnett, D. Garcia, A. and Thielmann, F. (2006). Measuring moisture sorption and diffusion kinetics on proton exchange membranes using a gravimetric vapor sorption apparatus. *Journal of Power Sources,* 160, pp 426-430.

Cabrerizo, J. and Garay-Aramburu, G. 2013. Intravitreal dexamethasone implant fragmentation. *Canadian Journal of Ophthalmology*, 48, pp 343.

Cairncross, R. Ramaswamy, S. and O'connor, R. (2007). Moisture sorption and transport in polylactide. *International Polymer Processing,* 22, pp 33-37.

Cantor, L. (2006). Brimonidine in the treatment of glaucoma and ocular hypertension. *Therapeutics and Clinical Risk Management,* 2, pp 337-346.

Chandak, A. and Verma, P. (2008). Development and Evaluation of HPMC Based Matrices for Transdermal Patches of Tramadol. *Clinical Research and Regulatory Affairs,* 25, pp 13-30.

Chisholm, M. (2010). Concerning the ring-opening polymerization of lactide and cyclic esters by coordination metal catalysts. *Pure Applied Chemistry,* 82, pp 1647–1662.

Choonara, Y. Pillay, V. Danckwerts, M. Carmichael, T. and Du Toit, L. (2009). A review of implantable intravitreal drug delivery technologies for the treatment of posterior segment eye diseases. *Journal of Pharmaceutical Sciences,* 99, pp 2219-2239.

Chuo, W. Tsai, T. Hsu, S. and Cham, T. (1996). Development of nifedipine-loaded albumin microspheres using a statistical factorial design. *International Journal of Pharmaceutics,* 134, pp 247-251.

Coleman, A. Lum, F. Velentgas, P. Su, Z. and Gliklich, R. (2016). Practice patterns and treatment changes for open-angle glaucoma: The RiGOR study. *Journal of comparative effectiveness research*, 5, pp 79-85.

Contreras, M. and Sãnchez, R. (2002). Application of a factorial design to the study of specific parameters of a Carbopol ETD 2020 gel. Part I. Viscoelastic parameters. *International Journal of Pharmaceutics,* 234, pp 139-147.

Costa, P. and Sousa Lobo, J. (2001). Modeling and comparison of dissolution profiles. *European Journal of Pharmaceutical Sciences,* 13, pp 123-133.

Costa, V. Harris, A. Stefánsson, E. Flammer, J. Krieglstein, G. Orzalesi, N. Heijl, A. Renard, J. and Serra, L. (2003). The effects of antiglaucoma and systemic

medications on ocular blood flow. *Progress in Retinal and Eye Research,* 22, pp 769-805.
Cown, J. (1975). Some general features of Tg-M relations for oligomers and amorphous polymers. *European Polymer Journal,* 11, pp 297-300.
Crank, J. 1975. The Mathematics of Diffusion, 2nd ed, Oxford University, Press: New York.
D'souza, S. Dorati, R and Patrick, P. (2014). Effect of Hydration on Physicochemical Properties of End-Capped PLGA. *Advances in Biomaterials*. pp 9
Davis, E. Minelli, M. Giacinti Baschetti, M. And Elabd, Y. (2013). Non-Fickian Diffusion of Water in Polylactide. *Industrial* and *Engineering Chemistry Research,* 52, pp 8664-8673.
De Jong, S. Arias, E. Rijkers, D. Van Nostrum, C. Kettenes-Van Den Bosch, J. and Hennink, W. (2001). New insights into the hydrolytic degradation of poly(lactic acid): participation of the alcohol terminus. *Polymer,* 42, pp 2795-2802.
De Souza, J. Maia, K. De Oliveira, P. Fernandes-Cunha, G. Da Silva, M. De Matos Jensen, C. and Da Silva, G. (2016). Ocular inserts based on chitosan and brimonidine tartrate: Development, characterization and biocompatibility. *Journal of Drug Delivery Science and Technology,* 32, pp 21-30.
Dechy-Cabaret, O. Martin-Vaca, B. And Bourissou, D. (2004). Controlled ring-opening polymerization of lactide and glycolide. *Chemical Reviews,* 104, pp 6147-76.
Dejaegher, B. And Vander, Y. (2010). Experimental designs and their recent advances in set-up, data interpretation, and analytical applications. *Journal of Pharmaceutical and Biomedical Analysis,* 56, pp 141-158.
Del Amo, E. And Urtti, A. (2008). Current and future ophthalmic drug delivery systems: A shift to the posterior segment. *Drug Discovery Today,* 13, pp 135-143.
Del Nobile, M. Buonocore, G. Palmieri, L. Aldi, A. And Acierno, D. (2002). Moisture transport properties of polyamides copolymers intended for food packaging applications. *Journal of Food Engineering,* 53, 287-293.
Deniz, G. And Turk, J. (1999). Synthesis, Characterization and *in vitro* Degradation of Poly(DL-Lactide)/Poly(DL-Lactide-co-Glycolide) Films. *Turkish Journal of Chemistry,* 23, 153 -161.
Deokule, S. Baffi, J. Guo, H. Nazzaro, M. And Kaneko, H. (2012). Evaluation of extended release brimonidine intravitreal device in normotensive rabbit eyes. *Acta Ophthalmologica,* 90, pp 344-348.
Dipti M. Patel, P. And Patel, N. (2009). Formulation and optimization of two days ophthalmic inserts of Brimonidine tartrate. *Journal of Pharmacy Research 2009,* 2, pp 1234-1236.
Du, A. (2012). *The Study of Water Transport in Polylactide and Polylactide Derivatives.* Doctor of Philosophy in Chemical Engineering, Drexel University.
Eljarrat-Binstock, E. Pe'er, J. And Domb, A. (2010). New techniques for drug delivery to the posterior eye segment. *Pharmacetuical Research,* 27, pp 530-43.

Elkheshen, S. Badawi, S. And Badawi, A. (1996). Optimization of a Reconstitutable Suspension of Rifampicin Using 24 Factorial Design. *Drug Development and Industrial Pharmacy,* 22, pp 623-630.

Engelund, E. Klamer, M. And Venås, T. (2010). Acquisition of sorption isotherms for modified woods by the use of dynamic vapour sorption instrumentation. Principles and Practice. *International Research Group on Wood Protection*

Erbetta, C. Alves, R. Resende, J. Freitas, R. And De Sousa, R. (2012). Synthesis and Characterization of Poly(D,L-Lactide-co-Glycolide) Copolymer. *Journal of Biomaterials and Nanobiotechnology,* 3, pp 208-225.

Faisant, N. Siepmann, J. And Benoit, J. (2002). PLGA-based microparticles: elucidation of mechanisms and a new, simple mathematical model quantifying drug release. *European Journal of Pharmaceutical Sciences,* 15, pp 355-366.

Fedorchak, M. Conner, I. Medina, C. Wingard, J. Schuman, J. And Little, S. (2014). 28-day intraocular pressure reduction with a single dose of brimonidine tartrate-loaded microspheres. *Experimental Eye Research,* 125, pp 210-216.

Félix, R. Leeuwenburgh, S. Wolke, J. And Jansen, J. A. (2011). *In vitro* degradation rate of apatitic calcium phosphate cement with incorporated PLGA microspheres. *Acta Biomaterialia,* 7, pp 3459-3468.

Feng, S. Nie, L. Zou, P. And Suo, J. (2015). Effects of drug and polymer molecular weight on drug release from PLGA-mPEG microspheres. *Journal of Applied Polymer Science,* 132.

Frank, A. Rath, S. And Venkatraman, S. (2005). Controlled release from bioerodible polymers: effect of drug type and polymer composition. *Journal of Controlled Release,* 102, pp 333-344.

Fredenberg, S. (2011). *PLG films in controlled release pharmaceuticals—release mechanisms.* Doctoral Dissertation, Lund University, Sweden.

Fredenberg, S. Wahlgren, M. Reslow, M. And Axelsson, A. (2011). The mechanisms of drug release in poly(lactic-co-glycolic acid)-based drug delivery systems - A review. *International Journal of Pharmaceutics,* 415, pp 34-52.

Friess, W. And Schlapp, M. (2002). Release mechanisms from gentamicin loaded poly(lactic-co-glycolic acid) (PLGA) microparticles. *Journal of Pharmaceutical Sciences,* 91, pp 845-55.

Fu, Y. And Kao, W. (2010). Drug release kinetics and transport mechanisms of non-degradable and degradable polymeric delivery systems. *Expert Opinion on Drug Delivery,* 7, pp 429-444.

Fulgêncio, G. Fernando, V. Raul, R. Yoshida, M. Faraco, A. And Cunha, A. (2012). New Mucoadhesive Chitosan Film for Ophthalmic Drug Delivery of Timolol Maleate: *In vivo* Evaluation. *Journal of Ocular Pharmacology and Therapeutics.,* 28, pp 350-358.

Gao, Q. Lan, P. Shao, H. And Hu, X. (2002). Direct Synthesis with Melt Polycondensation and Microstructure Analysis of Poly(L-lactic acid-co-glycolic acid). *Polymer Journal,* 34, pp 786-793.

Gasmi, H. Danede, F. Siepmann, J. And Siepmann, F. (2015). Does PLGA microparticle swelling control drug release? New insight based on single particle swelling studies. *Journal of Controlled Release,* 213, pp 120-127.

Gasper, M. Blanco, D. Cruz, M. And Alonso, M. (1998). Formulation of L-asparaginase-loaded poly(lactide-co-glycolide) nanoparticles: influence of polymer properties on enzyme loading, activity and *in vitro* release. *Journal Control Release,* 52, pp 53-62.

GHATE, D. M. and EDELHAUSER, H. F. 2008. Barriers to Glaucoma Drug Delivery. *Journal of Glaucoma,* 17, 147-156.

Giannakou, S. Dallas, P. Rekkas, D. And Choulis, N. (2002). *In vitro* evaluation of nimodipine permeation through human epidermis using response surface methodology. *International Journal of Pharmaceutics,* 241, pp 27-34.

Gilding, D. And Reed, A. (1979). Biodegradable polymers for use in surgery—polyglycolic/poly(actic acid) homo- and copolymers. *Polymer,* 20, pp 1459-1464.

Hanafy, A. El-Egaky, A. Mortada, S. And Molokhia, A. (2009). Development of implants for sustained release of 5-fluorouracil using low molecular weight biodegradable polymers. *Drug Discovery Therapry,* 3, pp 287-95.

Hancock, B. And Zografi, G. (1994). The relationship between the glass transition temperature and the water content of amorphous pharmaceutical solids. *Pharmaceutical Research,* 11, pp 471-7.

Hatakeyama, H. And Hatakeyama, T. (1998). Interaction between water and hydrophilic polymers. *Thermochimica Acta,* 308, pp 3-22.

Hatakeyama, T. Nakamura, K. And Hatakeyama, H. (2000). Vaporization of bound water associated with cellulose fibres. *Thermochimica Acta,* 352, pp 233-239.

Hausberger, A. And Deluca, P. (1995). Characterization of biodegradable poly(d,l-lactide-co-glycolide) polymers and microspheres. *Journal of Pharmaceutical and Biomedical Analysis,* 13, pp 747-760.

Hermann, M. Papaconstantinou, D. Muether, P. Georgopoulos, G. And Diestelhorst, M. (2011). Adherence with brimonidine in patients with glaucoma aware and not aware of electronic monitoring. *Acta Ophthalmology,* 89, pp 300-5.

Hibbert, D. (2012). Experimental design in chromatography: A tutorial review. *Journal of Chromatography B*.

Hiltunen, K. Seppälä, J. And Härkönen, M. (1997). Lactic acid based poly(ester-urethane): The effects of different polymerization conditions on the polymer structure and properties. *Journal of Applied Polymer Science,* 64, pp 865-873.

Hitesh, B. And Jayvadan, K. (2013). Long Acting Betaxolol Ocular Inserts based on Polymer Composite. *Current Drug Delivery,* 10, pp 384-393.

Hodge, R. Bastow, T. Edward, G. Simon, G. And Hill, A. (1996). Free Volume and the Mechanism of Plasticization in Water-Swollen Poly(vinyl alcohol). *Macromolecules,* 29, pp 8137-8143.

Houchin, M. And Topp, E. (2009). Physical properties of PLGA films during polymer degradation. *Journal of Applied Polymer Science,* 114, pp 2848-2854.

Huang, C. Kumar, S. Tan, J. Boey, F. Venkatraman, S. Steele, T. And Loo, J. (2013). Modulating drug release from poly(lactic-co-glycolic acid) thin films through terminal end-groups and molecular weight. *Polymer Degradation and Stability,* 98, pp 619-626.

Hunter, N. Frampton, C. Craig, D. And Belton, P. (2010). The use of dynamic vapour sorption methods for the characterization of water uptake in amorphous trehalose. *Carbohydrate Research,* 345, pp 1938-1944.

Ibrahim, M. Abd-Elgawad, A. Soliman, O. And Jablonski, M. (2013). Novel topical ophthalmic formulations for management of glaucoma. *Pharmaceutical Research,* 30, pp 2818-31.

Ibrahim, M. Abd-Elgawad, A. Soliman, O. And Jablonski, M. 2015. Natural Bioadhesive Biodegradable Nanoparticle-Based Topical Ophthalmic Formulations for Management of Glaucoma. *Translational Vision Science Technology,* 4, pp 12.

Insel, P. (1996). α2-Adrenergic receptors: structure, function and therapeutic implications. *Trends in Pharmacological Sciences,* 19, pp 116.

Jranca, G. Foureaux, L. Fuscaldi, T. Ribeiro, L. Rodrigues, R. Bravo, R. Castilho, M. Yoshida, V. Cardoso, S. Fernandes, S. Conemberger, A. And. Faraco, A. (2014). Bimatoprost-loaded ocular inserts as sustained release drug delivery systems for glaucoma treatment: *in vitro* and *in vivo* evaluation*,* 9.

Jain, R. (2000). The manufacturing techniques of various drug loaded biodegradable poly(lactide-co-glycolide) (PLGA) devices. *Biomaterials,* 21, pp 2475-2490.

Jeromenok, J. And Weber, J. (2013). Restricted Access: On the Nature of Adsorption/Desorption Hysteresis in Amorphous, Microporous Polymeric Materials. *Langmuir,* 29, pp 12982-12989.

Jung, Y. Kim, T. Park, S. And Lee, S. (2010). Metabolic engineering of Escherichia coli for the production of polylactic acid and its copolymers. *Biotechnology and Bioengineering,* 105, pp 161-171.

Kamaly, N. Fredman, G. Subramanian, M. Gadde, S. Pesic, A. Cheung, L. Fayad, Z. Langer, R., Tabas, I. And Cameron Farokhzad, O. (2013). Development and *in vivo* efficacy of targeted polymeric inflammation-resolving nanoparticles. *Proceedings of the National Academy of Sciences,* 110, pp 6506-6511.

Kang, J. And Schwendeman, S. (2007). Pore Closing and Opening in Biodegradable Polymers and Their Effect on the Controlled Release of Proteins. *Molecular Pharmaceutics,* 4, pp 104-118.

Karikari, A. (2006). *Synthesis and Characterization of Functional Biodegradable Polyesters.* PhD, Virginia Polytechnic Institute and State University.

Karlsson, O. Stubbs, J. Karlsson, L. And Sundberg, D. (2001). Estimating diffusion coefficients for small molecules in polymers and polymer solutions. *Polymer,* 42, pp 4915-4923.

Keegan, M. Royce, S. Fahmy, T. And Saltzman, W. 2006. *In vitro* evaluation of biodegradable microspheres with surface-bound ligands. *Journal of controlled release,* 110, pp 574-580.

Kiefer, J. And Wolfowitz, J. (1959). Optimum Designs in Regression Problems. *The Annals of Mathematical Statistics* 30, pp 271-294.

Klose, D. Siepmann, F. Elkharraz, K. Krenzlin, S. And Siepmann, J. (2006). How porosity and size affect the drug release mechanisms from PLGA-based microparticles. *International Journal of Pharmaceutics,* 314, pp 198-206.

Klose, D. Siepmann, F. Elkharraz, K. And Siepmann, J. (2008). PLGA-based drug delivery systems: Importance of the type of drug and device geometry. *International Journal of Pharmaceutics,* 354, pp 95-103.

Kobori, Y. Iwata, T. Doi, Y. And Abe, H. (2004). Synthesis, Solid-State Structure, and Surface Properties of End-Capped Poly(l-lactide). *Biomacromolecules,* 5, pp 530-536.

Koopaei, M. Maghazei, M. Mostafavi, S. Jamalifar, H. Samadi, N. Amini, M. Malek, S. Darvishi, B. Atyabi, F. And Dinarvand, R. (2012). Enhanced antibacterial activity of roxithromycin loaded pegylated poly lactide-co-glycolide nanoparticles. *Journal of Pharmaceutical Sciences,* 20, pp 92-92.

Korhonen, H. Helminen, A. And Seppälä, J. (2001). Synthesis of polylactides in the presence of co-initiators with different numbers of hydroxyl groups. *Polymer,* 42, pp 7541-7549.

Korsmeyer, R. Gurny, R. Doelker, E., Buri, P. And Peppas, N. A. 1983. Mechanisms of solute release from porous hydrophilic polymers. *International Journal of Pharmaceutics,* 15, pp 25-35.

Kovach, J. And Cho, B. (2009). A D-optimal design approach to constrained multiresponse robust design with prioritized mean and variance considerations. *Computers and Industrial Engineering,* 57, pp 237-245.

Kranz, H. Ubrich, N. Maincent, P. And Bodmeier, R. 2000. Physicomechanical properties of biodegradable poly(D,L-lactide) and poly(D,L-lactide-co-glycolide) films in the dry and wet states. *Journal of Pharmaceutical Sciences,* 89, pp 1558-66.

Langer, R. And Peppas, N. (1983). *Chemical and Physical Structure of Polymers as Carriers for Controlled Release of Bioactive Agents: A Review*.

Lee, S. Hughes, P. Ross, A. And Robinson, M. (2010). Biodegradable Implants for Sustained Drug Release in the Eye. *Pharmaceutical Research,* 27, pp 2043-2053.

Lee, V. And Robinson, J. (1986). Topical ocular drug delivery: recent developments and future challenges. *J Ocul Pharmacol,* 2, pp 67-108.

Lee, W. Losito, I. Gardella, J. And Hicks, W. (2001). Synthesis and Surface Properties of Fluorocarbon End-Capped Biodegradable Polyesters. *Macromolecules,* 34, pp 3000-3006.

Li, S. Shen, Y. Li, W. And Hao, X. (2006). A common profile for polymer-based controlled releases and its logical interpretation to general release process. *Journal of Pharmaceutical Sciences,* 9, pp 238-44.

Lin, Y. (1990). Entanglement and the molecular weight dependence of polymer glass transition temperature. *Macromolecules,* 23, pp 5292-5294.

Linlin, Li. Nikki, K. Robishaw, J. And Rinaldi, P. (2011). Microstructure characterization of polymers by modern NMR techniques. *Polymer Preprints,* 52, pp 282.

Liu, C. And Lin, W. 2012. Polymeric nanoparticles conjugate a novel heptapeptide as an epidermal growth factor receptor-active targeting ligand for doxorubicin. *International Journal of Nanomedicine,* 7, pp 4749-67.

Lonngren, U. Napankangas, U. Lafuente, M. Mayor, S. Lindqvist, N. Vidal-Sanz, M. And Hallbook, F. (2006). The growth factor response in ischemic rat retina and superior colliculus after brimonidine pre-treatment. *Brain Research Bulletin,* 71, pp 208-18.

Lu, L. Tsai, J. And Liu, J. (2017). Novel Pharmacologic Candidates for Treatment of Primary Open-Angle Glaucoma. *Yale Journal of Biology Medicine,* 90, 111-118.

Macoul, K. And Pavan-Langston, D. (1975). Pilocarpine ocusert system for sustained control of ocular hypertension. *Archives of Ophthalmology,* 93, pp 587-90.

Maeda, Y. Ide, M. And Kitano, H. (1999). Vibrational spectroscopic study on the structure of water in polymer systems. *Journal of Molecular Liquids,* 80, pp 149-163.

Majsztrik, P. Satterfield, M. Bocarsly, A. And Benziger, J. (2007). Water sorption, desorption and transport in Nafion membranes. *Journal of Membrane Science,* 301, pp 93-106.

Mallick, J. Devi, L. Malik, P. And Mallick, J. (2016). Update on Normal Tension Glaucoma. *Journal of Ophthalmic* and *Vision Research,* 11, pp 204-208.

Mandal, T. Bostanian, L. Graves, R. And Chapman, S. (2002). Poly(d,l-Lactide-Co-Glycolide) Encapsulated Poly(Vinyl Alcohol) Hydrogel as a Drug Delivery System. *Pharmaceutical Research,* 19, pp 1713-1719.

Manickavasagam, D. And Oyewumi, M. (2013). Critical Assessment of Implantable Drug Delivery Devices in Glaucoma Management. *Journal of Drug Delivery*.

Mannarswamy, A. Munson-Mcgee, S. And Andersen, P. (2010). D-optimal designs for the Cross viscosity model applied to guar gum mixtures. *Journal of Food Engineering,* 97, pp 403-409.

Mantravadi, A. And Vadhar, N. 2015. Glaucoma. *Primary Care: Clinics in Office Practice,* 42, pp 437-449.

Mathew, S. Devi, S. And Sandhya, K. (2007). Formulation and evaluation of ketorolac tromethamine-loaded albumin microspheres for potential intramuscular administration. *AAPS PharmSciTech,* 8, pp 100-108.

Mealy, J. Fedorchak, M. And Little, S. (2014). *In vitro* characterization of a controlled-release ocular insert for delivery of brimonidine tartrate. *Acta Biomaterialia,* 10, pp 87-93.

Merkli, A. Tabatabay, C. Gurny, R. And Heller, J. (1998). Biodegradable polymers for the controlled release of ocular drugs. *Progress in Polymer Science,* 23, pp 563-580.

Mermoud, A. Salmon, J. Barron, A. Straker, C. And Murray, A. (1993). Surgical management of post-traumatic angle recession glaucoma. *Ophthalmology,* 100, pp 634-42.

Mikkelson, T. Chrai, S. And Robinson, J. (1973). Competitive inhibition of drug-protein interaction in eye fluids and tissues. *J Pharm Sci,* 62, pp 1942-5.

Miyajima, M. Koshika, A. Okada, J. Kusai, A. And Ikeda, M. (1998). The effects of drug physico-chemical properties on release from copoly (lactic/glycolic acid) matrix. *International Journal of Pharmaceutics,* 169, pp 255-263.

Mollo, A. And Corrigan, O. (2003). Effect of poly-hydroxy aliphatic ester polymer type on amoxycillin release from cylindrical compacts. *International Journal of Pharmaceutics,* 268, pp 71-79.

Montgomery, D. 2009. *Design and Analysis of Experiments. Seventh Edition*, Willey, New York.

Moraillon, A. Gouget-Laemmel, A. Ozanam, F. And Chazalviel, J. (2008). Amidation of Monolayers on Silicon in Physiological Buffers: A Quantitative IR Study. *The Journal of Physical Chemistry C,* 112, pp 7158-7167.

Munk, S. Harcourt, D. Arasasingham, P. Gluchowski, C. Wong, H. Burke, J. Kharlamb, A. Manlapaz, C. Padillo, E. Williams, L. Wheeler, L. And Garst, M. (1995). Analogs of UK 14,304: Structural features responsible for α_2 adrenoceptor activity. *Bioorganic* and *Medicinal Chemistry Letters,* 5, pp 1745-1750.

Myers, R. Montgomery, D. And Anderson-Cook, C. (2009) *Response Surface Methodology: Process and Product Optimization Using Designed Experiments, Third Edition*, John Wiley and Sons, Inc.

Nagarwal, R. Srinatha, A. And Pandit, J. (2009). In situ forming formulation: development, evaluation, and optimization using 3(3) factorial design. *AAPS PharmSciTech,* 10, 977-84.

Naik, A. Sawant, S. Kavishwar, G. And Kavishwar, S. (2010). *Novel process for the synthesis of brimonidine and derivative*.

Narasimhan, B. And Langer, R. (1997). Zero-order release of micro- and macromolecules from polymeric devices: the role of the burst effect. *Journal of Controlled Release,* 47, pp 13-20.

Nasr, M. Awad, G. Mansour, S. Al Shamy, A. And Mortada, N. (2011). A reliable predictive factorial model for entrapment optimization of a sodium bisphosphonate into biodegradable microspheres. *Journal of Pharmaceutical Sciences,* 100, pp 612-621.

Navarro, M. Benetti, E. Zapotoczny, S. Planell, J. And Vancso, G. (2008). Buried, Covalently Attached RGD Peptide Motifs in Poly(methacrylic acid) Brush Layers: The Effect of Brush Structure on Cell Adhesion. *Langmuir,* 24, pp 10996-11002.

Nuo, W. Xue Shen, W. Chaoli, L. And Mei, F. (2000). Synthesis, characterization, biodegradation, and drug delivery application of biodegradable lactic/ glycolic acid oligomers: I. Synthesis and characterization. *Journal of Biomaterials Science, Polymer Edition,* 11, pp 301-318.

Ofokansi, K. And Kenechukwu, F. (2013). Formulation Development and Evaluation of Drug Release Kinetics from Colon-Targeted Ibuprofen Tablets Based on Eudragit RL 100-Chitosan Interpolyelectrolyte Complexes. *ISRN Pharmaceutics,* 2013, 8.

Olthoff, C. Schouten, J. Van De Borne, B. And Webers, C. (2005). Noncompliance with ocular hypotensive treatment in patients with glaucoma or ocular hypertension an evidence-based review. *Ophthalmology,* 112, pp 953-61.

Ouyang, C. Ma, G. Zhao, S. Wang, L. Wu, L. Wang, Y. Song, C. And Zhang, Z. (2011). Preparation and characterization of the molecular weight controllable poly(lactide-co-glycolide). *Polymer Bulletin,* 67, pp 793-803.

Pan, J. Tang, J. Weng, Y. Wang, J. And Huang, N. (2006). Preparation, characterization and anticoagulation of curcumin-eluting controlled biodegradable coating stents. *Journal of Control Release,* 116, pp 42-9.

Park, J. And Kang, S. (2013). A Study on Surface, Thermal and Mechanical Properties of Absorbable PLGA Plate. *International Journal of Control and Automation,* 6, pp 73-82.

Park, J. Mattessich, T. Jay, S. Agawu, A., Saltzman, W. And Fahmy, T. 2011. Enhancement of surface ligand display on PLGA nanoparticles with amphiphilic ligand conjugates. *Journal of Control Release,* 156, pp 109-15.

Park, T. (1994). Degradation of poly(d,l-lactic acid) microspheres: effect of molecular weight. *Journal of Controlled Release,* 30, pp 161-173.

Park, T. Lu, W. And Crotts, G. (1995). Importance of *in vitro* experimental conditions on protein release kinetics, stability and polymer degradation in protein encapsulated poly (d,l-lactic acid-co-glycolic acid) microspheres. *Journal of Controlled Release,* 33, pp 211-222.

Patel, S. And Spaeth, G. (1995). Compliance in patients prescribed eyedrops for glaucoma. *Ophthalmic Surgery,* 26, pp 233-6.

Peppas, N. And Brannon-Peppas, L. 1994. Water in Foods Fundamental Aspects and Their Significance in Relation to Processing of Foods Water diffusion and sorption in amorphous macromolecular systems and foods. *Journal of Food Engineering,* 22, pp 189-210.

Peppas, N. And Sahlin, J. (1989). A simple equation for the description of solute release. III. Coupling of diffusion and relaxation. *International Journal of Pharmaceutics,* 57, pp 169-172.

Ping, L. And Wang, W. 2009. H-NMR Spectroscopy Analysis of Homo and Copolymers of L-lactic Acid *Journal of Fiber Bioengineering and Informatics,* 2.

Ping, Z. Nguyen, Q. Chen, S. Zhou, J. And Ding, Y. (2001). States of water in different hydrophilic polymers — DSC and FTIR studies. *Polymer,* 42, pp 8461-8467.

Plazek, D. And Ngai, K. (2007). The Glass Temperature. *Physical Properties of Polymers Handbook.* Secaucus, NJ, USA: Springer.

Pozuelo, J. And Baselga, J. (2002). Glass transition temperature of low molecular weight poly(3-aminopropyl methyl siloxane). A molecular dynamics study. *Polymer,* 43, pp 6049-6055.

Qian, H. Wohl, A. Crow, J. Macosko, C. And Hoye, T. (2011). A Strategy for Control of “Random” Copolymerization of Lactide and Glycolide: Application to Synthesis of PEG-b-PLGA Block Polymers Having Narrow Dispersity. *Macromolecules,* 44, pp 7132-7140.

Quigley, H. (2011). Glaucoma. *The Lancet,* 377, pp 1367-1377.

Quigley, H. And Broman, A. (2006). The number of people with glaucoma worldwide in 2010 and 2020. *British Journal of Ophthalmology,* 90, 262-267.

Raman, C. Berkland, C. Kim, K. And Pack, D. (2005). Modeling small-molecule release from PLG microspheres: effects of polymer degradation and nonuniform drug distribution. *Journal of Controlled Release,* 103, 149-158.

Rishi, P., Mathur, G. And Rishi, E. (2012). Fractured Ozurdex™ implant in the vitreous cavity. *Indian Journal of Ophthalmology,* 60, 337-338.

Ritger, P. And Peppas, N. (1987). A simple equation for description of solute release II. Fickian and anomalous release from swellable devices. *Journal of Controlled Release,* 5, pp 37-42.

Roman-Gutierrez, A. Mabille, F. Guilbert, S. And Cuq, B. (2003). Contribution of Specific Flour Components to Water Vapor Adsorption Properties of Wheat Flours. *Cereal Chemistry Journal,* 80, pp 558-563.

Roy, R. And Hegde, S. (2013). Split Ozurdex implant: a caution. *Canadian Journal of Ophthalmology,* 48, pp 15-6.

Saettone, M. And Salminen, L. (1995). Ocular inserts for topical delivery. *Advanced Drug Delivery Reviews,* 16, pp 95-106.

Sam, S. Touahir, L. Salvador J. Allongue, P. Chazalviel, J. Gouget-Laemmel, A. Henry De Villeneuve, C. Moraillon, A. Ozanam, F. Gabouze, N. And Djebbar, S. (2010). Semiquantitative Study of the EDC/NHS Activation of Acid Terminal Groups at Modified Porous Silicon Surfaces. *Langmuir,* 26, pp 809-814.

Samadi, N. Abbadessa, A. Di Stefano, A. Van Nostrum, C. Vermonden, T. Rahimian, S. Teunissen, E. Van Steenbergen, M. Amidi, M. And Hennink, W. (2013). The effect of lauryl capping group on protein release and degradation of poly(d,l-lactic-co-glycolic acid) particles. *Journal of Controlled Release,* 172, pp 436-443.

Sankalia, M. Mashru, R. Sankalia, J. And Sutariya, V. (2007). Reversed chitosan-alginate polyelectrolyte complex for stability improvement of alpha-amylase: Optimization and physicochemical characterization. *European Journal of Pharmaceutics and Biopharmaceutics,* 65, pp 215-232.

Sasaki, T. Yamauchi, N. Irie, S. And Sakurai, K. (2005). Differential scanning calorimetry study on thermal behaviors of freeze-dried poly(L-lactide) from dilute solutions. *Journal of Polymer Science Part B: Polymer Physics,* 43, pp 115-124.

Sauraabh, G. And Gilhotra, R. (2011). Enhancement of antiglaucoma potential by novel ocular drug delivery system. *International Journal of Pharmacy and Pharmaceutical Sciences,* 3.

Servat, J. And Bernardino, C. (2011). Effects of Common Topical Antiglaucoma Medications on the Ocular Surface, Eyelids and Periorbital Tissue. *Drugs* and *Aging,* 28, pp 267-282.

Sharp, J. Forrest, J. And Jones, R. (2001). Swelling of Poly(dl-lactide) and Polylactide-co-glycolide in Humid Environments. *Macromolecules,* 34, pp 8752-8760.

Shen, J. Caydamli, Y. Gurarslan, A. Li, S. And Tonelli, A. (2017). The glass transition temperatures of amorphous linear aliphatic polyesters. *Polymer,* 124, pp 235-245.

Siepmann, J. Faisant, N. Akiki, J. Richard, J. And Benoit, J. (2004). Effect of the size of biodegradable microparticles on drug release: experiment and theory. *Journal of Controlled Release,* 96, pp 123-134.

Siepmann, J. And Göpferich, A. (2001). Mathematical modeling of bioerodible, polymeric drug delivery systems. *Advanced Drug Delivery Reviews,* 48, pp 229-247.

Siepmann, J. And Siepmann, F. 2008. Mathematical modeling of drug delivery. *International Journal of Pharmaceutics,* 364, 328-343.

Silva, A. Cardoso, B. Silva, M. Freitas, R. And Sousa, R. (2015). Synthesis, Characterization, and Study of PLGA Copolymer *in vitro* Degradation. *Journal of Biomaterials and Nanobiotechnology*, pp 8-19.

Singh, B. Tripathi, C. Bhatowa, R. And Kapil, R. (2011). Developing micro-/nanoparticulate drug delivery systems using "design of experiments". *International Journal of Pharmaceutical Investigation,* 1, pp 75-87.

Singh, S. Parhi, R. And Garg, A. (2011) Formulation of Topical Bioadhesive Gel of Aceclofenac Using 3-Level Factorial Design. *Iranian Journal of Pharmaceutical Research,* 10, pp 435-445.

Singh, V. (2008). *Synthesis of Polylactide with Varying Molecular Weight and Aliphatic Content: Effect on Moisture Sorption.* Master of Science in Chemical Engineering, Drexel University.

SINGH, V. M., KOO, D., PALMESE, G. R. and CAIRNCROSS, R. A. 2011b. Synthesis of polylactide with varying molecular weight and aliphatic content: Effect on moisture sorption. *Journal of Applied Polymer Science,* 120, 2543-2549.

Mohammadi, S. Salehi, R. Amini, N. and Davaran, S. (2012). Synthesis and Physicochemical Characterization of Biodegradable PLGA-based Magnetic Nanoparticles Containing Amoxicilin. *Bulletin Korean Chemical Society,* 33.

Sperling, L. (2001). *Introduction to Physical Polymer Science,* John Wiley and Sons Inc.

Susan, S. Patrick, H. Aron, D. and Robinson, M. (2011). Drug Product Development for the Back of the Eye. *AAPS Advances in the Pharmaceutical Sciences Series.*

Takeuchi, I. Yamaguchi, S. Goto, S. and Makino, K. (2017). Drug release behavior of hydrophobic drug-loaded poly (lactide-co-glycolide) nanoparticles: Effects of glass transition temperature. *Colloids and Surfaces A: Physicochemical and Engineering Aspects,* 529, pp 328-333.

Tamaddon, L. Mostafavi, S. Karkhane, R. Riazi-Esfahani, M. Dorkoosh, F. and Rafiee-Tehrani, M. (2015). Design and development of intraocular polymeric implant systems for long-term controlled-release of clindamycin phosphate for toxoplasmic retinochoroiditis. *Advanced Biomedical Research,* 4, pp 32.

Thrimawithana, T. Young, S. Bunt, C. Green, C. and Alany, R. (2011). Drug delivery to the posterior segment of the eye. *Drug Discovery Today,* 16, pp 270-277.

Tobiesen, F. and Michielsen, S. (2002). Method for grafting poly(acrylic acid) onto nylon 6,6 using amine end groups on nylon surface. *Journal of Polymer Science Part A: Polymer Chemistry,* 40, pp 719-728.

Tracy, M. Ward, K. Firouzabadian, L. Wang, Y. Dong, N. Qian, R. and Zhang, Y. (1999). Factors affecting the degradation rate of poly(lactide-co-glycolide) microspheres *in vivo* and *in vitro*. *Biomaterials,* 20, pp 1057-1062.

Tsai, W. Hedenqvist, M. S., Laiback, Å., Melin, H., Ngo, M., Trollsås, M. And Gedde, U. W. 2016. Physical changes and sorption/desorption behaviour of amorphous and semi-crystalline PLLA exposed to water, methanol and ethanol. *European Polymer Journal,* 76, 278-293.

Tsuji, H. and Muramatsu, H. (2001). Blends of aliphatic polyesters. IV. Morphology, swelling behavior, and surface and bulk properties of blends from hydrophobic poly(L-lactide) and hydrophilic poly(vinyl alcohol). *Journal of Applied Polymer Science,* 81, pp 2151-2160.

Vaishya, R. Khurana, V. Patel, S. and Mitra, A. (2014). Controlled ocular drug delivery with nanomicelles. *Wiley Interdisciplinary Reviews: Nanomedicine and Nanobiotechnology,* 6, pp 422-437.

Velez, G and Whitcup, S. (1999). New developments in sustained release drug delivery for the treatment of intraocular disease. *British Journal of Ophthalmology* 83, pp 1225–1229.

Verhoeven, E. Siepmann, F. De Beer, T. Van Loo, D. Van Den Mooter, G. Remon, J. Siepmann, J. and Vervaet, C. (2009). Modeling drug release from hot-melt extruded mini-matrices with constant and non-constant diffusivities. *European Journal of Pharmaceutics and Biopharmaceutics,* 73, pp 292-301.

Walter, E. Dreher, D. Kok, M. Thiele, L. Kiama, S. Gehr, P. and Merkle, H. (2001). Hydrophilic poly(dl-lactide-co-glycolide) microspheres for the delivery of DNA to human-derived macrophages and dendritic cells. *Journal of Controlled Release,* 76, pp 149-168.

Wang, C. Yan, Q. Liu, H. Zhou, X. and Xiao, S. (2011). Different EDC/NHS Activation Mechanisms between PAA and PMAA Brushes and the Following Amidation Reactions. *Langmuir,* 27, pp 12058-12068.

Wang, C. Wang, W. Meyer, R. Liang, Y. Winey, K. and Siegel, S. (2010). A rapid method for creating drug implants: translating laboratory-based methods into a scalable manufacturing process. *Journal of Biomedical Materials Research Part B: Applied Biomaterials* , 93, pp 562-72.

Wang, J. Wang, B. and Schwendeman, S. (2002). Characterization of the initial burst release of a model peptide from poly(d,l-lactide-co-glycolide) microspheres. *Journal of Controlled Release,* 82, pp 289-307.

Weinreb, R. (2016). Medical Treatment: Neuroprotection. *Pearls of Glaucoma Management.* Berlin, Heidelberg: Springer Berlin Heidelberg.

Wheeler, L. Woldemussie, E. and Lai, R. (2003). Role of Alpha-2 Agonists in Neuroprotection. *Survey of Ophthalmology,* 48, pp S47-S51.

Whitcup, S. and Robinson, M. (2015). Development of a dexamethasone intravitreal implant for the treatment of noninfectious posterior segment uveitis. *Annals of the New York Academy of Sciences,* 1358, pp 1-12.

Widmer, M. Gupta, P. Lu, L. Meszlenyi, R. Evans, G. Brandt, K. Savel, T. Gurlek, A. Patrick, C. and Mikos, A. (1998). Manufacture of porous biodegradable polymer conduits by an extrusion process for guided tissue regeneration. *Biomaterials,* 19, pp 1945-1955.

Wilson, C. Zhu, Y. Frier, M. Rao, L. Gilchrist, P. and Perkins, A. (1998). Ocular contact time of a carbomer gel (GelTears) in humans. *The British Journal of Ophthalmology,* 82, pp 1131-1134.

Wilson, C. Badawi, M. Hillery, A. Borooah, S. Megaw, R. and Dhillon, B. (2016). Ophthalmic Drug Delivery. *In Drug Delivery: Fundamentals and Applications, Second Edition.* CRC Press Taylor and Francis.

Wu, X. and Wang, N. (2001). Synthesis, characterization, biodegradation, and drug delivery application of biodegradable lactic/glycolic acid polymers. Part II: biodegradation. *Journal of Biomaterials Science, Polymer Edition*, 12, pp 21-34.

Yamaguchi, Y. Takenaga, M. Kitagawa, A. Ogawa, Y. Mizushima, Y. and Igarashi, R. (2002). Insulin-loaded biodegradable PLGA microcapsules: initial

burst release controlled by hydrophilic additives. *Journal of Controlled Release,* 81, pp 235-249.

Yasukawa, T. Ogura, Y. Tabata, Y. Kimura, H. Wiedemann, P. and Honda, Y. (2004). Drug delivery systems for vitreoretinal diseases. *Progress in Retinal and Eye Research,* 23, pp 253-281.

Yeo, Y. and Park, K. (2004). Control of encapsulation efficiency and initial burst in polymeric microparticle systems. *Archives of Pharmaceutical Research,* 27, pp 1-12.

Yoon, J. Jung, H. Kim, M. and Park, E. (2000). Diffusion coefficient and equilibrium solubility of water molecules in biodegradable polymers. *Journal of Applied Polymer Science,* 77, pp 1716-1722.

YU, L. (2008). Pharmaceutical Quality by Design: Product and Process Development, Understanding, and Control. *Pharmaceutical Research,* 25, pp 781-791.

Yu, X. Schmidt, A. Bello-Perez, L. and Schmidt, S. (2008). Determination of the Bulk Moisture Diffusion Coefficient for Corn Starch Using an Automated Water Sorption Instrument. *Journal of Agricultural and Food Chemistry,* 56, pp 50-58.

Zhou, S. Deng, X., Li, X., Jia, W. And Liu, L. 2004. Synthesis and Characterization of Biodegradable Low Molecular Weight Aliphatic Polyesters and Their Use in Protein-Delivery Systems. *Journal of Applied Polymer Science,* 91, pp 1848 –185.

Zolnik, B. Leary, P. and Burgess, D. (2006). Elevated temperature accelerated release testing of PLGA microspheres. *Journal of Controlled Release,* 112, pp 293-300.

Zougagh, M. Rudner, P. Garcia De Torres, A. and Cano J. (2000). Application of Doehlert matrix and factorial designs in the optimization of experimental variables associated with the on-line preconcentration and determination of zinc by flow injection inductively coupled plasma atomic emission spectrometry. *Journal of Analytical Atomic Spectrometry,* 15.